



**KTH Engineering Sciences**

## **Studies of sound generation and propagation in flow ducts**

**Fabrice Ducret**

Licentiate Thesis

Stockholm 2006

The Marcus Wallenberg Laboratory for Sound and Vibration Research (MWL)

Department of Aeronautical and Vehicle Engineering

The Royal Institute of Technology (KTH)

Akademisk avhandling som med tillstånd av Kungliga Tekniska Högskolan i Stockholm framläggs till offentlig granskning för avläggande av teknologie licentiatexamen fredagen den 16 juni 2006, kl 10.00 i Sal MWL 74, Teknikringen 8, KTH, Stockholm. Fakultetsopponent är Dr Andy Moorhouse, University of Salford, England, UK.

TRITA-AVE-2006:34

ISSN-1651-7660

---

***Postal address***

Royal Institute of Technology  
MWL  
SE-100 44 Stockholm  
Sweden

***Visiting address***

Teknikringen 8  
Stockholm

***Telephone/E-mail/Web-page***

+46 8 7907903  
fabrice\_ducret@hotmail.com  
<http://www.ave.kth.se/>



## **Abstract**

This thesis contains three papers investigating problems of interest for noise control in ducts.

The first part of this thesis treats the sound propagation in rectangular ducts with flexible walls. Various experimental techniques are performed to measure the internal sound propagation and radiation to the surrounding. An analytical model is derived to calculate the coupled propagation wavenumber and radiated sound power. The two-port formalism is used.

The second part starts with the sound propagation in open ended circular straight pipe with airflow (a tailpipe). Various aspects such as: acoustic damping, reflection and transmission at the open termination are investigated. Sound absorption due to vorticity shed at the opening is also treated. The geometry of the opening is then modified (oblique cuts, diffusers) and comparisons with the reference straight pipe is made for the sound transmission and flow induced noise generation. The effect of an upstream bend close to the opening is also investigated.

In the third part the acoustic impedance of perforated plates are investigated. In particular the application to small perforation ratios ( $\approx 1\%$ ) and holes or slits with apertures of sub-millimetre size, so called micro-perforated plates, are of interest. Linear and non-linear regimes are investigated. A model is derived to calculate the linear acoustic impedance of perforated elements.

**Keywords:** two-port, plane wave, HVAC system, tailpipe, exhaust system, flexible duct, pipe, reflection coefficient, impedance, flow noise, vorticity, damping, scaling laws, impedance, transmission loss, perforated plate, slit, non linearity.



## **Content**

### *Paper I*

Low frequency sound propagation in rectangular ducts

### *Paper II*

Aeroacoustic behaviour of tailpipes

### *Paper III*

Linear and non linear acoustic regimes of perforated plates

## **Fundings**

The author gratefully acknowledges the financial support from the following sources:

Paper I has been funded by the **Rådet för ArbetsLivsForskning** project (dnr 1999-0082).

Paper II has been funded by the European commission under the Artemis project (contract number: G3RD-CT-2001-00511).

Paper III has been funded by the European commission under the EDSVS programme in partnership with Acoustic Technology, Ørsted, DTU, Lyngby, Denmark.

## **Related conference papers**

*Low frequency sound propagation in rectangular ducts*, Tenth International Congress on Sound and Vibration, 2003, Stockholm, Sweden.

*Aeroacoustics behaviour of different exhaust pipe geometries*, Eleventh International Congress on Sound and Vibration, 2004, St. Petersburg, Russia.

*Aeroacoustics behaviour of a straight pipe*, Twelfth International Congress on Sound and Vibration, 2005, Lisbon, Portugal.

*Development of micro-perforated acoustic elements for vehicle applications*, Twelfth International Congress on Sound and Vibration, 2005, Lisbon, Portugal.



## **Acknowledgments**

For his willingness to teach me and share his acoustic knowledge, I am grateful to Mats Åbom.

I am indebted to Susann Boij for the numerous enlightening discussions on the dimensionless but certainly not pointless Strouhal number. She has provided invaluable guidance on the writing of this document. Any errors that remain are, of course, my own. Ragnar Glav has also to be thanked for his time spent on the interpretation of the results concerning the modelling of the exhaust lines.

I have greatly benefited from the help given to me by Hans Bodén in various areas.

My stay in Denmark could not have been possible without the support of Finn Jacobsen, Acoustic Technology, Ørsted, DTU, Lyngby, Denmark.

Down in the lab, technical and moral assistance after rig blowouts has been kindly provided by Kent Lindgren and Danilo Prelevic.

I have immensely appreciated my friendship with Daniel Backström. I have listened with great interest to his Gaussian's theory of life. Спасибо тебе, Даниель, за твое внимание и компанию. Я очень надеюсь поддерживать наши отношения, вне зависимости от расстояний, разделяющих нас.

I would like to thank the staff members at MWL for encouragements and support.





### ***Acoustic poetry***

*“if you would blow on my heart, near the sea, weeping,  
it would sound with a dark noise,  
with the sound of sleepy train wheels,  
like wavering waters,  
like a leafy autumn,  
like blood,  
with a noise of moist flames burning the sky,  
sounding like dreams or branches or rains,  
or foghorns in a dreary port”*

*Extract from “Bacarole”, Pablo Neruda (1904-1973)*

*The type of noise you certainly do not want to attenuate...*



# *Studies of sound generation and propagation in flow ducts*

## **Table of contents**

1	Introduction .....	1
2	Summary of the papers .....	3
2.1	Paper I. Low frequency sound propagation in rectangular ducts .....	3
2.1.1	Summary of the results .....	6
2.2	Paper II. Aeroacoustic behaviour of tailpipes .....	10
2.2.1	Summary of the results .....	12
2.3	Paper III. Linear and non linear acoustic regimes of perforated plates .....	25
2.3.1	Summary of the results .....	26
3	Main contributions.....	31
4	Future research .....	32
5	References .....	33



# 1 Introduction

Airflow is required to expel exhaust fumes and particulates formed during the combustion process in an internal combustion engine. In a ventilation system, air blown by fans is required to transport heat to ensure comfort. In addition, noise produced by elements such as fans, engines or by the flow itself when flow separation occurs is borne by the flow. Therefore, two fields (acoustic and flow) coexist. **Aeroacoustics** is the branch that investigates interaction between these two fields.

Paper I in this thesis deals with the sound propagation in ventilation systems. The flow speed is of magnitude less than 10 m/s. Thus, phenomena associated with flow is not investigated in this part. Influence of the flow is considered in paper II where exhaust tailpipes and various terminations is analysed. For this case flow effects on the sound propagation and on the sound generation are studied. The main application of this investigation concerns the automotive industry. No flow investigation has been performed in paper III where perforated plates are studied. However, flow effects can play a role to understand the acoustical behaviour of such systems.

In an internal combustion engine, pulsating exhaust gas flow excites the structure. Engine elements such as the piston generate structural vibrations. This energy is transmitted through the other components and radiates as sound. In a ventilation system, the ducted elements are sometimes made of thin flexible aluminium sheets. These panels are easily excited either by vibrations or by the sound and flow fields present in the airway and transmit structural vibrations. Vibrating structures are also found in shells of silencers. **Vibroacoustics** deals with the types and the behaviour of the different structural waves that can exist. In paper II and paper III the pipe wall and perforated samples are considered rigid and therefore structural vibration is neglected. Paper I includes vibroacoustic effects as the rectangular ventilation ducts studied are allowed to vibrate and radiate acoustic energy.

**Thermal effects and thermoacoustics** are not considered in this thesis. Temperature gradients are known to be of importance for the sound propagation in an exhaust system. This is particular true for exhaust element closest to the engine, e.g., catalytic

converters. But for the tailpipes investigated here, the effect of temperature gradients is not important. The tests reported in paper III have therefore been done at cold conditions (ambient temperature  $\approx 20^{\circ}C$  ).

This thesis focuses on three acoustic elements found in buildings and cars or trucks, namely, a duct ventilation system (Paper I), an exhaust system (Paper II) and a perforated element (Paper III). Noise in fluid machinery systems can be reduced directly at the source or along the propagation parts which is studied here. The walls of a, e.g., ventilation system, can be stiffened to shift the resonance frequency and reduce the radiating sound. Porous materials can be applied on the walls to absorb outgoing sound waves. An internal additional sound treatment is often required. The easiest consists of placing sound absorbing material within the ventilation duct. However, sufficient sound reduction requires the use of bulky material that takes up space. Thin perforated panels are often preferred. They are placed in front of walls and form panel absorbers. At specific frequencies depending on the geometries of the perforations and depth of the backing cavity, resonance occurs and an enhanced reduction of noise is obtained. Absorbing sheets and materials can be placed in the cavity to improve the sound reduction level. Another interesting approach is to reduce the size of the perforations to the sub-millimetre range, creating so-called micro-perforated panels. For minute dimensions, it has been shown that acoustic losses occur within the perforations. The other advantage of sound reduction through micro-perforated elements is the low frequency efficiency and large bandwidth.

## **2 Summary of the papers**

### **2.1 Paper I. Low frequency sound propagation in rectangular ducts**

Ducts with thin flexible vibrating walls are used in buildings for airflow transportation between the various locations for ensuring better living conditions. Ventilation systems are also operated in many other applications, e.g., cars and trains. The manufacturing process usually consists of folding thin aluminium or steel sheets into rectangular ducts. Although, the main purpose is the transportation of a fluid such as air, noise is also carried out along the duct. Various sources can be thought of, the most obvious one is the fan or fluid machine connected to the duct. Other sources are flow induced noise due to flow separation, speech and other external sources which enters the duct via openings or via breakin through duct walls. The sound transmission to the external environment is sometimes referred as the breakout effect. This is a low frequency process and promotes the extraction of the internal acoustic energy. This is of interest as a sound reduction effect as long as the external environment is not populated. Another effect called structural flanking transmission takes place when the acoustic energy is transmitted to the structure and is carried away until it radiates into the core of the duct. Radiation bypass occurs when the noise is first transmitted out of the duct, propagates in the external environment and re-enters the duct. Porous materials are lined onto the walls to maximise the sound absorption and bars or corrugations are applied to stiffen the structure. The acoustic effects (external radiation to the outside, transmission along and internal absorption) need to be quantified for the case when the flexible duct is part of an entire system composed of other duct elements. An analytical approach is preferred for its simplicity and ease of implementation for calculations involving multiple acoustic elements. For the low frequency plane wave range, which is of main interest here, a building block technique where the duct elements are represented as acoustic two-ports can be applied.

Transmission of sound through walls of flexible ducts has been exhaustively treated by Cummings (1978). An accurate calculation of the radiation from the complete rectangular structure requires the solving of the equations of the motion of the walls. The structural wave theory is used to predict the wall admittance and attenuation in the wall. Cummings (1978) derives a simple low frequency model based on coupled

acoustic/structure wave system. Cummings (1978) treats the radiating duct as a finite length source with a single travelling wave. Cummings (1978) obtains good comparison with experimental results up to  $2/3$  of the cut-on frequency of the lowest cross-mode of the equivalent rigid walled. An extreme test of the theory is made (Cummings (1978)) on a short duct with rigid termination and gives good prediction using the single wave model.

A high frequency approximate asymptotic model has been derived by Cummings (1983) based on the “mass law” wall impedance and including a single higher order mode. The duct is treated as a radiating circular cylinder with the same surface velocity distribution. The predicted radiated power is slightly underestimated. External lagging consisting of wrapping up the duct with porous material such as mineral wool and glass fibre covered by an impervious layer such as plaster or sheet metal has been treated theoretically by Cummings (1979). External lagging is used for two purposes: thermal insulation and sound reduction. A study of the stiffness control of the duct walls has been performed by Cummings (1981) by using materials (Fimalite, polystyrene, honeycomb) with different stiffness/mass ratios to reduce low frequency acoustic breakout related to transverse resonances and to increase the fundamental transverse resonance frequency of the walls. A low frequency approximate method is given to calculate the transmission loss of ducts. Flanking transmission effects (structural and breakout/breakin) have been modelled by Cummings (1995) using the reciprocity theorem. A more accurate and refined modelling has been performed using a finite element scheme (Astley & Cummings (1984)) for acoustic transmission through ducts with flexible walls. This study has shown that the radiation damping is negligible in comparison to structural damping. Moreover, the investigation of the relation between near field and far field has demonstrated the simplicity of the far field radiation pattern.

The internal reduction of sound in a duct with flexible walls and porous material has been treated analytically by Astley (1990). A functional is derived based on the wave equations in the airway, the porous material and the flexible structure. The dispersion relationship obtained is solved to compute the propagating coupled wavenumber. The imaginary part is converted to a loss factor.



Paper I focuses on two aspects of low frequency (plane wave) sound propagation in rectangular ducts. The first one concerns the internal attenuation of sound waves inside a lined duct with flexible walls. From a functional based on boundary conditions and wave equations in the structure and fluid, the fundamental characteristics of sound in flexible ducts are computed. The model used is based on Astley (1990).

The second aspect deals with the radiation of sound by the same duct. Using the equations derived for the internal sound attenuation model, one can analytically estimate the radiation. An analytical model, which regards the duct as a line of monopole sources, is used. This procedure is applicable and gives good results as long as only the fundamental plane mode is investigated. The model used in this case is based on Cummings (1978, 1979).

These two theoretical models have been validated experimentally using different test ducts. The two-microphone technique was used and radiation measurements were performed in a reverberation room at the MWL laboratory. All measurements were done in the plane wave range of the test ducts (0-2000 Hz).

One aim of this research is to implement the models in the software code SID (“Sound in ducts”) developed at MWL to simulate sound propagation in duct networks (Nygård (2000)).



Figure 1: Industrial ventilation duct.

### 2.1.1 Summary of the results

#### *Internal transmission loss*

Theoretical and measurement results of the internal transmission loss for a lined and unlined corrugated duct are shown in Figure 2. In the lined case, only the bottom wall was lined with polyurethane foam (thickness: 22 mm, length: 2m).

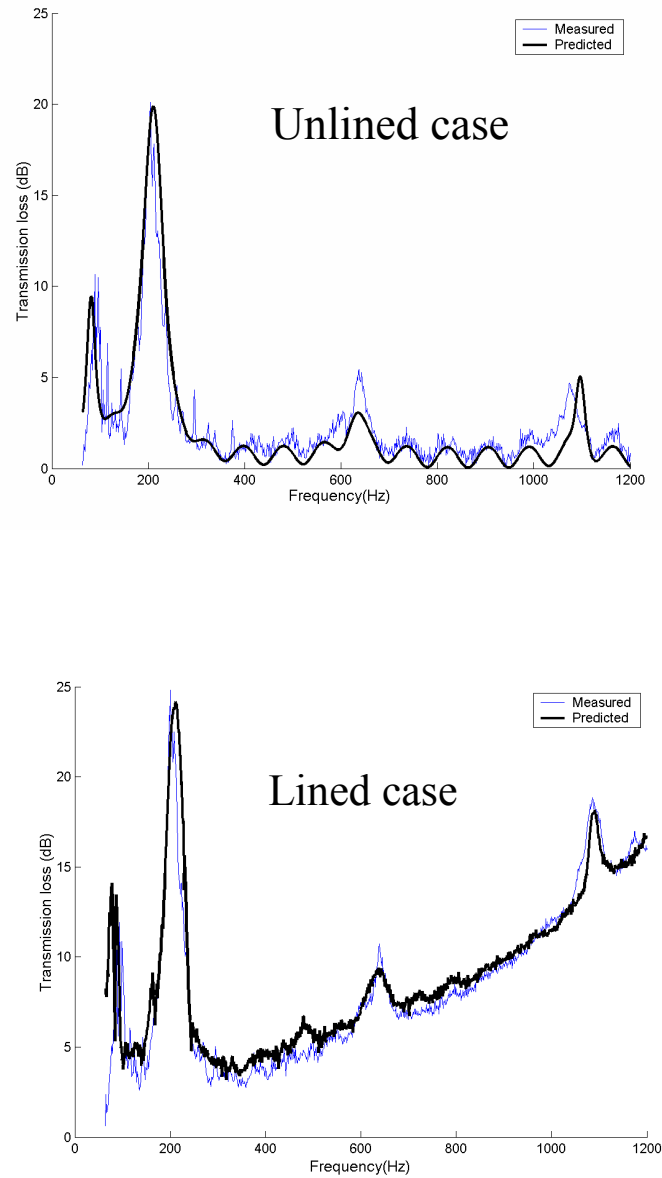


Figure 2: Predicted and measured internal transmission loss for the unlined and lined corrugated steel duct. Duct length:  $l=2\text{m}$ , cross-section area:  $150 \times 200 \text{ mm}^2$ , wall thickness: 1 mm.

The measurement results are in close agreement with data obtained from the theoretical models. Both plots display four resonance peaks due to the presence of two pairs of walls of different lengths (150 and 200 mm). At these frequencies maximum transmission loss occurs. It can be seen that in the lined case (right plot), the trend is for the transmission loss to increase as frequency rises. This is due to the presence of the lining material which is more acoustically efficient for higher frequencies. No noticeable deterioration between measurement and theory can be observed for frequencies above the cut-off frequency of the corrugated duct (850 Hz) for which higher-order mode perturbations would be expected. Inspection of the left plot (unlined case) reveals a standing-wave like pattern. This can be explained by reflected waves produced at the duct termination. Figure 3 shows the internal transmission loss for the three tested duct

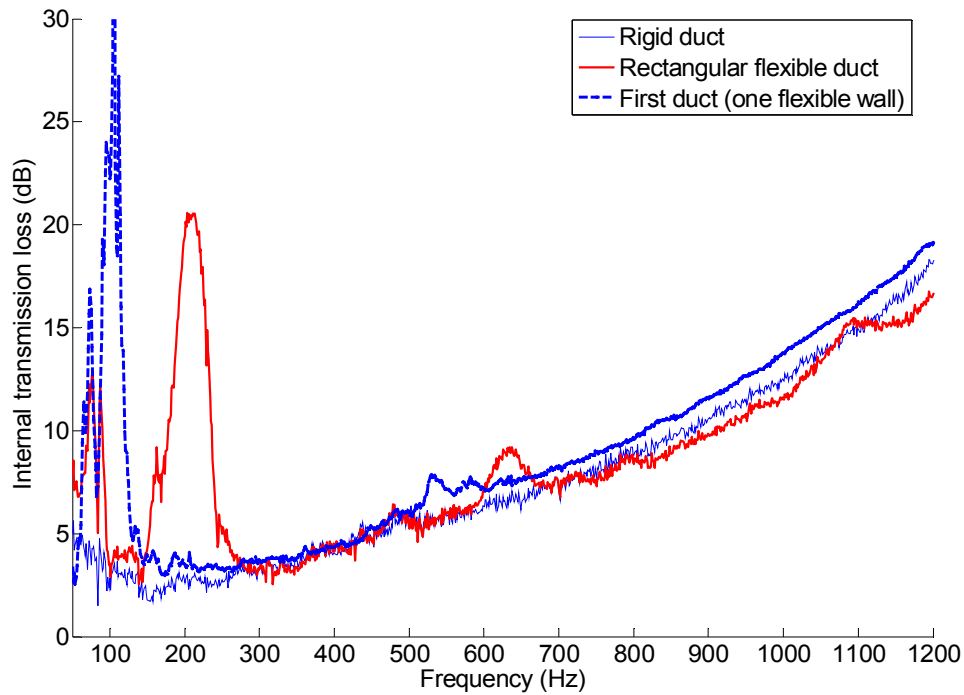


Figure 3: Comparison of measured internal transmission loss for the three lined ducts investigated.

Except at the first bending wave resonances the lined flexible ducts behave as a rigid duct.

### ***Radiation transmission loss***

Theoretical and measured results of the radiation transmission loss for the lined and unlined corrugated duct are shown in Figure 4. As for the transmission loss analysis, the bottom wall was lined with the same material (polyurethane foam).

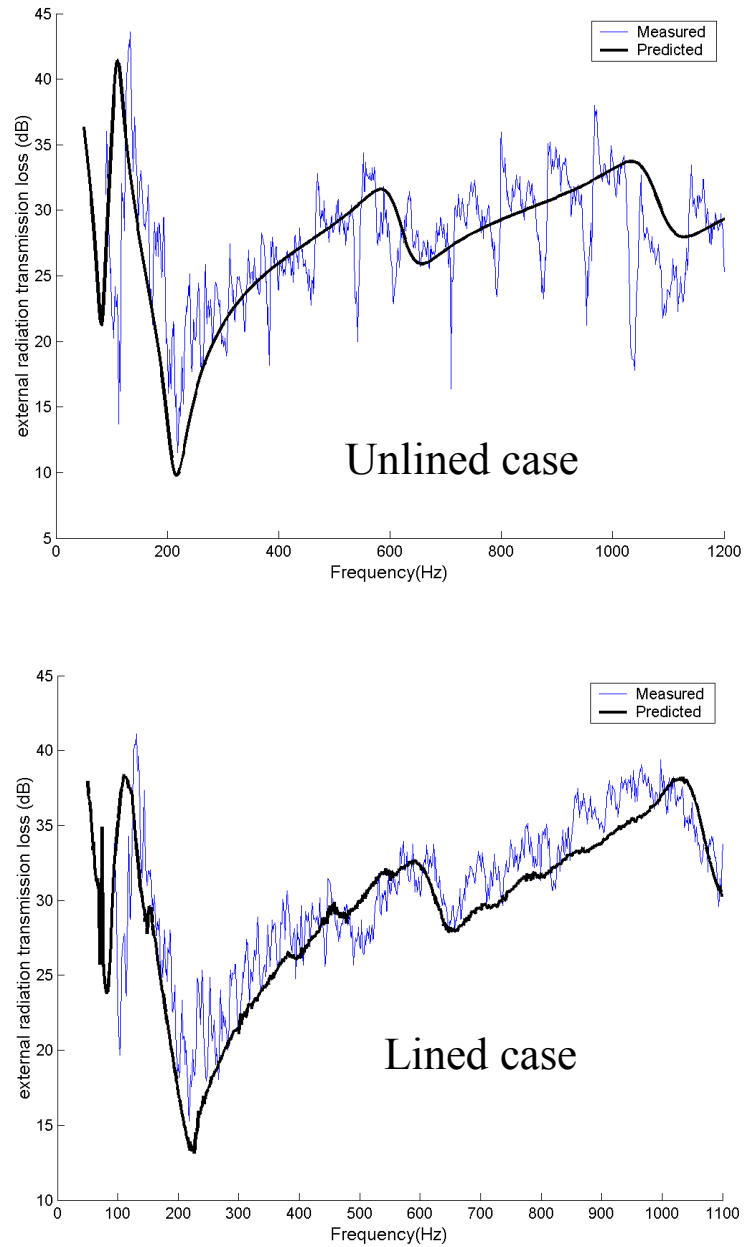


Figure 4: Predicted and measured radiation transmission loss for the unlined and lined corrugated duct

Good agreement between theory and measurement is observed even for frequencies above the corrugated duct cut-off frequency (850 Hz). This time, four dips are displayed at the frequencies for which the internal transmission loss reaches a peak (resonance frequencies of the flexible walls). The reason for this behaviour is that the acoustical energy is mostly attenuated in the structure. No deviation occurs at resonance frequencies although the radiation model based on monopole distribution was expected to be violated. Comparison of the unlined and lined cases shows that the presence of the lining does not greatly influence the radiation magnitude of the duct.

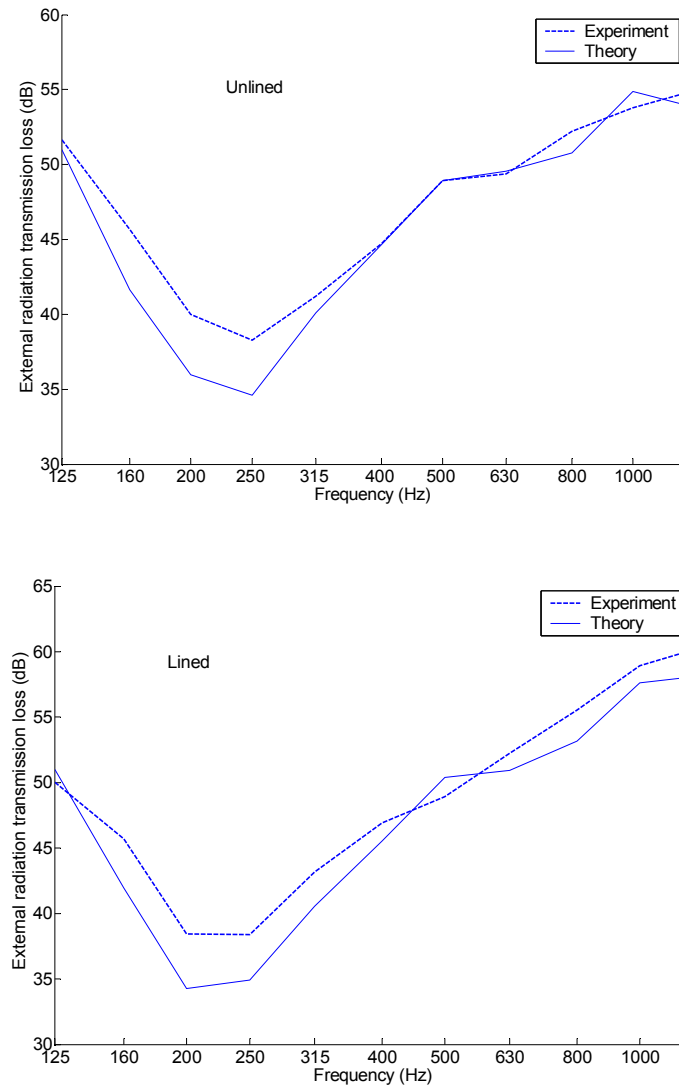


Figure 5: Same as in Figure 4 but in 1/3-octave band.

## **2.2 Paper II. Aeroacoustic behaviour of tailpipes**

The exhaust system of a car is typically composed of various elements such as the silencer and termination (tailpipe). An efficient exhaust system implies the tuning of all the elements respective to each other. The silencer has been exhaustively investigated. The termination of the exhaust system has on the other hand received less attention.

A classical theoretical work on the sound radiation from an open end straight pipe with no flow has been done by Lewine & Schwinger (1948). They obtain numerically the reflection coefficient for the velocity potential and the amplitude of the diverging spherical wave in the far field. The reciprocity relation is employed to relate the radiation characteristics to the attenuation of the plane sound waves.

Another major work on the radiation of sound from an open ended straight pipe with flow has been performed by Munt (1977, 1990). The mathematical model involves the use of the Wiener-Hopf technique and a full Kutta condition (boundary conditions at the lips stating that the flow velocity is fixed and finite). The model describes the air jet as a semi-infinite cylinder pipe bounded by an unstable boundary layer. Cargill (1982) derived analytical expressions for the far field radiation and pressure reflection coefficient at the opening of a flow pipe. The agreement with Munt's model is good.

The aeroacoustic behaviour of an open pipe has been treated experimentally with a multimicrophone technique by Peters and al. (1993). The technique enables the measurement of the acoustical attenuation due to visco-thermal effects along the wall and the determination of the impedance, the pressure reflection coefficient and end correction at the opening. The authors point out that the geometry of the opening does not affect the low frequency reflection coefficient. The internal acoustic damping along the walls of a straight pipe with an open end has also been treated by Dokumaci (1998), Davies (1988) and Howe (1995). The attenuation in the core of the fluid is usually neglected.

Flow diffusers and bends have been characterised by Dequand and al. (2002), van Lier and al. (2001). A parallel has been drawn between the two geometries. It has been found that the aeroacoustic behaviour is accurately predicted by a quasi-stationary model

when the flow separation occurs at sharp edges. Non-linear effects are more important for smooth geometries and can not be predicted by an incompressible quasi-steady theory. In the case of a smooth bend, it is theoretically preferable to replace the element with an equivalent smooth straight pipe. The study of flow diffuser (van Lier and al. (2001)) has shown that at low and moderate sound amplitude, the diffuser is a source of sound at a specific Strouhal number. At high excitation level, the diffuser behaves as a sound sink.

Paper II starts by describing the acoustics of a straight pipe with circular termination which is used as a reference case. A second part treats modified tailpipes, i.e., a straight pipe terminated with different configurations such as oblique cuts, diffusers and with upstream bends

### ***Straight pipe***

An experimental investigation is carried out on the propagation and radiation of plane waves from an open end in a pipe. This study seeks to analyse the acoustic response of tailpipes commonly found in an exhaust system. The silencer located upstream has to be designed in accordance with this response. The flow velocity was varied over a Mach number range of 0-0.2. Using an array of six in-duct flush mounted microphones associated with an iterative method; one can extract the rate of acoustical energy attenuation through internal visco-thermal effects. Reflection coefficient and impedance at the opening are obtained in a similar fashion. Munt's model (Munt (1977, 1990)) is run to compute these quantities for confrontation with experimental data. A rotating microphone placed in the far field of a reverberation room is employed to measure the rate of attenuation through vorticity in the flow jet. An analytical model (Bechert (1980)) regarding the opening as a point monopole and a point dipole is coded to predict the radiated power in the far field and consequently the acoustical energy dissipation in the jet.

### ***Tailpipes***

An experimental investigation is carried out on the transmission, reflection, and generation of low frequency acoustical energy from different exhaust pipe geometries

(oblique cuts, diffusers and bends). Measured data are compared with theoretical models based on Munt (1977, 1990). A low frequency experimental investigation has shown that the diffuser elements deviate from the straight pipe case when flow is present. It has been found that the magnitude of the pressure reflection coefficient for the diffusers is larger than 1 and increase with the diffuser angle and flow Mach number. The measured impedance data for flow diffusers are implemented in the modelling of exhaust lines to test the potential of such elements in reducing sound radiation.

Another aspect of interest is the determination of flow-induced noise emitted from the same geometries; no other sources of sound being present. The main purpose being to estimate the level of extra-noise generated by the elements compared to the reference case (straight pipe). Based on this data, scaling laws could be obtained for the elements after collapse of measured sound power levels as function of Strouhal number. The velocity dependence found is of importance to understand the mechanism governing the flow noise generation.

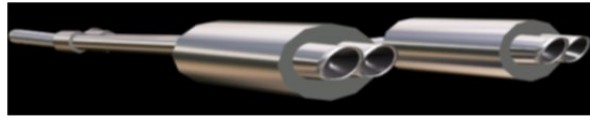


Figure 6: Exhaust system with double tailpipe configuration.

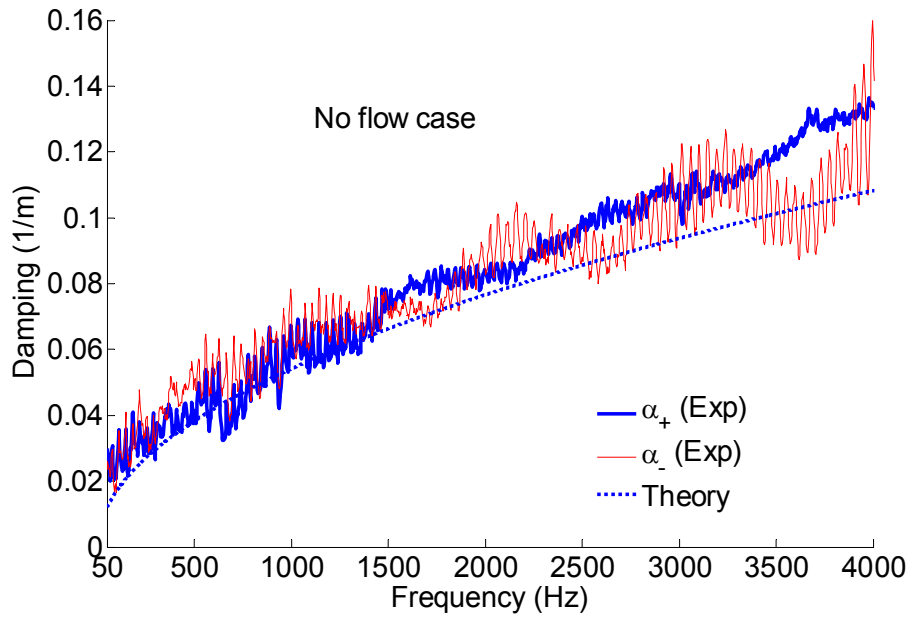
### 2.2.1 Summary of the results

#### *Straight pipe*

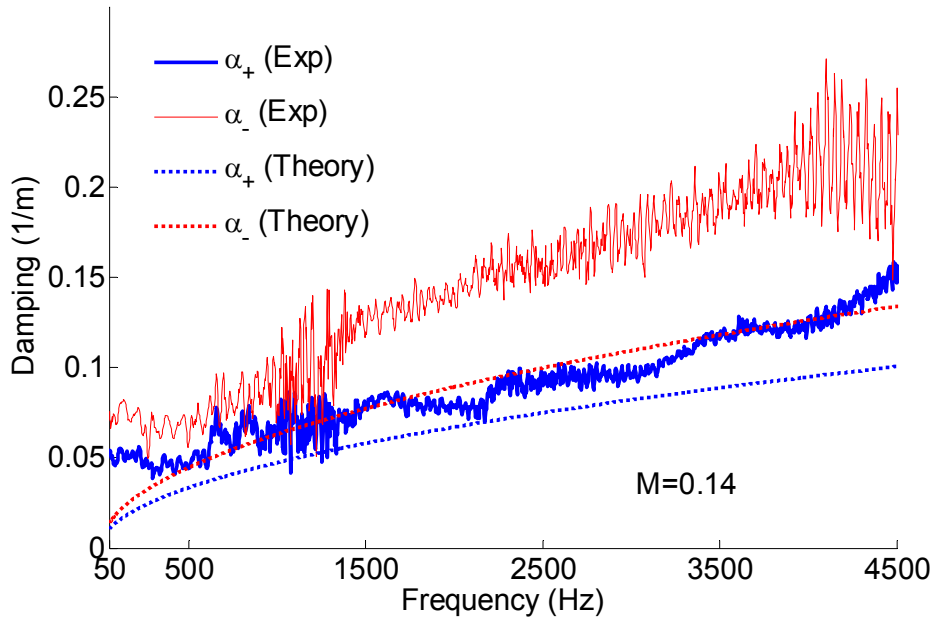
##### *Experimental results for internal damping in the boundary layer*

The influence of flow on acoustic damping can be seen in Figure 7. The theoretical damping presented in Figure 7 corresponds to the absolute value of the imaginary part of the wavenumbers  $k_{+/-}$  obtained from the cluster technique. The experimental results for the no flow case in Figure 7(a) agree well with the classical Kirchhoff (1868) formulation. However, with flow (Figure 7(b)), the often quoted formulation by Davies (1988) does not work and can significantly under predict the damping.





(a)

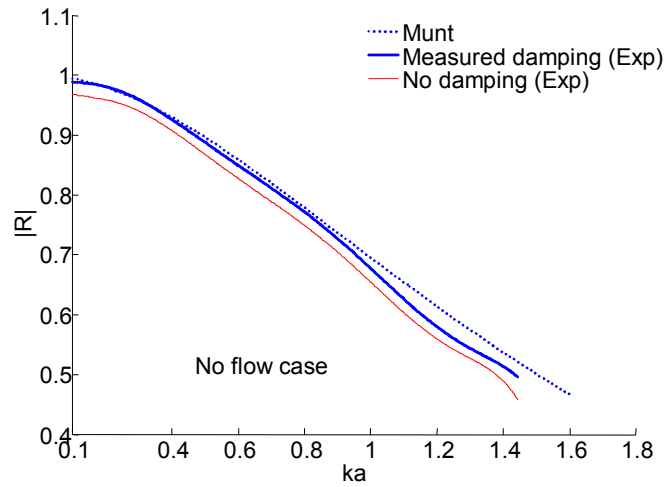


(b)

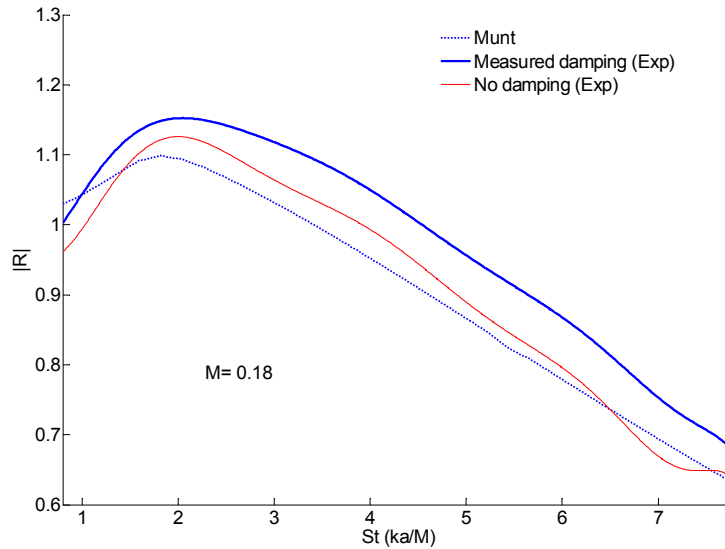
Figure 7: Acoustical attenuation rate in a straight pipe with and without flow.

### ***Reflection coefficient at the opening***

Experimental data presented in Figure 8 are obtained using the cluster technique without iteration (two-microphone technique, Bodén & Åbom (1986)) and a pure real wavenumber  $k=\omega/c$  (no damping) and with iteration. The latter corresponding to the case for which the measured damping is included in the experimental determination of the reflection coefficient  $R$  using the complete wavenumber  $k=\omega/c-i\alpha$ , where  $\alpha$  is the attenuation rate.



(a)



(b)

Figure 8: Measured reflection coefficient and comparison with Munt's model (1990).

Attenuation along the pipe does not greatly modify the reflection coefficient  $|R|$  when no flow is present in the pipe (Figure 8(a)). As can be seen from Figure 8(b) the Munt model agrees quite well with the measured data except for Strouhal numbers  $< 1$ .

### ***End correction results***

Munt's model allows for the determination of the complex value of the reflection coefficient  $R$  at the opening. In this section, the phase of  $R$  is converted into an end-correction term. Both experimental and theoretical results are presented and shown in Figure 9(a), (b).

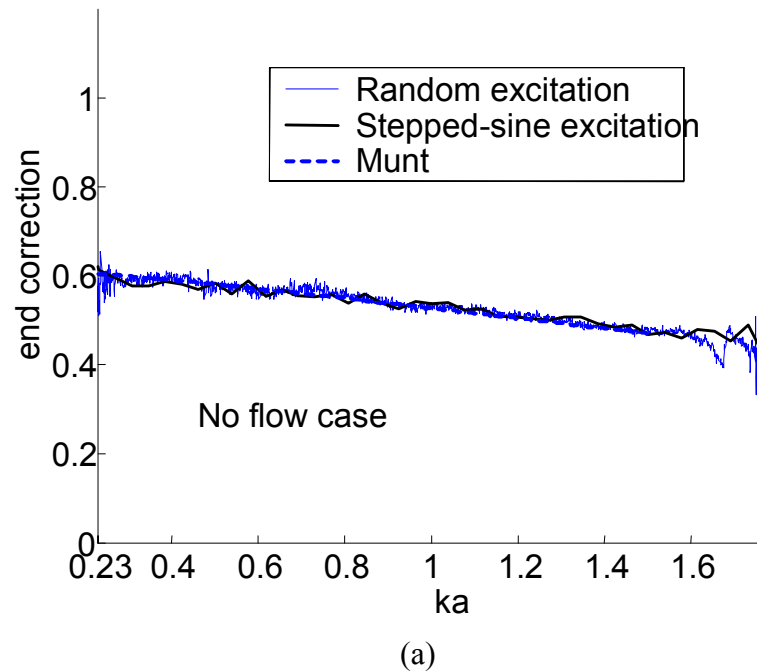


Figure 9 (a): End correction for an open end.

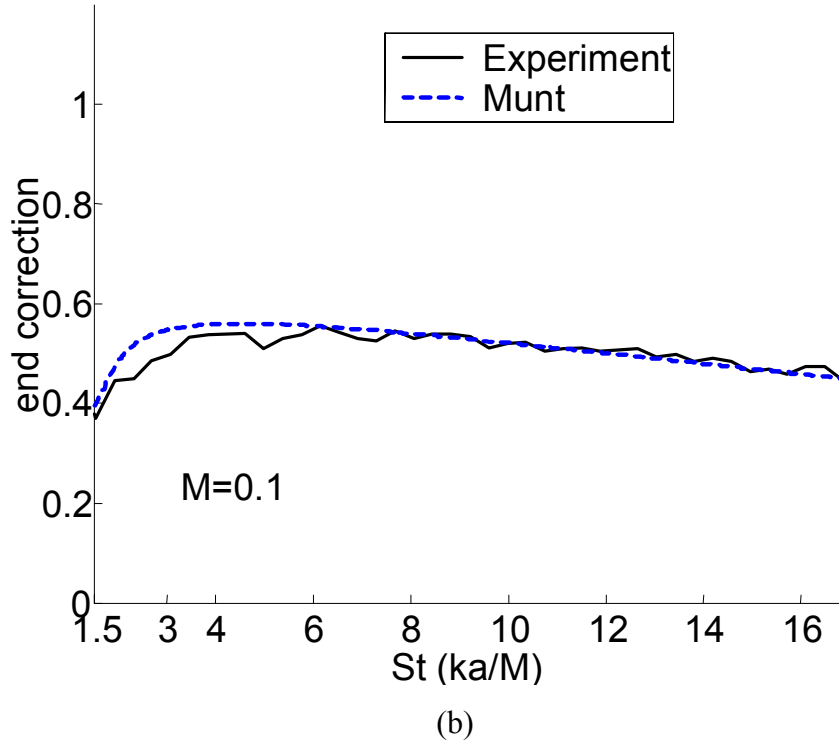


Figure 9 (b): End correction for an open end.

For the no flow case, prediction of the end correction agrees well with the experimental value. The low frequency limit obtained experimentally is very close to the value of 0.6133 derived by Levine & Schwinger (1948). An interesting and already noticed feature is observed in the high Strouhal number region. In this portion of the plot ( $St=ka/M \gg 1$ ), one can see from comparison with the no flow case that the flow does not change the value of the end correction. The theory tends to overestimate the end correction at low Strouhal numbers ( $St < 5$ ). It can also be seen that the measurements clearly support the drop in the end correction for small  $St$ -numbers predicted by Munt's model. For small  $St$ -numbers the flow field plays an active part and coupling between the acoustic field and the flow field is of importance. This coupling is imposed by Munt theoretically through the full Kutta condition. This condition governs the transfer of energy between the acoustic field and the flow field.

#### ***Sound absorption by vorticity shedding***

The presence of mean flow in the pipe influences the rate of sound radiated to the far field. The results presented in Figure 5 show that acoustic losses due to vorticity is

dominantly a low frequency process. The upper frequency limitation of the theory developed by Bechert (1980) is indicated by a vertical dashed line in Figure 10.

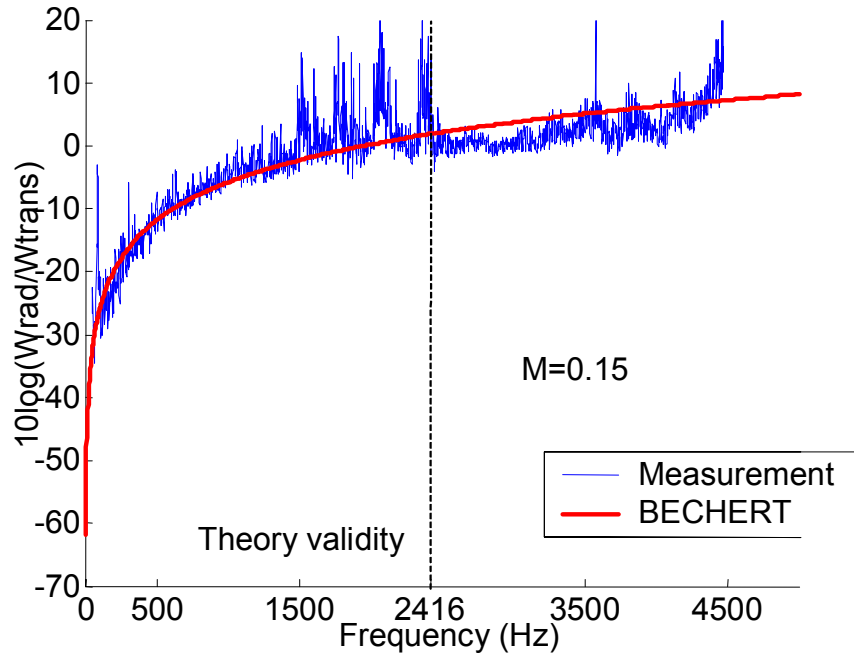
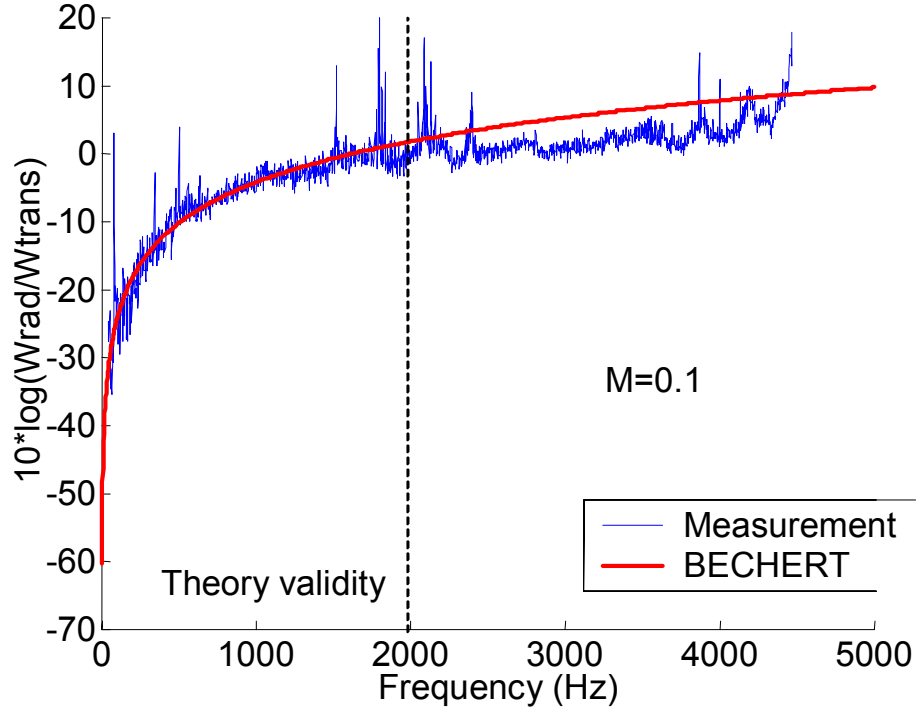


Figure 10: Theoretical (Bechert (1980)) and measured sound absorption by vorticity.

## Tailpipes

### Reflection coefficient

The experimental and theoretical results presented in this section have been obtained at the inlet of the elements.

### Oblique cuts

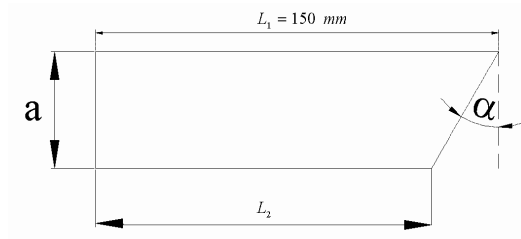


Figure 11 presents the oblique cut dependence for the magnitude  $|R|$  of the reflection coefficient for the case of no flow. Theoretical models for one oblique cut case ( $\alpha=45^\circ$ ,  $M=0$ ) are validated against measurement in Figure 12.

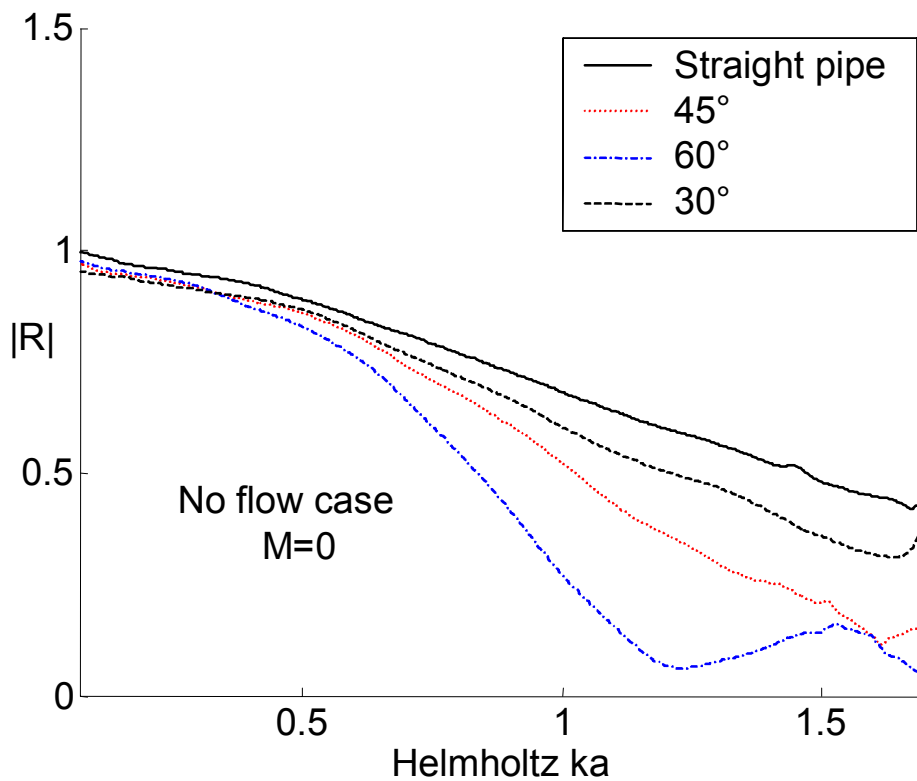


Figure 11: Reflection coefficient for oblique cuts in terms of Helmholtz number for no flow case.

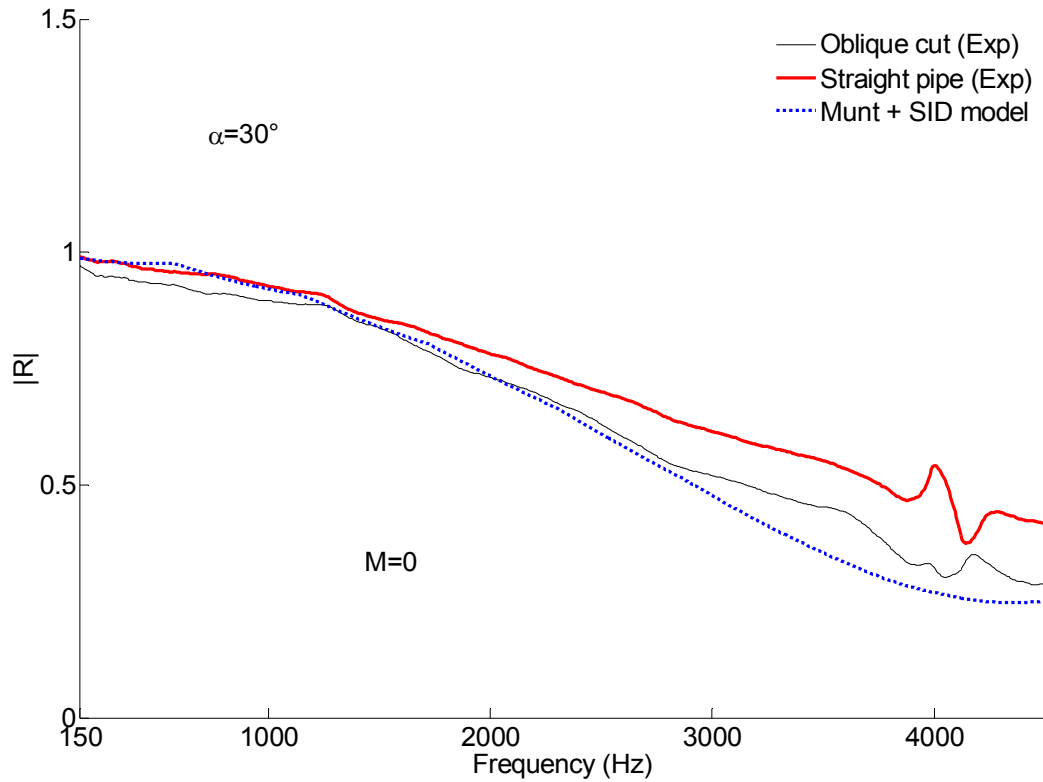


Figure 12: Models for reflection coefficient for an oblique cut (45°) and no flow.

Inspection of Figure 11 reveals the major feature of these geometries. The reflection coefficient magnitude drops and the transmission increases. This can have a positive effect since one problem with normal tailpipes is resonances, which amplify the radiated sound at certain frequencies. For a fixed frequency the transmission increases with the angle and for a fixed angle the effect increases with the frequency. Figure 12 shows that increasing the cross-section area, i.e, using an equivalent radius at the opening is not sufficient to predict the reflection coefficient. In other words, the obliquity has also an effect on the acoustical propagation. To take this geometrical effect into account, a model based on parallel coupled pipes with different lengths was developed.

## Diffusers

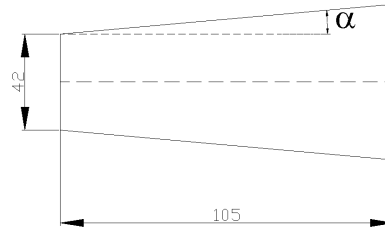


Figure 13 and Figure 14 illustrate the diffuser case for two angles  $5^\circ$  and  $7.5^\circ$  for the no flow case and a case with flow.

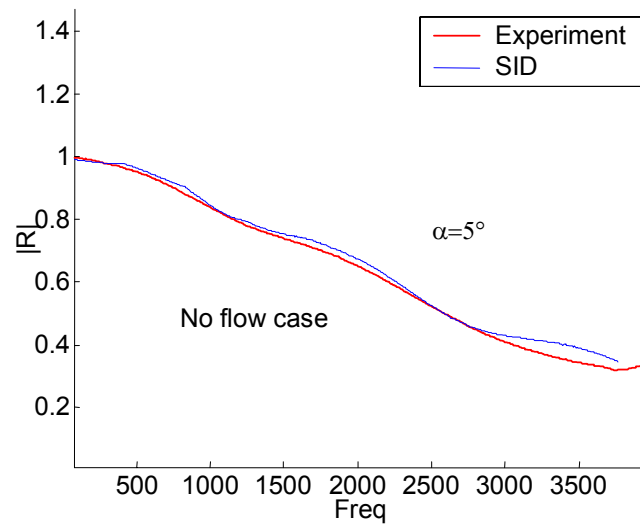


Figure 13: Experimental and theoretical reflection coefficient for diffuser ( $5^\circ$ ) for the no flow case.

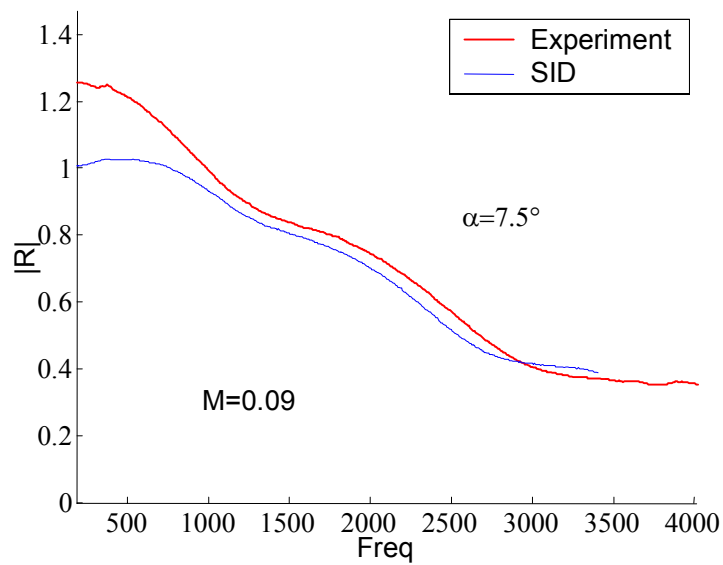
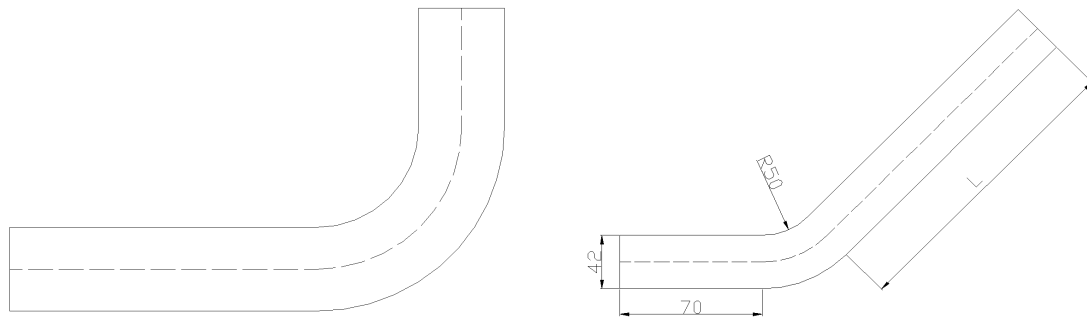


Figure 14: Experimental and theoretical reflection coefficient for diffuser ( $7.5^\circ$ ) and  $M = 0.09$ .



The simple model used to predict the reflection coefficient for the no flow case agrees well with the experimental data. The model is based on the conical element in the SID code<sup>2</sup> terminated by an impedance obtained from Munt's theory (1977, 1990). Modelling of the standing wave pattern (undulation) is achieved theoretically. The discrepancy between the calculated and measured values for lower frequency when flow is present in the rig (Figure 14) is suspected to be due to the flow separation that occurs for this angle. Dequand and al. (2002) showed for diffusers of this type the flow separation point is not fixed and moved along the inner walls of the elements. Munt's model used at the outlet cross-section is based on a sharp-edged condition with a thin shear boundary layer. Due to the flow separation the boundary layer at the opening is substantially thicker violating the simple flow separation model used by Munt.

### ***Bends***



The reflection coefficient results for tailpipes with an upstream bend confirms the findings of Dequand and al. (2002). The bends can be replaced theoretically by a straight pipe.

### ***Flow noise***

#### ***Oblique cuts***

Figure 15 draws an experimental comparison for the flow induced sound power level for the oblique cut. Only the last case corresponding to the most pronounced angle (60°) is shown since it is obviously the “loudest”. It is compared to the measurement with no element (straight pipe reference case). No significant difference in terms of the sound

---

<sup>2</sup> Sound In Ducts (SID), a 2-port code developed at MWL/KTH (Nygård (2000)).

flow production can be observed for the oblique cuts. It behaves like a straight-pipe; no additional noise is generated due to the obliquity.

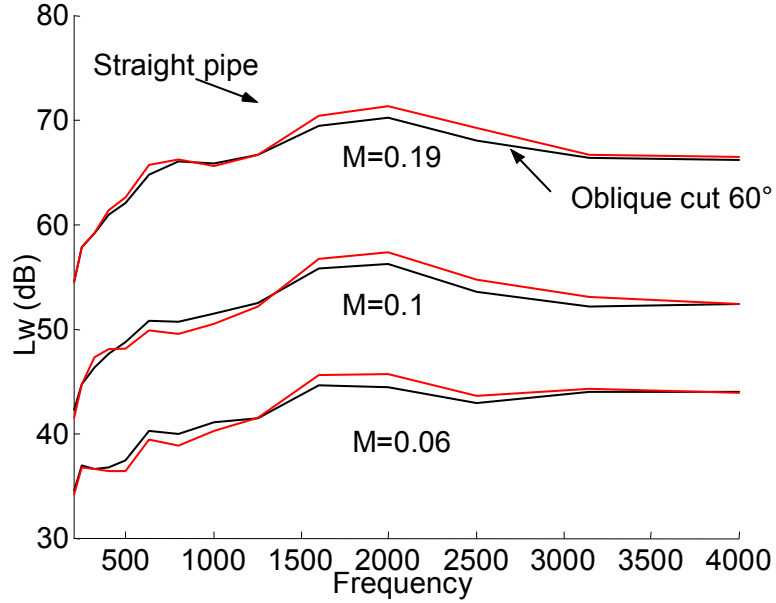


Figure 15: Measured sound flow power level for oblique cut (60°) and straight pipe.

### ***Diffusers and bends***

Dimensionless sound power spectra for diffusers and bends are presented in Figure 16. The dimensionless spectra  $L_s = 10 \log_{10}(F(St))$ , where  $St$  is the Strouhal number based on the pipe diameter for the bends and outlet diameter for the diffusers is based on the equation

$$W = \rho_0 U^3 D^2 M^\alpha C_L^2 F(St) \quad (2-1)$$

where  $W$  is the flow induced noise sound power,  $U$  is the flow speed,  $D$  is the pipe diameter. The exponent  $\alpha$  depends on the source type and the dimensionality of the sound field.

The velocity dependence for the bends is  $U^4$  and  $U^6$  for the diffusers (1/3-octave band). As expected bend 1 corresponding to the greatest curvature ( $R/D=1.6$ ) generates higher sound power level.

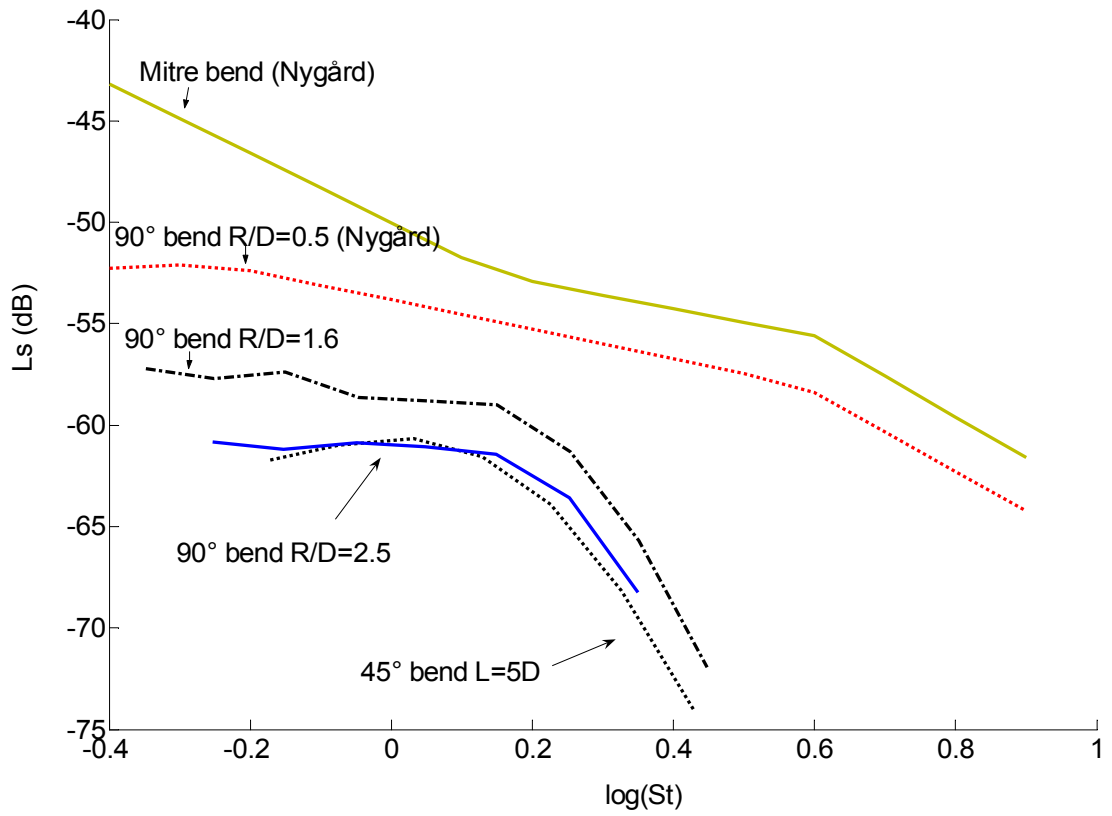
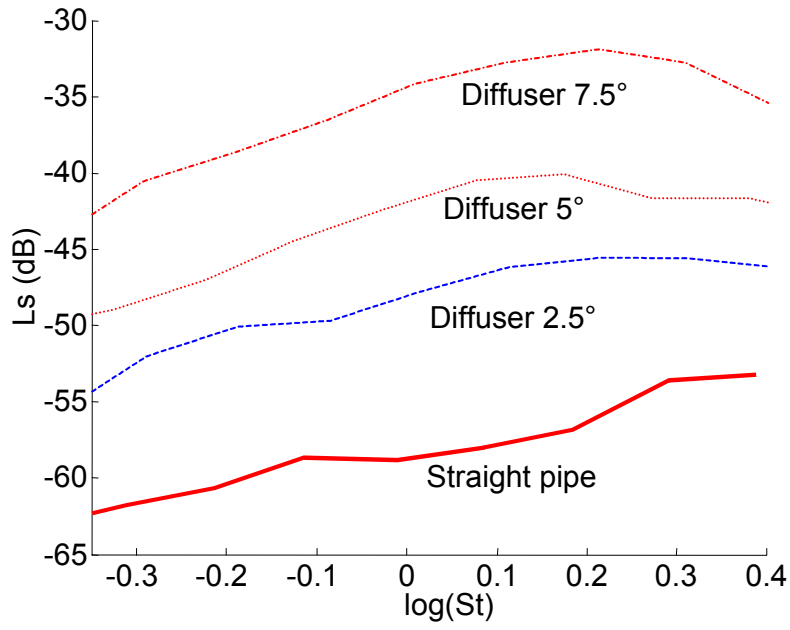


Figure 16: Complete sets of dimensionless spectra based on equation (2-1) obtained from our investigation and Nygård (2000).

A summary of the main findings for tailpipes are listed in Table 1.

<i>Elements</i>	<b>Reflection coefficient/Impedance</b>	<b>Flow noise</b>
Oblique cuts	Deviates from straight pipe at frequencies $> 1500$ Hz. No effect for low frequencies.	Equivalent to a straight pipe
Diffusers	Kutta condition not valid for $>5^\circ$ Deviations from the straight pipe at low frequencies and with flow	$1^\circ$ : equivalent to a straight pipe $2.5^\circ, 5^\circ, 7.5^\circ$ : Flow noise sound power level at opening $\propto U^6$
Bends	Equivalent to a straight pipe	$45^\circ$ bend( $L=0$ ): Equivalent to a straight pipe $45^\circ$ bend( $L=5D$ ), $90^\circ$ bends ( $R/D=1.6, 2.5$ ): Flow noise sound power level at the bend $\propto U^4$

Table 1: Comparison between the tailpipes and the straight pipe.

### **Modelling of exhaust lines**

The measured load impedances for flow diffusers have been implemented in the calculation of the insertion loss ( $IL$ ) of exhaust lines. Figure 17 demonstrates the potentiality of flow diffusers to increase the losses at the tailpipe resonances.

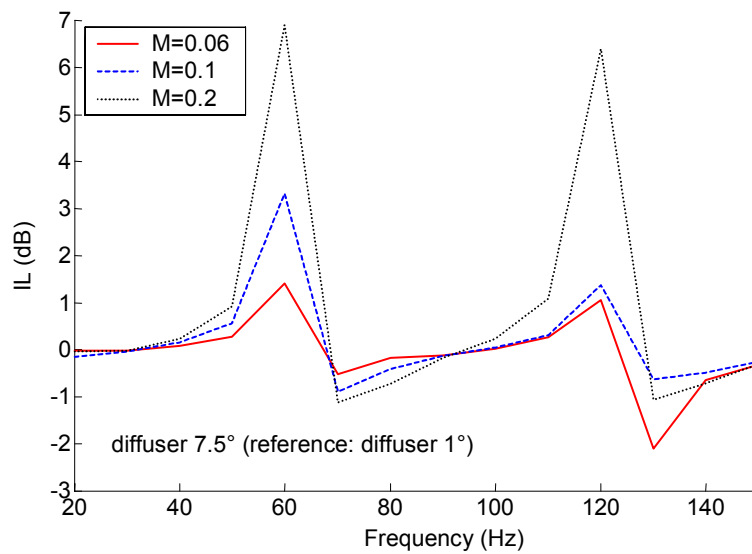


Figure 17: Increase in  $IL$  for the diffuser  $7.5^\circ$  at various flow Mach numbers  $M$ .

### **2.3 Paper III. Linear and non linear acoustic regimes of perforated plates**

Sound absorbers are traditionally made of porous materials of fibrous types. The drawbacks of these types of materials are numerous: they are brittle therefore hazardous, bulky and inefficient at low frequencies. A new trend in the automotive industry is to use thin micro-perforated panels to enhance the noise reduction. These panels are required to be made with perforations of sub-millimetre size in order to obtain high acoustic attenuation without the drawbacks of the traditional porous materials. An analytical treatment has been suggested by Maa (1998) to model the ratio of the acoustic pressure drop through a panel made of micro-circular holes to the acoustic particle velocity over the panel. This ratio is called the acoustic (flow) impedance and is used to characterise the material. Based on Maa's formulation, a similar analytical expression for panels made of rectangular apertures is derived in paper III.

Measurement of the impedance of single rectangular and circular apertures at low and high excitation amplitudes has been performed by Sivian (1935). An analytical model consisting of the various internal and external linear acoustics terms of an aperture is also detailed. However, only non linear resistive results are presented. Sivian (1935) neglects the role of the reactance on the overall acoustics of the opening.

Ingard (1967, 1974) has investigated the acoustics of apertures. Numerous effects such as interaction effects between neighbouring apertures, non linear effects, the effects of the geometry of the plane (baffled, unbaffled, circular, rectangular) in which the aperture is located are treated by Ingard.

Randeberg (2000, 2002) has derived a model for a slitted plate with multiple layers. The analytical model is coupled to a finite element scheme to predict the absorption coefficient of the complete assembly. The modelling is checked with a slitted sample mounted in an impedance tube. In paper III various experiments are carried out on perforated samples with single or multiple apertures of square, circular and rectangular geometries mounted in a rig to measure the linear and non-linear impedance. Empirical observations and experimental comparisons between the different plates investigated are made. A technique is suggested to measure the perforation area ratio (porosity)  $\sigma$  of these samples.

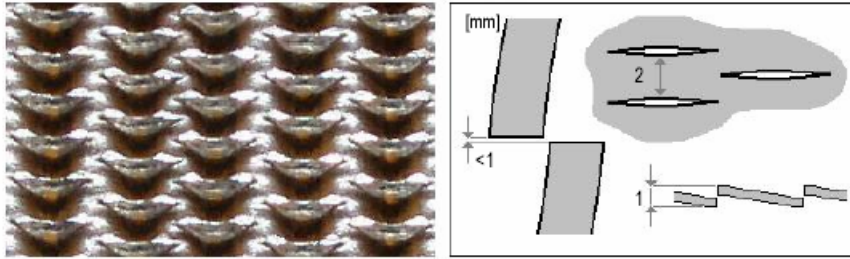
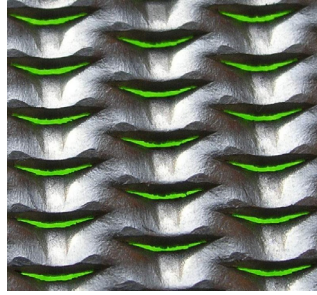


Figure 18 : An example of a commercial micro-perforated plate (Acustimet) with slit -shaped apertures.

### 2.3.1 Summary of the results

Figure 19 shows the flow impedance of single apertures of square and rectangular geometries. It can be seen that the more elongated the aperture, the lower is the reactance due to that the end correction term is reduced.

Figure 20 demonstrates the differences between square, rectangular and circular geometries with the same cross-sectional area. It can be seen that the square and circular apertures have the same acoustics behaviour. An elongation of the aperture towards a rectangular geometry results in the reduction of the end correction as observed for Figure 19.

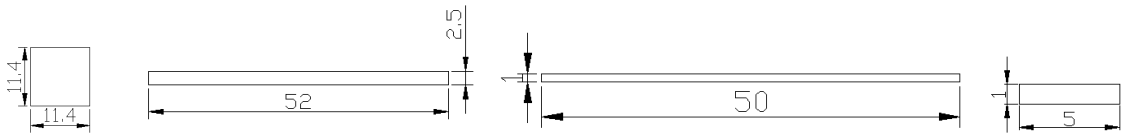
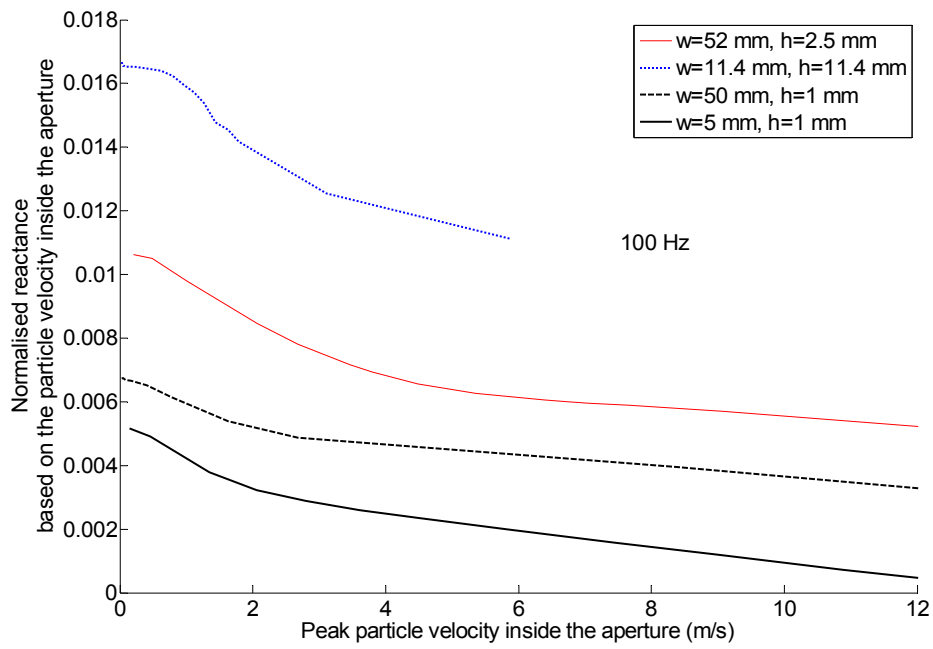
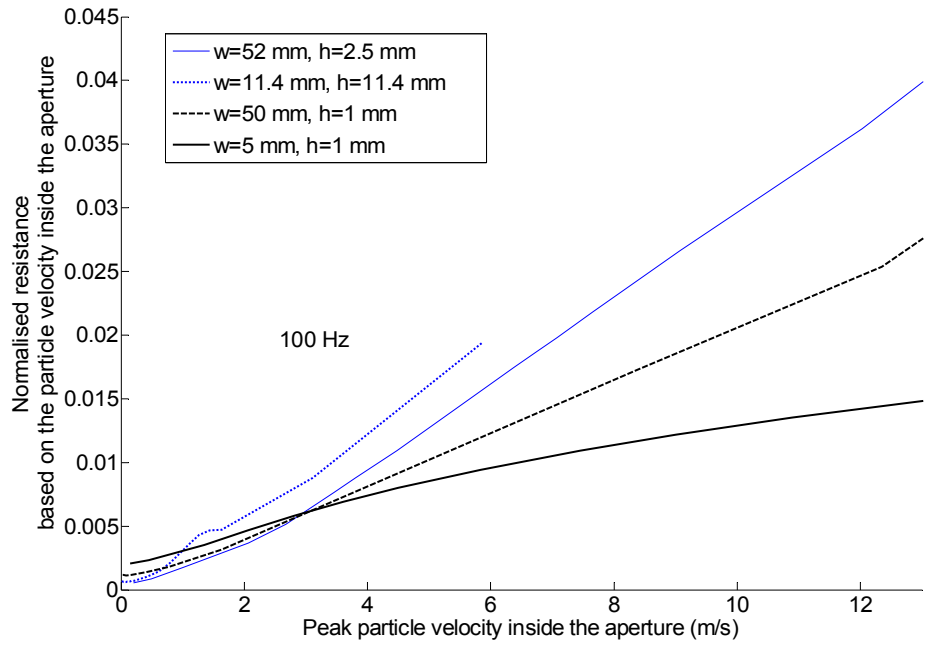


Figure 19: Normalised flow impedance  $\zeta_s$  based on the interior particle velocity  $V$  for plates with single square and rectangular apertures.

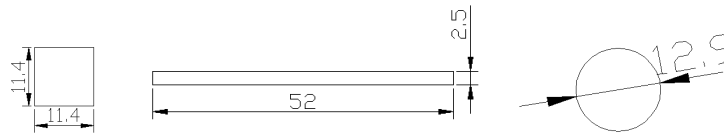
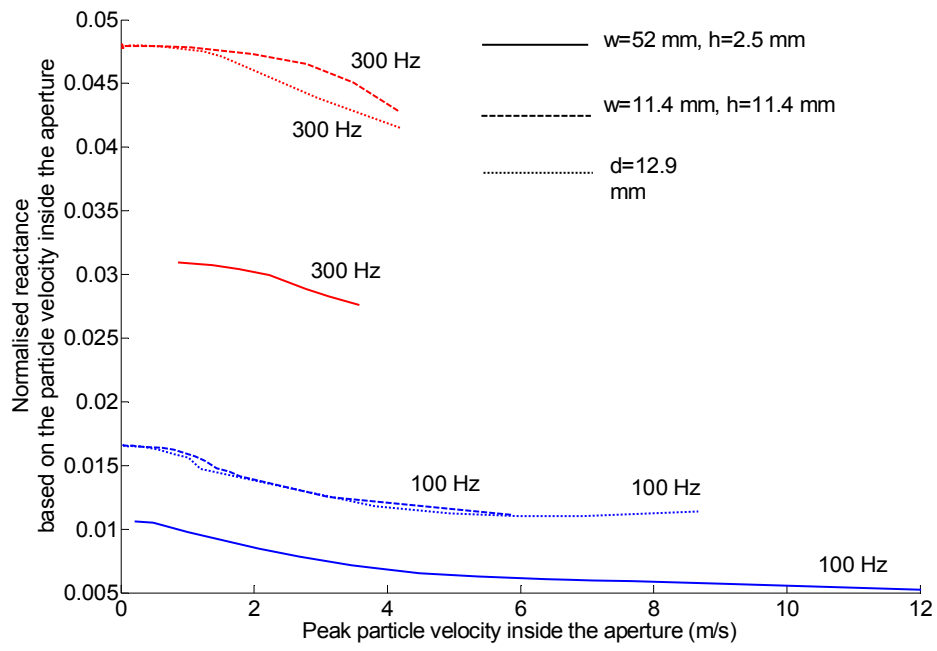
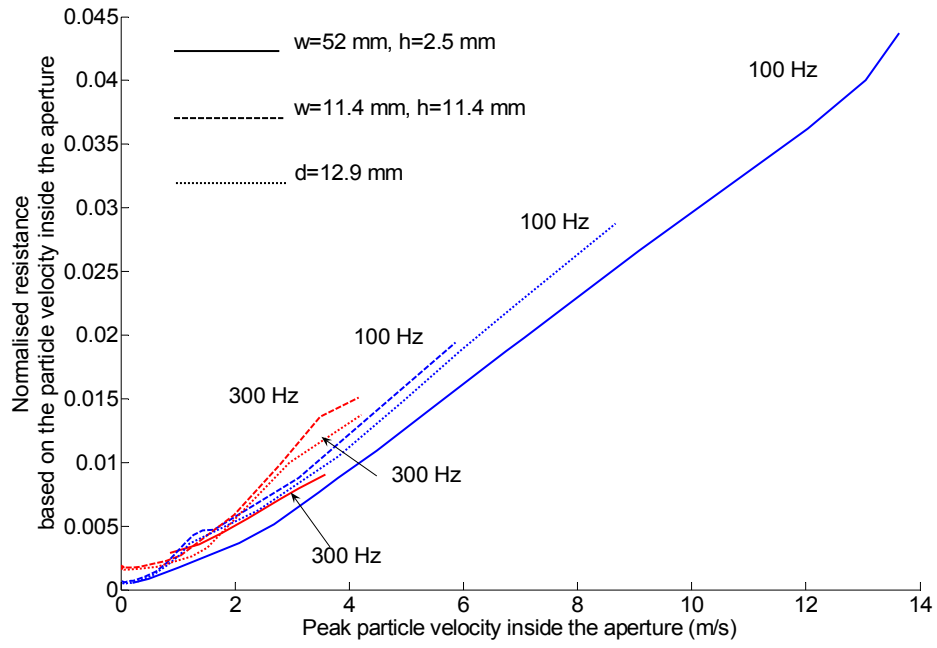


Figure 20: Normalised impedance  $\zeta'_s$  based on the interior particle velocity  $V$  for plates with single square, rectangular and hole orifices ( $\sigma=0.0265$ ).



Figure 21 shows the impedance for samples composed of multiple apertures with the same geometry (width  $w$ : 5 mm, height  $h$ : 1 mm). Interaction effects are observed as the number of slits increases. A comparison between the linear slit model (straight line) and linear and non-linear measurement carried out on a slitted plate is given in Figure 22 and shows good agreement.

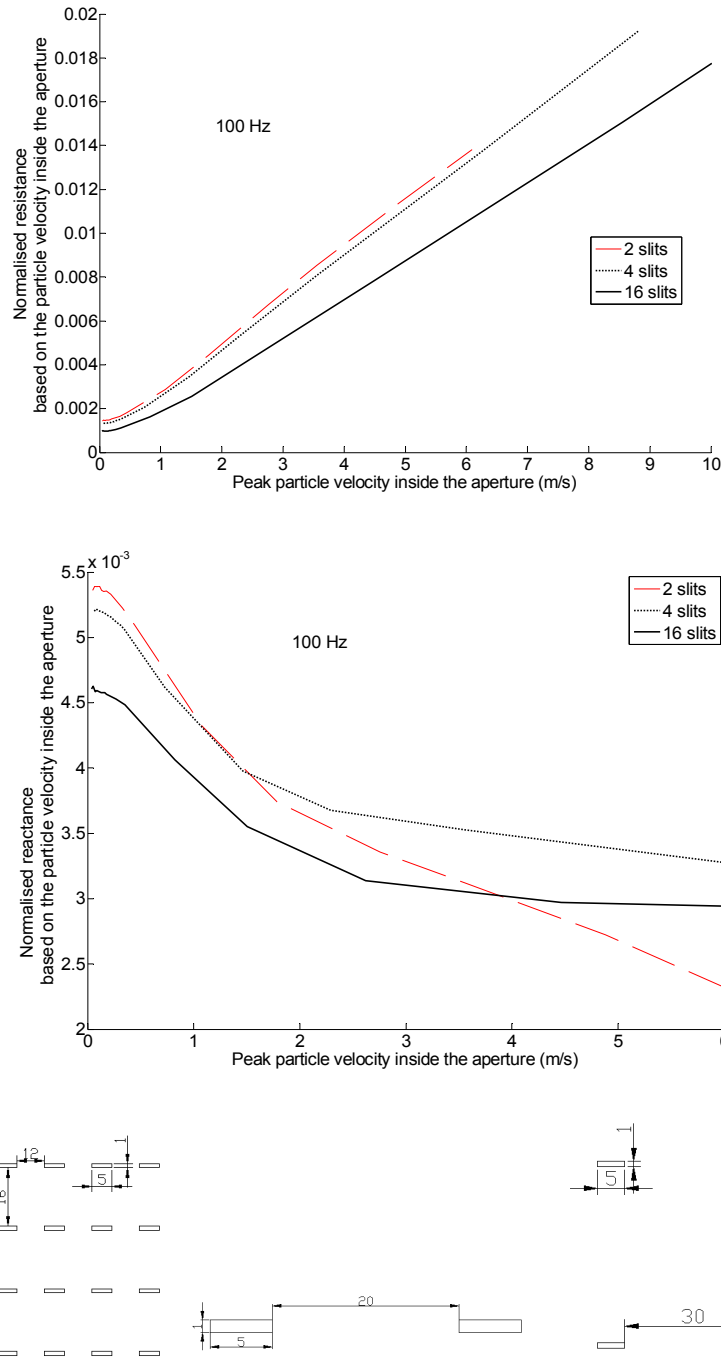


Figure 21: Single aperture normalised flow impedance  $\zeta'_s$  for plates with multiple rectangular apertures ( $w=5$  mm,  $h=1$  mm).

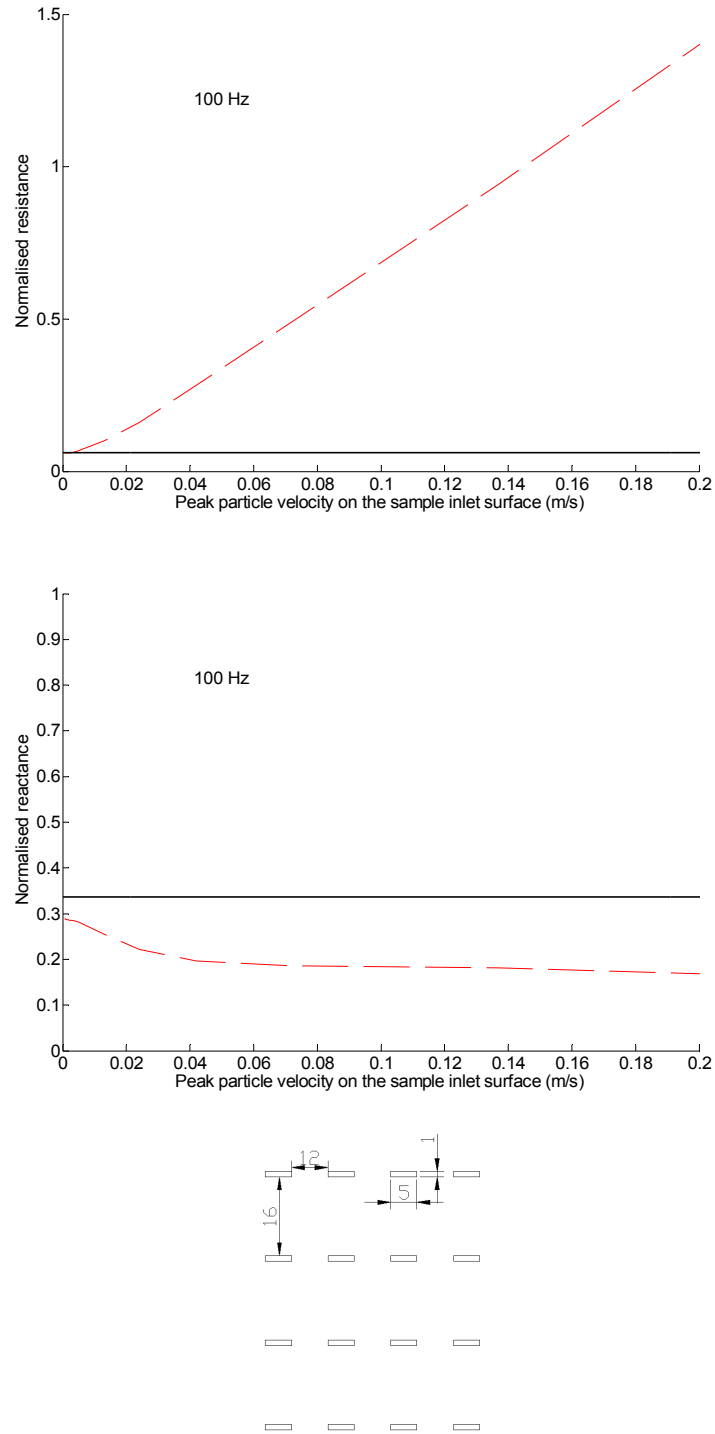


Figure 22: Normalised flow impedance  $\zeta_s$  for a plate with sixteen rectangular apertures ( $w=5$  mm,  $h=1$  mm,  $\sigma=0.016$ ).

### **3 Main contributions**

Paper I: A new two-port model for rectangular flexible ducts has been developed.

Paper II: First systematic investigation of tailpipe aeroacoustics.

Paper III: A new analytical model for the acoustic impedance of slitted plates has been derived.

The papers also contain a number of results and conclusion of practical interest.

Paper I has demonstrated that except at the first wall bending wave resonance the effect of flexible walls can be neglected in practice. It has been shown that the lining position is not of importance in the low frequency (plane wave) range..

Paper II has shown that an outlet diffuser can significantly modify the low frequency reflection coefficient and reduce the effect of low frequency tailpipe resonances. An oblique cut tailpipe opening can reduce the reflection coefficient at high frequencies and reduce the effect of high frequency tailpipe resonances. Other results of the study are summarised in Table 1.

Paper III has presented an experimental technique to obtain the porosity of perforated plates.

## 4 Future research

### ***Paper I. Low frequency sound propagation in rectangular ducts***

To improve the presented two-port model, in particular around the cut-on frequencies for the structural bending waves, a complete 1-D wave model could be derived. Such a model should include not only the acoustic wave types but also the structural bending waves and could be build on the works presented by Martin (1991) and Martin and al. (2004). Another topic of interest is to investigate the effect of flow and the existence of instability waves. Such waves could exist close to the cut-on frequency of the bending waves where the wall impedance is close to “zero”.

### ***Paper II. Aeroacoustic behaviour of tailpipes***

The model of Munt (1977, 1990) has been coded to predict the acoustics at the opening. However, in its full application, sound absorption in the near field and the sound radiation can also be calculated. This could be used for a more complete validation of the dissipation by vorticity at the opening and to investigate the far-field directivity. It has been shown that flow diffusers can reduce the sound radiation at low frequencies by reducing the effect of tailpipe resonances. However, a diffuser will also increase the flow noise at low and mid frequencies. A more detailed experimental study of these two effects would reveal the true potential of this type of acoustic elements. Non-linear effects could be also investigated since high noise amplitude propagates in exhaust systems.

### ***Paper III. Linear and non linear acoustic regimes of perforated plates***

Here the work should focus on developing models for non-linear impedance effects for rectangular (slit) apertures. Also the effect of grazing flow on the impedance of micro-perforated plates is important for vehicles applications. A large amount of works exist for perforated pipes and aircraft liners (Elnady (2004)). These works present semi-empirical models, but the data are based on plates with larger holes and higher perforation ratios than what is typical for micro-perforated plates.

## 5 References

1. Åbom M., 1989, *Studies of sound propagation in ducts and mufflers*, Doctoral Thesis, Department of Aeronautical and Vehicle Engineering, Royal Institute of Technology, Stockholm, Sweden.
2. Åbom M., 1999, *Determination of porous material data via two-port measurements*, Inter-Noise 99, Florida, USA, 589-594.
3. Åbom M., Bodén H., 1988, *Error analysis of two-microphone measurements in ducts with flow*, Journal of the Acoustical Society of America, **83**, 2429-2438.
4. Allam S., 2004, *Acoustic modelling and testing of advanced exhaust system components for automotive engines*, Doctoral Thesis, Department of Aeronautical and Vehicle Engineering, Royal Institute of Technology, Stockholm, Sweden.
5. Allard J.F., 1993, *Propagation of sound in porous media, modelling sound absorbing materials*, Elsevier, London.
6. Almgren M., 1982, *Prediction of sound pressure level outside a closed ventilation duct – a literature survey*, Report F82-03, Chalmers University of Technology, Department of Building Acoustics.
7. Astley, R. J., 1990, *Acoustical modes in lined ducts with flexible walls. A variational approach*, Proceedings of Inter-Noise **90**, 575-578.
8. Astley R. J., 1991, *A finite element scheme for acoustic propagation in flexible-walled ducts with bulk-reacting liners, and comparison with experiment*, Journal of Sound and Vibration, **150**(1), 119-138.
9. Astley R.J., Cummings A., Sormaz N., 1991, *A finite element scheme for acoustical propagation in flexible walled ducts with bulk reacting liners, and comparison with experiment*, Journal of Sound and Vibration, **150**, 119-138.

10. Astley R. J., Cummings A., 1984, *A finite element scheme for acoustic transmission through the walls of rectangular ducts: comparison with experiment*, Journal of Sound and Vibration, **92**(3), 387-409.
11. Astley R.J., Cummings A., 1987, *A finite element scheme for attenuation in ducts lined with porous material: comparison with experiment*, Journal of Sound and Vibration, **116**(2), 239-263.
12. Baxa D. E., 1989, *Noise control in combustion engines*, Krieger Pub Co.
13. Bechert D. W., 1980, *Sound absorption caused by vorticity shedding, demonstrated with a jet flow*, Journal of Sound and Vibration, **70**, 389-405.
14. Bierkens J., 2002, *Calculation of the reflection coefficient of a jet pipe with subsonic jet flow*, Master Thesis, Department of Aeronautical and Vehicle Engineering, Royal Institute of Technology, Stockholm, Sweden.
15. Blevins R. D., 1984, *Applied fluid dynamics handbook*, New York: Van Nostrand Reinhold.
16. Bodén H., 1989, *Characterization of fluid machines as sources of fluid borne noise*, Doctoral Thesis, Department of Aeronautical and Vehicle Engineering, Royal Institute of Technology, Stockholm, Sweden.
17. Bodén H., Åbom M., 1986, *Influence of errors on the two-microphone method for measuring acoustic properties in ducts*, Journal of the Acoustical Society of America, **79**(2), 541-549.
18. Bodén H., Carlsson U., Glav R., Wallin H. P., Åbom M., 2001, *Ljud och vibration*, Norstedts Tryckeri AB, Stockholm.
19. Boij S., 2003, *Acoustic scattering in ducts and influence of flow coupling*, Doctoral Thesis, Department of Aeronautical and Vehicle Engineering, Royal Institute of Technology, Stockholm, Sweden.

20. Brown G. L., Rennison D. C., 1974, *Sound radiation from pipes excited by plane acoustic waves*, Noise, Shock & Vibration Conference, Monash University, Melbourne.
21. Callow G.D., Peat K.S., 1988, *Insertion loss of engine intake and exhaust silencers*, IMechE C19/88, 39-46.
22. Cargill A. M., 1982, *Low frequency acoustic radiation from a jet pipe- a second order theory*, Journal of Sound and Vibration, **83**, 339-354.
23. Cabelli A., 1985, *The propagation of sound in a square duct with a non-rigid side wall*, Journal of Sound and Vibration, **103**(3), 379-394.
24. Cabelli A., 1985, *Application of the time dependent finite difference theory to the study of sound and vibration interactions in ducts*, Journal of Sound and Vibration, **103**, 13-23.
25. Chung J.Y., Blaser D.A., 1980, *Transfer function method of measuring in-duct acoustic properties I. Theory*, Journal of the Acoustical Society of America, **68**, 907-913.
26. Crandall I. B., 1927, *Theory of vibrating systems and sound*, Appendix A: Resistance coefficients for cylindrical conduits, Macmillan and co, limited.
27. Cremer L., Müller H. A., 1976/1982, *Principles and applications of room acoustics*, vol. II, Applied Science Publisher, London.
28. Cummings, A., 1976, *Sound attenuation in ducts lined on two opposite walls with porous material, with some applications to splitters*, Journal of Sound and Vibration, **49**(1), 9-35.
29. Cummings, A., 1978, *Low frequency acoustic transmission through the walls of rectangular ducts*, Journal of Sound and Vibration, **61**(3), 327-345.
30. Cummings, A., 1979, *Low frequency sound transmission through the walls of rectangular ducts: further comments*, Journal of Sound and Vibration, **63**(3), 463-465.
31. Cummings, A., 1979, *The effects of external lagging on low frequency sound transmission through the walls of rectangular ducts*, Journal of Sound and Vibration, **67**(2), 187-201.

32. Cummings, A., 1980, *Low frequency acoustic radiation from duct walls*, Journal of Sound and Vibration, **71**(2), 201-226.
33. Cummings, A., 1981, *Design charts for low frequency acoustic transmission through the walls of rectangular ducts*, Journal of Sound and Vibration, **78**, 269-289.
34. Cummings, A., 1981, *Stiffness control of low frequency acoustic transmission through the walls of rectangular ducts*. Journal of Sound and Vibration, **74**, 351-380.
35. Cummings, A. 1983, *Approximate asymptotic solutions for acoustic transmission through the walls of rectangular ducts*, Journal of Sound and Vibration, **90**(2), 211-227.
36. Cummings, A., 1983, *Higher order mode acoustic transmission through the walls of rectangular ducts*, Journal of Sound and Vibration, **90**(2), 193-209.
37. Cummings, A. 1994, *The attenuation of sound in unlined ducts with flexible walls*, Journal of Sound and Vibration, **174**(4),
38. Cummings, A., 2001, *Sound transmission through duct walls*, Journal of Sound and Vibration, **239**(4), 731-765.
39. Cummings A., Astley R.J., 1995, *The effects of flanking transmission on sound attenuation in lined ducts*, Journal of Sound and Vibration, **179**, 617-646.
40. Davies P.O.A.L., 1988, *Practical flow duct acoustics*, Journal of Sound and Vibration, **124**(1), 91-115.
41. Davies P.O.A.L., Coelho J. L. B., Bhattacharya M., 1980, *Reflection coefficients for an unflanged pipe with flow*, Journal of Sound and Vibration, **72**, 543-546.
42. Dequand S., van Lier L., Hirschberg A., Huijnen J., 2002, *Aeroacoustics response of diffusers and bends: comparison of experiments with quasi-steady incompressible flow models*, Journal of Fluids and Structures, **16**, 957-969.
43. Dokumaci E., 1998, *On transmission of sound in circular and rectangular narrow pipes with superimposed mean flow*, Journal of Sound and Vibration, **210**, 375-389.



44. Ducret F., 2005, *Aeroacoustics behaviour of a straight pipe*, Twelfth International Congress on Sound and Vibration, Lisbon, Portugal.
45. Ducret F., Åbom M., 2004, *Aeroacoustics behaviour of different exhaust pipe geometries*, Eleventh International Congress on Sound and Vibration, St. Petersburg, Russia.
46. Ducret F., Åbom M., 2003, *Low frequency sound propagation in rectangular ducts*, Tenth International Congress on Sound and Vibration, Stockholm, Sweden.
47. Ducret F., Jacobsen F., Åbom M., 2005, *Development of micro-perforated acoustic elements for vehicle applications*, Twelfth International Congress on Sound and Vibration, Lisbon, Portugal.
48. Elnady T., 2002, *On the use of liners to reduce aircraft jet engine noise*, Licenciate Thesis, Royal Institute of Technology, Department of Aeronautical and Vehicle engineering, TRITA-FKT 2002:26.
49. Elnady T., 2004, *Modelling and characterization of perforates in lined ducts and mufflers*, Doctoral Thesis, KTH Aeronautical and Vehicle Engineering.
50. Fenech B., 2004, *Damping the acoustic modes in a closed cavity using a micro-perforated plate*, MSc Thesis, Acoustic Technology, Ørsted, DTU, Denmark.
51. Gijrath H., Nygård S., Åbom M., 2001, *Modelling of flow generated sound in ducts*, Eight International Congress on Sound and Vibration, Hong-Kong, China.
52. Glav R., 1994, *On acoustic modelling of silencers*, Doctoral thesis, Royal Institute of Technology, Department of Aeronautical and Vehicle engineering, TRITA-FKT Report 9435.
53. Goldstein M., 1976, *Aeroacoustics*, McGraw-Hill, New York.
54. Gomperts M.C., 1964, *The "sound insulation" of circular and slit-shaped apertures*, *Acustica*, **14**(1), 1-16.

55. Gomperts M.C., 1965, *The influence of viscosity on sound transmission through small circular apertures in walls of finite thickness*, *Acustica*, **15**(4).
56. Gomperts M.C, Kihlman T., 1967, *The sound transmission loss of circular and slit-shaped apertures in walls*, *Acustica*, **18**, 144-150.
57. Hirschberg A., Bruggeman J. C., Wijnands A. P. J., Morgenstern M., 1988, *The whistler nozzle and horn as aero-acoustic sound sources in pipe systems*, *Proc. Inst. Acoust.*, 10, 701-708.
58. Howe M. S., 1980, *The dissipation of sound at an edge*, *Journal of Sound and Vibration*, **70**, 407-411.
59. Howe M. S., 1995, *The damping of sound by turbulent shear layers*, *Journal of the Acoustical Society of America*, **98**, 1723-1730.
60. Huijnen J.H., 1998, *Aero-acoustics of a bend: quasi-stationary models*, Technische universiteit eindhoven, Report R1476A.
61. Ingard U., 1953, *On the Theory and Design of Acoustic Resonators*, *Journal of the Acoustical Society of America*, **25**(6), 1037-1061.
62. Ingard U., Ising H., 1967, *Acoustic nonlinearity of an orifice*, *Journal of the Acoustical society of America*, **42**(1), 6-17.
63. Ingard U., Singhal V. K., 1974, *Sound attenuation in turbulent pipe flow*, *Journal of the Acoustical Society of America*, **55**, 535-538.
64. Ingerslev F., Kjerbye Nielsen A., 1944, *On the transmission of sound through small apertures and narrow slits*, Publication Nr.1 from The Acoustical Laboratory of the Academy of Technical Sciences, Copenhagen.

65. in't panhuis P., 2003, *Calculations of the sound pressure reflection coefficient and the acoustic end correction of a semi-infinite pipe issuing a subsonic cold or hot jet with co-flow*, Master Thesis, Department of Aeronautical and Vehicle Engineering, Royal Institute of Technology, Stockholm, Sweden.
66. ISO 3741, 1994, *Acoustics: Determination of sound power levels of noise sources using sound pressure, precision methods for reverberation rooms*.
67. ISO 3747, 1998, *Acoustics: Determining the sound power level of noise sources from sound pressure measurement*.
68. Jacobsen F., 2005, *Propagation of sound waves in ducts*, Note 31260, Acoustic Technology, Ørsted-DTU, Denmark.
69. Kinsler L. E., Frey A. R., Coppens A. B., Sanders J. V., 1982, *Fundamentals of acoustics*, John Wiley & Sons, Inc
70. Kirby R., Cummings A., 1998, *Structural/acoustic interaction in air-conditioning ducts in the presence of mean flow*, Proceedings of ISMA23, Leuven, Belgium, 677-684.
71. Kirchhoff G., 1868, *Über den einfluss der wärmeleitung in einem gase auf die schallbewegung*, Pogg. Ann., **134(6)**, 177-193.
72. Kristiansen U.R., Vigran T.E., 1994, *On the design of resonant absorbers using a slotted plate*, Applied Acoustics, **43**, 39-48.
73. Kuhn G.F., Morfey C.L., 1976, *Noise due to fully developed turbulent flow exhausting from straight and bend pipes*, Journal of Sound and Vibration, **44**, 27-35.
74. Lamb H., 1910, *The dynamical theory of sound*, London.
75. Levine, H., Schwinger H., 1948, *On the radiation of sound from an unflanged circular pipe*, Physical Review, **73**, 383-406.

76. Maa D-Y., 1983, *Direct and accurate impedance measurement of microperforated panel*, Inter Noise, Edinburg, UK.
77. Maa D-Y., 1987, *Microperforated-panel wideband absorbers*, Noise Control Engineering Journal, **29**(3).
78. Maa D-Y., 1994, *Microperforated panel at high sound intensity*, Inter Noise, Yokohama Japan, August 29-31.
79. Maa D-Y., 1998, *Potential of microperforated panel absorber*, Journal of the Acoustical Society of America, **105**(5), 2861-2866.
80. Martin V., 1991, *Perturbation of fluid-guided waves introduced by bending plates*, Journal of Sound and Vibration, **144**, 331-353.
81. Martin V., Cummings A., Gronier C., 2004, *Discrimination of coupled structural/acoustic duct modes by active control: principles and experiments results*, Journal of Sound and Vibration, **274**, 583-603.
82. Mechel F.P., 1994, *Helmholtz resonators with slotted neck plates*, Acustica, **80**, 321-331.
83. Melling T.H., 1973, *The acoustic impedance of perforates at medium and high sound pressure levels*, Journal of Sound and Vibration, **29**(1), 1-65.
84. Morfey C.L., 1969, *Acoustic properties of openings at low frequencies*, Journal of Sound and Vibration, **9**(3), 357-366.
85. Morfey C.L., 1971, *Sound transmission and generation in ducts with flow*, Journal of Sound and Vibration, **14**(1), 37-55.
86. Morse, P.M., Ingard K.U., 1968, *Theoretical acoustics*, McGrawHill, St.Louis.
87. Munt R.M., 1977, *The interaction of sound with a subsonic jet issuing from a semi-infinite cylindrical pipe*, Journal of Fluid Mechanics, **83**, 609-61040.

88. Munt R. M., 1990, *Acoustic transmission properties of a jet pipe with subsonic jet flow: I. the cold jet reflection coefficient*, Journal of Sound and Vibration, **142**, 413-436.
89. Nelson P.A., Morfey C.L., 1981, *Aerodynamic sound production in low speed flow ducts*, Journal of Sound and Vibration, **79**, 263-289.
90. Nygård S., 2000, *Modelling of low frequency sound in duct networks*, Licenciate Thesis, Royal Institute of Technology, Department of Aeronautical and Vehicle engineering, TRITA-FKT 2000:57.
91. Oldham D. J., Ukpoho A. U., 1990, *A pressure-based technique for predicting regenerated noise levels in ventilation systems*, Journal of Sound and Vibration, **140**, 259-272.
92. Peters M.C.A.M., Hirschberg A., Reijnen A.J., Wijnands A.P.J., 1993, *Damping and reflection coefficient measurements for an open pipe at low Mach and Low Helmholtz numbers*, Journal of Fluid Mechanics **256**, 499-534.
93. Pierce A.D., 1989, *Acoustics: an introduction to its physical principles and applications*, Acoustical Society of America, Mc Graw Hill Inc., New York.
94. Regaud P. L., 2001, *Modelling of compact resonators*, Licenciate Thesis, Royal Institute of Technology, Department of Aeronautical and Vehicle engineering, TRITA-FKT 2001:31.
95. Lord Rayleigh, 1878, *The theory of sound*, Macmillan and Co.
96. Randeberg R.T., 2000, *A Helmholtz resonator with a lateral elongated orifice*, Acta Acustica/Acustica, **86**, 77-82.
97. Randeberg R. T., 2002, *Adjustable slitted panel absorber*, Acta Acustica/Acustica, **88**, 507-512.
98. Rienstra S.W., Hirschberg A., 2004, *An introduction to acoustics*, Report IWDE 01-03, Eindhoven University of Technology, can be downloaded at:  
<http://www.win.tue.nl/%7Esjoerdr/papers/boek.pdf>

99. Ronneberger D., 1975, *Genaue messung der schalldämpfung und der phasengeschwindigkeit in durchströmten rohren im hinblick auf die wechselwirkung zwischen schall und turbulenz*, Habilitationsschrift mathematische-naturwissenschaftliche fakultät der universität Göttingen.
100. Sauter A., Soroka W.W., 1970, *Sound transmission through rectangular slots of finite depth between reverberant rooms*, Journal of the Acoustical Society of America, **47**(1), 5-11.
101. Schlichting H., 1968, *Boundary layer theory*, McCraw Hill Inc., New York.
102. Schlinker R.H., 1979, *The transmission of acoustic plane waves as a jet exhaust*, Journal of Aircraft, **16**(3).
103. Sivian L.J., 1935, *Acoustic impedance of small orifices*, Journal of the Acoustical Society of America, **7**, 94-101.
104. Smits J.M.A, Kosten C.W., 1951, *Sound absorption by slit resonators*, Acustica, **1**, 114-122.
105. Tijdeman H., 1975, *On the propagation of sound in cylindrical tubes*, Journal of Sound and Vibration, **39**, 1-33.
106. van Lier L., Dequand S., Hirschberg A., Gorter J., 2001, *Aeroacoustics of diffusers: An experimental study of typical industrial diffusers at Reynolds numbers of  $O(10^5)$* , Journal of the Acoustical Society of America, **109**, 108-115.
107. van Lier L.J., 1999, *An experimental study of the dynamic response of diffusers with application to gas transport system*, Technische universiteit Eindhoven, Report R-1493-A.
108. VDI3733,1996, Noise at pipes, VDI manual noise reduction guidelines, <http://www.vdi.de/vdi/kontakt/index.php>, Verein Deutscher Ingenieure e.V., VDI Guidelines Department P.O. Box 10 11 39, 40002 Duesseldorf, Germany.

## ***Paper I. Low frequency sound propagation in rectangular ducts***

### **Abstract**

HVAC (heating, ventilation and air-conditioning) systems can be found in buildings and are commonly used to transport airflow to different locations to ensure optimum living and working conditions. The duct walls are sometimes made of thin flexible aluminium or steel sheets. Noise generating by the units (fans, compressors) can propagate and radiate to another locations. An investigation of the internal sound propagation and radiation to the surrounding is conducted in this paper. Flow effects are neglected due to the relative low airflow velocity ( $< 10$  m/s) and only low frequency (plane wave) sound is treated. Various experimental techniques are employed to validate analytical models. Two main theoretical treatments are conducted to predict the propagation along the duct and transmission through its walls. Good agreements are obtained between measurement and theoretical models for future implementation in 2-port based simulation codes. These codes are necessary to facilitate the predictions of internal sound propagation and radiation in complex duct network.





# Table of Contents

1. Introduction .....	1
2. Theory.....	5
2.1    Governing equations, functional and dispersion relationship .....	5
2.1.1    Air-borne waves .....	6
2.1.2    Waves in the liner .....	6
2.1.3    Structure-borne waves .....	7
2.1.4    Boundary conditions.....	8
2.1.5    Derivation of the functional.....	9
2.1.6    Analytical formulation.....	9
2.2    Flexible duct transfer matrix formulation.....	11
2.2.1    Theoretical duct impedance.....	12
2.3    The line source method for acoustic radiation/breakout from duct walls .....	13
3. Methods and materials.....	17
3.1    Rig description.....	17
3.1.1    Types of ducts.....	17
3.1.2    Electronic equipment.....	22
3.2    Internal experimental measurement techniques .....	22
3.2.1    Experimental duct transfer matrix .....	22
3.2.2    Incident power and duct internal sound power.....	23
3.3    Duct radiated sound power (external measurement) .....	25
4. Results and discussion .....	27
4.1    In-duct investigation.....	28
4.1.1    Duct with one flexible wall (internal propagation) .....	28
4.1.2    Corrugated duct (Internal propagation) .....	30
4.1.3    Internal sound propagation for the rigid walled duct .....	32
4.2    Sound radiation investigation .....	33
4.3    Parameter investigations.....	35
4.3.1    Effect of liner positioning.....	35
4.3.2    Effect of structural conditions .....	36
4.3.3    Effect of the reflection in the airway .....	37
5. Conclusions .....	39
6. References .....	41
Appendix A    A note on measurement of liner properties .....	45



# 1. Introduction

HVAC (heating, ventilation and air-conditioning) systems are commonly found in buildings and vehicles. They are used to transport airflows to ensure comfortable working or living conditions. The ducts used in HVAC systems have either a circular or a rectangular cross section. For the case of rectangular ducts, wall vibrations are easily excited and radiate sound. The walls are sometimes lined with porous material that provides efficient acoustical attenuation at medium and high frequencies. Noise produced by the units (fans, compressor) or picked up along the system from other sources such as speech (breakin effects), propagates along the entire system and is radiated (breakout effects) into other locations. These ventilation systems also carry airflows with speeds up to 10 m/s corresponding to a Mach number  $M$  less than 0.05. This implies that mean flow effects (convection) can be neglected in the analysis.

For high frequencies, well above the plane wave range, power based analysis methods as described in standard procedures, e.g., ASHRAE (2003). However, such methods do not apply to the low frequency plane wave region where standing wave effects can be important. For the plane wave range, the most efficient is to model the duct system as a network of acoustical 2-ports (Munjal (1987), Davies (1988)). Each element in a network is characterised by its acoustic 2-port. The building block technique consists of combining these elements to form complex networks of elements. The overall performance of the entire system can then be calculated.

The aim of this study is to investigate low frequency propagation in rectangular ducts and transmission through the walls and derive analytical models for implementation in 2-port codes, e.g., the SID code developed at KTH (Nygård (2000)).

Various analytical and numerical methods have been developed (Astley (1990, 1991), Astley & Cummings (1984, 1987), Cabelli (1985<sup>a</sup>), Cummings (1978, 1979<sup>b</sup>) to predict the propagation of sound in ducts with flexible walls. A time-dependent finite difference method (Cabelli (1985<sup>b</sup>)) has been used. The variational technique has been employed by Cummings & Astley (1995). A finite element technique has been used by Astley &

Cummings (1987), Astley and al. (1991), Martin (1991) and Kirby & Cummings (1998).

Astley (1991) derives a dispersion relationship for the case of infinite-length lined elastic ducts. The formulation starts with deriving the governing equations in the duct cross-section in the different media (structure, airway, liner). The boundary conditions of the geometry gives a functional which can form the basis for various theoretical techniques and is defined for the low frequency range of interest corresponding to the frequency range below the cut-off frequency of the duct. A uniformly distributed pressure profile (plane wave) is assumed over the duct cross section.

Authors such as Cabelli (1985<sup>a</sup>) uses a Fourier series to define the pressure distribution on the duct wall due to the presence of higher-order modes. A comparison of both models of internal sound field (non-uniform in Cabelli and uniform in Cummings) has been made by Cummings (2001). It turns out that up to the cut-on frequency of the equivalent rigid duct, no deviation is observed between these two ways of expressing the internal sound field acting on the flexible walls. Thus, it is not greatly in error to consider only uniform pressure over the duct cross-section.

With this simplifying assumption, the minimisation of the functional is straightforward and leads directly to a dispersion relationship. Implementation of an iterative technique such as the Newton-Raphson scheme for solving the roots of this dispersive equation is done to obtain the propagating coupled wavenumber along the duct axis. The novelty in this paper is the derivation of the transfer matrix after theoretical derivation of the duct wavenumber and impedance. The internal transmission loss is obtained from the elements of this transfer matrix.

The analytical approach taken in this paper to obtain the radiated sound power level and transmission loss has been derived by Cummings (1979<sup>b</sup>, 1980) based on the line source model from Rennisson & Brown (1974). It regards the vibrating duct as a distribution of monopole sources of infinite length. A radiation efficiency is introduced to compensate for the finite length of the duct.

A finite element based analysis of the sound radiation from finite length rectangular ducts has been performed by Astley & Cummings (1984).

The experimental apparatus used in this thesis consists of a broadband noise excitation generated from a loudspeaker located on each side of the tested rectangular ducts. Using an experimental technique involving measurement of the acoustical upstream and downstream<sup>1</sup> conditions, one can experimentally obtain the transfer matrix (Åbom (1999)). No measurement is conducted inside the rectangular duct. In contrast, Cummings (1978) used a traverse probe to scan the sound field inside the duct as done in an impedance tube apparatus.

Radiation effects (breakout) are measured from a rotating microphone located in a reverberation chamber. Liner properties required in the full prediction is measured separately in a special rigid walled duct. All the measurements are done with no flow. Noise retransmitted to the inside after reflection from the surrounding (breakin-breakout bypass effect) is not treated.

The paper structure can be broken into two main parts: the first one accounts for the internal propagation of the plane wave and the second part treats the radiation. Both aspects are detailed theoretically with derivation of simple analytical models and confronted with results from different experiments. Various experimental techniques are described to characterise the sound fields in the different regions of the rig (circular pipe sections, internal flexible duct and external region). Experimental investigations of the termination effects in the airway and in the structure are also presented.

---

<sup>1</sup> It should be noted that the upstream and downstream sections refer to the circular pipes placed on both sides of the test ducts (see Figure 9). No airflow has been used in the paper.



## 2. Theory

In this section, mathematical derivations are presented for two theoretical models investigated in this paper. The first one concerns the propagation of sound waves inside a flexible walled duct and is based on a method derived by Astley (1990, 1991). A dispersion relationship derived from a functional describing coupled fluid-structure waves is used to compute the fundamental characteristics of the propagation of low frequency (plane) waves within a duct. The result is further implemented into a two-port formulation which is the main contribution of the present work.

The second part of this section deals with the radiation of sound from duct walls. Using the equations derived for the internal sound propagation, one can analytically estimate the level of sound emitted by the duct walls. The model used is based on a work by Cummings (1978) on the so-called duct “breakout” effects. It regards the duct as a line of monopole sources. This method gives good results as long as only the fundamental (plane wave) propagation mode is investigated.

### 2.1 Governing equations, functional and dispersion relationship

A schematic outline of the duct with homogeneous properties along its  $z$ -axis is shown in Figure 1.

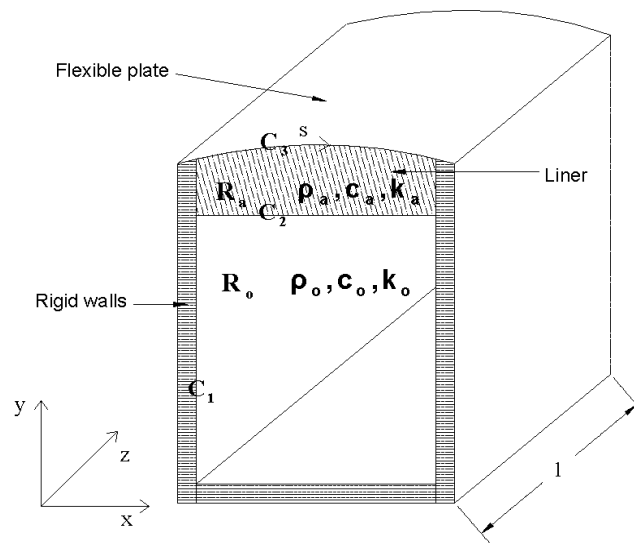


Figure 1: Definition of duct coordinate system and symbols used.

where  $R$  is the cross-section area,  $C$  is the boundary,  $s$  is the length coordinate for the flexible wall,  $c$  is the speed of sound ( $c_0 = 343 \text{ m.s}^{-1}$  in the airway),  $\rho$  is the density and  $k$  is the wavenumber. Waves propagating in lined flexible walled ducts are present in three different media (wall, liner, air) with different acoustical characteristics. Acoustic energy is transmitted along the duct in the form of coupled fluid-structured waves where the wave energy is split between the fluid (air and liner) and the structure.

### 2.1.1 Air-borne waves

The acoustic pressure in the airway is assumed to be harmonic and has the following form

$$p_0(x, y, z, t) = \hat{p}_0(x, y)e^{i(\omega t - \alpha z)}, \quad (2-1)$$

where  $\hat{\phantom{x}}$  denotes a complex valued (Fourier) quantity,  $z$  is the direction of the wave propagation, i.e., along the axial direction of the duct and  $p_0$  is the pressure mode shape. It is assumed that no airflow is present in the duct.

The wave equation governing the propagation of the first harmonic mode in the air filled region (Region  $R_0$ ) is

$$\nabla^2 \hat{p}_0 + k^2(1 - \alpha'^2)\hat{p}_0 = 0, \quad (2-2)$$

where the subscript  $0$  denotes the airway,  $k = \omega/c_0$  is the plane wave number,  $\alpha = \alpha'k$  is the fluid-structure coupled complex axial wavenumber. Solution of the dispersion relationship derived later in this section gives the frequency dependent dimensionless wave number  $\alpha'$ .

### 2.1.2 Waves in the liner

The acoustic pressure in the liner is also assumed to be harmonic and is written as

$$p_a = \hat{p}_a(x, y)e^{i(\omega t - \alpha t)}. \quad (2-3)$$

In the liner (Region  $R_a$ ), the propagation of sound waves is characterised by the following equation

$$\nabla^2 \hat{p}_a + (k_a^2 - \alpha^2)\hat{p}_a = 0, \quad (2-4)$$

where the subscript  $a$  denotes the liner.  $k_a$  is the frequency dependent liner complex wavenumber which can be determined by standard models or experimentally using various acoustical measurement techniques (cf Appendix).



### 2.1.3 Structure-borne waves

The flexible walls vibrate and radiate energy to the surrounding environment. This structural vibration significantly influences the internal propagation of sound wave.

Assuming thin plate theory, the equation governing the normal displacement  $u$  of such flexible walls is represented by

$$u(s, z, t) = \hat{u}(s) e^{i(\omega t - \alpha z)}, \quad (2-5)$$

where  $s$  and  $z$  are the spatial coordinates for the flexible wall/plate.

Assuming only bending waves in the plate; the standard equation for a thin plate gives

$$m \frac{\partial^2 u}{\partial t^2} = -B \nabla^4 u + p_u, \quad (2-6)$$

where  $m = \rho_s h$ ,  $B = Eh^3 / (12(1 - \nu^2))$  and  $k_p^4 = \frac{\omega^2 m}{B}$ .  $\rho_s$  is the plate density,  $h$  its thickness,  $E$  its elastic Young's modulus and  $\nu$  its Poisson's ratio.

Substituting (2-5) into (2-6).

$$B \left[ \frac{\partial^4 \hat{u}}{\partial s^4} - 2\alpha^2 \frac{\partial^2 \hat{u}}{\partial s^2} + (\alpha^4 - k_p^4) \hat{u} \right] = \hat{p}_u. \quad (2-7)$$

The pressure or dynamic loading applied on the plate (the pressure difference between the upper and lower surface) is represented by  $p_u$  (the subscript  $u$  denotes the flexible wall) and can have different forms. However, the pressure along the wall is assumed to be uniform in this paper due to the low frequency plane wave propagation.

Regarding the acoustical losses, three types exist:

- Structural internal loss factor
- Boundary loss factor
- Radiation loss factor

In the model they are comprised in only one single loss factor, the structural loss factor  $\eta$  in the plate used in conjunction with the Young's modulus  $E$

$$E = E_0(1 + i\eta), \quad (2-8)$$

where  $E_0$  is the standard Young's modulus which can be found in any engineering hand book. For example:  $E_0 = 19.5 \times 10^{10} \text{ Pa}$  (*Steel*).

The general solution of (2-7) is

$$\hat{u}(s) = A \cosh(k_s s) + B \sinh(k_s s) + C \cos(k_s s) + D \sin(k_s s) - \frac{\hat{p}_u}{B(\alpha'^4 - k_p^4)}, \quad (2-9)$$

where  $k_s = \sqrt{(\alpha' k)^2 - k_p^2}$  and  $A, B, C, D$  are boundary coefficients.

For rectangular flexible ducts with pairs of vibrating walls oriented along  $x$  and  $y$ , the displacement fields are given by

$$\hat{u}_x(s) = A \cos(k_s s) + B \sinh(k_s s) + C \cos(k_s s) + D \sin(k_s s), \quad (2-10)$$

$$\hat{u}_y(s) = E \cos(k_s s) + F \sinh(k_s s) + G \cos(k_s s) + H \sin(k_s s), \quad (2-11)$$

where  $s$  varies between 0 and  $S_x$  and  $S_y$  respectively.

Determination of the eight coefficients from  $A$  through  $H$  are established using the following eight boundary conditions (Cummings (1979<sup>a</sup>)).

No displacement at the corners

$$\hat{u}_x(0) = \hat{u}_x(S_x) = 0, \quad (2-12)$$

$$\hat{u}_y(0) = \hat{u}_y(S_y) = 0, \quad (2-13)$$

A fixed 90° angle between adjacent walls, e.g.,

$$\frac{\partial \hat{u}_x(0)}{\partial s} = -\frac{\partial \hat{u}_y(0)}{\partial s}, \quad (2-14)$$

The uniform internal pressure assumption (plane wave range) implies that the displacement for each plate has a slope equal to zero in the middle of the plate.

$$\frac{\partial \hat{u}_x(S_x/2)}{\partial s} = 0, \quad (2-15)$$

$$\frac{\partial \hat{u}_y(S_y/2)}{\partial s} = 0, \quad (2-16)$$

Balance of the transverse bending moments for adjacent walls.

$$B_x \frac{\partial^2 \hat{u}_x(0)}{\partial s^2} = B_y \frac{\partial^2 \hat{u}_y(0)}{\partial s^2}. \quad (2-17)$$

#### 2.1.4 Boundary conditions

In order to express the problem in a variational form, one needs to state the different boundary conditions of the problem.

At the interface between two media, the pressure  $p$  and the normal displacement should be conserved, i.e., be continuous across the interface.

Using the appropriate momentum equation relating the pressure and the displacement, it is possible to write down the different boundary conditions.

On  $C_1$  (along the rigid wall), the velocity in the direction of the normal is zero, it implies that

$$\nabla \hat{p}_a \cdot n_1 = 0. \quad (2-18)$$

On  $C_2$  (between the liner and the airway), there should be continuity in the particle displacement along the normal, i.e.,

$$\frac{1}{\rho_0 \omega^2} (\nabla \hat{p}_0 \cdot n_2) = \frac{1}{\rho_a \omega^2} (\nabla \hat{p}_a \cdot n_2). \quad (2-19)$$

On  $C_3$  (along the plate), there should be continuity in the displacement in the normal direction, i.e.,

$$\frac{1}{\rho_a \omega^2} \nabla \hat{p}_a \cdot n_3 = \hat{u} \quad (2-20)$$

### 2.1.5 Derivation of the functional

From the wave equations ((2-2), (2-4) and (2-7) and boundary conditions ((2-18), (2-19) and (2-20)) for this problem, it is now possible to create a single expression called a functional. This functional is stationary for acoustic and vibration fields that satisfy the equations and the boundary conditions. This functional is then used to setup finite element schemes or to derive approximate solutions using suitable ansatz functions. After some manipulations, it is found (Astley (1990)) that the functional  $F$  for this problem is given by

$$\begin{aligned} F(\hat{u}, \hat{p}) = & \rho_0 \omega^2 \int_{C_3} \left[ \frac{1}{2} g \left\{ \left( \frac{\partial^2 \hat{u}}{\partial s^2} \right)^2 + 2k^2 \alpha'^2 \left( \frac{\partial \hat{u}}{\partial s} \right)^2 + (k^4 \alpha'^4 - k_p^4) \hat{u}^2 \right\} - \hat{u} \hat{p}_u \right] ds \\ & + \frac{1}{2} \int_{R_0} \{ \nabla \hat{p}_0 \cdot \nabla \hat{p}_0 - k^2 (1 - \alpha'^2) \hat{p}_0^2 \} dx dy + \frac{\rho_0}{2 \rho_a} \int_{R_a} \{ \nabla \hat{p}_a \cdot \nabla \hat{p}_a - (k_a^2 - k^2 \alpha'^2) \hat{p}_a^2 \} dx dy. \end{aligned} \quad (2-21)$$

### 2.1.6 Analytical formulation

The functional (2-21) forms the basis for a simple analytical analysis from which a dispersion relationship is obtained. However, one has to make complementary assumptions to further proceed. Generally, when the acoustic wavelength is larger than the characteristic dimension of the duct, it may be suitable to see the wave as a plane

wave, that is, all acoustic properties such as pressure and velocity can be considered as constant over the cross-section of the duct. Thus,

$$\hat{p}(x, y) = \hat{p}_u = \hat{p}_a = \hat{p}_0 = \hat{p}_{int} = \text{const} \quad (2-22)$$

This also implies that the external radiation load is neglected.

Looking back at (2-7) (the equation describing the motion of the flexible walls) it can be further noted that the solution  $\hat{u}(s)$  can be expressed in the form

$$\hat{u}(s) = \hat{p}_{int} \hat{u}'(s, \alpha'), \quad (2-23)$$

where  $\hat{p}_{int}$  represents the uniform pressure applied on the inner surface of the flexible wall and  $\hat{u}'(s, \alpha')$  is the solution of (2-7) for which  $\hat{p}_{int}$  is set to unity (unit pressure).

Incorporating this into (2-21) the functional  $F$  is rewritten in the form

$$F = \frac{1}{2} ik \bar{\beta}(\alpha') S \hat{p}_{int}^2 + \frac{1}{2} k^2 \hat{p}_{int}^2 \left[ R_0 \{ \alpha'^2 - 1 \} + R_a \frac{\rho_0}{\rho_a} \left\{ \alpha'^2 - \left( \frac{k_a}{k} \right)^2 \right\} \right], \quad (2-24)$$

where  $S$  represents the total length of flexible walls and

$$\bar{\beta}(\alpha') = (1/S) \int \beta ds = (i \omega \rho_0 c_0 / S) \int \hat{u}' ds \quad (2-25)$$

is the averaged wall admittance  $\beta$  over the vibrating length  $S$ .  $\rho_a$  and  $k_a$  correspond respectively to the liner density and wavenumber. Minimisation of this functional with respect to  $\hat{p}_{int}$  (plane wave approximation) gives the dispersion relationship (2-26) from which the roots  $\alpha'$  are sought

$$G(\alpha') = \frac{1}{2} ik \bar{\beta}(\alpha') S + \frac{1}{2} k^2 \left[ R_0 \{ \alpha'^2 - 1 \} + R_a \frac{\rho_0}{\rho_a} \left\{ \alpha'^2 - \left( \frac{k_a}{k} \right)^2 \right\} \right]. \quad (2-26)$$

Solving this dispersion relationship through a Newton-Raphson scheme gives the dimensionless frequency dependent complex axial coupled wavenumbers  $\alpha' = \alpha/k$ .

Such iterative method requires an initial guess, in an attempt to predict the different wavenumbers in this problem, two initial guesses were tested corresponding to the plane wave number  $\alpha' = 1 - 0.1i$  and to the bending wave number  $\alpha' = k_p/k = c/\sqrt{\omega} \sqrt[4]{m/B}$ .

The result that emerges is that the root obtained from this scheme converges to the same coupled wave number for any initial guess. The reason for this is the ansatz in (2-23) which will always track an acoustic type of mode, i.e., the one that transports acoustic energy in the air. For the in-duct sound transmission problems of interest here, it will be

assumed that it is sufficient to only include this mode type in the analysis.

## 2.2 Flexible duct transfer matrix formulation

The predicted coupled propagating wavenumber  $\alpha$  is now used to build the 2-port transfer matrix corresponding to the flexible duct element. This transfer matrix is suitable for calculation of the element transmission loss index or can be inserted in an acoustic network composed of various other elements for which the transfer matrices are known. The block technique consists of multiplying the transfer matrices to obtain the network transfer matrix.

The transfer matrix for an element is characterised by two independent state variables: acoustic pressure  $p$  and volume velocity  $q$  on each side of the element.

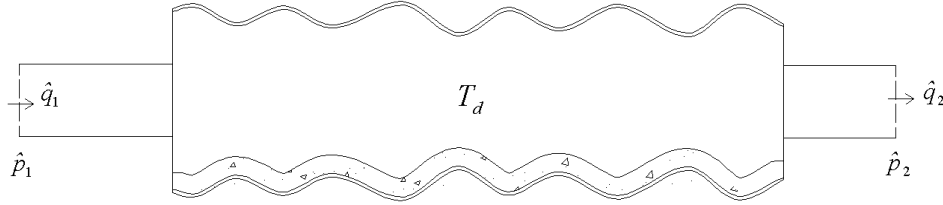


Figure 2: Duct transfer matrix defining a relationship between the plane wave state variables  $(p, q)$  at the input 1 and the output 2 cross sections.

One can define the duct transfer matrix  $T_d$  as

$$\begin{pmatrix} \hat{p}_1 \\ \hat{q}_1 \end{pmatrix} = T_d \begin{pmatrix} \hat{p}_2 \\ \hat{q}_2 \end{pmatrix}. \quad (2-27)$$

Assuming a straight homogenous duct section along  $z$  with length  $l$  and low Mach number ( $M \ll 1$ ) (cf Figure 1), the duct transfer matrix is (Munjal (1987), Davies(1988))

$$T_d = \begin{pmatrix} T_{11} & T_{12} \\ T_{21} & T_{22} \end{pmatrix} = \begin{pmatrix} \cos(\alpha l) & iZ_d \sin(\alpha l) \\ \frac{i \sin(\alpha l)}{Z_d} & \cos(\alpha l) \end{pmatrix}, \quad (2-28)$$

where  $Z_d$  is the duct impedance defined as

$$Z_d = \sqrt{\frac{T_{12}}{T_{21}}}. \quad (2-29)$$

$Z_d$  can be obtained theoretically as described in the following section. The wavenumber  $\alpha = \alpha'k$  is obtained after solving (2-26).

The duct internal transmission loss  $ITL$  is computed using the following relation for no

flow and equal input and output impedance  $Z_p = \rho_0 c_0 / R$  where  $R$  is the cross-section area of the pipe.

$$ITL = 10 \log_{10} \left( \frac{1}{4} \left| T_{11} + \frac{T_{12}}{Z_p} + Z_p T_{21} + T_{22} \right|^2 \right). \quad (2-30)$$

### 2.2.1 Theoretical duct impedance

The duct transfer matrix  $T_d$  formulated in (2-28) necessitates the coupled wavenumber  $\alpha$  obtained after solving the dispersion relationship (2-26) and the duct internal impedance  $Z_d$  evaluated as follows

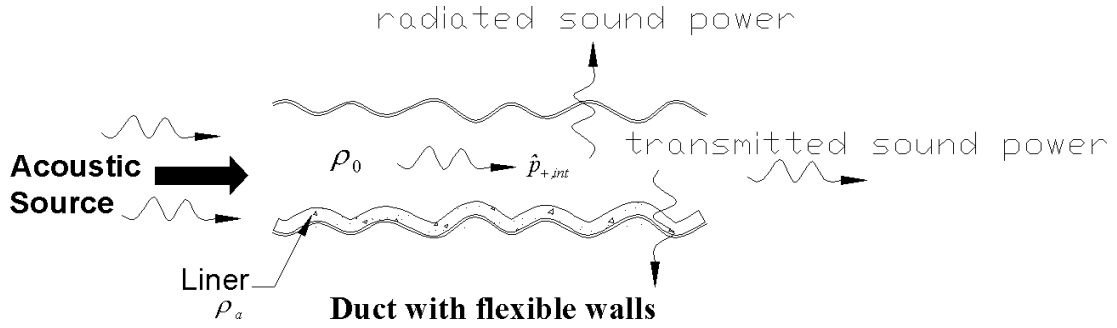


Figure 3: Schematic of wave propagation in lined duct with flexible walls.

Assuming a harmonic particle velocity  $v$  and pressure  $p$ , the linearized equation of motion is given by

$$\rho \frac{\partial \vec{v}}{\partial t} = -\nabla p. \quad (2-31)$$

Thus, one gets in the absorber and in the airway for waves in positive direction

$$\text{Absorber: } \rho_a i \omega \hat{v}_a = \hat{p}_{+,int} i \alpha, \quad (2-32)$$

$$\text{Airway: } \rho_o i \omega \hat{v}_o = \hat{p}_{+,int} i \alpha, \quad (2-33)$$

Rearranging (2-32) and (2-33) gives

$$\hat{p}_{+,int} = \frac{\omega}{\alpha} \rho_a \hat{v}_a^+ = \frac{\omega}{\alpha} \rho_0 \hat{v}_0^+. \quad (2-34)$$

The volume velocity is given by

$$\hat{q}^+ = R_a \hat{v}_a^+ + R_0 \hat{v}_0^+. \quad (2-35)$$

The duct impedance  $Z_d$  is defined from (2-34) and (2-35)

$$Z_d = \frac{\hat{p}_{+,int}}{\hat{q}^+} = \frac{\omega}{\alpha \left( \frac{R_a}{\rho_a} + \frac{R_0}{\rho_0} \right)}. \quad (2-36)$$

The same results with a change of sign will apply to negative direction.

### 2.3 The line source method for acoustic radiation/breakout from duct walls

Attention is now brought to the calculation of acoustic energy propagation through flexible walls. A radiation transmission loss index  $RTL$  can be derived to estimate the level of sound radiated.

The model to predict the radiated power was first derived by Brown & Rennison (1974) for circular pipes and adapted to rectangular ducts by Cummings (1978). This model regards the duct as a distribution of monopole sources. The source strength of these sources is obtained from the duct wall displacement integrated and averaged around the duct wall perimeter.

It can be shown (Cummings (1978)) that the radiated sound power per unit length for an infinitely long line source with supersonic waves can be calculated using

$$W_\infty = \frac{\omega \rho_0 |\hat{q}|^2}{8}, \quad (2-37)$$

where  $\hat{q}$  is the volume velocity per unit length and can be expressed in terms of the averaged wall admittance  $\bar{\beta}$  as

$$\hat{q} = \frac{\hat{p}_{int}}{\rho_0 c_0} S \bar{\beta}. \quad (2-38)$$

The averaged wall admittance  $\bar{\beta}$  depends on the geometry of the flexible wall and is expressed in equation (2-25).

For a duct of finite length  $l$ , the radiated sound power for any type of waves is obtained using a radiation efficiency factor  $C_r$ . Equation (2-37) then becomes

$$W_{rad} = W_\infty C_r = \frac{C_r \omega \rho_0 |\hat{q}|^2}{8}. \quad (2-39)$$

$C_r$  is obtained graphically from Figure 4 and is taken from Cummings (1978) where

$k=\omega/c_0$  and  $\alpha=\alpha'k$  is the axial propagating wave obtained from the dispersion relationship (2-26).

The line source model derived originally by Brown & Rennison (1974) only considered one single travelling wave. In an attempt to refine this model, Cummings (1980) incorporates an additional reflected wave. A modified radiation efficiency factor  $C_r$  is thus derived from the assumption of two sinusoidal travelling waves. Cummings (1980) claims that it does not affect the total radiated power. Therefore, the single wave assumption for the radiation model is valid even when structural reflections occur.

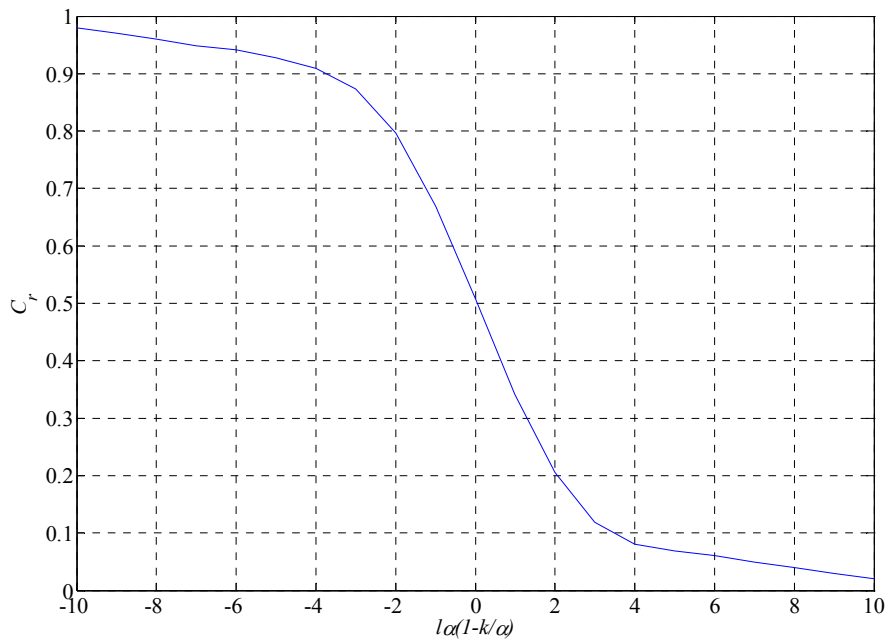


Figure 4: Radiation efficiency  $C_r$  of a source with finite length  $l$ .

Concerning now the internal sound power in the positive direction  $W_{+,int}$ , it is defined from

$$W_{+,int} = |\hat{p}_{+,int}|^2 \operatorname{Re}\left(\frac{1}{Z_d}\right), \quad (2-40)$$

where  $Z_d$  is the duct impedance obtained from (2-36).

Using the definition for *RTL* (radiation transmission loss)

$$RTL = 10 \log_{10} \left( \frac{W_{+,int}}{W_{rad}} \right). \quad (2-41)$$

Equations (2-39) and (2-40) are used to derive the expression for the radiation



transmission loss  $RTL$  of the flexible duct

$$RTL = 10 \log_{10} \left( \frac{8 \rho_0 c_0^2 \operatorname{Re}[\alpha(R_a/\rho_a + R_0/\rho_0)]}{C_r \omega^2 S^2 |\bar{\beta}|^2} \right). \quad (2-42)$$

Theoretical models have been derived concerning the internal propagation and radiation of plane waves in rectangular ducts with flexible walls. The models give the transmission loss due to the internal propagation and the radiation (“breakout” effect). Experimental evaluation is presented in the next section in order to validate the theory.



### 3. Methods and materials

In order to test the theory, three ducts have been constructed and the tests have been in a reverberation room. This acoustical environment is practical to measure the transmission loss due to the radiation of sound waves through the flexible walls.

This section presents the equipment and procedures used to carry out the measurements of the internal propagation and radiation through the flexible walls. The measurement of the liner properties are described in the appendix.

#### 3.1 Rig description

##### 3.1.1 Types of ducts

###### Duct with one flexible plate

The geometry of the first duct tested can be seen in Figure 5 and Figure 6. This duct has been built at MWL and represents a first benchmark test for the theory. The idea was to have a duct with a single flexible wall and with well defined boundary conditions. Different duct types are tested. The first one, shown in Figure 6, consists of three wooden rigid walls and a flexible wall made of steel (thickness: 0.5 mm).

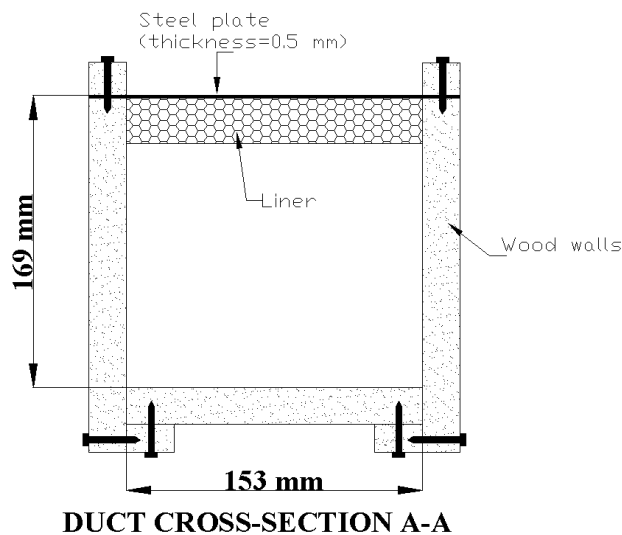


Figure 5: Specification of the duct with a single flexible wall (length  $l=2\text{m}$ ). The liner has a thickness of 22 mm.



Figure 6: Measurement set-up in the reverberation room of MWL.

A sheet of porous material (Figure 8) of thickness 22 mm is made slightly larger than the transverse dimensions of the duct so no glue or support is required for this liner and the arrangement allows the air spacing between the liner and the wall to be easily varied. The transverse dimensions for this duct is 169 by 153 mm (cut-off frequency: 1000 Hz). The edges of this plate are rigidly fixed onto the walls to satisfy the clamped-clamped boundary conditions used in the theory (Figure 7).

Figure 9 shows the experimental apparatus for the duct with one flexible wall and the circular plastic pipes (diameter 0.150 m, cut-off frequency 1350 Hz) on which the microphones are mounted. The microphones on the left and right hand side are used for the plane wave decomposition using the two-microphone technique (Bodén & Åbom (1986)). Three microphones are used on each side to extend the frequency range. The transfer matrix is determined via the so-called source switching technique (Åbom (1999)) using loudspeaker LS I and LS II.

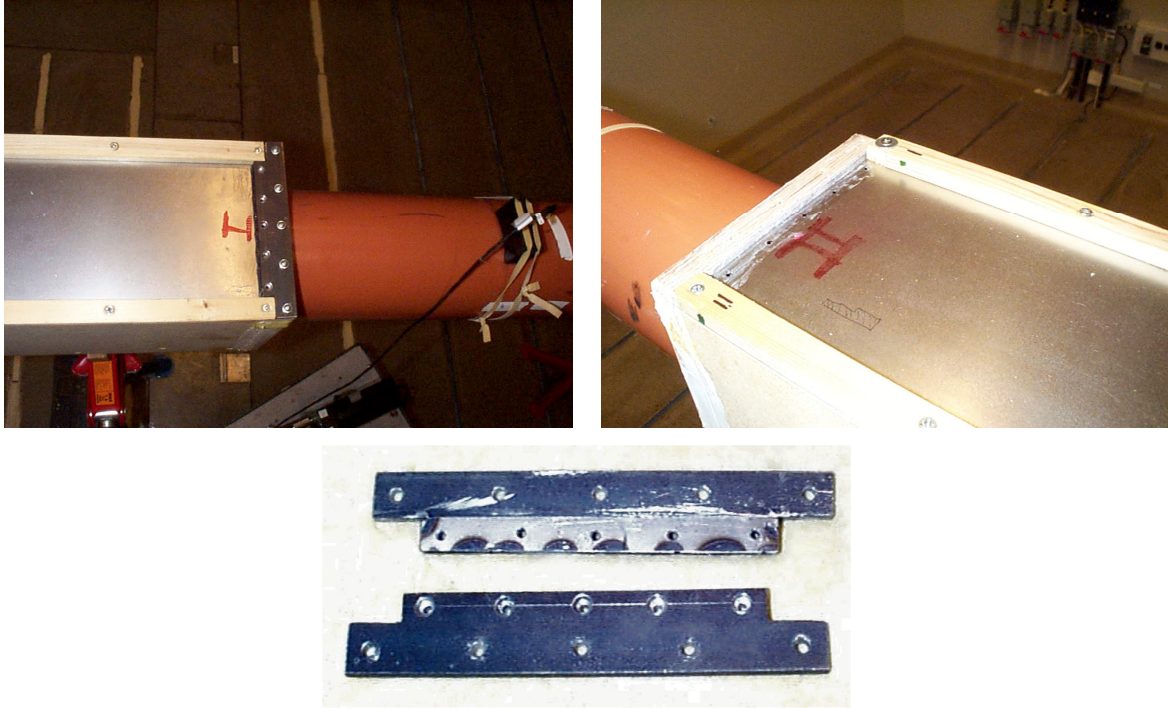


Figure 7: Variation of the boundary conditions at the inlet and outlet section, I : clamped, II: unclamped.

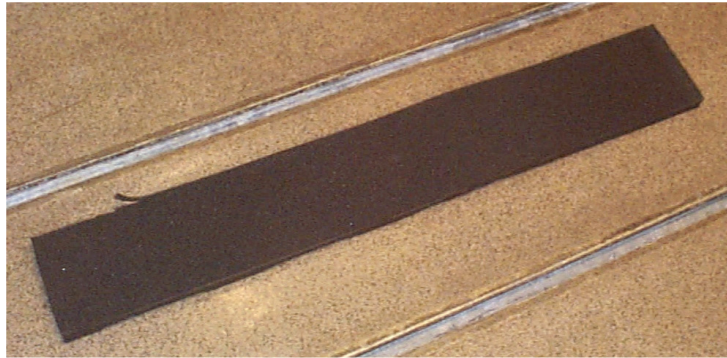


Figure 8: Porous material (Polyurethane foam).

The set-up is also used for the corrugated and rigid ducts. Some mineral wool material encloses the flexible plate (Figure 6) when internal propagation measurement is performed in order to avoid any breakin-breakout bypass effects. The radiating length of the three ducts is 2 m.

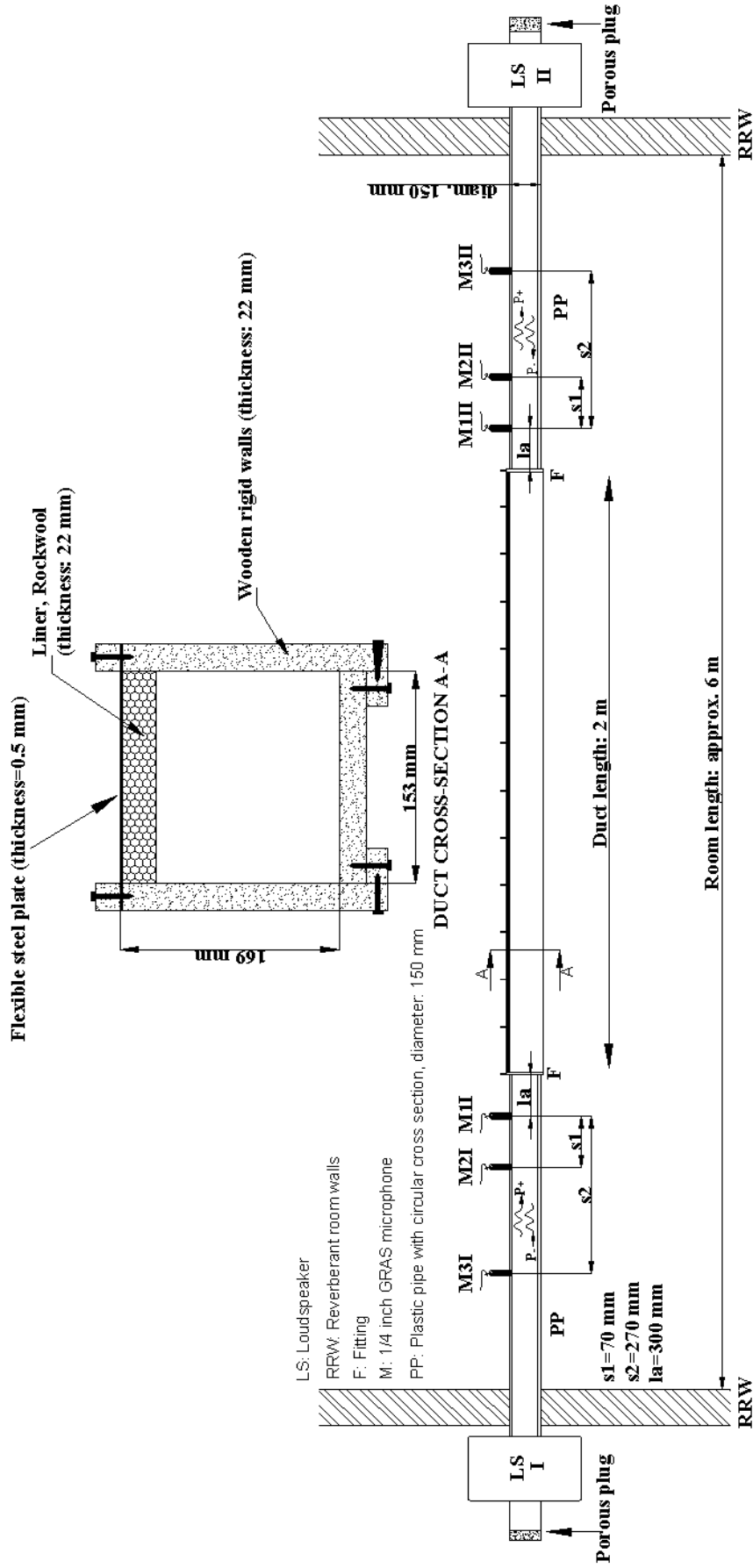


Figure 9: Schematic of the experimental rig.



### Corrugated duct

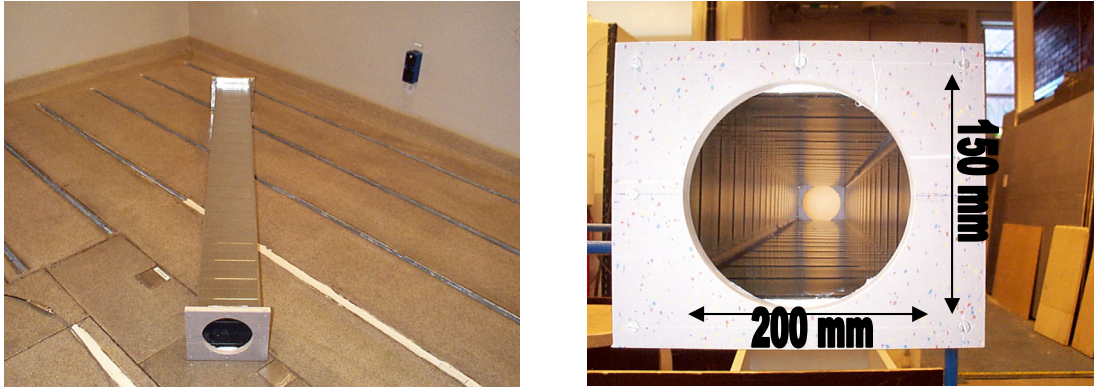


Figure 10: Corrugated duct.

Figure 10 shows a picture of the second duct investigated: a rectangular corrugated industrial duct made of four flexible steel walls. The transverse dimensions are 150 by 200 mm (cut-off frequency: 850 Hz). Specifications of the manufacturer give a thickness of about 1 mm. The radiating length of this corrugated duct is also 2 m. The corrugated duct is mounted without supports to the circular pipes used for the measurement (Figure 9).

### Rigid walled duct

The duct with a single flexible wall is also used to obtain the liner properties (cf Appendix for more details). It is necessary to remove the flexible plate and replaced it with a thick wooden plate. The duct is then made completely rigid as shown in Figure 11.



Figure 11: Rigid walled duct. The polyurethane foam is lined at the bottom.

### 3.1.2 Electronic equipment

Sound waves are generated from two loudspeakers (Figure 9) connected to a Tektronix signal processor which is used to produce the signal fed to the loudspeaker. The microphone is connected to the second channel. Correlation between the input signal and microphone response is performed. The spacing between the microphone locations dictates the range of frequency under investigation. For a measurement frequency ranging between 50 and 2000 Hz, a minimum spacing of 70 mm and of maximum spacing of 270 mm are required.

## 3.2 Internal experimental measurement techniques

The experimental procedures used to measure the sound fields in the different duct sections are now described. The separate measurement techniques to characterise the liner properties are given in the appendix.

### 3.2.1 Experimental duct transfer matrix

The standard two-microphone technique (Bodén & Åbom (1986)) applied separately on the upstream and downstream pipe is used to determine the duct transfer matrix  $T_d$  of the acoustical element tested. The procedure used is based on the so-called source switching technique described for instance by Åbom (1999).

One can define the duct transfer matrix  $T_d$  as

$$\begin{aligned} \begin{pmatrix} \hat{p}_1 \\ \hat{q}_1 \end{pmatrix} &= \begin{bmatrix} T_{11} & T_{12} \\ T_{21} & T_{22} \end{bmatrix} \begin{pmatrix} \hat{p}_2 \\ \hat{q}_2 \end{pmatrix} \\ &= \left\{ \begin{array}{l} \text{straight duct with constant} \\ \text{properties along its axis} \end{array} \right\} \left\{ \begin{array}{cc} \cos(\alpha l) & iZ_d \sin(\alpha l) \\ \frac{i \sin(\alpha l)}{Z_d} & \cos(\alpha l) \end{array} \right\} \begin{pmatrix} \hat{p}_2 \\ \hat{q}_2 \end{pmatrix}, \end{aligned} \quad (3-1)$$

where  $\alpha$  is the propagation wavenumber and  $Z_d = \sqrt{T_{12}/T_{21}}$  is the internal duct impedance.

Only one microphone is used at six different locations (Figure 9). Although it is time consuming to move the microphone to the various locations, the necessary phase calibration between multiple microphones is eliminated.

First measurements of the transfer functions between the loudspeaker voltage and one of the six microphone positions are done using loudspeaker LS I (Figure 9).



The procedure is then repeated for the second loudspeaker LS II. A total of 12 measurement files are then collected during each measurement session. A Matlab code is used to obtain the transfer matrix  $T_d$  and internal transmission loss  $ITL$  (see (2-30))

### 3.2.2 Incident power and duct internal sound power

The test ducts are positioned between the two circular pipes. Measurement of transfer functions at different microphone positions is carried out to decompose the waves as shown in Figure 12.

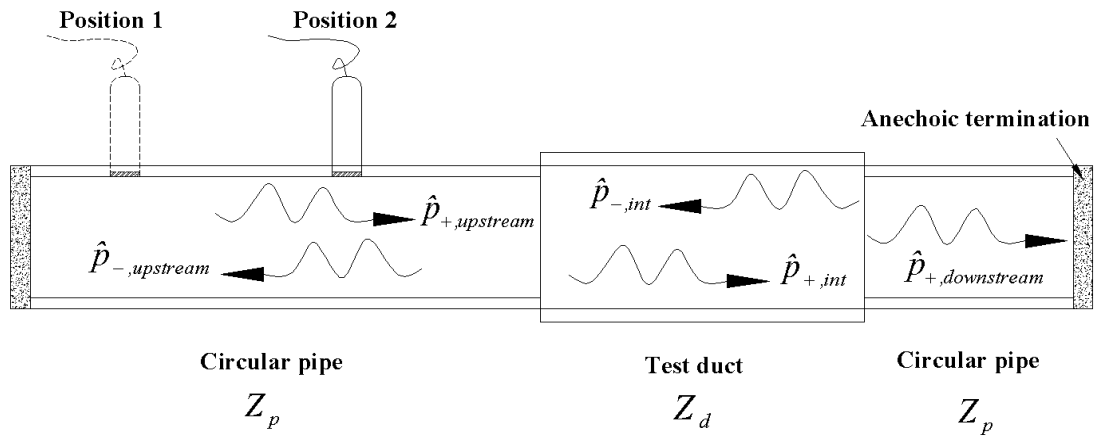


Figure 12: Schematic of the travelling plane wave pressures.

By placing a microphone at different positions  $x$  as shown in Figure 9 and measuring the transfer function between the position and the loudspeaker and calling the result  $H_{Lp/x}$ , it is possible to determine the travelling waves  $\hat{p}_{+,upstream}$  and  $\hat{p}_{-,upstream}$ . Using the impedance of both the pipe and the test duct, one calculates the travelling pressures  $\hat{p}_{+,int}$  and  $\hat{p}_{-,int}$  propagating in the duct. The circular pipe impedance is taken as  $Z_p = \rho_0 c_0 / R$  and the internal duct impedance  $Z_d$  is obtained from the duct transfer matrix (3-1).

#### *Travelling pressure waves in the pipe ( $\hat{p}_{+,upstream}$ , $\hat{p}_{-,upstream}$ )*

Using one separation, for example, position 1 and 2 and referring to Figure 12, the relation between the travelling pressure waves and  $\hat{p}_1$  (reference position 1)

and  $\hat{p}_2$  (position 2) is given by

$$\begin{aligned}\hat{p}_1 &= \hat{p}_{+,upstream} + \hat{p}_{-,upstream}, \\ \hat{p}_2 &= \hat{p}_{+,upstream} e^{-iks} + \hat{p}_{-,upstream} e^{iks},\end{aligned}\tag{3-2}$$

where  $s$  is the distance between microphone positions 1 and 2. In matrix form this becomes

$$\begin{bmatrix} \hat{p}_1 \\ \hat{p}_2 \end{bmatrix} = \begin{bmatrix} 1 & 1 \\ e^{-iks} & e^{iks} \end{bmatrix} \begin{bmatrix} \hat{p}_{+,upstream} \\ \hat{p}_{-,upstream} \end{bmatrix}.\tag{3-3}$$

Rearranging (3-3) to extract  $\hat{p}_{+,upstream}$  and  $\hat{p}_{-,upstream}$  (wave decomposition) yields

$$\hat{p}_{+,upstream} = \left( \frac{\hat{p}_1 e^{iks} - \hat{p}_2}{2i \sin ks} \right),\tag{3-4}$$

$$\hat{p}_{-,upstream} = \left( \frac{-\hat{p}_1 e^{-iks} + \hat{p}_2}{2i \sin ks} \right).\tag{3-5}$$

Dividing formally by the loudspeaker voltage  $\hat{e}$ , this gives

$$H_{\hat{e}/\hat{p}_{+,upstream}} = \frac{H_{\hat{e}/1} e^{iks} - H_{\hat{e}/2}}{2i \sin ks},\tag{3-6}$$

$$H_{\hat{e}/\hat{p}_{-,upstream}} = \frac{-H_{\hat{e}/1} e^{-iks} + H_{\hat{e}/2}}{2i \sin ks}.\tag{3-7}$$

Recalling that

$$\left| H_{\hat{e}/\hat{p}_{+,upstream}} \right|^2 = \frac{S_{\hat{p}_+\hat{p}_+}}{S_{\hat{e}\hat{e}}},\tag{3-8}$$

$$\left| H_{\hat{e}/\hat{p}_{-,upstream}} \right|^2 = \frac{S_{\hat{p}_-\hat{p}_-}}{S_{\hat{e}\hat{e}}},\tag{3-9}$$

where  $S_{\hat{p}_-\hat{p}_-}$  and  $S_{\hat{p}_+\hat{p}_+}$  are the uncalibrated autospectra of the incident  $\hat{p}_{+,upstream}$  and reflected wave  $\hat{p}_{-,upstream}$  and  $S_{\hat{e}\hat{e}}$  the loudspeaker autospectrum.

The true autospectra for the travelling waves are given by

$$S_{\hat{p}_+\hat{p}_+}^t = K_{cal}^2 \times S_{\hat{p}_+\hat{p}_+} = K_{cal}^2 \times \left| H_{\hat{e}/\hat{p}_{+,upstream}} \right|^2 \times S_{\hat{e}\hat{e}},\tag{3-10}$$

$$S_{\hat{p}_-\hat{p}_-}^t = K_{cal}^2 \times S_{\hat{p}_-\hat{p}_-} = K_{cal}^2 \times \left| H_{\hat{e}/\hat{p}_{-,upstream}} \right|^2 \times S_{\hat{e}\hat{e}},\tag{3-11}$$

where  $K_{cal}$  is the calibration factor [Pa/V] of the quarter-inch microphone mounted on the circular pipe.

***Travelling pressure waves inside the duct ( $\hat{p}_{+,int}$ ,  $\hat{p}_{-,int}$ ) and duct internal power  $W_{+,int}$***

Due to the reflection free termination of the duct,  $\hat{p}_{-,int}$  is small and neglected. The duct internal pressure  $\hat{p}_{+,int}$  is derived as

$$\hat{p}_{+,int} = T\hat{p}_{+,upstream}, \quad (3-12)$$

where the transmission factor  $T$  is

$$T = \frac{2}{1 + Z_p/Z_d}, \quad (3-13)$$

where  $Z_p$  and  $Z_d$  are the pipe and duct impedances respectively. The duct internal power  $W_{+,int}$  is calculated using (2-40).

### **3.3 Duct radiated sound power (external measurement)**

Measurements are performed in the reverberation room at MWL using a Brüel & Kjaer reference source with calibrated third octave band frequency data. Conversion of these data to smallband with the same frequency resolution as the one obtained from the one used in the in-duct measurements

$$L_{wnB} = L_{w1/3} - 10 \log_{10}(n), \quad (3-14)$$

where  $L_{wnB}$  is the sound power level in narrowband,  $L_{w1/3}$  is the sound power level in 1/3-octave band from the source calibration data sheet and  $n$  is the number of narrow band points within a 1/3 octave band. White noise within each band is assumed. A rotating half-inch microphone in the reverberation room at a distance of at least 1m away of any reflecting surface is used to measure the sound radiated. A room factor  $K$  is determined according to

$$K(f) = \frac{W_{ref\ source}}{S_{pp}}, \quad (3-15)$$

where  $W_{ref\ source}$  is the narrow band converted reference source calibration data and  $S_{pp}$  is the rotating microphone autospectrum. Once the room factor  $K$  has been obtained, the sound power radiated per unit length by the duct of length  $l$  is given by

$$W_{rad} = KS_{pp(duct)}/l. \quad (3-16)$$

The radiation transmission loss  $RTL$  defined in equation (2-41) can now be obtained by combining the measured in-duct sound power  $W_{int}$  and radiated power  $W_{rad}$ .



## 4. Results and discussion

In the following section, attention is brought to the comparison between measured and predicted data. The results derived from the two theoretical models (internal and radiation) and experimental data for the three test ducts are compared. For specifications of the three ducts (duct with single flexible wall, corrugated duct and rigid duct) investigated, the reader is referred to section 3.1.1. The same porous material (liner) is used in all three ducts. The influence of the liner position is tested. The effect of different boundary conditions both in the fluid and in the structure is also tested.

A special problem when using the models described earlier is the choice of the loss factor  $\eta$  for the flexible walls. Cummings (2001) points out that he uses anomalously high structural loss factor in his model.

This loss factor is especially important at the eigenfrequencies of the flexible walls. To handle this problem, the loss factors are determined experimentally and fitted to the formulas given below

For the duct with one flexible wall

$$\eta = \eta_1 e^{\left(-bw_1 \left(\frac{f-f_{r1}}{f_{r1}}\right)^2\right)} + \eta_2 e^{\left(-bw_2 \left(\frac{f-f_{r2}}{f_{r2}}\right)^2\right)} \quad (4-1)$$

and for the corrugated duct

$$\eta = \eta_1 e^{\left(-bw_1 \left(\frac{f-f_{r1}}{f_{r1}}\right)^2\right)} + \eta_2 e^{\left(-bw_2 \left(\frac{f-f_{r2}}{f_{r2}}\right)^2\right)} + \eta_3 e^{\left(-bw_3 \left(\frac{f-f_{r3}}{f_{r3}}\right)^2\right)} + \eta_4 e^{\left(-bw_4 \left(\frac{f-f_{r4}}{f_{r4}}\right)^2\right)} \quad (4-2)$$

where  $f_r$  corresponds to the resonance frequencies so that a maximum loss factor occurs at these frequencies and  $b_w$  corresponds to the bandwidth factor. These parameters are set to the values tabulated in Table 1.

Duct	$\eta_1$	$\eta_2$	$\eta_3$	$\eta_4$	$bw_1$	$bw_2$	$bw_3$	$bw_4$
First duct with one flexible wall	6%	1.5%			10	10		
Corrugated duct	20%	22%	3.5%	2%	10	10	10	10

Table 1: Structural loss factors.

## 4.1 In-duct investigation

### 4.1.1 Duct with one flexible wall (internal propagation)

#### *Internal sound propagation for the unlined duct with one flexible wall*

The first series of measurements are performed on a duct with three rigid walls and a flexible plate made of steel (thickness: 0.5 mm). Measured and predicted internal transmission loss results are shown in Figure 13.

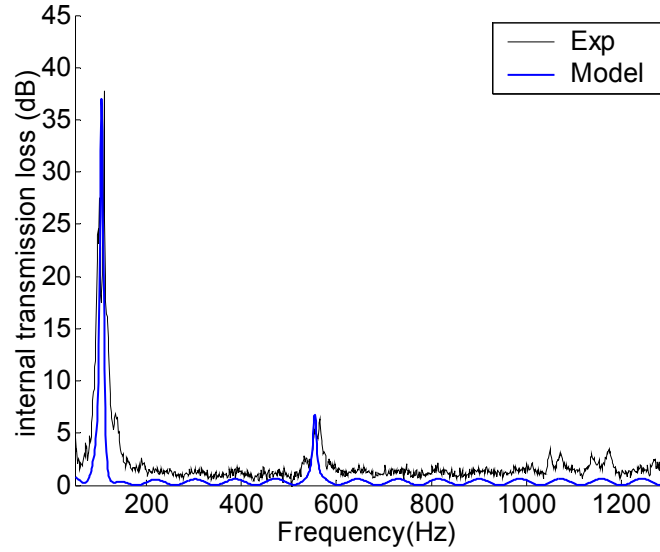


Figure 13: Predicted and measured internal transmission loss for the unlined rigid duct with one flexible plate.

The predictions are in acceptable agreement with the measured data, the discrepancy being approximatively 1 dB over the whole range frequency. The largest transverse dimension for this duct is 169 mm yielding a cut-off frequency of 1000 Hz. This can be seen in the measured plot with an increase of the number of peaks for frequencies above this cut-off frequency. Concerning now the resonances in the flexible wall corresponding to the peaks in the transmission loss, they occur twice within the investigated frequency range. The first one is attributed to a frequency of 93 Hz and 510 Hz for the second resonance. It can be mentioned that it has been necessary to adjust the value of the plate Young's modulus used in the model so both measured and theoretical resonance peaks would coincide. The value has to be increased by 40%. Inspection of the plate revealed that due to its small thickness (only 0.5 mm) it has been buckled and it is not flat when mounted.

### ***Internal sound propagation for the lined duct with one flexible wall***

Theoretical and measured internal transmission loss results are illustrated in Figure 14 and Figure 15 for the case when the polyurethane foam sheet is lined with no air gap.

In order to achieve this experimentally, the steel plate is taken off the duct and the liner piece is put in place so part of it comes off the top of the duct. The liner is then pushed evenly downwards with the aid of the flexible wall to ensure no air gap between the wall and the liner. The effect of lining the flexible wall with polyurethane foam on the measured internal transmission loss is seen in Figure 14.

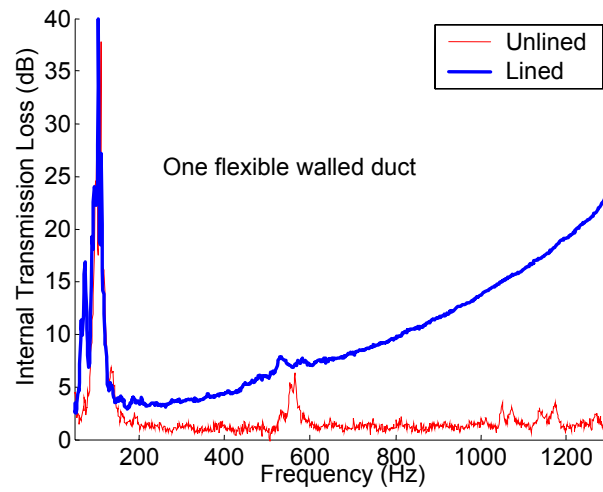


Figure 14: Experimental transmission loss for the one walled flexible duct.

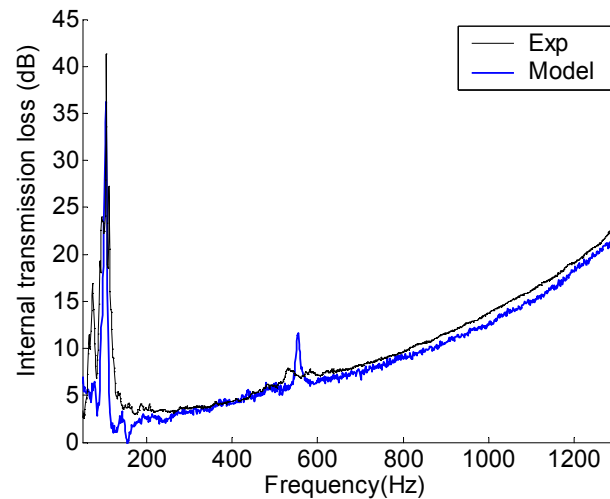


Figure 15: Predicted and measured internal transmission loss for the lined rigid duct with one flexible plate.

As seen from Figure 15, the presence of the liner does not shift the two resonance frequencies; however, the magnitudes are reduced. The first resonance occurring at a

frequency of 93 Hz is still the dominant peak. As expected lining the duct, even on only one wall improves drastically the internal transmission loss at high frequencies.

#### 4.1.2 Corrugated duct (Internal propagation)

The same measurements are performed on a corrugated duct of rectangular geometry. This time not only one but four walls vibrate.

##### *Internal sound propagation the unlined corrugated duct*

The transmission loss result for an empty duct is shown in Figure 16.

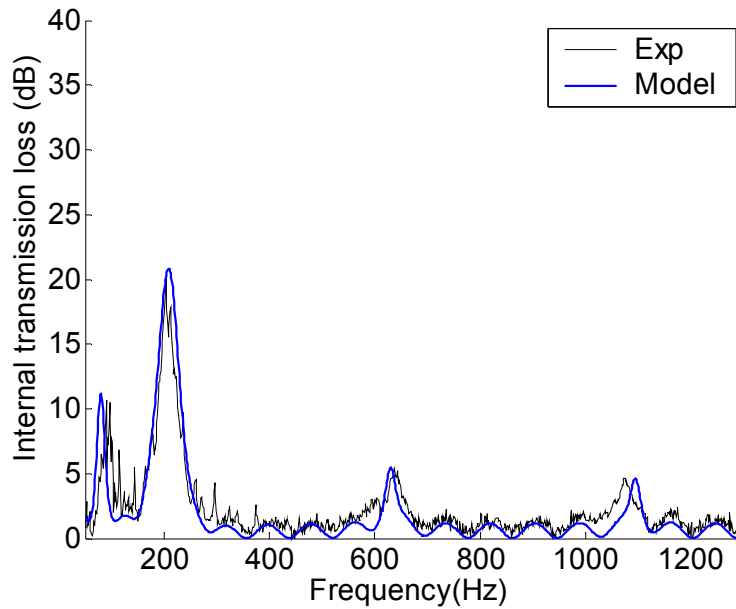


Figure 16: Predicted and measured internal transmission loss for the unlined corrugated duct.

Due to the fact that two pairs of walls of different lengths (150 and 200 mm) are excited, four resonance peaks are seen in Figure 16. A further analysis shows that these resonances occur at the following frequencies

Corrugated walls	Observed resonance frequencies
150 mm	82 Hz, 640 Hz
200 mm	213 Hz, 1109 Hz

Table 2: Resonance frequencies of the corrugated duct.

For each pair of walls, the first peak (82 Hz and 213 Hz) is the most dominant. In other



words, the transmission loss is maximal at these frequencies (10 dB and 20 dB respectively). The discrepancy between the fourth peak at the computed frequency of 1109 Hz and the measured resonance is mainly due to the cut-off frequency. For this corrugated duct, the cut-off frequency is 850 Hz, thus higher-order modes are propagating above this frequency. The thickness of the plate which gave the best fit to the resonance peak values was 1.02 mm, close to the 1 mm thickness obtained for the manufacturer's specifications. A sinusoidal oscillation in the transmission loss between resonance peaks can be observed. It is caused by the relatively inefficiency of the walls to attenuate the acoustic energy (less than 2 dB attenuation). A standing wave pattern composed of minima and maxima is created by the reflected waves interacting with the incident waves. This pattern does not differ greatly with the one observed in Figure 13 in the case of the duct with one flexible wall as both ducts have the same length (2m).

#### ***Internal sound propagation for the lined corrugated duct***

The porous material used previously in the first duct is now put on the bottom wall of the corrugated duct. As for the duct with one flexible wall (Figure 14), lining the corrugated duct modified the measured internal transmission loss curve in a similar fashion (Figure 17). Experimental and theoretical data for this lined corrugated duct are shown in Figure 18.

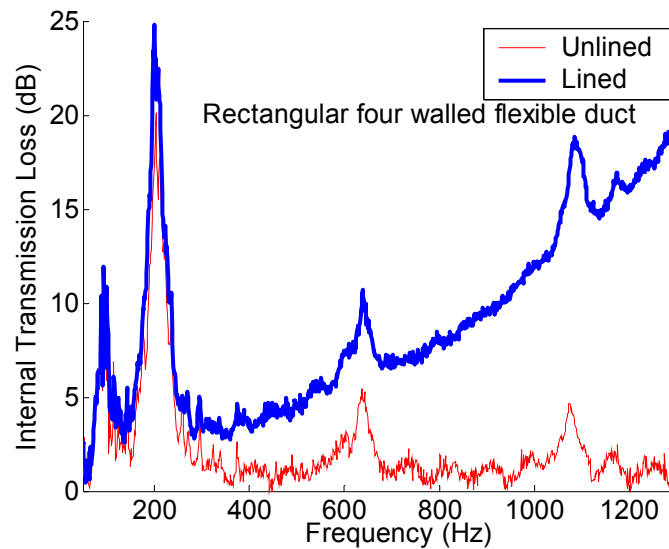


Figure 17: Experimental internal transmission loss for the lined corrugated duct.

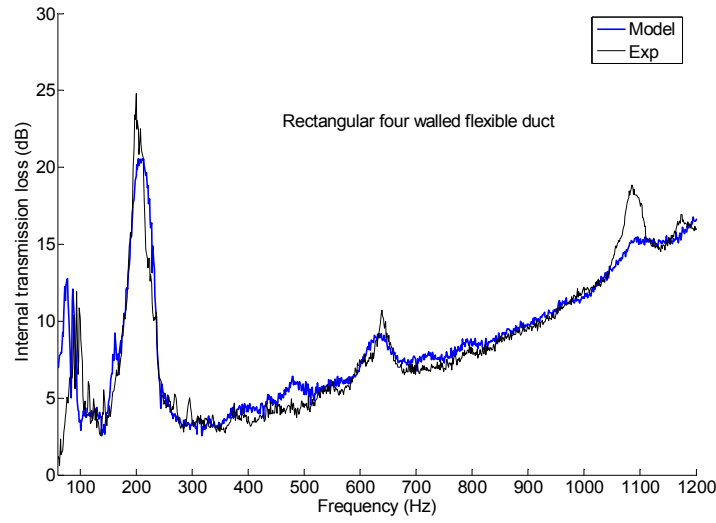


Figure 18: Internal transmission loss for the lined corrugated duct.

Comparison of Figure 15 (lined duct with one flexible wall) and Figure 18 (lined corrugated duct) shows, except at the peaks, transmission loss values that are more or less equal. In practice, this implies that the effect of flexible walls in a lined duct is only of importance around structural resonances, in particular the first.

#### 4.1.3 Internal sound propagation for the rigid walled duct

Measurements on the liner mounted in a rigid walled duct have also been performed to determine the liner properties, see appendix A. From these results, the transmission loss for a lined rigid walled duct can be obtained, see Figure 19.

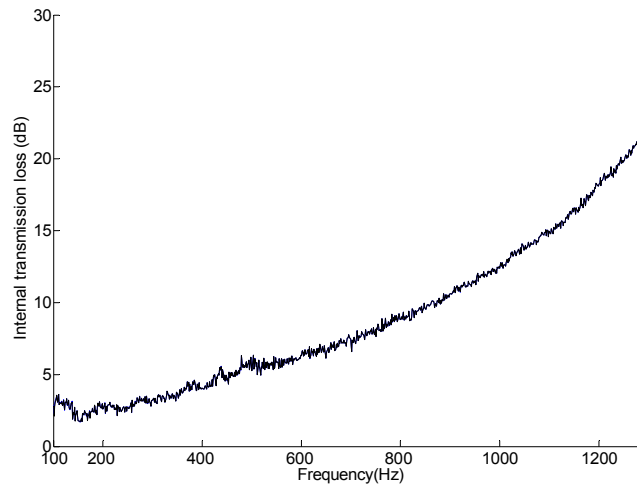


Figure 19: Measured internal transmission loss for the lined completely rigid duct.

In Figure 20, the transmission loss for all the three tested lined ducts is presented. As can be seen the differences are small except at the first resonance peak.

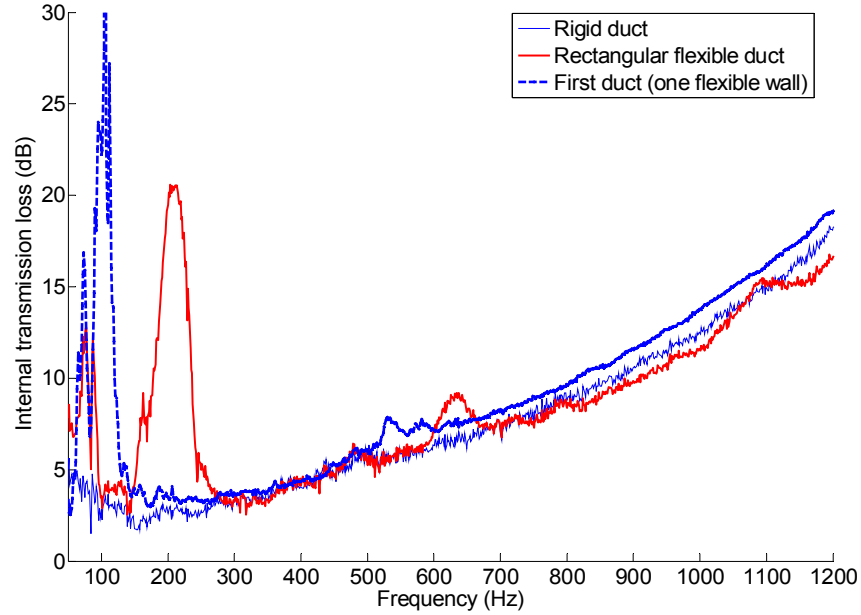


Figure 20: Comparison of measured internal transmission loss for the three lined ducts investigated.

## 4.2 Sound radiation investigation

The sound radiation from the ducts is measured and theoretically evaluated in the following section. Due to the uncertainties of the dynamic properties of the duct with a single flexible wall, only the sound radiation results for the corrugated are presented.

### *Sound radiation transmission loss for the corrugated unlined duct*

Measurement and theoretical radiation transmission loss results for the unlined corrugated duct are shown in Figure 21 in narrow band with the duct impedance  $Z_d$  determined experimentally (see (2-29)) or theoretically (see (2-36)) and in Figure 22 in 1/3 octave band.

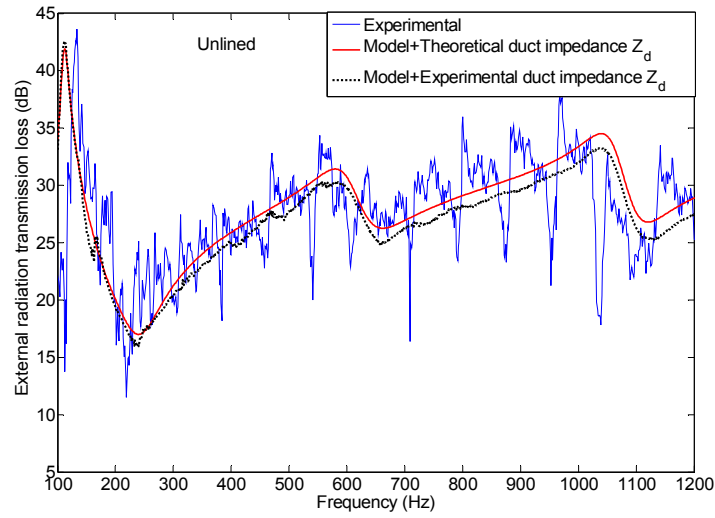


Figure 21: Radiation transmission loss for the unlined corrugated duct.

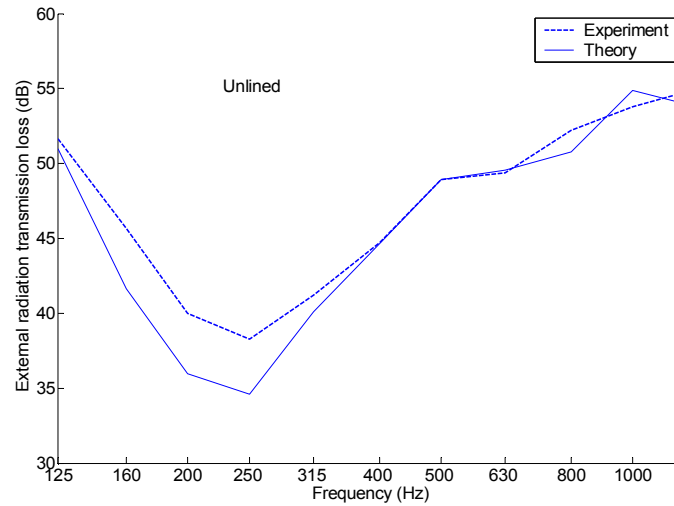


Figure 22: 1/3 octave band radiation transmission loss for the unlined corrugated duct.

A reasonable agreement between theory and measurement is observed. Four resonance dips are displayed at the same frequencies as the resonance peaks of the structural waves, see Figure 16.

### ***Sound radiation transmission loss for the corrugated lined duct***

The effect of lining the bottom of the corrugated duct on the radiation transmission loss is shown in Figure 23 and Figure 24.

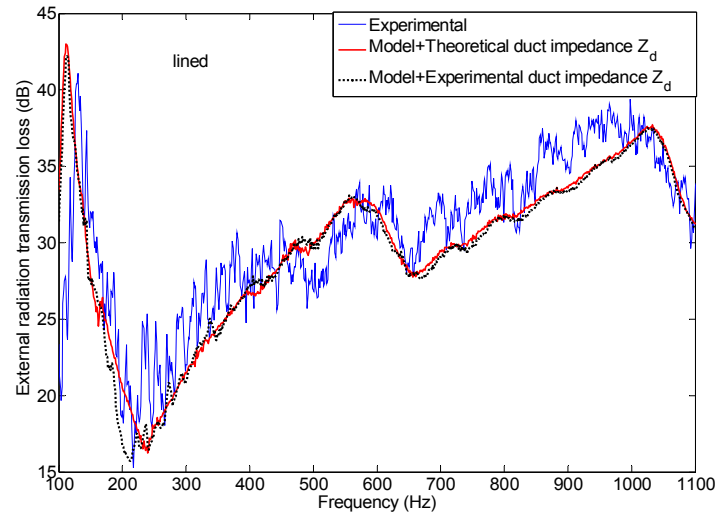


Figure 23: Predicted and measured radiation transmission loss for the lined corrugated duct.

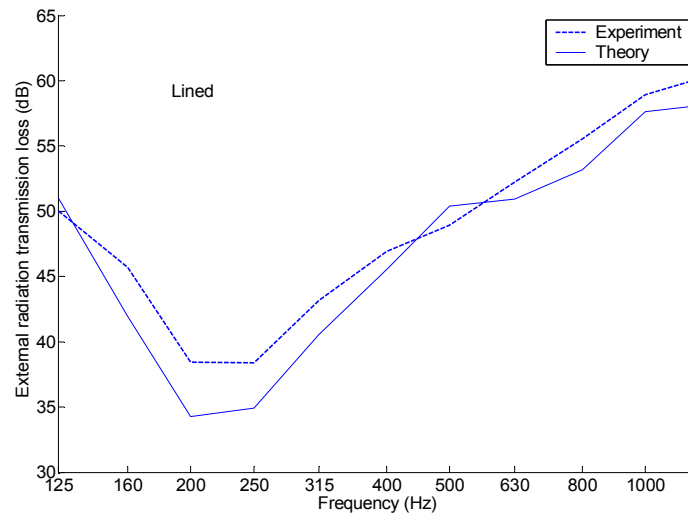


Figure 24: 1/3 octave band radiation transmission loss for the lined corrugated duct.

### 4.3 Parameter investigations

The effects of some parameters on the interior sound transmission are now investigated.

#### 4.3.1 Effect of liner positioning

The effect of the position of the liner material inside the duct with one flexible plate is now studied. Measurement of the transmission loss is performed and shown in Figure 25 for two different lining methods.

The liner is positioned at the flexible wall and at the opposite side against the rigid wall. In both cases there is no air gap between the liner and the wall.

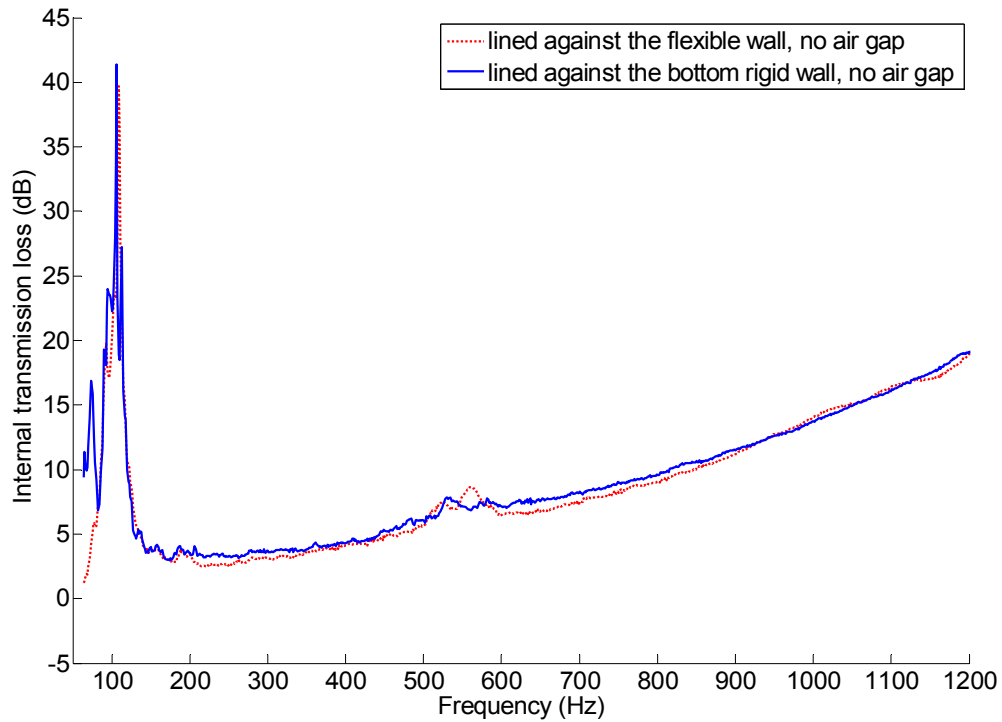


Figure 25: Influence of the lining position within the one walled flexible duct.

As can be seen from Figure 25 the position of the liner is not critical.

#### 4.3.2 Effect of structural conditions

Structural termination effects on the internal transmission loss for the first duct (single flexible wall) are studied and experimental results are given in Figure 26. Two termination conditions are studied: clamped and unclamped (Figure 7). The coupling between the acoustic and the structural wave is mainly important around the structural resonances. This is clear for instance from comparing the transmission loss for the lined flexible duct and the lined rigid duct in Figure 20. Also in Figure 26 one can see that the termination conditions affect the behaviour around the structural resonances.

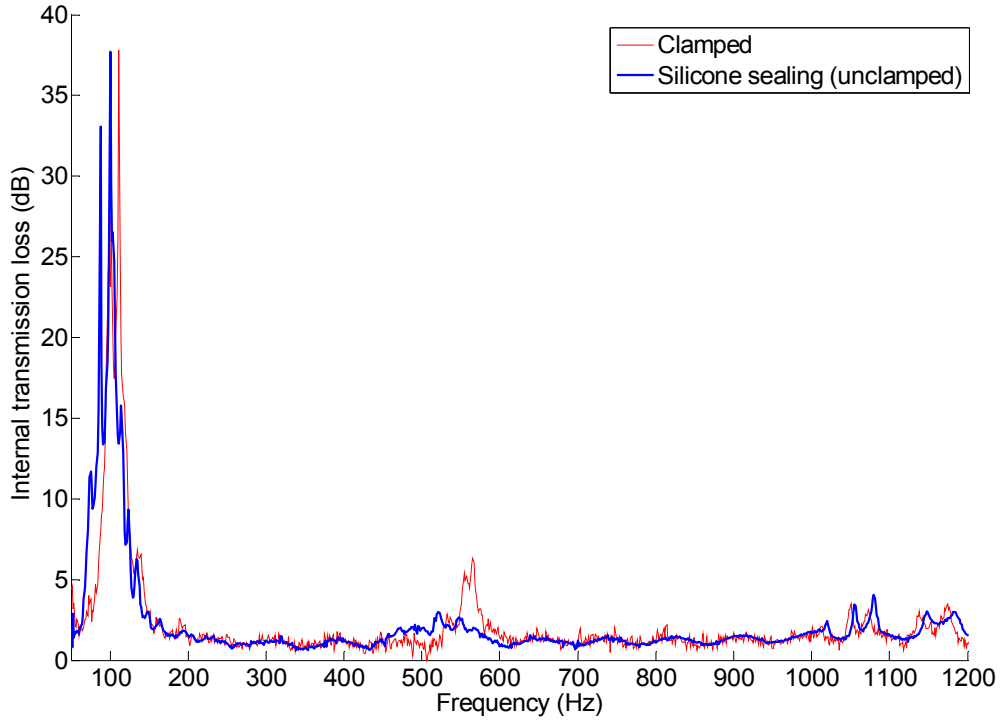


Figure 26: Internal transmission loss in the one walled unlined flexible duct with different experimental axial boundary conditions.

#### 4.3.3 Effect of the reflection in the airway

For a thorough treatment of the radiation to the surrounding, the calculation of the total internal sound pressure  $\hat{p}_{int}$  should include the reflected internal sound pressure waves  $\hat{p}_{-int}$  as

$$\hat{p}_{int}(z, t) = \hat{p}_{+,int} e^{i(\omega t - \alpha z)} + \hat{p}_{-,int} e^{i(\omega t + \alpha z)}. \quad (4-3)$$

That leads to

$$|\hat{p}_{int}|^2 = |\hat{p}_{+,int}|^2 + |\hat{p}_{-,int}|^2 + 2|\hat{p}_{+,int}||\hat{p}_{-,int}|\cos(2kz). \quad (4-4)$$

An average duct internal pressure is now defined

$$\langle |\hat{p}_{int}|^2 \rangle = \frac{1}{l} \int_0^l |\hat{p}_{int}|^2(z) dz = |\hat{p}_{+,int}|^2 + |\hat{p}_{-,int}|^2 + \frac{|\hat{p}_{+,int}| \times |\hat{p}_{-,int}|}{2kl} \sin(2kl), \quad (4-5)$$

where  $l$  is the axial length of the duct. As long as  $kl \gg 1$  the cross term can be neglected. Maximum reflectivity ( $R=1$ ) at the outlet of the duct implies then that  $\hat{p}_{+,int} = \hat{p}_{-,int}$  leading to a maximum internal duct power increase of 3 dB.





## **5. Conclusions**

In this paper low frequency (plane wave) transmission in lined ducts with flexible walls has been studied.

These models have been compared with experimental data and a satisfactory agreement has been obtained, especially for an industrial corrugated duct. The results are in accordance with the findings of Astley (1990) concerning the internal propagation and Cummings (1980) for the radiation. Peaks and dips attributed to resonances in the walls are well predicted.

The main contribution in this work is the implementation of the results in 2-port or transfer matrix form. The model can be implemented in the software code SID (developed at MWL) or in other codes based on this formulation.



## 6. References

1. Åbom M., 1999, *Determination of porous material data via two-port measurements*, Proceedings of Inter-Noise 99.
2. Almgren M., 1982, *Prediction of sound pressure level outside a closed ventilation duct – a literature survey*, Report F82-03, Chalmers University of Technology, Department of Building Acoustics.
3. ASHRAE, 2003, *ASHRAE HVAC Applications Handbook*, chapter 47: Sound and Vibration Control
4. Astley, R. J., 1990, *Acoustical modes in lined ducts with flexible walls. A variational approach*, Proceedings of Inter-Noise **90**, 575-578.
5. Astley R. J., 1991, *A finite element scheme for acoustic propagation in flexible-walled ducts with bulk-reacting liners, and comparison with experiment*, Journal of Sound and Vibration, **150**(1), 119-138.
6. Astley R. J., Cummings A., 1984, *A finite element scheme for acoustic transmission through the walls of rectangular ducts: comparison with experiment*, Journal of Sound and Vibration, **92**(3), 387-409.
7. Astley R.J., Cummings A., 1987, *A finite element scheme for attenuation in ducts lined with porous material: comparison with experiment*, Journal of Sound and Vibration, **116**(2), 239-263.
8. Astley R.J., Cummings A., Sormaz N., 1991, *A finite element scheme for acoustical propagation in flexible walled ducts with bulk reacting liners, and comparison with experiment*, Journal of Sound and Vibration, **150**, 119-138.
9. Bodén H., Åbom M., 1986, *Influence of errors on the two-microphone method for measuring acoustic properties in ducts*, Journal of the Acoustical Society of America, **79**(2), 541-549.
10. Bodén H., Carlsson U., Glav R., Wallin H. P., Åbom M., 2001, *Ljud och vibration*, Norstedts Tryckeri AB, Stockholm.

11. Brown G. L., Rennison D. C., 1974, *Sound radiation from pipes excited by plane acoustic waves*, Noise, Shock & Vibration Conference, Monash University, Melbourne.
12. Cabelli A., 1985<sup>a</sup>, *The propagation of sound in a square duct with a non-rigid side wall*, Journal of Sound and Vibration, **103**(3), 379-394.
13. Cabelli A., 1985<sup>b</sup>, *Application of the time dependent finite difference theory to the study of sound and vibration interactions in ducts*, Journal of Sound and Vibration, **103**, 13-23.
14. Cummings, A., 1976, *Sound attenuation in ducts lined on two opposite walls with porous material, with some applications to splitters*, Journal of Sound and Vibration, **49**(1), 9-35.
15. Cummings, A., 1978, *Low frequency acoustic transmission through the walls of rectangular ducts*, Journal of Sound and Vibration, **61**(3), 327-345.
16. Cummings, A., 1979<sup>a</sup>, *Low frequency sound transmission through the walls of rectangular ducts: further comments*, Journal of Sound and Vibration, **63**(3), 463-465.
17. Cummings, A., 1979<sup>b</sup>, *The effects of external lagging on low frequency sound transmission through the walls of rectangular ducts*, Journal of Sound and Vibration, **67**(2), 187-201.
18. Cummings, A., 1980, *Low frequency acoustic radiation from duct walls*, Journal of Sound and Vibration, **71**(2), 201-226.
19. Cummings, A., 1981<sup>a</sup>, *Design charts for low frequency acoustic transmission through the walls of rectangular ducts*, Journal of Sound and Vibration, **78**, 269-289.
20. Cummings, A., 1981<sup>b</sup>, *Stiffness control of low frequency acoustic transmission through the walls of rectangular ducts*. Journal of Sound and Vibration, **74**, 351-380.
21. Cummings, A. 1983<sup>a</sup>, *Approximate asymptotic solutions for acoustic transmission through the walls of rectangular ducts*, Journal of Sound and Vibration, **90**(2), 211-227.
22. Cummings, A., 1983<sup>b</sup>, *Higher order mode acoustic transmission through the walls of rectangular ducts*, Journal of Sound and Vibration, **90**(2), 193-209.
23. Cummings, A. 1994, *The attenuation of sound in unlined ducts with flexible walls*, Journal of Sound and Vibration, **174**(4),

24. Cummings, A., 2001, *Sound transmission through duct walls*, Journal of Sound and Vibration, **239**(4), 731-765.
25. Cummings A., Astley R.J., 1995, *The effects of flanking transmission on sound attenuation in lined ducts*, Journal of Sound and Vibration, **179**, 617-646.
26. Davies P. O. A. L., 1988, *Practical flow duct acoustics*, Journal of Sound and Vibration, **124**(1), 91-115.
27. Ducret F, Åbom M., 2003, *Low frequency sound propagation in rectangular ducts*, Tenth International Congress on Sound and Vibration, Stockholm, Sweden.
28. Elnady T., 2002, *On the use of liners to reduce aircraft jet engine noise*, Licenciate Thesis, Royal Institute of Technology, Department of Aeronautical and Vehicle engineering, TRITA-FKT 2002:26.
29. Glav R., 1994, *On acoustic modelling of silencers*, Doctoral thesis, Royal Institute of Technology, Department of Aeronautical and Vehicle engineering, TRITA-FKT Report 9435.
30. Kinsler L. E., Frey A. R., Coppens A. B., Sanders J. V., 1982, *Fundamentals of acoustics*, John Wiley & Sons, Inc.
31. Kirby R., Cummings A., 1998, *Structural/acoustic interaction in air-conditioning ducts in the presence of mean flow*, Proceedings of ISMA23, Leuven, Belgium, 677-684.
32. Martin V., 1991, *Perturbation of fluid-guided waves introduced by bending plates*, Journal of Sound and Vibration, **144**, 331-353.
33. Martin V., Cummings A., Gronier C., 2004, *Discrimination of coupled structural/acoustic duct modes by active control: principles and experiments results*, Journal of Sound and Vibration, **274**, 583-603.
34. Munjal M.L., 1987, *Acoustics of ducts and mufflers*, Wiley Interscience, New York.
35. Nygård S., 2000, *Modelling of low frequency sound in duct networks*, Licenciate Thesis, Royal Institute of Technology, Department of Aeronautical and Vehicle engineering, TRITA-FKT 2000:57.

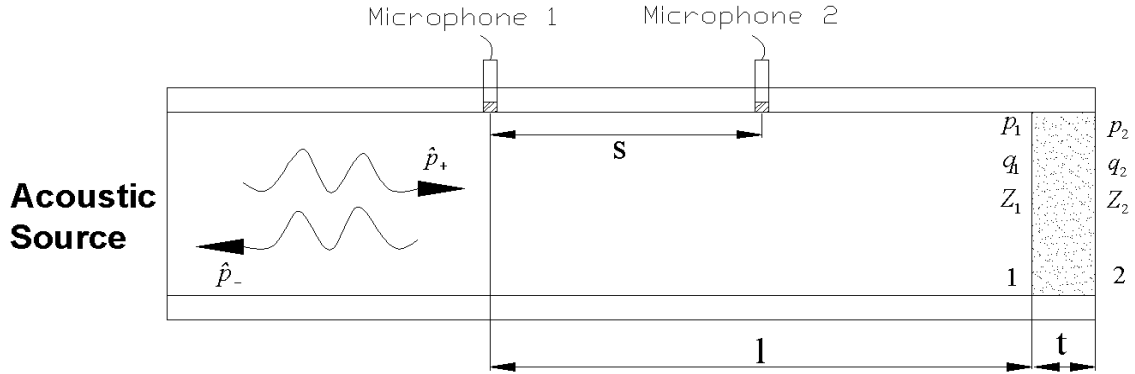


## Appendix A A note on measurement of liner properties

This section is devoted to the techniques used to measure liner properties; mainly the frequency dependent liner density  $\rho_a$  and complex wavenumber  $k_a$ . These parameters are necessary for analytical predictions of sound propagation through lined flexible ducts. Three techniques described in this section are tested. Results obtained from the one and two-sided techniques show some characteristics (resonances) which are not observed when the porous material is mounted in the test ducts. It is believed that these resonances are coupled to the mounting conditions used in these techniques since samples had to be cut and fit into a circular pipe. The last technique where the sample is mounted along a duct similar to the case of interest gave the most satisfactory results.

### *Two-microphone technique measurement (one-sided technique)*

The sample is mounted at the end of tube as shown in the following picture.



A two-microphone technique (Bodén & Åbom (1986)) is used to determine the normalized impedance  $\zeta_l$  on the surface of the sample of thickness  $t$ . Using the transfer function  $H_{12}$  between the microphone positions 1 and 2, the normalized impedance on the surface sample 1 is found to be

$$\frac{Z_1}{\rho c} R_a = \zeta_l = \frac{1 + R_1}{1 - R_1} = j \frac{H_{12} \sin kl - \sin k(l-s)}{\cos k(l-s) - H_{12} \cos kl}, \quad (\text{A-1})$$

where  $R_a$  is the sample cross-section area.

Employing the sample transfer matrix

$$\begin{bmatrix} \hat{p}_1 \\ \hat{q}_1 \end{bmatrix} = \begin{bmatrix} \cos(k_a t) & iZ_a \sin(k_a t) \\ i \sin(k_a t)/Z_a & \cos(k_a t) \end{bmatrix} \begin{bmatrix} \hat{p}_2 \\ \hat{q}_2 \end{bmatrix}, \quad (\text{A-2})$$

where  $Z_a = \rho_a c_a / R_a$ .

This leads to

$$Z_1 = \frac{\hat{p}_1}{\hat{q}_1} = \frac{\cos(k_a t) Z_2 + i Z_a \sin(k_a t)}{(i \sin(k_a t) / Z_a) Z_2 + \cos(k_a t)}, \quad (\text{A-3})$$

where  $Z_2 = \hat{p}_2 / \hat{q}_2$ .  $Z_a$  and  $\gamma_a$  are thus determined from the measurement of the normal incident impedance  $Z_1$  for samples of two different thickness  $t$ .

For an open end termination, three measurements are necessary:

-Measurement on an empty duct (no sample) for determination of  $Z_2$  (radiation impedance)

-Measurement of  $Z_{1,\text{sample } 1}$  and  $Z_{1,\text{sample } 2}$  for two samples of two different thicknesses  $t_1$  and  $t_2$

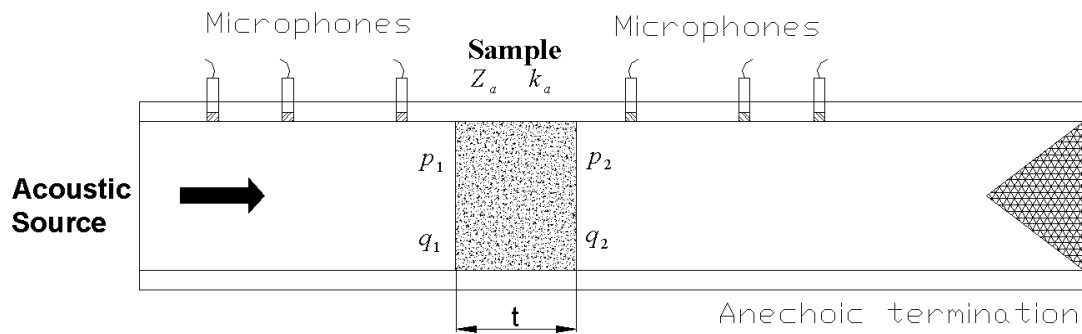
It follows that

$$Z_{1,\text{sample } 1} (i \sin(k_a t_1) Z_2 + Z_a \cos(k_a t_1)) - Z_a \cos(k_a t_1) Z_2 + i Z_a^2 \sin(k_a t_1) = 0, \quad (\text{A-4})$$

$$Z_{1,\text{sample } 2} (i \sin(k_a t_2) Z_2 + Z_a \cos(k_a t_2)) - Z_a \cos(k_a t_2) Z_2 + i Z_a^2 \sin(k_a t_2) = 0, \quad (\text{A-5})$$

Equations (A-4) and (A-5) can be solved iteratively using a Newton-Raphson scheme to obtain  $Z_a$  and  $k_a = \omega / c_a$ .

### ***Two-port measurement (two-sided technique)***



The sample is mounted in a rigid pipe. Cautions have to be taken to ensure no air gap between the wall of the pipe and the sample.

Measurement on each side of the sample using the two-microphone technique allows determination of the sample transfer matrix  $T$  (Åbom (1999))



$$\begin{pmatrix} \hat{p}_1 \\ \hat{q}_1 \end{pmatrix} = [T] \begin{pmatrix} \hat{p}_2 \\ \hat{q}_2 \end{pmatrix} = \begin{bmatrix} T_{11} & T_{12} \\ T_{21} & T_{22} \end{bmatrix} \begin{pmatrix} \hat{p}_2 \\ \hat{q}_2 \end{pmatrix} = \begin{bmatrix} \cos(k_a t) & iZ_a \sin(k_a t) \\ i \sin(k_a t) / Z_a & \cos(k_a t) \end{bmatrix} \begin{pmatrix} \hat{p}_2 \\ \hat{q}_2 \end{pmatrix}. \quad (\text{A-6})$$

Using the elements of the sample transfer matrix  $T$ , the sample properties can be derived as

$$Z_a = \frac{\rho_a c_a}{R_a} = \sqrt{\frac{T_{12}}{T_{21}}}, \quad (\text{A-7})$$

$$k_a = \frac{\omega}{c_a} = \frac{\ln\left(\frac{1}{2}(T_{11} + T_{22} + T_{12}/Z_a + T_{21}Z_a)\right)}{it}. \quad (\text{A-8})$$

### **Rigid duct**

Here the liner is mounted similar to the test cases but in a rigid walled duct as shown in Figure 27.

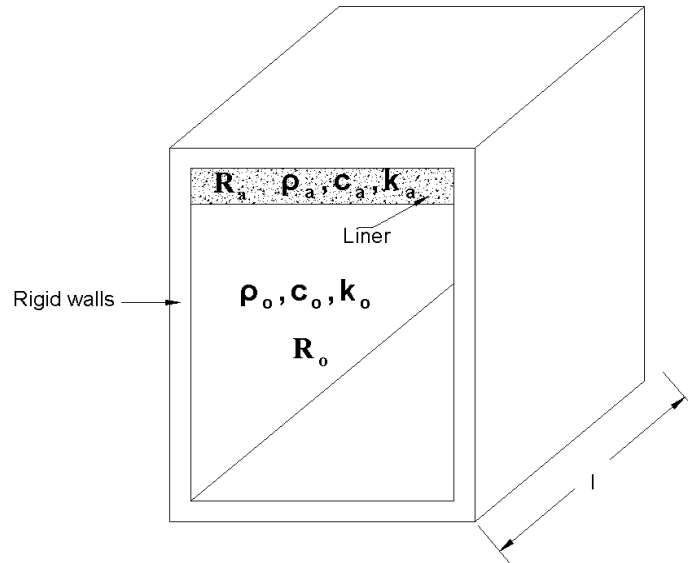


Figure 27: Rigid walled duct with liner.

The same pieces of liner remained in the bottom of the rigid duct. Using the two-microphone technique upstream and downstream of the duct as in the double-sided technique, it was possible to measure the transfer matrix for this complete rigid lined duct given as

$$\begin{pmatrix} \hat{p}_1 \\ \hat{q}_1 \end{pmatrix} = [T_d] \begin{pmatrix} \hat{p}_2 \\ \hat{q}_2 \end{pmatrix} = \begin{bmatrix} T_{11} & T_{12} \\ T_{21} & T_{22} \end{bmatrix} \begin{pmatrix} \hat{p}_2 \\ \hat{q}_2 \end{pmatrix} = \begin{pmatrix} \cos(\alpha l) & iZ_d \sin(\alpha l) \\ \frac{i \sin(\alpha l)}{Z_d} & \cos(\alpha l) \end{pmatrix} \begin{pmatrix} \hat{p}_2 \\ \hat{q}_2 \end{pmatrix}. \quad (\text{A-9})$$

Using this measured transfer matrix and assuming no reflected wave, it yields the experimental duct impedance  $Z_d$  expressed as (see (2-36))

$$Z_d = \frac{\hat{p}_+}{\hat{q}_+} = \frac{\omega}{\alpha \left( \frac{R_a}{\rho_a} + \frac{R_o}{\rho_o} \right)} = \sqrt{\frac{T_{12}}{T_{21}}}. \quad (\text{A-10})$$

The liner density  $\rho_a$  is hence

$$\rho_a = \frac{Z_d \alpha \rho_o R_a}{\omega \rho_o - R_o Z_d \alpha}. \quad (\text{A-11})$$

The complex axial wavenumber  $\alpha$  is obtained from the elements  $T_{11}$  and  $T_{12}$  in the measured transfer matrix  $T_d$  using (A-8).

For a rigid walled duct with no mean flow, Astley (1990) expresses the propagating coupled wavenumber  $\alpha$  as

$$\alpha = \sqrt{\frac{R_a \rho_o k_a^2 + R_o \rho_a k^2}{R_a \rho_o + R_o \rho_a}} \quad (\text{A-12})$$

Combining (A-11) and (A-12) gives the wavenumber  $k_a$  in the liner

$$k_a = \sqrt{\frac{R_o (\alpha^2 - k^2) \rho_a + R_a \rho_o \alpha^2}{R_a \rho_o}}. \quad (\text{A-13})$$

## ***Paper II. Aeroacoustic behaviour of tailpipes***

### **Abstract**

This paper investigates the influence of the opening geometry and upstream bends on the propagation and generation of sound in exhaust-system tailpipes found in cars or trucks. The muffler positioned upstream has to be acoustical designed in accordance with these termination effects. Starting with a reference straight pipe case, the author describes the acoustical behaviour in different regions. For the investigation of sound propagation, the acoustical excitation is provided at the inlet of the test rig by loudspeakers. The flow Mach number was varied over the range 0-0.2. Damping of the acoustical waves corresponding to the acoustical attenuation along the inside walls of the pipe is experimentally derived in conjunction with an array of six microphones. End effects are estimated from the pressure reflection coefficient and impedance at the opening. Sound transmission to the far-field is obtained with a rotating microphone in a reverberant room. This enables the determination of acoustical losses due to the vorticity after comparison with the incident acoustical power obtained from in-duct measurement. Two main mathematical models were employed to validate experimental data. The end effects are predicted from a model of Munt (1977, 1990) and validity of assumptions made in the model are discussed and experimentally proved. Absorption in the vorticity is calculated from an analytical model derived by Bechert (1980). The next step corresponds of an investigation on the influence of the opening geometry on the acoustic of the termination and on flow induced noise (loudspeaker turned off). Three main types are considered: oblique cuts, diffusers and bends. Flow generated noise is measured in the far-field by means of a rotating microphone for each termination for different Mach numbers. Empirical laws (scaling laws) can then be derived by combining the data from different flow speeds. The velocity dependence of these laws is of great importance to determine the aeroacoustic mechanism governing the sound generation.



## Table of Contents

1. Introduction .....	1
1.1 Earlier related work .....	2
1.1.1 Propagation in straight pipes .....	2
1.1.2 Radiation from openings .....	2
1.1.3 Flow generated noise .....	2
1.2 Pressure reflection coefficient and impedance at openings .....	5
1.3 Description of the airflow facility and two-microphone technique .....	6
2. Acoustics of a straight pipe .....	9
2.1 Methods and materials .....	9
2.1.1 Presentation of the straight pipe rig .....	9
2.1.2 Damping of plane wave .....	13
2.1.3 End correction .....	13
2.1.4 Sound absorption by vorticity shedding in the near field .....	14
2.2 Results and discussion .....	17
2.2.1 Internal damping in the boundary layer of a straight pipe .....	17
2.2.2 End correction .....	21
2.2.3 Sound absorption due to vorticity shedding .....	23
2.3 Summary .....	26
3. Acoustics of tailpipes .....	27
3.1 Methods and materials .....	27
3.1.1 Presentation of the tailpipe rig .....	27
3.1.2 Presentation of the tailpipe elements .....	29
3.1.3 Modelling of pressure reflection coefficients and impedances .....	33
3.1.4 Experimental procedures .....	36
3.2 Results and discussion .....	36
3.2.1 Reflection coefficient and impedance .....	36
3.3 Summary .....	64
4. Modelling of exhaust lines .....	65
4.1 Description of an exhaust line .....	65
4.2 The automotive exhaust line .....	67
4.3 The single pipe exhaust line .....	71
4.4 Summary .....	74
5. Flow noise for a straight pipe and tailpipes .....	75
5.1 Methods and materials .....	75
5.1.1 Measurement of flow-induced noise in a reverberant room .....	75
5.1.2 Flow noise generation for a straight pipe .....	76
5.1.3 Scaling laws .....	78
5.2 Results and discussion .....	82
5.2.1 Scaling law results for a straight pipe .....	82
5.2.2 Flow-induced noise and scaling law results for tailpipes .....	82
5.2.3 Scaling laws review .....	89
5.3 Summary .....	92
6. Summary and conclusions .....	93
7. References .....	97



# **1. Introduction**

A typical modern exhaust system is composed of one or several mufflers, a device for exhaust gas cleaning and an exhaust pipe also called tailpipe. Exhaust pipes are inevitably associated with cars, trucks and motorcycles. They can also be found in gas turbine and jet engine systems. Exhaust noise is an important source of noise from an internal combustion (IC) engine and effective exhaust mufflers are therefore needed. Exhaust noise can also radiate mainly from the shell of expansion chamber mufflers. Exhaustive research has been conducted on mufflers to find efficient types that with a minimum pressure drop can sufficiently reduce the pressure pulsations emitted from the engine manifold.

Mufflers are also to be found also in heating, ventilation and air-conditioning systems. Two types of muffler exist. Reactive mufflers based on impedance mismatching that create reflection of sound; this is usually done by a sudden change of geometry such as an expansion chamber. Dissipative mufflers are characterised by the presence of porous material or flow constrictions. Acoustical energy is dissipated through visco-thermal effects in the porous material or via turbulence dissipation. Usually, both of these mechanisms are present in a muffler. The impedance mismatch is used for low frequencies (tones) and the dissipative mechanism at mid and high frequencies. For high flow speeds, care must be taken so that the aeroacoustic noise produced by the muffler itself does not become a problem. Mufflers have to be compact to fit , e.g., under a car.

In this paper the aeroacoustics of different exhaust tailpipes is investigated. Both the acoustic impedance and the flow generated noise are investigated experimentally.

We start by investigating the different regions of a straight pipe with open end termination. This study aims to set the foundations for another investigation concerning the effects of changing the termination geometry (oblique cuts, diffusers and bends).

## **1.1 Earlier related work**

### **1.1.1 Propagation in straight pipes**

The standard analytical model for sound attenuation (damping) inside a pipe with no flow is that of Kirchhoff (1868). Davies (1988) has suggested an ad hoc modification of the Kirchhoff formula for the flow case. Howe (1995) also discusses the damping of sound in the internal shear boundary layer of a pipe. Measurement of the damping with a multi-microphone technique has been previously carried out by Peters and al. (1993) and is reproduced in this thesis. A six-microphone array technique which treats individually two clusters of three flush mounted microphones is performed. The technique allows computations of complex wavenumber from which the attenuation can be extracted.

### **1.1.2 Radiation from openings**

Theoretical investigation on the acoustics of the opening of a straight pipe without a mean flow has been done by Levine & Schwinger (1948). Munt (1977, 1990) has extended this work to the case with flow. The main assumptions in Munt's model are the use of a full Kutta condition at the opening and the description of the jet out of the semi-infinite pipe as cylindrical and bounded by an unstable vortex layer.

A flow jet at the opening of a straight pipe is unstable and turbulent. Forced vortex shedding at the duct outlet edge can absorb acoustical energy before it reaches the far field (Bechert (1980), Howe (1980)). A method using in-duct measurement to determine the incident power and a measurement (radiated power) in a reverberation room enables the investigation of the rate of the acoustic energy converted into vorticity for a straight pipe. The experimental data is compared with the analytical model of Bechert (1980). Experimental and theoretical studies of sound propagation in diffusers and bends can be found in Dequand and al. (2002), van Lier (1999), van Lier and al. (2001) and Huijnen (1998).

### **1.1.3 Flow generated noise**

Concerning the noise generated by the airflow the work of Kuhn & Morfey (1976) can be mentioned. The scaling law technique proposed by Nelson & Morfey (1981) is used here to derive scaling laws for various tailpipe geometries. These laws are necessary to



predict the flow noise sound power level for a specific configuration and flow speed. Nelson & Morfey (1981) regard the flow separation process as a dipole type of source. In other words, the physical mechanism of flow noise sound production can be summarized as a fluctuating force acting at a specific position in the element. A similar investigation on flow noise has been performed earlier for other geometries by Girath and al. (2001) and Nygård (2000).

The present document consists of four main parts. The first one concerns only the straight pipe for which open-end reflection coefficient and impedance are treated theoretically and experimentally under the variation of the flow Mach number. The damping of the sound wave inside the pipe, the end correction and the absorption by vorticity are also discussed.

The second part deals with tailpipes of various geometries (oblique cuts, diffusers and bends). Only one aspect is considered for the tailpipe investigation: the sound pressure reflection coefficient and impedance at the inlet and outlet. Measured low frequency diffuser termination impedances are used in section three for calculation of the performance of an exhaust line terminated by a diffuser. This shows the influence of diffusing geometries and the flow Mach number on the efficiency to attenuate sound at low frequency in an exhaust line. The fourth section concerns the sound power levels of flow generated noise and presents scaling laws for the straight pipe and tailpipes. The methodology systematically undertaken in this section is the comparison of the flow noise produced by the tailpipes with the straight-pipe (reference case) results.



# 1. General methodology

This section describes the experimental rigs and theoretical analysis used for the investigation of the acoustics of a straight pipe and tailpipes. The flow noise generated from a straight pipe and tailpipes is treated in a separate chapter.

For both rigs, a rotating microphone is located in a reverberant room to measure the flow noise. An additional measurement was performed using the rotating microphone for the first straight pipe; the radiation of the sound from the straight pipe rig. It is required to estimate the sound absorption in the vorticity.

## 1.2 Pressure reflection coefficient and impedance at openings

### *Prediction of pressure reflection coefficient and impedance at openings*

Evaluation of the performance of exhaust systems requires the determination of the acoustic properties at the opening such as the pressure reflection coefficient  $R$ . The calculation of this pressure reflection coefficient has been performed using a MATLAB model coded by two master students (Bierkens (2002), in't panhuis (2003)) from the Eindhoven university of Technology (TUE). Their model calculates the complex valued pressure reflection coefficient  $R$  at an opening of radius  $r$  and with outlet flow Mach number  $M$  based on two papers written by Munt (1977, 1990). It is believed that this rather mathematically involved model is presently the most refined and accurate .

Starting with the wave equation with velocity potential as variable, Munt (1977, 1990) splits the problem in terms of the polar coordinate system. In the radial direction, the solution can be solved analytically as the mode shape is known and is function of the radial direction  $r$ . The axial direction aspect is treated through the Wiener-Hopf technique (Fourier transform of the wave equation with specific boundary conditions). The wave is assumed to be monochromatic for ease of mathematical derivation. The boundary condition states that at the lips the velocity is finite (full Kutta condition) and the flow jet is leaving the pipe uniformly with a thin cylindrical boundary layer. This assumption is experimentally obtained for sharp edged pipe lips.

### 1.3 Description of the airflow facility and two-microphone technique

Air flow was provided from the flow facility located on the KTH/MWL service floor ; a maximum flow rate of  $10 \text{ m}^3/\text{s}$  and pressure up to  $10 \text{ kPa}$  can be achieved. The flow is taken to an anechoic room acting as a settling chamber. The pressurised anechoic room then creates a flow in the test duct mounted between this room and the reverberation room (see Figure 2).

A smooth inlet cone situated in the anechoic room is connected to the inlet of the rig to ensure minimum flow background noise. Preliminary tests showed dips in the measurement of the coherence function at the microphones due to resonances in the pipe. In order to reduce these standing waves in the rig, an ordinary car muffler is inserted upstream in the rig. Sufficient levels of excitation during measurement at higher flow speeds is provided by two loudspeakers mounted onto the pipe further downstream.

The airflow Mach number  $M$  measurement procedure consists of a Pitot tube connected to a pressure transducer to ensure measurements of flow speeds in the pipe. The Pitot tube is aligned with the centreline of the pipe where measurement of maximum velocities is performed. For  $4 \times 10^3 \leq \text{Re} \leq 3.2 \times 10^6$ , the ratio of the mean to the maximum velocity is  $U_{\text{mean}}/U_{\text{max}} = 0.8$  (Schlichting (1968)). The flow Mach number  $M$  and wavenumber  $k_{+/-}$  are assumed to be independent of the axial position (Peters and al. (1993)).

For the plane wave decomposition in the pipes, the two microphone technique described in Åbom & Bóden (1988) is used. It is based on the transfer function between two flush mounted microphones. The reflection coefficient and normal impedance can then be calculated and moved to a specific position in the pipe.

The normalised<sup>1</sup> acoustic impedance  $Z$  is calculated from the complex reflection coefficient  $R$  using

$$Z = (1 + R)/(1 - R). \quad (1-1)$$

The measurable frequency range in the two-microphone technique is determined from the distance  $s$  between the microphones and is given (for no flow) as

---

<sup>1</sup> In this paper  $Z$  refers to both the specific and normalised acoustic impedance. This is not completely correct, the normalised impedance should be denoted as  $\zeta$  as in paper III.

$$f_{min} = \frac{0.05c_0}{S} \leq f \leq f_{max} = \frac{0.4c_0}{S}, \quad (1-2)$$

where  $c_0$  is the speed of sound.

The acoustical excitation is provided by a loudspeaker mounted upstream. Random noise is generated for lower velocity cases (up to 40 m/s). In cases of a Mach number greater than 0.1, a stepped-sine acoustic excitation was shown to be more satisfactory to reach a good signal-to-noise ratio.

The straight pipe rig consists of an array of six microphones whereas three microphones are used for the tailpipes studied (different rig). The measured pressure reflection coefficient  $R_l$  at microphone 1 for either rig is for example moved to the opening as follows

$$R_{opening} = R_l e^{(2ikl/(1-M^2))}, \quad (1-3)$$

where  $k=\omega/c_0$ ,  $M$  is the Mach number and  $l$  is the distance separating the reference microphone to the straight pipe open end or to the tailpipe inlet as shown in Figure 1. The acoustical damping over the length  $l$  is neglected.

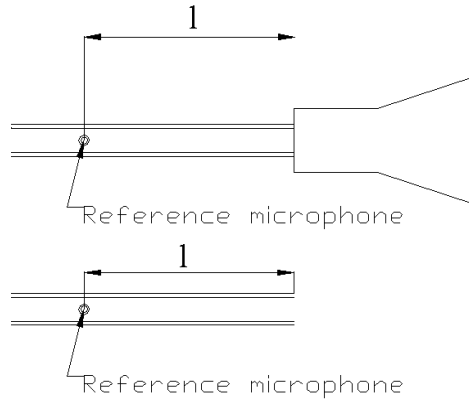


Figure 1: Distance reference microphone to pipe opening or tailpipe inlet.



## 2. Acoustics of a straight pipe

This section details the experimental techniques and models used to determine the damping, reflection coefficient and impedance at the opening and losses due to vorticity shedding for a straight pipe. The results of the experimental investigations are also presented.

### 2.1 Methods and materials

#### 2.1.1 Presentation of the straight pipe rig

The rig as shown in Figure 2 was constructed entirely of a single straight steel pipe of length of 6 m, thickness of 2 mm and inner diameter of 35 mm (cut-off frequency of 5800 Hz). Six microphones are flushed mounted and are arranged in two clusters. Cluster I is composed of microphones 1, 2 and 3 and cluster II corresponds to microphones 4, 5 and 6.

The two-microphone technique frequency criteria (see equation (1-2)) implies

	Cluster I		Cluster II	
	Microphone 1 and 2, $s_{12}=28$ mm	Microphone 1 and 3, $s_{13}=218$ mm	Microphone 6 and 5, $s_{65}=28$ mm	Microphone 6 and 4, $s_{64}=173$ mm
<b>Two- microphone frequency criteria (Hz)</b>	$610 \leq f \leq 4900$	$80 \leq f \leq 640$	$610 \leq f \leq 4900$	$100 \leq f \leq 800$

The measurement is performed for various flow speeds in the pipe measured with a Pitot-tube probe and is tabulated

<b>Pitot-tube reading (m/s) (maximum velocity at the pipe centreline)</b>	18	32	47	61	76
---	----	----	----	----	----

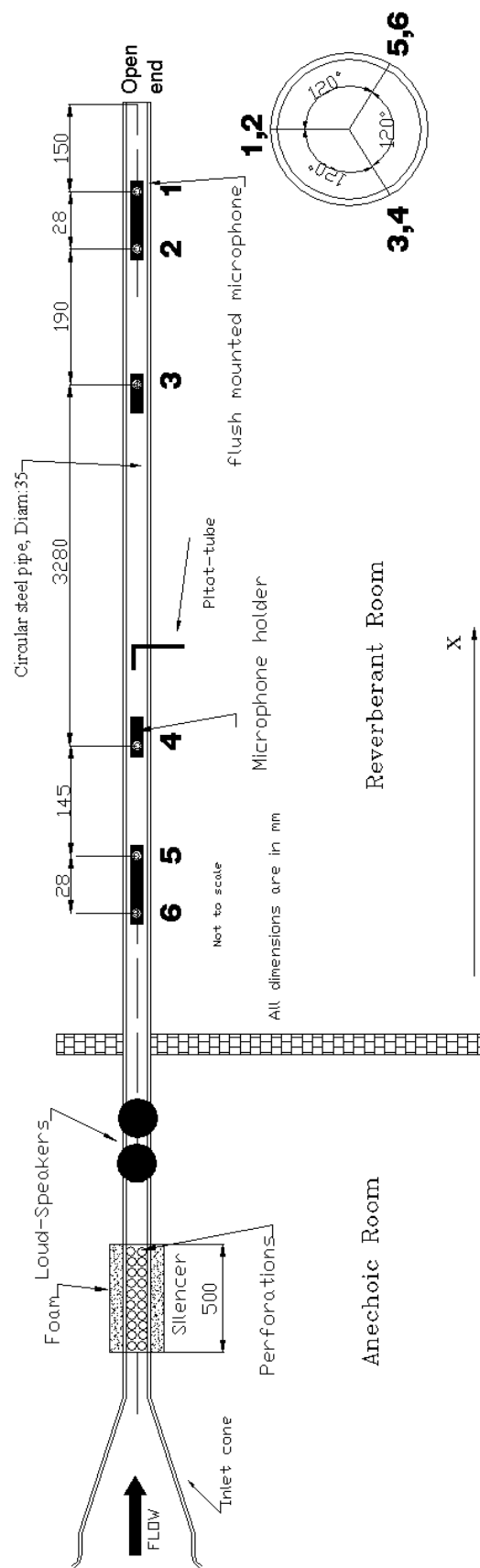


Figure 2: Layout of the straight pipe rig.



### Cluster technique

A refined experimental determination of the sound propagation in a pipe is carried out with an array of six microphones located into two distant clusters. In each cluster, one microphone signal is chosen as reference for determination of the reflection coefficient through the means of the standard two-microphone technique (Åbom & Bodén (1988)). Microphone 1 in cluster I was preferred as reference for its proximity to the opening of the pipe. In cluster II microphone 6 which is closest to the loudspeaker was chosen.

The complex valued pressure  $\hat{p}_n(x) = \hat{p}_n^+(x) + \hat{p}_n^-(x)$  at the microphone  $n$  consists of two travelling pressure waves  $\hat{p}_n^+$  and  $\hat{p}_n^-$ .

This implies at Cluster II: microphones 4, 5, 6 (reference)

$$\hat{p}_6 = \hat{p}_6^+ + \hat{p}_6^-, \quad (2-1)$$

$$\hat{p}_5 = \hat{p}_6^+ e^{-ik_+(x_5-x_6)} + \hat{p}_6^- e^{ik_-(x_5-x_6)}, \quad (2-2)$$

$$\hat{p}_4 = \hat{p}_6^+ e^{-ik_+(x_4-x_6)} + \hat{p}_6^- e^{ik_-(x_4-x_6)}, \quad (2-3)$$

where  $k_{\pm}$  are the wavenumbers in the positive and negative directions.

Evaluation in matrix form gives

$$\begin{pmatrix} \hat{p}_6^+ \\ \hat{p}_6^- \end{pmatrix} = \frac{1}{e^{ik_-(x_5-x_6)} - e^{-ik_+(x_5-x_6)}} \begin{pmatrix} e^{ik_-(x_5-x_6)} & -1 \\ -e^{-ik_+(x_5-x_6)} & 1 \end{pmatrix} \begin{pmatrix} \hat{p}_6 \\ \hat{p}_5 \end{pmatrix}, \quad (2-4)$$

which leads to

$$\hat{p}_6^+ = \frac{1}{e^{ik_-(x_5-x_6)} - e^{-ik_+(x_5-x_6)}} (e^{ik_-(x_5-x_6)} \hat{p}_6 - \hat{p}_5), \quad (2-5)$$

$$\hat{p}_6^- = \frac{1}{e^{ik_-(x_5-x_6)} - e^{-ik_+(x_5-x_6)}} (-e^{-ik_+(x_5-x_6)} \hat{p}_6 + \hat{p}_5). \quad (2-6)$$

This implies that

$$R_6 = \frac{\hat{p}_6^-}{\hat{p}_6^+} = \frac{-e^{-ik_+(x_5-x_6)} \hat{p}_6 + \hat{p}_5}{e^{ik_-(x_5-x_6)} \hat{p}_6 - \hat{p}_5}. \quad (2-7)$$

To minimise the effect of noise on the measured data, equation (2-7) can be written in terms of transfer functions  $H_{en} = \hat{e}_n / \hat{e}$  where  $\hat{e}_n$  is the output voltage from microphone  $n$  and  $\hat{e}$  is the voltage to the loudspeaker in the test rig.

Equations ((2-5), (2-6), (2-7) can be rewritten in terms of these measured transfer functions

$$H_{\hat{e}\hat{e}_6} = \frac{1}{e^{ik_-(x_5-x_6)} - e^{-ik_+(x_5-x_6)}} \left( e^{ik_-(x_5-x_6)} H_{\hat{e}_6} - H_{\hat{e}_5} / H_{65c} \right), \quad (2-8)$$

$$H_{\hat{e}\hat{e}_6^-} = \frac{1}{e^{ik_-(x_5-x_6)} - e^{-ik_+(x_5-x_6)}} \left( -e^{-ik_+(x_5-x_6)} H_{\hat{e}_6} + H_{\hat{e}_5} / H_{65c} \right), \quad (2-9)$$

where  $H_{65c} = H_{\hat{e}_5c} / H_{\hat{e}_6c}$  is obtained from the microphone calibration procedure in which the two microphones are exposed to the same acoustic pressure.

Equations (2-8) and (2-9) imply that the pressure reflection coefficient at microphone 6 is

$$R_6 = H_{\hat{e}\hat{e}_6^-} / H_{\hat{e}\hat{e}_6^+}. \quad (2-10)$$

Using the same procedure with the microphone pair 4 and 6 a lower frequency range is covered.

The procedure is repeated for cluster I composed of microphones 3, 2, 1(reference) to obtain the pressure reflection  $R_I$  at microphone 1.

Referring to cluster I, one derives for microphone 1 and 2

$$H_{\hat{e}\hat{e}_1^+} = \frac{1}{e^{-ik_-(x_2-x_1)} - e^{ik_+(x_2-x_1)}} \left( e^{-ik_-(x_2-x_1)} H_{\hat{e}_1} - H_{\hat{e}_2} / H_{12c} \right), \quad (2-11)$$

$$H_{\hat{e}\hat{e}_1^-} = \frac{1}{e^{-ik_-(x_2-x_1)} - e^{ik_+(x_2-x_1)}} \left( -e^{ik_+(x_2-x_1)} H_{\hat{e}_1} + H_{\hat{e}_2} / H_{12c} \right), \quad (2-12)$$

$$R_1 = H_{\hat{e}\hat{e}_1^-} / H_{\hat{e}\hat{e}_1^+}. \quad (2-13)$$

The cluster technique can be used to determine the damping in the pipe. Two formulations can be used. The first one (performed by the author) uses the travelling pressure to determine the complex wavenumber whereas the second method (derived by Peters and al. (1993)) uses the pressure reflection coefficient. The damping technique consists essentially in combining the results obtained separately from the two clusters of microphones.

It can be demonstrated that the relations between the travelling pressures at microphone 1 and 6 can be written as

$$e^{-ik_+(x_1-x_6)} = \hat{p}_1^+ / \hat{p}_6^+ = \left( H_{\hat{e}\hat{e}_1^+} / H_{\hat{e}\hat{e}_6^+} \right) H_{16c}, \quad (2-14)$$

$$e^{ik_-(x_1-x_6)} = \hat{p}_1^- / \hat{p}_6^- = \left( H_{\hat{e}\hat{e}_1^-} / H_{\hat{e}\hat{e}_6^-} \right) H_{16c}. \quad (2-15)$$

Experimentally derived wavenumbers  $k_{+/-}$  are extracted from (2-14) and (2-15) and reinserted into the two-microphone technique ((2-8) and (2-11),(2-9) and (2-12)) for

each cluster iteratively until convergence is obtained. As starting values for the iteration technique the classical no flow value for the wavenumber are used, i.e.,  $k_{+/-} = \omega/c_0$ . A damping coefficient  $\alpha_{+/-}$  is finally obtained from the absolute value of the imaginary part of  $k_{+/-}$ . An improved value for the complex reflection coefficient is thus obtained from this method.

### 2.1.2 Damping of plane wave

#### *Damping modelling*

The interior losses in the fluid can normally be neglected (Pierce (1989)). Kirchhoff (1868) derived a formulation (2-16) for the visco-thermal damping that occurs in the boundary layer in a straight pipe without flow. The second term in (2-16) proportional to  $(1/Sh^2)$  was added by Ronneberger (1975) and Tijdeman (1975). The attenuation of acoustical energy  $\alpha$  is expressed as the imaginary part ( $\alpha = \text{Im}(k)$ ) of the wave number  $k_{no\ flow}$  expressed as

$$k_{no\ flow} = \frac{\omega}{c_0} \left( 1 + \frac{1-i}{\sqrt{2}} \frac{1}{Sh} \left( 1 + \frac{\gamma-1}{Pr^{1/2}} \right) - \frac{i}{Sh^2} \left( 1 + \frac{\gamma-1}{Pr^{1/2}} - \frac{1}{2} \gamma \frac{\gamma-1}{Pr} \right) \right) = \frac{\omega}{c_0} - i\alpha, \quad (2-16)$$

where  $\gamma$  is the specific heat ratio,  $Sh = a\sqrt{(\rho_0\omega/\mu)}$  is the shear wavenumber of a pipe of radius  $a$ ,  $\rho_0$  is the density and  $\mu$  is the shear viscosity coefficient,  $Pr = \mu C_p / \kappa$  is the Prandtl number,  $C_p$  is the specific heat coefficient and  $\kappa$  is the thermal diffusivity.

The modified Kirchhoff's formulation suggested by Davies (1988) for the acoustic wavenumber  $k_+$  and  $k_-$  propagating respectively with and against the flow is expressed as

$$k_+ = \frac{k_{no\ flow}}{1 + M}, \quad k_- = \frac{k_{no\ flow}}{1 - M}. \quad (2-17)$$

The corresponding attenuations are  $\alpha_+ = \text{Im}(k_+)$  and  $\alpha_- = \text{Im}(k_-)$ .

### 2.1.3 End correction

#### *Definition*

The end correction corresponds to the extended length required to obtain a phase shift of  $180^\circ$  between the incident and reflected wave. Its value normalised with respect of the pipe radius is influenced by the opening geometry (Peters and al. (1993)) and by flow

(Boij (2003)). The low and high Strouhal limits of the magnitude of the end correction have been found experimentally and theoretically to not be modified under the variation of flow Mach number  $M$ . However, for intermediate Strouhal number around the vicinity of  $St=1$ , the end correction behaviour is changed for different flow conditions due to the strong coupling flow-acoustic fields in this region.

### ***End correction determination***

The end correction  $\delta$  can be defined as the extra length that must be added to the pipe to produce a reflection coefficient of -1. This implies

$$R = |R_0| e^{i\left(\theta + \frac{2k\delta}{1-M^2}\right)} = |R_0| e^{i\pi} , \quad (2-18)$$

where  $R$  is the reflection coefficient at the opening.

The definition of the normalised end-correction  $\delta$  is

$$\frac{\delta}{a} = \frac{(\theta - \pi)(1 - M^2)}{2ka} , \quad (2-19)$$

where  $\theta$  is the phase of the reflection coefficient  $R$  obtained from theoretically Munt's model (1977, 1990) or experimentally from the cluster technique and  $a$  is the pipe radius.

Another way to derive the end correction is through the imaginary part of the termination impedance  $Z$ ,

$$Z = \frac{\hat{p}}{\hat{q}} = R_Z + jX_Z . \quad (2-20)$$

The end correction  $\delta$  can then be derived from the reactance  $X_Z$  as

$$\frac{X_Z}{\rho_0 c_0} S = k\delta , \quad (2-21)$$

where  $S$  is the pipe cross-section.

The normalised reactance  $X_Z$  is obtained from (1-1).

### **2.1.4 Sound absorption by vorticity shedding in the near field**

This section looks at the sound dissipation through vorticity. Flow separation at the lips of the pipe (vorticity shedding) is known to absorb the acoustic energy (Bechert (1980), Howe (1980)). The sound wave energy is converted into vortex kinetic energy. The

vortices are propagating further downstream before they break up into turbulence and converted into heat. An analytical model derived by Bechert (1980) is reviewed and used to predict the losses due to vorticity shedding. An experimental method is presented to obtain these losses. It requires the separate measurement of the incident and radiated sound energies.

### ***Analytical formulation for the sound absorption in the vorticity shedding***

Bechert (1980) derives an analytical model based on a multipole distribution at the opening. By assuming a monopole and a dipole source at the opening of the pipe and deriving the power radiated into the far field by these two sources, Bechert (1980) obtains

$$W_r = (\pi a^2 / 2 \rho_0 c_0) |\hat{p}_1^+|^2 (\omega a / c_0)^2 \left(1 + \frac{4}{3} M^2\right). \quad (2-22)$$

The transmitted power  $W_t$  at low frequency is expressed as

$$W_t = (2\pi a^2 / \rho_0 c_0) M |\hat{p}_1^+|^2. \quad (2-23)$$

It follows that the ratio of radiated sound power  $W_r$  to the transmitted sound power  $W_t$  is

$$W_r / W_t = \left[ \left(1 + \frac{4}{3} M^2\right) / 4M \right] (\omega a / c_0)^2. \quad (2-24)$$

### ***Experimental investigation of the sound absorption in the vorticity shedding***

Measurement of the losses through vorticity requires the determination of the incident power in order to estimate the acoustic power coming out of the pipe (transmitted power). A separate measurement in a reverberation room allows the radiated acoustic powers to be measured. The losses are obtained by comparison of the transmitted and radiated powers.

In order to obtain experimentally the incident wave amplitude  $|\hat{p}_+|$  at the opening, an induct measurement is performed using the microphone cluster located next to the opening (cluster I, cf Figure 2).

Using the definition of the microphone calibration factor  $K_I [V/Pa]$

$$S_{\hat{e}_1^+ \hat{e}_1^+} = (K_I)^2 |\hat{p}_1^+|^2 = |H_{\hat{e} \hat{e}_1^+}|^2 S_{\hat{e} \hat{e}}, \quad (2-25)$$

where  $S_{\hat{e}_1^+ \hat{e}_1^+}$  is the autospectrum for the incident pressure expressed as  $V^2$ ,  $S_{\hat{e} \hat{e}}$  is the

loudspeaker voltage autospectrum.  $H_{\hat{e}\hat{e}_1^+}$  is given in (2-11).

It follows that the incident sound power  $W_i$  is

$$W_i = \frac{|\hat{p}_1^+|^2}{\rho_0 c_0} S_{pipe} (1 + M)^2 = \frac{|H_{\hat{e}\hat{e}_1^+}|^2 S_{\hat{e}\hat{e}}}{(K_1)^2 \rho_0 c_0} S_{pipe} (1 + M)^2. \quad (2-26)$$

The incident power  $W_i$  can be combined with the pressure reflection coefficient  $R_l$  (equation (2-13)) to determine the sound power  $W_t$  transmitted out of the pipe

$$W_t = \frac{|p_1^+|^2}{\rho_0 c_0} S_{pipe} \left[ (1 + M)^2 - |R_l|^2 (1 - M)^2 \right]. \quad (2-27)$$

The radiated sound power level  $W_r$  has been measured in a reverberation room by measuring the autospectrum from a rotating microphone and using a calibrated sound source (ISO 3747).

The noise due to the flow generation in the pipe and at the opening has been measured. It has been intended to compare this quantity to the sound power level transmitted from the loudspeaker to the room to ensure a good signal-to-noise ratio. The measurements are conducted using a broadband type of excitation as stipulated in standards for measurement in a reverberation room (ISO 3741).

The experimental ratio of radiated sound power  $W_r$  to transmitted sound power  $W_t$  is evaluated as

$$\frac{W_r}{W_t} = \frac{W_r}{\frac{|\hat{p}_1^+|^2}{\rho_0 c_0} S_{pipe} \left[ (1 + M)^2 - |R_l|^2 (1 - M)^2 \right]}. \quad (2-28)$$

## 2.2 Results and discussion

A mean value Mach number  $M$  and Kirchoff damping are explicitly assumed if not otherwise stated.

### 2.2.1 Internal damping in the boundary layer of a straight pipe

The influence of flow on acoustic damping can be seen in Figure 3. The theoretical damping  $\alpha$  (see (2-16) and (2-17)) presented in Figure 3 corresponds to the absolute value of the imaginary part of the calculated wavenumber  $k_{+/-}$ .

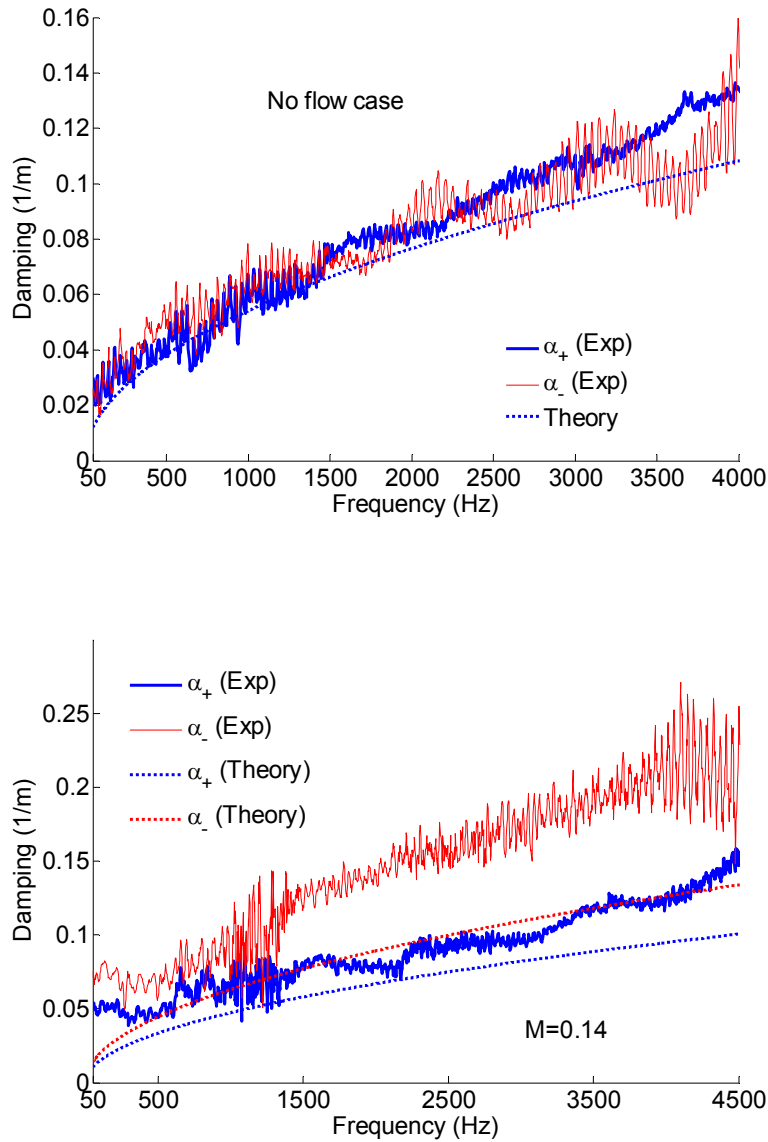


Figure 3: Acoustical attenuation rate in a straight pipe ( $M=0, 0.14$ ).

The experimental results are obtained using the two-microphone and cluster techniques and with formulation based on travelling pressures (cf (2-14), (2-15)). The cluster technique consists of an array of six in-duct flushed mounted microphone.

The experimental results for the no flow case in Figure 3(a) agree well with the calculated results using the Kirchoff formulation (see (2-16)). No significant difference in damping is seen between the upstream and downstream propagating waves. Comparison of the plots in Figure 3 shows that introducing flow into the pipe does not significantly change the damping  $\alpha_+$  of the downstream propagating wave. An increase in the damping is however observed for the upstream propagating wave  $\alpha_-$  (reflected wave). It also appears that Davies' modified theory (Davies 1988) of Kirchoff for the case with flow (see equation (2-17)) underpredicts the damping.

A transmission loss  $TL$  [dB/m] due to the viscous-damping can be calculated from the value of the damping  $\alpha$  [1/m] measured and shown in Figure 3. The  $TL$  is given as

$$TL = 8.7\alpha . \quad (2-29)$$

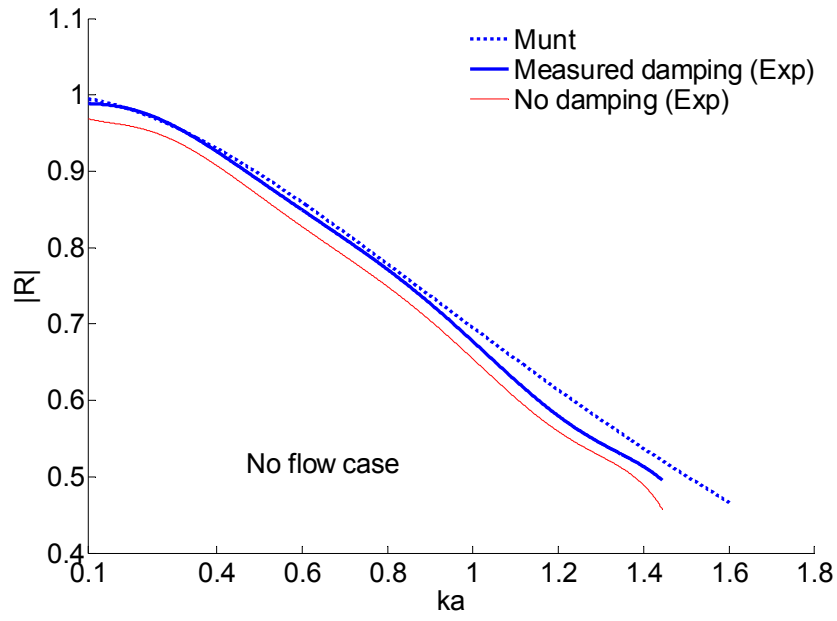
Using the maximum value ( $\alpha=0.2$ ) observed at 4.5 KHz for the flow case  $M=0.14$  gives a  $TL$  of 2 dB/m.

This result shows that attenuation through viscous boundary layer along the inner wall of a pipe is not an efficient method to prevent acoustic energy propagation. The value of the damping will increase for smaller pipe diameter, i.e., it can be of importance in narrow pipes as found in catalytic converters (Allam (2004)).

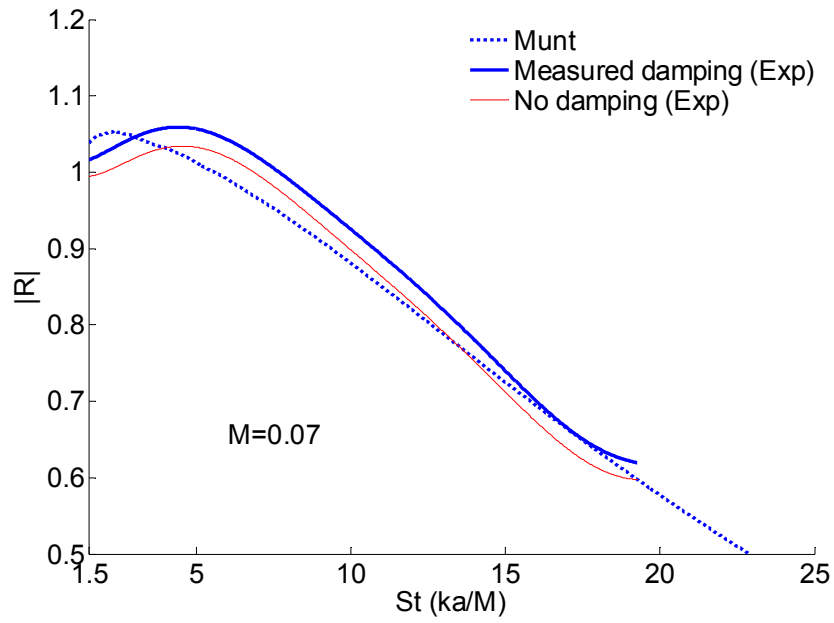
### ***On the influence of the internal sound attenuation on the measured reflection coefficient***

The experimental data presented in Figure 4 plotted as function of the Helmholtz number  $ka$  for the case without flow and Strouhal number  $St = ka/M$  for the flow cases) are obtained using the cluster technique without iteration (two-microphone technique) and a real wavenumber  $k=\omega/c_0$  (no damping) and with iterations corresponding to the case for which the measured damping is included in the experimental determination of the reflection coefficient  $R$ . It can be seen from Figure 4 that the Munt's model predicts quite well the trends of the measured data (typical error <10%).





(a)



(b)

Figure 4 (a), (b): Magnitude of the pressure reflection coefficient  $R$  at the opening of the straight pipe measured with and without the effect of damping.

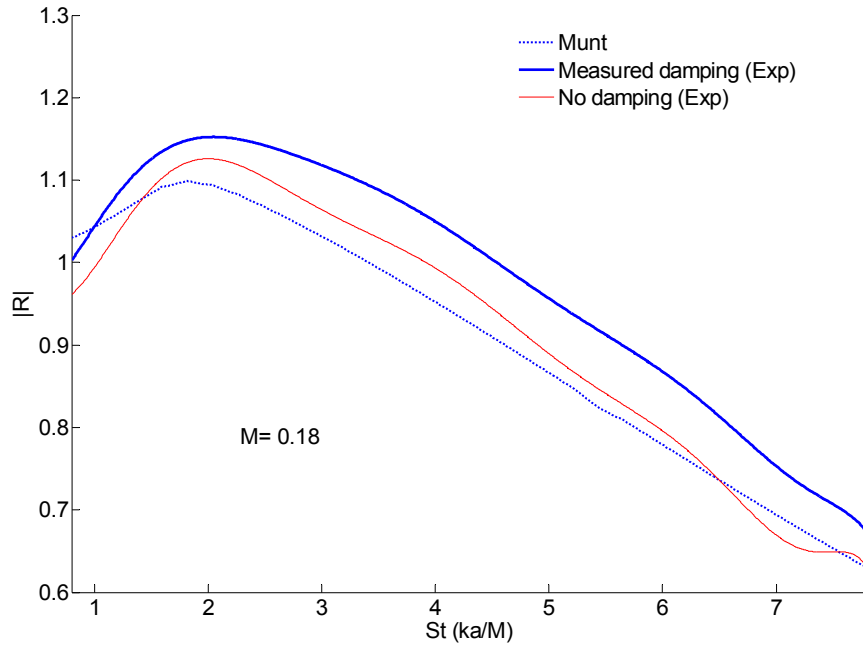


Figure 4 (c) : Magnitude of the pressure reflection coefficient  $R$  at the opening of the straight pipe measured with and without the effect of damping.

***On the velocity input for Munt's model***

Figure 5 studies the effect of the choice of the flow speed (maximum, mean) for computation of the reflection coefficient  $|R|$  using Munt's model (Munt (1977, 1990)).

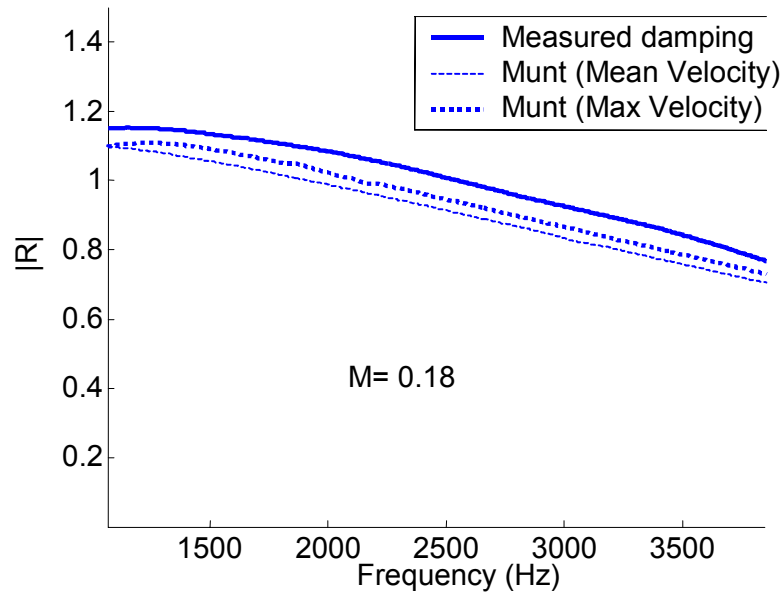
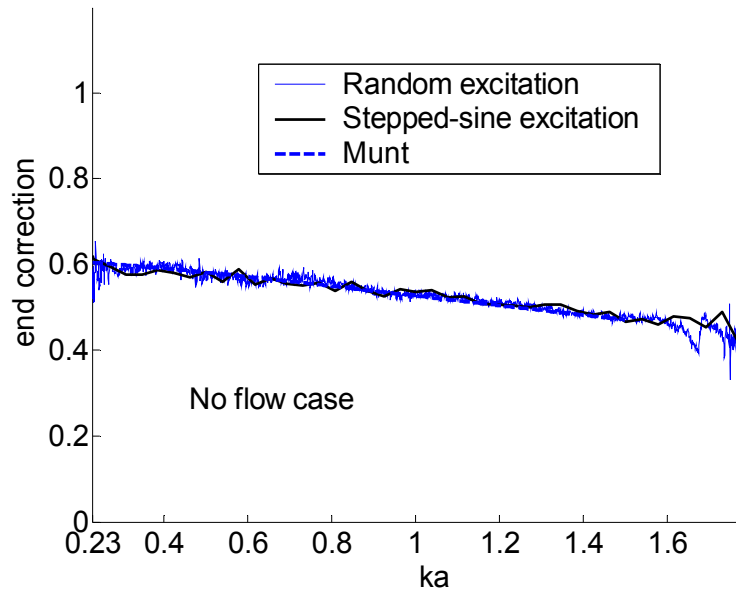


Figure 5: Reflection coefficient for straight pipe.

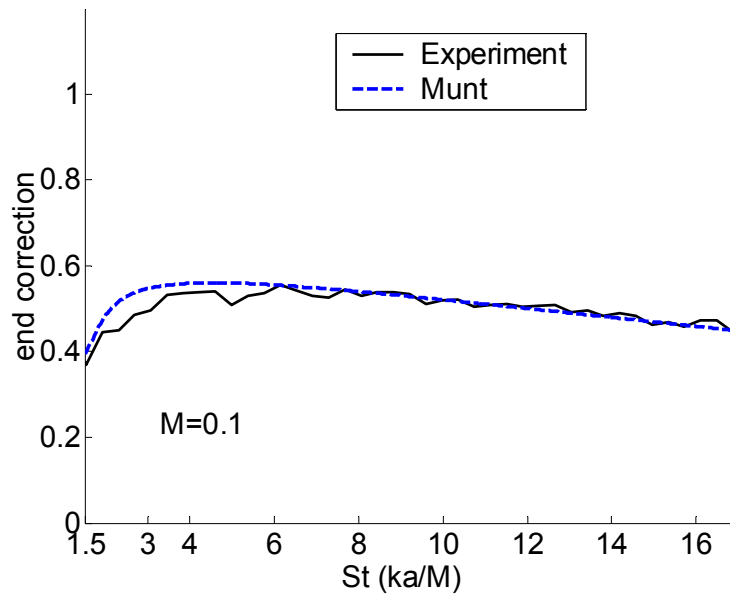
Experimentally, the maximum velocity is obtained with a Pitot-tube aligned with the centreline of the pipe. The relation between the maximum flow speed and the mean velocity over the cross section is given in Schlichting (1968). At the Reynolds number of this study, the mean velocity is 20% less than the maximum value. It can be seen from Figure 5 that using the maximum speed seems to improve the predictions.

### 2.2.2 End correction

Munt's model allows the determination of the complex value of the reflection coefficient  $R$  at the opening. In this section, the phase of  $R$  (measured and predicted) is converted into an end-correction term (see (2-18) and (2-19). Both experimental and theoretical results are presented and shown in Figure 6. For the no flow case (Figure 6 (a)), prediction of the end correction agrees well with the experimental value for which two types of excitation were tested: a broadband noise and steeped-sine excitation ranging from 0 to 5 KHz. No discrepancies between the predicted and measured no flow end correction appear even at low Helmholtz number for which experimental problems can be encountered (room acoustic, low driving efficiency of loud-speaker, etc..). The result for the low frequency limit obtained experimentally is very close to the value of 0.6133 derived by Levine & Schwinger (1948). An interesting feature is observed in the high Strouhal number region. In this region ( $St = ka/M \gg 1$ ), one can see from comparison with the no flow case that the flow does not change the value of the end correction. It can also be seen that the measurements clearly support the drop in the end correction for small  $St$ -number predicted by Munt's model. For small  $St$ -numbers the flow field plays an active part and coupling between the acoustic field and the flow field is of importance. This coupling is imposed by Munt theoretically through the full Kutta condition. This condition governs the transfer of energy between the acoustic field and the unstable vortex sheet outside the opening.



(a)



(b)

Figure 6 (a), (b): End correction for a straight pipe.

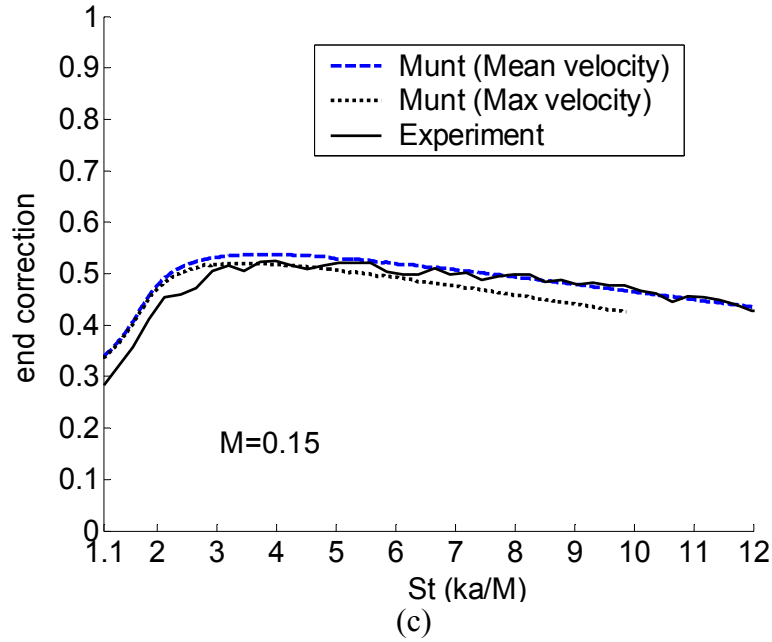


Figure 6 (c): End correction for a straight pipe.

Another investigation shown in Figure 6 (c) corresponds to the choice (mean or max) of the value of the Mach number to be used in Munt's model. The turnout is that the max speed gives a better prediction up to  $St \cong 4 - 5$  and for higher  $St$ -number the mean speed appears to be the best choice. The low frequency behaviour of the end correction has been checked by using a larger microphone separation. The experimental normalised end correction ( $\delta/a \approx 0.25$ ) obtained is very close to the predicted value for  $St \rightarrow 0, M = 0.2$ .

### 2.2.3 Sound absorption due to vorticity shedding

Measurement of the rate of the acoustic absorption related to vorticity production at the pipe opening requires an estimation of the background noise due to the wall friction and flow separation noise. Figure 7 shows the various levels of background noise. It is necessary to ensure that the radiated power is of at least 10 dB greater than the background noise generated by the flow and other rig noise. It is found from Figure 7 (a) that good SNR could not be obtained in the narrow region of 1.0 KHz. The measurements presented below have been therefore restricted to Mach numbers less than 0.2.

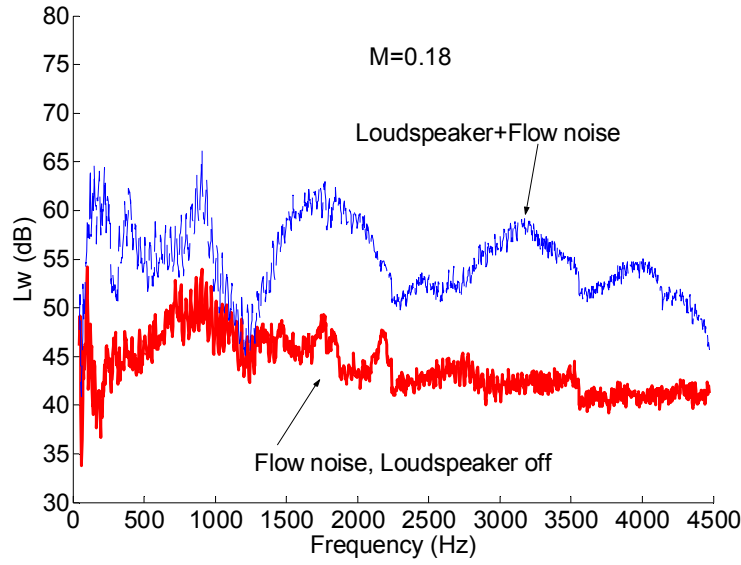


Figure 7: Various sound power levels externally measured with a rotating microphone.

#### ***Flow case sound absorption in the vorticity shedding***

The presence of mean flow in the pipe influences the rate of sound radiated to the far field. The results presented in Figure 16 shows that acoustic losses due to vorticity is dominantly a low frequency process. In contrast, sound attenuation through viscous damping within the pipe is a high frequency mechanism. Bechert (1980) demonstrates the connection between flow separation and sound reduction by conversion of the acoustical energy into kinetic energy of the flow field. The upper frequency limitation of the theory developed by Bechert (1980) is given as  $f < \sqrt{Mc}/\pi a$  and is indicated by a vertical dashed line in Figure 8. The analytical model derived by Bechert (1980) is in its form rather simplistic although good agreements are observed with our experimental data. Linear effects are usually encountered in the near field where low frequency sound absorption occurs. Thus, traditional and simple mathematical derivations are feasible in this region. An analytical approach as the one described by Bechert (1980) can thus be made.

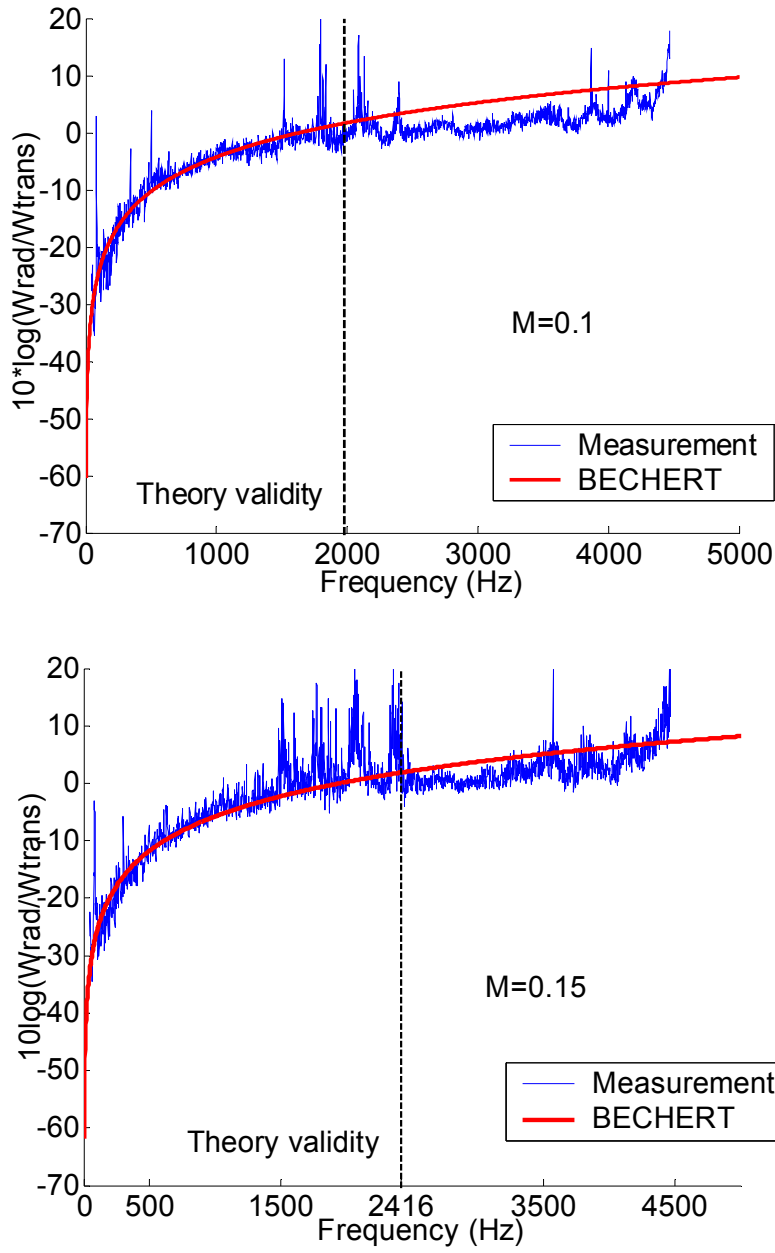


Figure 8: Theoretical and measured sound absorption by the vorticity.

Such a linear approach is not possible in the further downstream region where the flow breaks into turbulence and sound energy is converted into heat. Turbulence creates sound of quadrupole type much weaker than the absorption in the near field (dipole sound sink). Another interesting mechanism pointed out by Bechert (1980) is the noise conversion from narrow band to broader band in this region. The effects in this jet mixing region are small and can be neglected.

### 2.3 Summary

This chapter has dealt with the sound propagation in an open straight pipe. Different regions have been examined theoretically and experimentally and variation of the flow speed has been performed up to a Mach number of 0.2. The internal damping through viscous boundary layers has been measured with the means of a six-microphone array. The measured results of the damping agree well with the Kirchhoff's formula when no flow is present in the pipe. However, for flow conditions, the formulation suggested by Davies (Davies (1980)) based on Kirchhoff's no flow formula underpredicts the internal damping in the flow pipe. The experimental technique also allows to determine the pressure reflection coefficient and impedance at the opening. The prediction is conducted with a model derived by Munt (1977, 1990). A quite good agreement is observed between the theoretical and experimental results even at relatively high flow speeds.

The end correction derived from the experimental pressure reflection coefficient has been compared with that of Munt's model (Munt (1977, 1990)) derived for the theoretical pressure reflection coefficient. The trends are well predicted and limits at low frequency agree with the experimental data obtained at low frequency.

The acoustic losses caused by the shedding of vorticity at the opening of the flow pipe has been experimentally obtained from induct and external measurements. The analytical model of Bechert (1980) defines the opening as a distribution of monopole and dipole sources. This model has been used to predict the sound absorption in the vorticity shedding. Good agreement has been obtained with the experimental data.



### **3. Acoustics of tailpipes**

#### **3.1 Methods and materials**

Experimental and theoretical treatments of the pressure reflection coefficient  $R$  at the opening and flow noise in the far field for a number of different tailpipe geometries are presented. The aim of this section is to investigate the deviation of the results obtained from the straight pipe when the opening geometry is varied. The reflection coefficient and impedance at the opening and flow noise generated are studied.

##### **3.1.1 Presentation of the tailpipe rig**

The tailpipe experimental rig consists of several sections assembled as shown in Figure 9. The main difference compared to the rig used in the treatment of the aeroacoustics of the straight pipe is the number of microphone used. Here, three microphone locations are used in conjunction with the two microphone technique, whereas a six-microphone array is used in the straight pipe rig in order to also measure the acoustic damping. The arrangement is designed to permit flexibility between measurements. The microphones are flush mounted to minimise flow disturbances. The cut-off frequency based on the internal pipe radius (42 mm diameter, 2 mm thickness) for this pipe is 4.8 KHz. Pitot-tube results are shown in Table 1. A smooth inlet cone is used to minimise flow separation noise at the inlet of the rig.

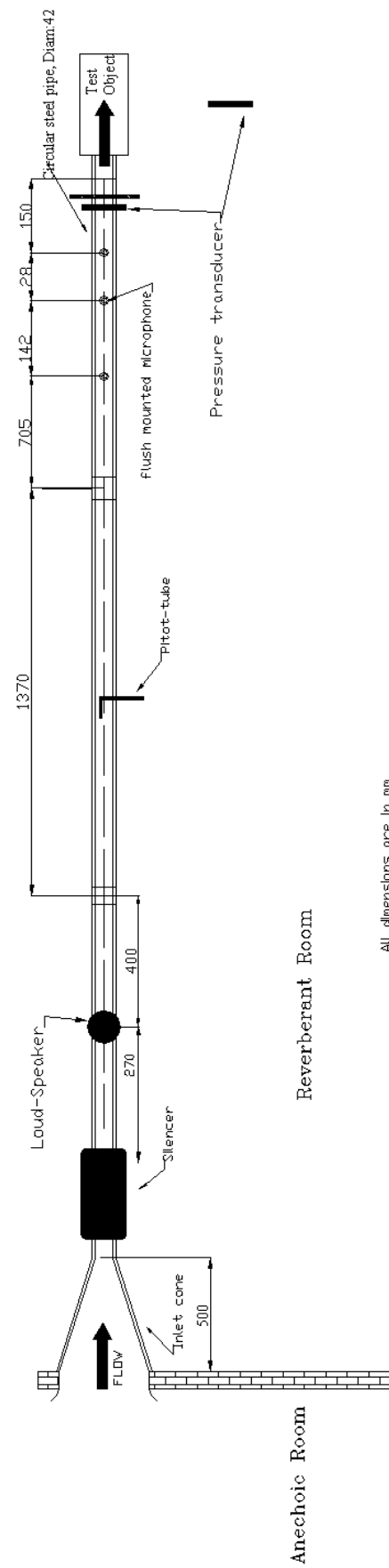


Figure 9: Layout of the experimental setup for tailpipes.

<i>Elements</i>	$V_{1,max}$	$V_{2,max}$	$V_{3,max}$
Straight pipe	25	43	80
Oblique cut 0°	25	43	80
Oblique cut 30°	24	42	80
Oblique cut 45°	24	42	80
Oblique cut 60°	24	43	80
Diffuser 1°	25	44	80
Diffuser 2.5°	27	47	90
Diffuser 5°	27	48	90
Diffuser 7.5°	25	48	91
45° Bend L=0	23	41	80
45° Bend L=1D	24	41	80
45° Bend L=2D	24	42	80
45° Bend L=5D	24	42	80
90° Bend 1 R/D=1.6	23	41	78
90° Bend 2 R/D=2.5	24	41	78

Table 1: List of tailpipes tested and the flow speeds used.

### 3.1.2 Presentation of the tailpipe elements

Schematic diagrams and pictures of the various elements tested are now presented. Three main categories are investigated: oblique cuts, diffusers and bends. Reflection coefficients and sound power levels of the flow generated noise are compared with the straight pipe case (reference).

#### *Oblique cut*

The steepness of the oblique cut at the outlet is given by the angle between the no cut case (straight pipe) and the oblique cut. This angle has a value of 30°, 45° and 60° as shown in the following drawings (Figure 10). It should be noticed that the total length of the element is constant (150 mm). The purpose of this cut is to reduce the reflection at the outlet and thereby reducing the effect of resonances.

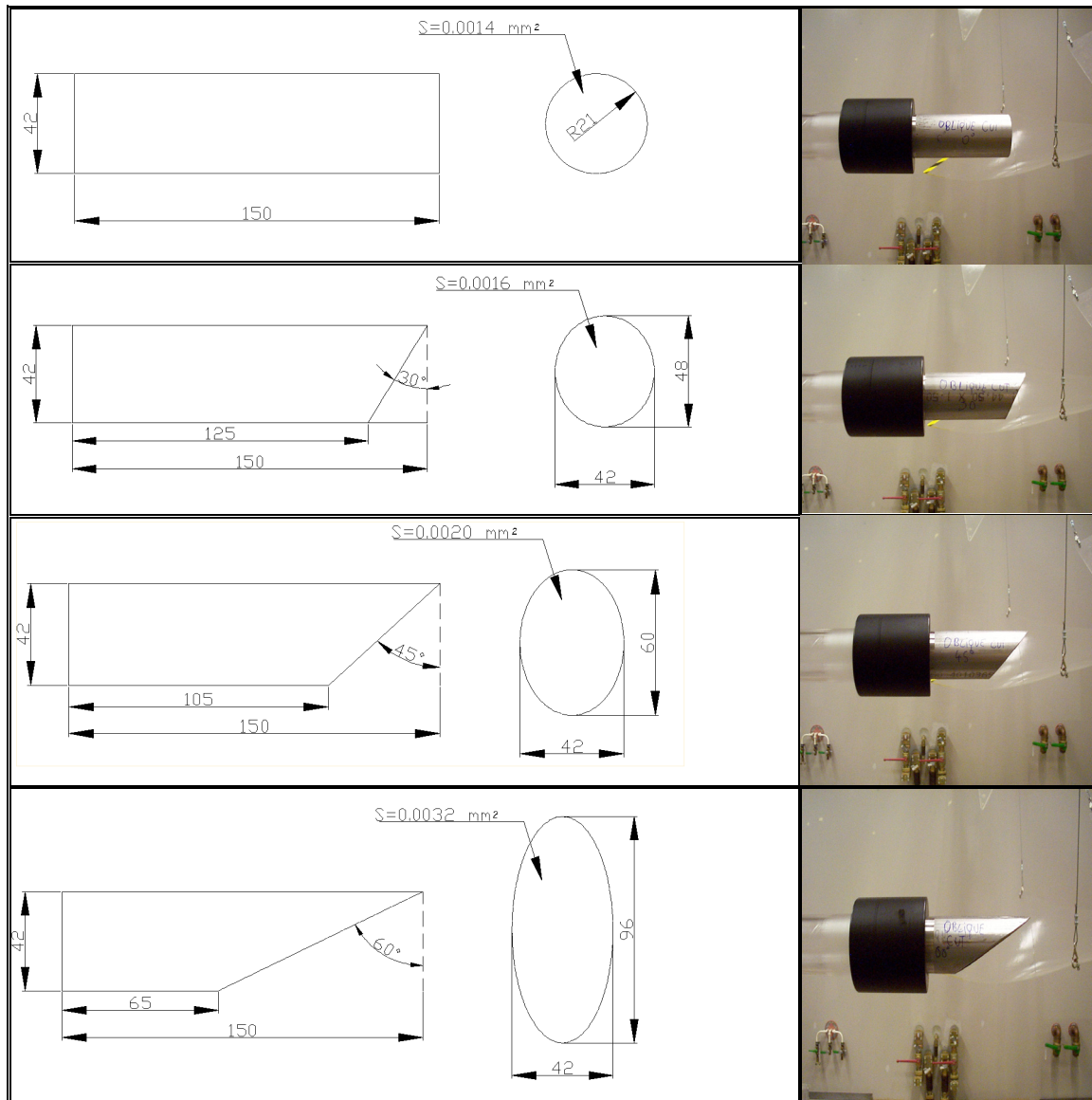


Figure 10: Oblique cuts in a circular pipe.

### ***Diffusers***

The second type of element investigated is the diffusing element (Figure 11). Slowly divergent conical elements having a fixed length of 105 mm are studied. Measurements on diffusers of semi angles of divergence of  $1^\circ$ ,  $2.5^\circ$ ,  $5^\circ$  and  $7.5^\circ$  are carried out. The diffuser can reduce reflections at an opening and possibly also reduce flow noise produced at the outlet.

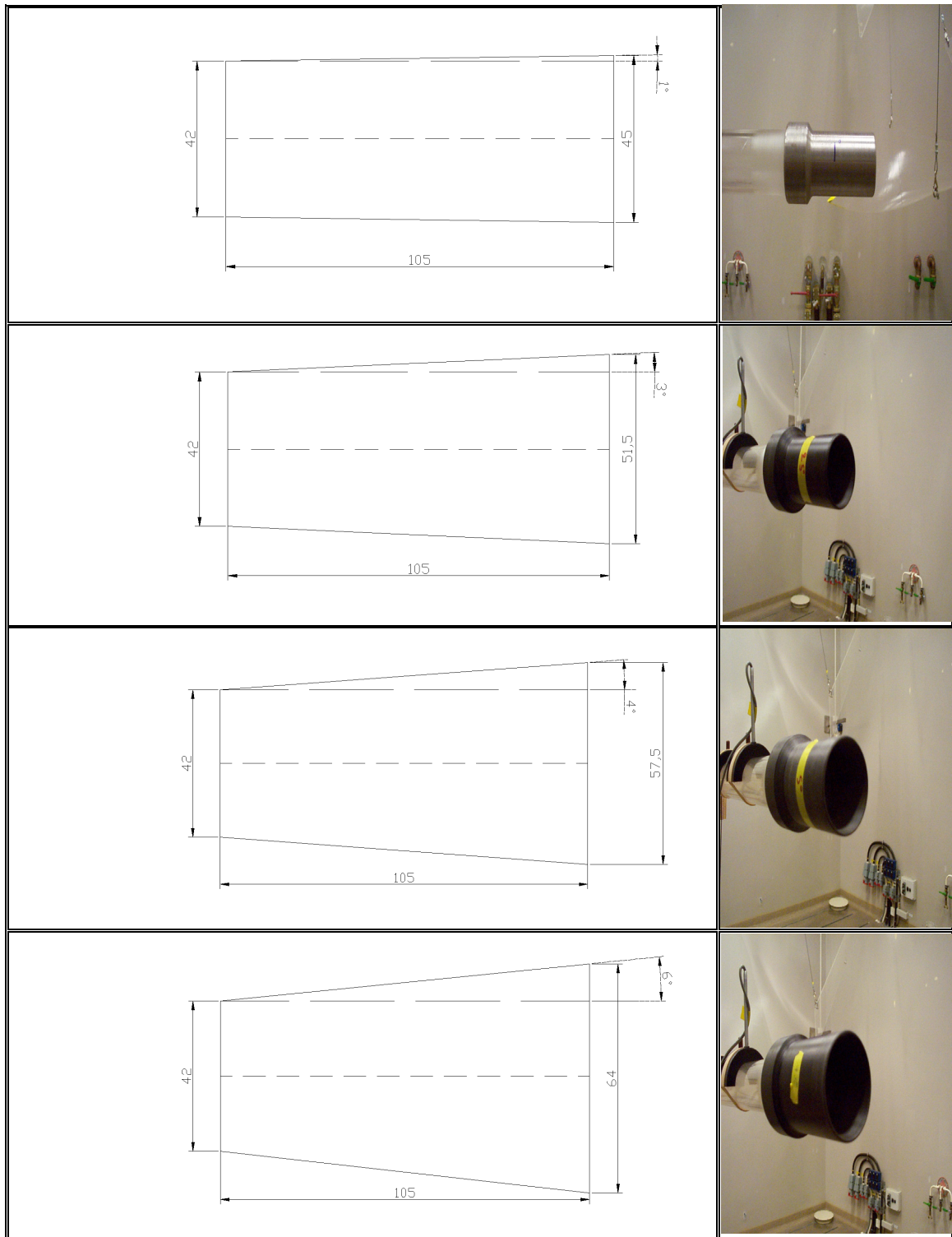


Figure 11: Diffusers.

### ***45° bends***

The bend elements consist of three parts, an upstream straight part, the bend and a downstream straight pipe. The upstream distance between the inlet and the bend edges

has a fixed value of 70 mm (Figure 12). The downstream section located after the curvature and extended to the outlet takes the length  $L$  of 0, 42, 82 and 210 mm. The curvature radius for the bends is 50 mm. An angle of  $45^\circ$  is found between the upstream and downstream sections.

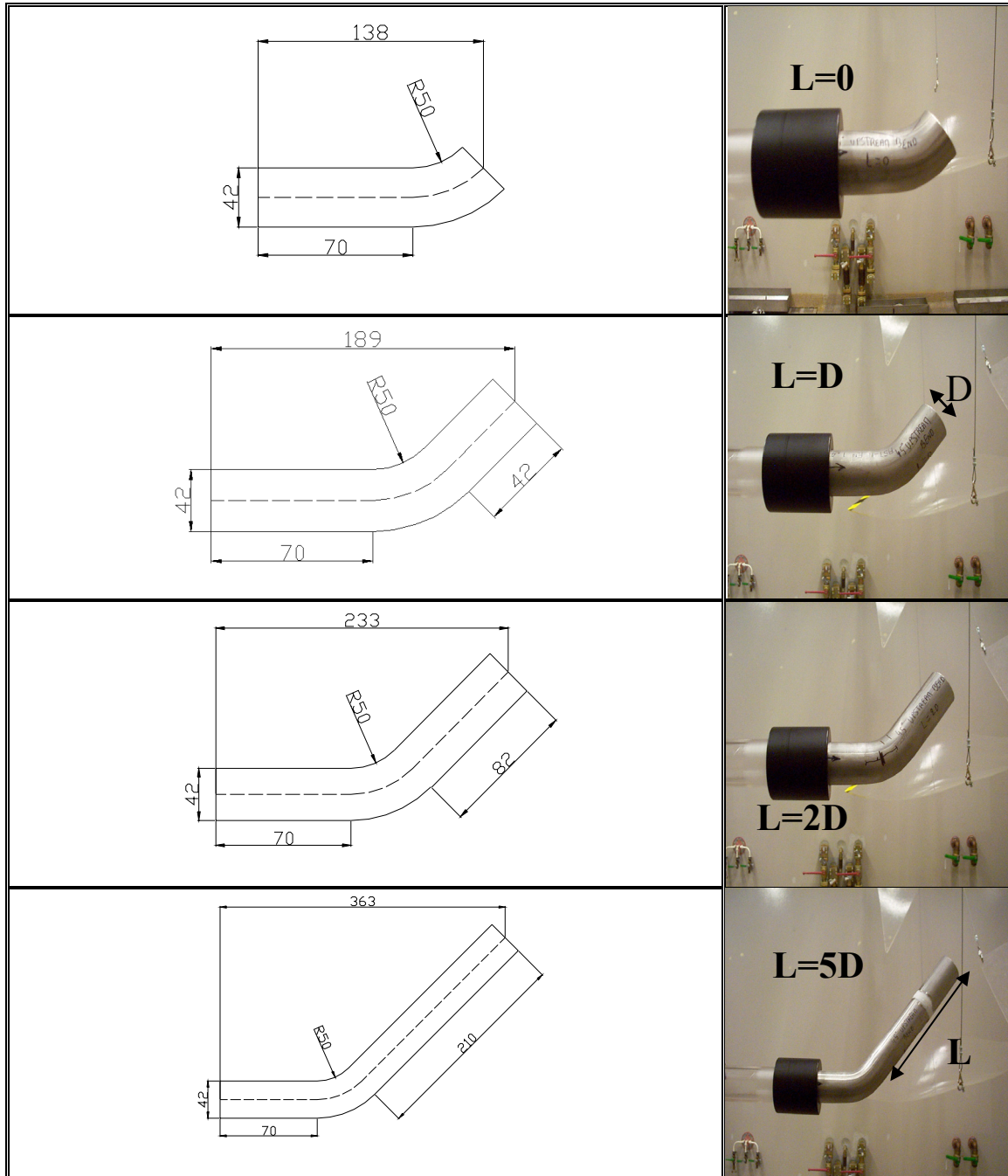


Figure 12:  $45^\circ$  bends.

### ***90° bends***

For the  $90^\circ$  bends the angle separating the upstream and downstream sections is  $90^\circ$

(Figure 13). Two radii of curvature (67 mm and 105 mm) at the bends permit ratios of curvature radius  $R$  to pipe diameter  $D$  to be of 1.6 and 2.5. The interest here is on the aeroacoustics of bends close to the tailpipe opening.

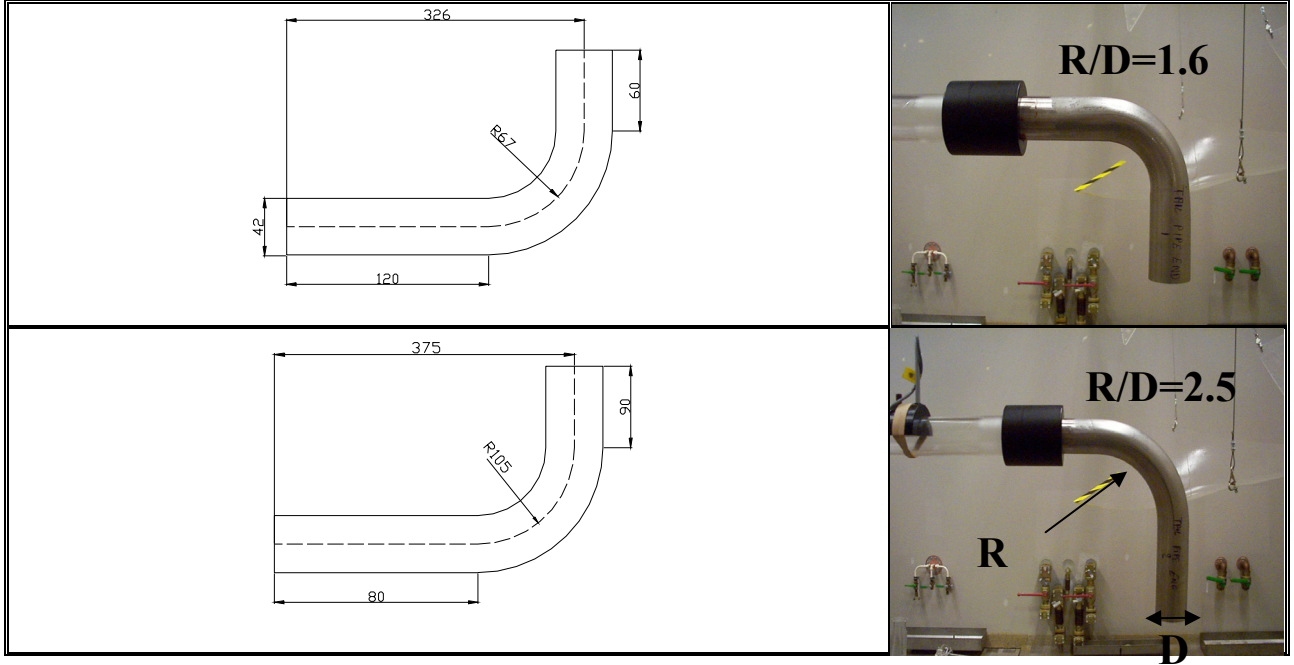


Figure 13: 90° bends.

### 3.1.3 Modelling of pressure reflection coefficients and impedances

Theoretical investigation of the reflection coefficient and impedance at the inlet and outlet of the elements differs slightly between the types of elements. Each case is now theoretically detailed.

The main approach is to calculate the reflection coefficient at the outlet of the element using Munt's model (Munt (1977, 1990)) and to move the results to the inlet through its transfer matrix calculated from SID (Nygård (2000)) (Sound in Duct software developed at MWL).

The outlet impedance  $Z_{out}$  is calculated after derivation of the outlet reflection coefficient  $R_{out}$  using the relation

$$Z_{out} = \left( \frac{1 + R_{out}}{1 - R_{out}} \right) \frac{\rho_0 c_0}{S}, \quad (3-1)$$

where  $R_{out}$  is calculated from Munt's model (Munt (1977, 1990)) based on the radius and mean Mach number  $M$  at the outlet for diffusers. For the oblique cuts, it was found preferable to use the inlet element radius.

The transfer matrix relating the pressure  $\hat{p}$  and volume flow speed  $\hat{q}$  between the inlet and outlet of the element is of the form

$$\begin{pmatrix} \hat{p}_{in} \\ \hat{q}_{in} \end{pmatrix} = \begin{pmatrix} T_{11} & T_{12} \\ T_{21} & T_{22} \end{pmatrix} \begin{pmatrix} \hat{p}_{out} \\ \hat{q}_{out} \end{pmatrix}. \quad (3-2)$$

Re-arranging this expression yields the impedance at the inlet

$$Z_{in} = \frac{\hat{p}_{in}}{\hat{q}_{in}} = \frac{T_{11}Z_{out} + T_{12}}{T_{21}Z_{out} + T_{22}}. \quad (3-3)$$

Using (3-1), the reflection coefficient  $R_{in}$  at the inlet can similarly be written

$$R_{in} = \frac{Z_{in}S/(\rho_0 c_0) - 1}{Z_{in}S/(\rho_0 c_0) + 1}. \quad (3-4)$$

The elements  $T_{11}$ ,  $T_{12}$ ,  $T_{21}$  and  $T_{22}$  are obtained from the transfer matrix calculated using SID.

Regarding the bends, no transfer matrix calculation is done; the reflection coefficient is shifted to the outlet through a straight pipe with same length.

### ***Oblique cut case***

It was primarily assumed that only the increase in the cross-section area at the outlet dominated the behaviour of the reflection coefficient. Therefore an equivalent radius has been calculated for this opening and used with Munt's model for same Mach number. However, the reflection coefficient obtained from Munt's model with this calculated radius did not agree well with the experimental data at high frequency. This discrepancy can be explained by the additional acoustical effect of the obliquity. As opposed to the other elements, the acoustical wave does not encounter the lips of the oblique cut at the same time, thus the wave is reflected at different time along the oblique cut introducing a phase difference. To model this, it was decided to split the oblique cut in a number of parallel pipes with varying length as shown in Figure 14.

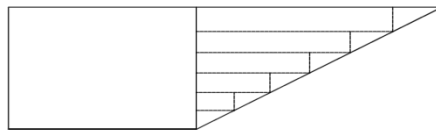


Figure 14: Pipe network for oblique cut transfer matrix calculation.



A network composed of these segments mounted in parallel enabled the determination of the transfer matrix for the entire element. This is done using the SID code.

The reflection coefficient at the outlet calculated from Munt's theory is based on the radius of the straight pipe and not on the equivalent radius of the oblique opening. The technique described from (3-1) to (3-4) allows determination of the reflection coefficient at the inlet of the network, i.e., the oblique cut.

### ***Diffuser case***

The theoretical transfer matrix for diffusers is derived from the software SID (Sound in Duct). The methodology used in SID is to split the overall diffuser into straight pipe segments connected to each other in serial. The user inputs for any diffuser elements are the inlet and outlet cross-section, the length and the number of straight pipe segments. Knowing the transfer matrix for each straight pipe and applying continuity of pressure and volume flow at the interface between two consecutive pipe elements, the transfer matrix for the entire network is derived. The centreline distance inlet-outlet, i.e., the length, for the diffusers has a fixed value of 105 mm. A number of 10 segments is chosen for the splitting as shown in Figure 15.

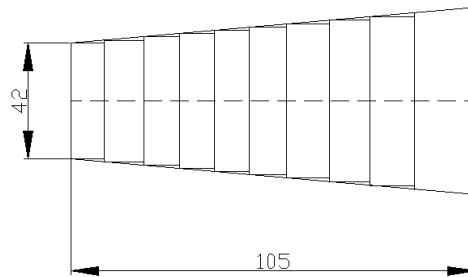


Figure 15: SID geometry for diffusers.

By combining the outlet pressure reflection coefficient  $R_{out}$  predicted from Munt's model with the diffuser transfer matrix, we can derive the inlet pressure reflection coefficient  $R_{in}$  and impedance  $Z_{in}$ .

### ***Bend case***

No transfer matrix calculation is performed for the bend cases. The reflection coefficient is calculated at the outlet of the bend using Munt's model and moved to the plane of interest by a centreline distance separating these two points. In other word, the

bend curvature is not taken into account for the prediction of the internal noise propagation in bends.

### 3.1.4 Experimental procedures

The experimental technique to measure the pressure reflection coefficient  $R$  for all elements is based essentially on the two microphone technique (Åbom & Bodén (1988)). The separations between the microphones in the rig yield a frequency range (see (1-2)) as follows

	<i>Microphone 1 and 2, <math>s_{12}=28\text{ mm}</math></i>	<i>Microphone 1 and 3, <math>s_{13}=170\text{ mm}</math></i>
<i>Two- microphone frequency criteria (Hz)</i>	$610 \leq f \leq 4900$	$100 \leq f \leq 800$

## 3.2 Results and discussion

Acoustic properties of the tailpipe geometries and the deviation from the straight pipe case are now studied. The circular straight pipe termination is replaced by various elements; oblique cuts, diffusers and bends as described in the previous section. Influence of the termination geometry and flow speed on the reflection coefficient and impedance and flow noise generated is investigated with comparison to the reference case, the straight pipe.

### 3.2.1 Reflection coefficient and impedance

Results for the reflection coefficient and impedance at the outlet of the tailpipe elements described in this section are now presented. The impedance for the tailpipe elements are moved assuming a straight pipe from the reference position (microphone 1) to the outlet opening. This procedure, which gives an equivalent radiation impedance, enables a direct comparison with the reference straight pipe case. Experimentally, it is obtained using three microphones with the one located the nearest to the pipe open end chosen as reference. Data are presented up to the straight pipe cut-off frequency (4800 Hz). Thus, only plane waves are considered in this analysis. An overview of experimental data collected for the elements are presented, and the influence of mean flow speed  $M$  is studied.

## ***Oblique cuts***

### ***Influence of the obliquity angle without flow***

Figure 16 shows the experimental reflection coefficients for the oblique cuts for various angles and for no flow condition. At low frequencies ( $<1500$  Hz), all the elements behave as a straight pipe. It can be explained by the relatively large wavelength compared to the opening characteristic dimension. In other words, at low frequency, the sound propagation is not influenced by the geometry of the elements. Bechert (1980), Peters and al. (1993) report the same observation.

Deviation between the elements is observed at high frequencies. The decrease in the reflection coefficient as the obliquity angle increases is related to the successive removal of a distinct cross section where the pipe terminates.

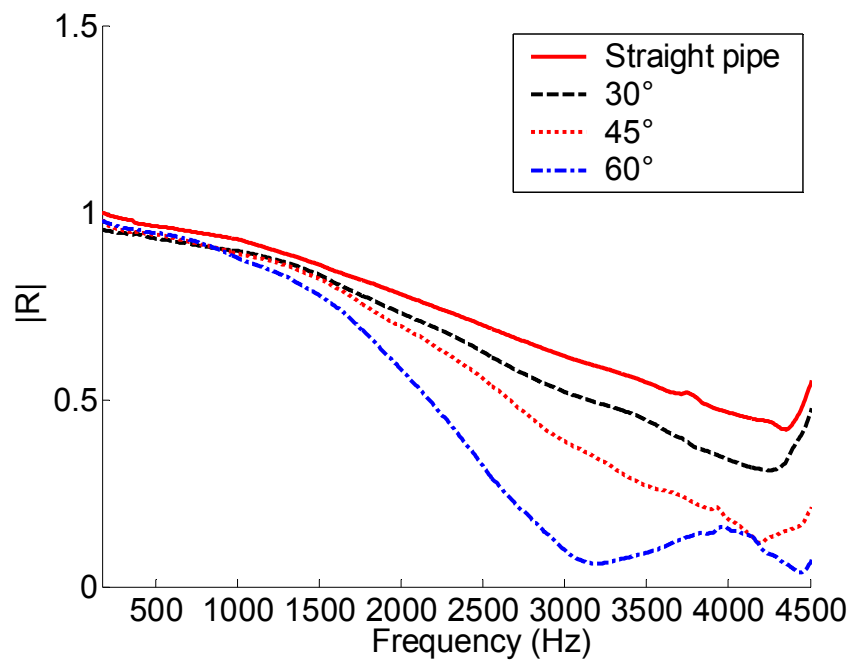
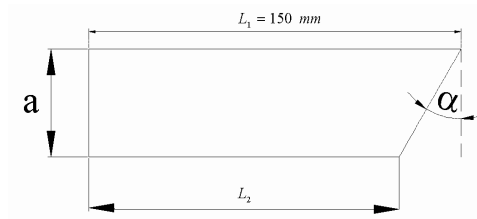
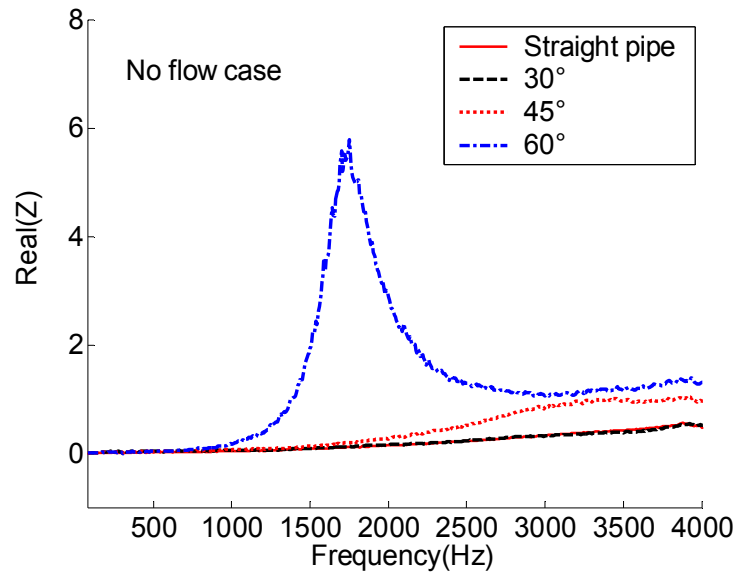


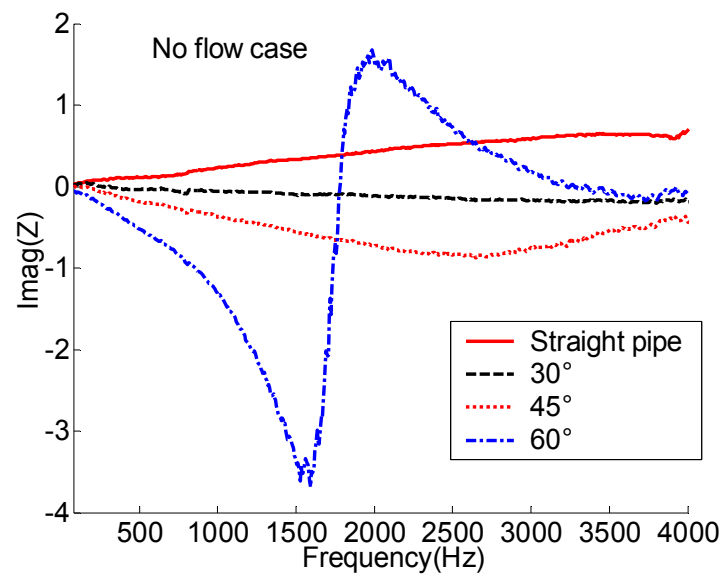
Figure 16: No flow reflection coefficient data for oblique cuts.



Results for the acoustic impedance  $Z$  are given in Figure 17.



(a)



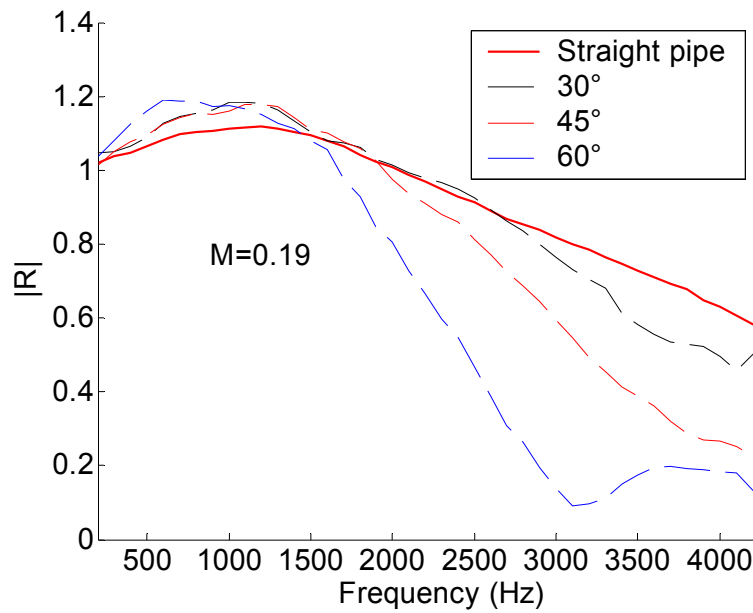
(b)

Figure 17: No flow opening impedance experimental data for oblique cuts.

As for the reflection coefficient, both the real and imaginary parts of the impedance tend to zero in the low frequency limit as for the straight pipe. It appears that the real part is not affected by the change of the obliquity. A deviation can be noticed, however, for the mid-frequency range when considering the imaginary part. A peak is observed for the sharpest cut ( $60^\circ$ ) for which a resonance seems to occur.

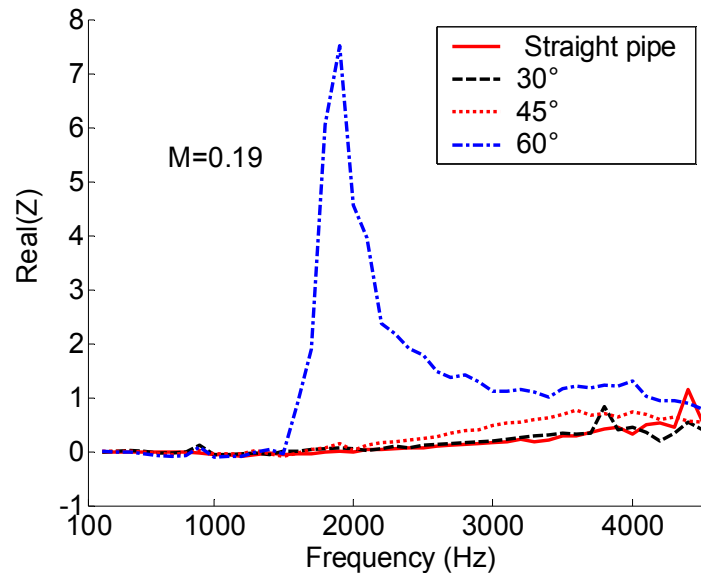
### ***Effect of mean flow***

Figure 18 shows the experimental values for the reflection coefficients and impedances for the oblique cut elements of different angles and straight pipe for flow Mach number of 0.19. Figure 18 shows that the general behaviour of the oblique cut elements is not ruled by the presence of the flow in the pipe.

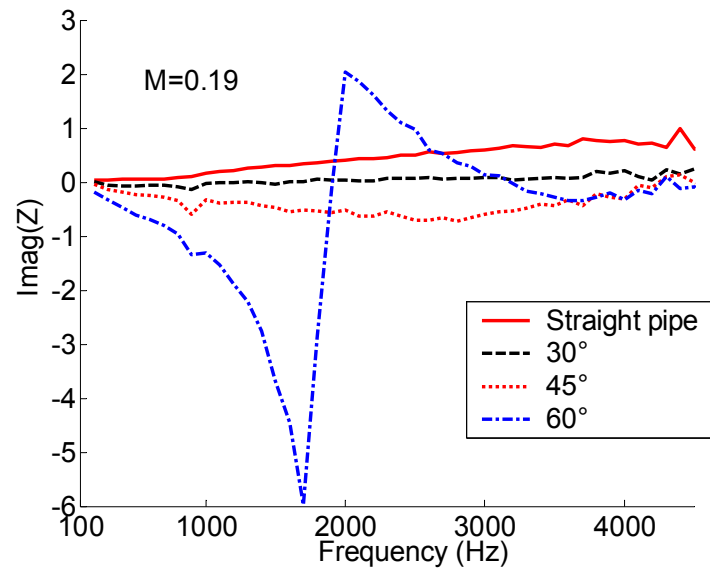


(a)

Figure 18 (a): Experimental reflection coefficient for flow oblique cuts.

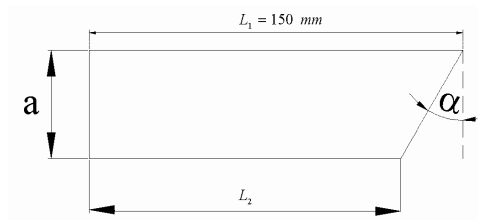


(b)



(c)

Figure 18 (b), (c): Experimental impedance for flow oblique cuts.



## Theoretical investigation

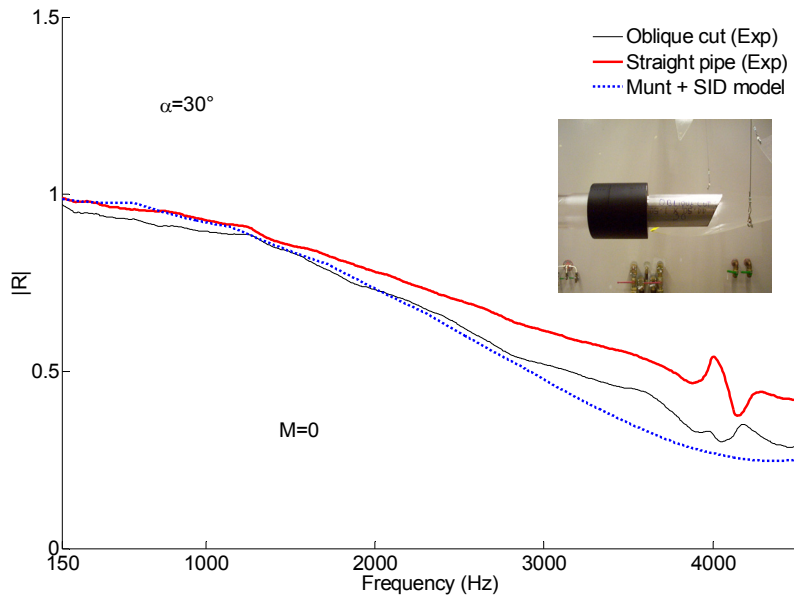


Figure 19: Theoretical analysis of no flow oblique cut case.

The prediction by the transfer matrix model including the geometrical effects agrees reasonably well with the experimental data. At even higher frequencies, the transfer matrix theory breaks up and deviates from the experimental result. A more refined model is certainly needed. shows the results obtained for the model including Munt's theory (Munt (1977, 1990)) and transfer matrix calculation.

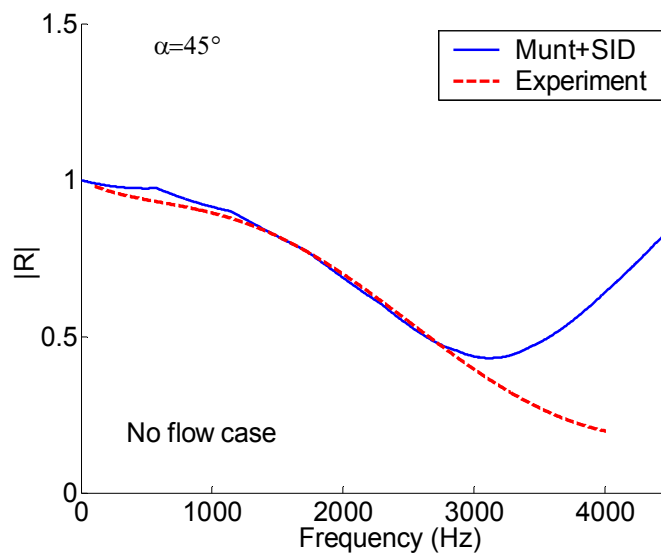


Figure 20: Modelling the opening reflection coefficient of oblique cuts.

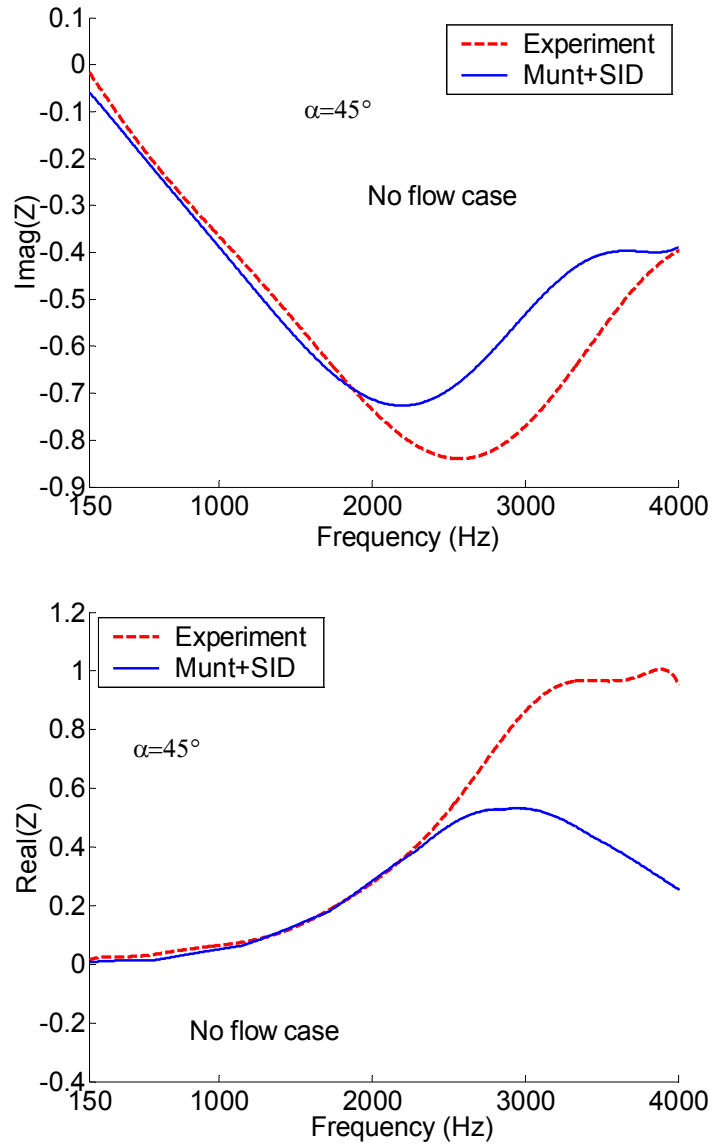


Figure 21: Modelling the opening reflection coefficient and impedance of oblique cuts.





### ***Diffusers***

The diffuser elements are now studied. Experimental data are presented for the diffusers and the straight pipe. It is followed by a comparison using the transfer matrix methodology. Discrepancies between the experiment and measured data are explained by a series of measurements performed at low frequencies.

### ***Influence of diffuser half-angle $\alpha$***

Figure 22 (no flow), Figure 23 (flow case) present the experimental results obtained for diffusers with different angles.

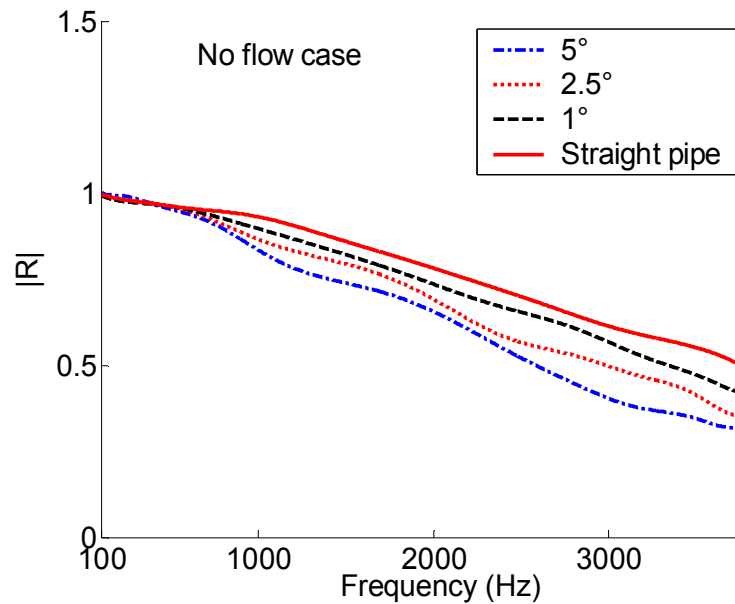


Figure 22: Diffuser experimental results at outlet (reflection coefficient) and no flow.

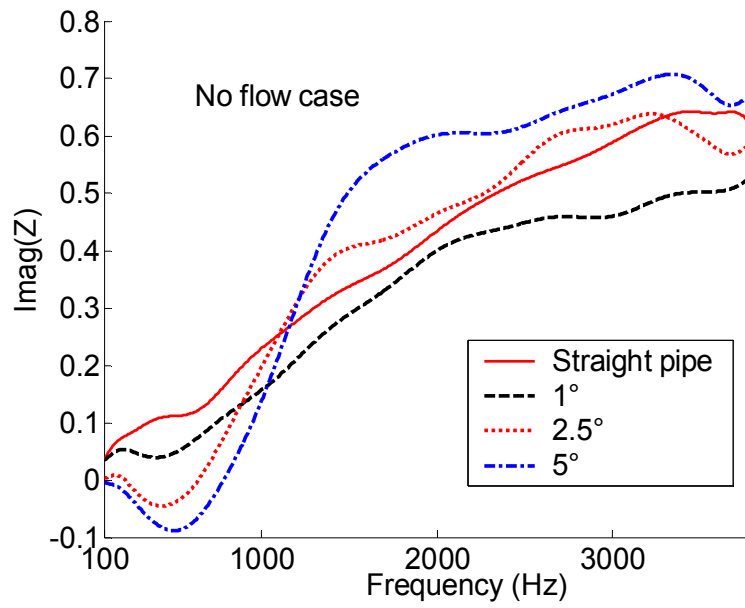
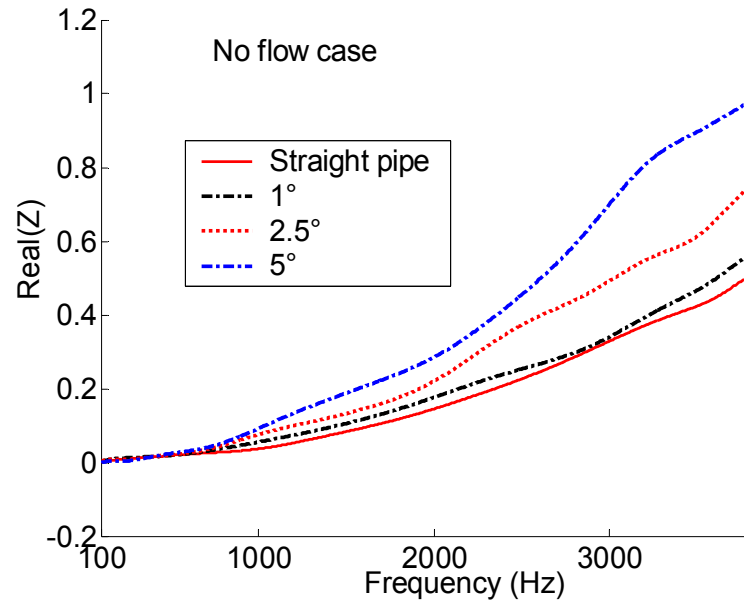


Figure 22: Diffuser experimental results at outlet (impedance) and no flow.

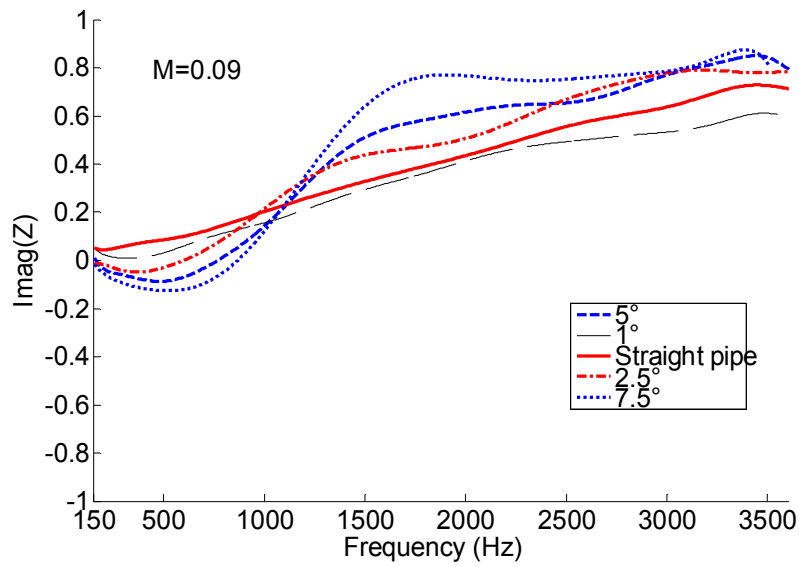
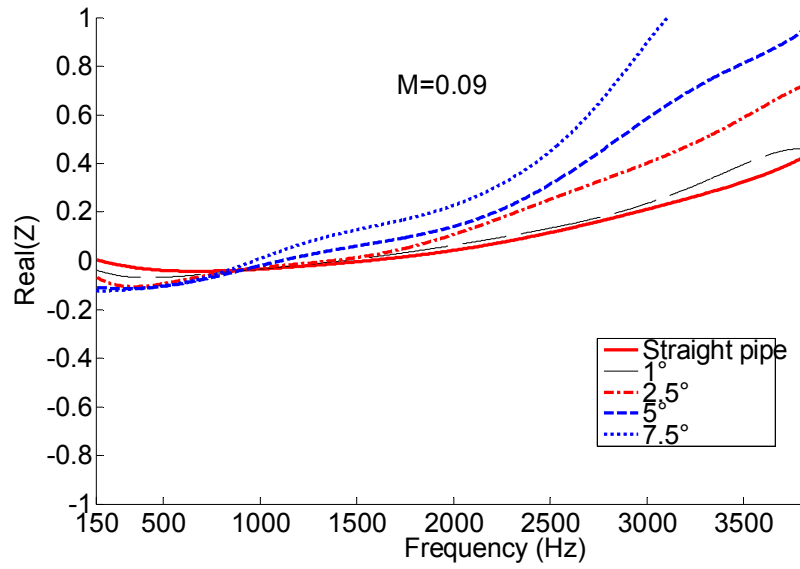


Figure 23: Diffuser experimental results at outlet (impedance) and with flow.

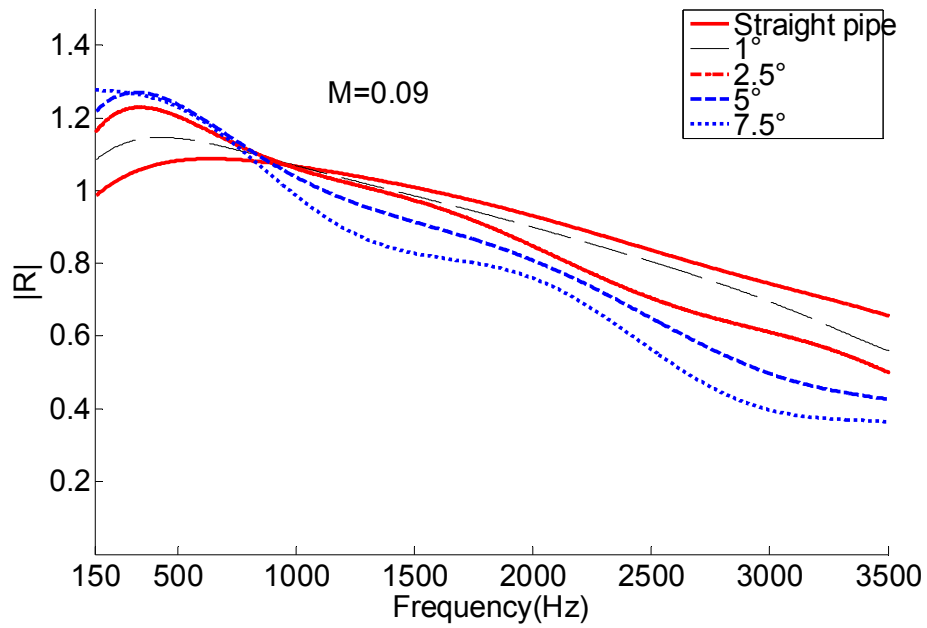


Figure 23: Diffuser experimental results at outlet (reflection coefficient) and with flow.

One interesting feature observed from the flow case is the significant increase for low frequencies of the reflection coefficient. Instead of approaching 1 as it always does for the straight pipe, it seems to approach a value larger than 1.

### ***Influence of flow Mach number***

Flow effects are shown for a specific diffuser angle in Figure 24 ( $1^\circ$ ) and Figure 25 ( $7.5^\circ$ ).

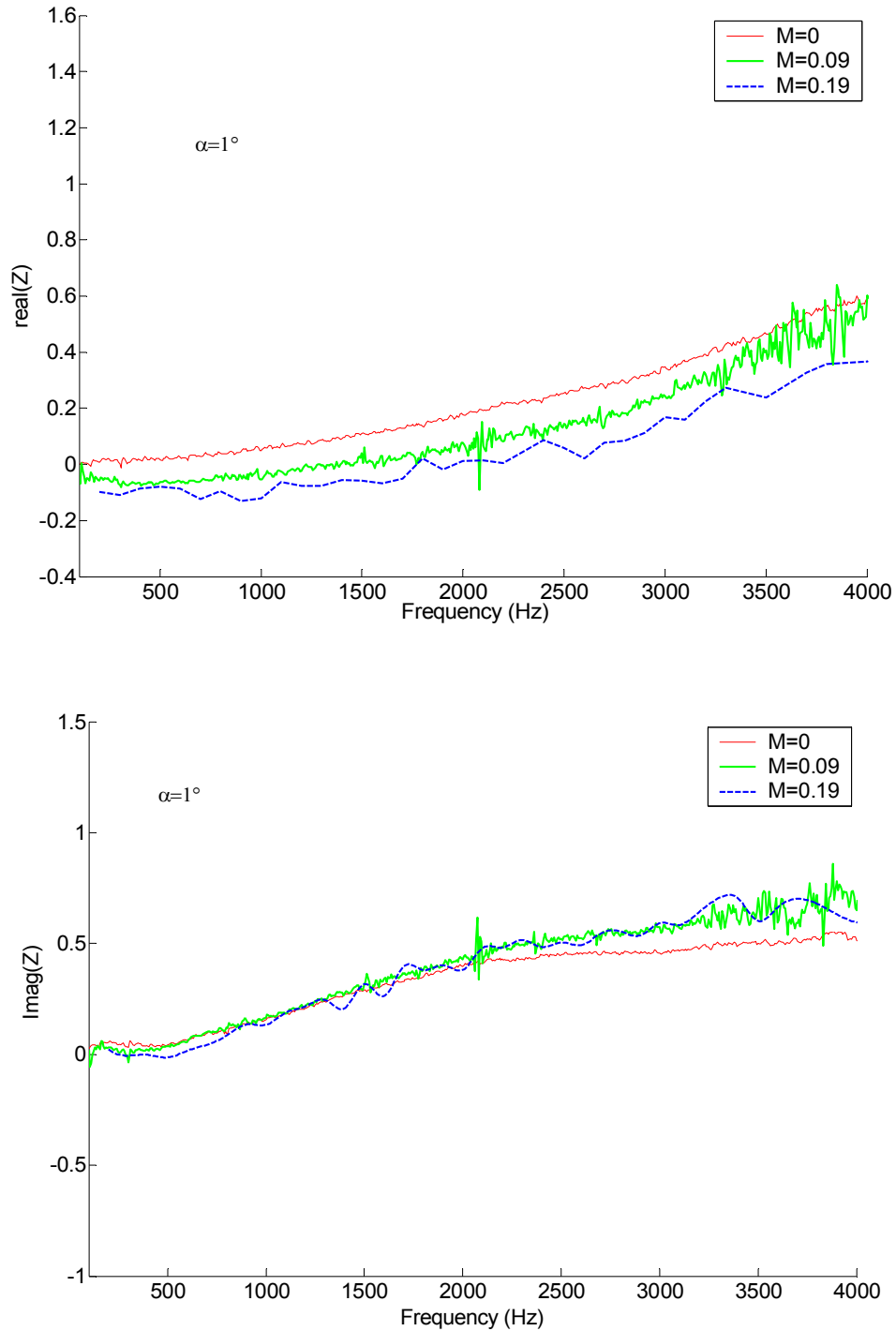
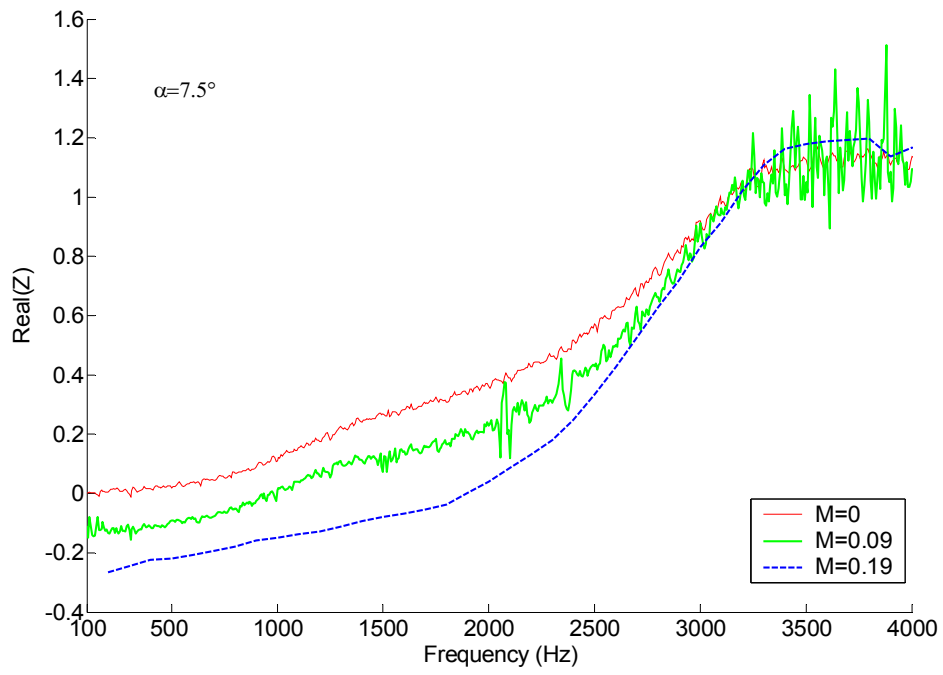
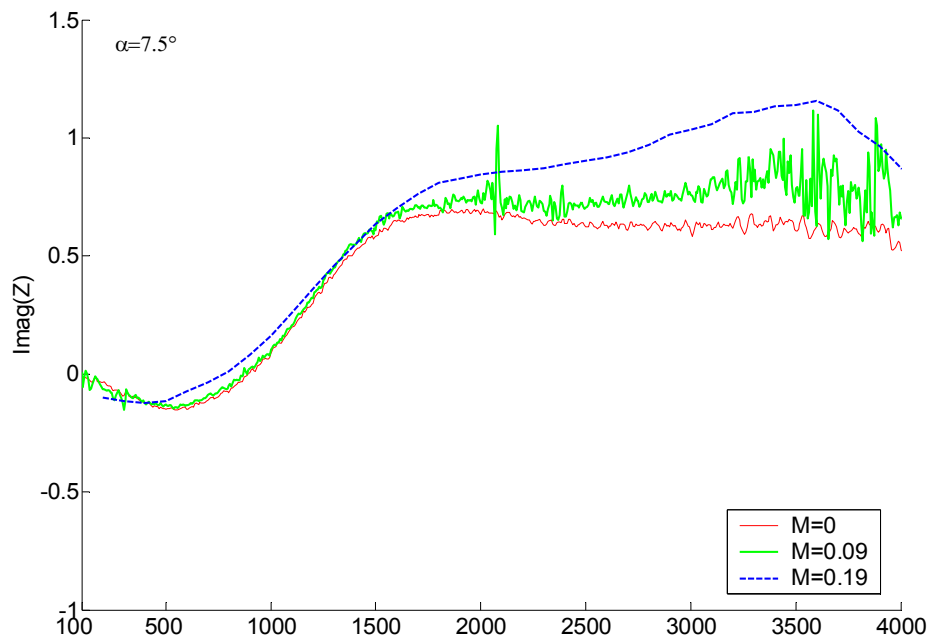


Figure 24: Influence of the Mach number on the outlet impedance of the diffuser  $1^\circ$ .

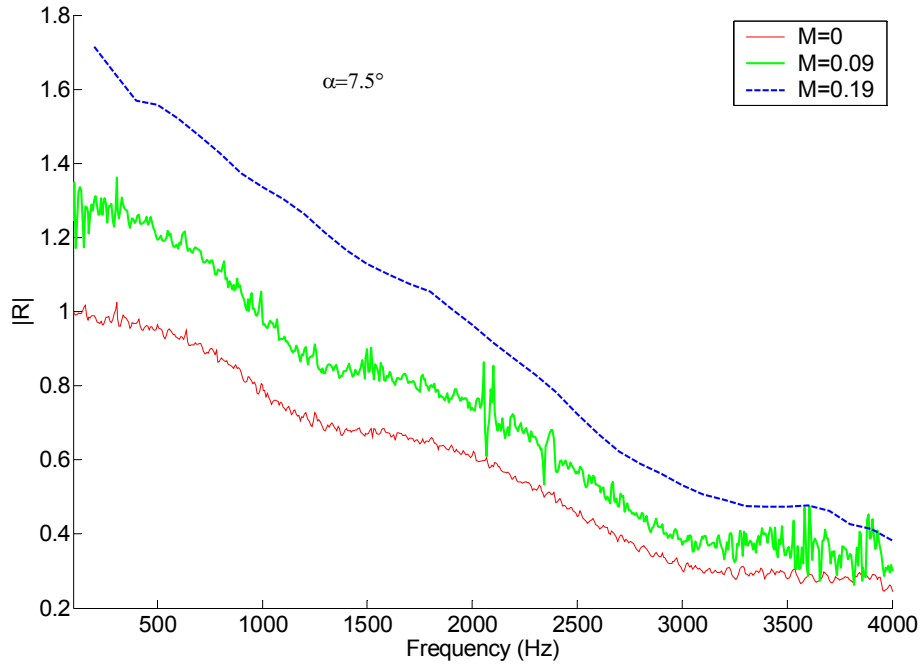


(a)



(b)

Figure 25(a), (b): Influence of the Mach number on the outlet impedance of the diffuser  $7.5^\circ$ .



(c)

Figure 25 (c): Influence of the Mach number on the pressure reflection coefficient and outlet impedance of the diffuser  $7.5^\circ$ .

It can be seen that an increase of the Mach number results in a reduction of the radiation resistance (real part of the load impedance  $Z$ ) at low frequency. The end correction (imaginary part of the load impedance  $Z$ ) is on the other hand unchanged at low frequency. At high frequency, the resistive term is not dependent on the flow speed whereas the end correction increases with the flow Mach number. The two cases presented here (also at low frequency, see Figure 26 and Figure 27) show that both the angle and flow influence the acoustics of the termination.

### ***Diffuser low frequency measurement***

The experimental investigation is repeated on the diffusers with a larger separation between the microphones in order to cover a lower frequency range (0-200 Hz). The full Kutta condition used in Munt's theory stipulates that the flow at the lips leaves the pipe as an uniform cylindrical flow with thin boundary layers. Flow separation inside the element violates this boundary condition. The low frequency limit of the pressure reflection coefficient  $R$  predicted with the Kutta condition is not valid anymore.

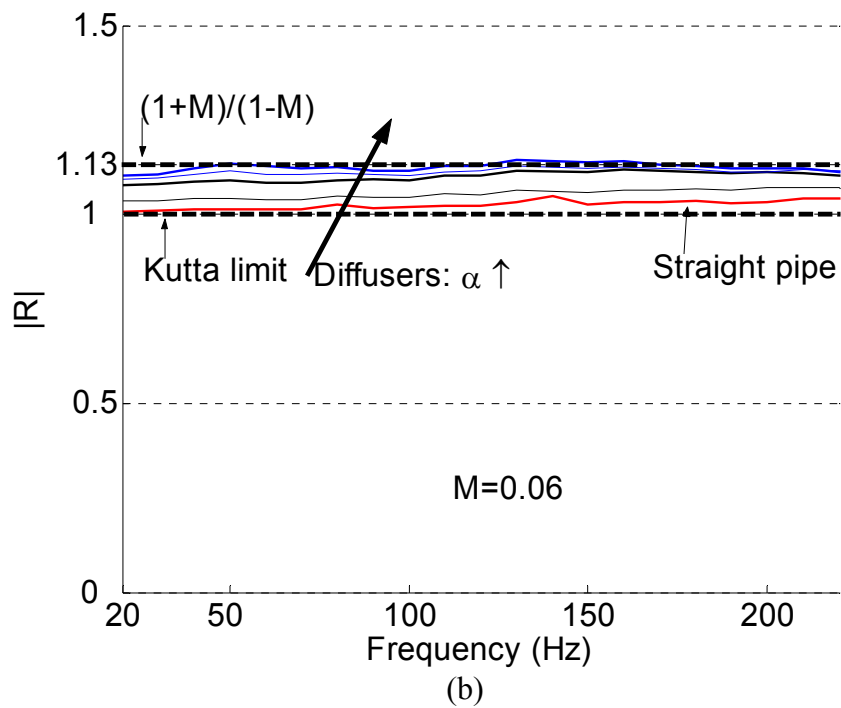
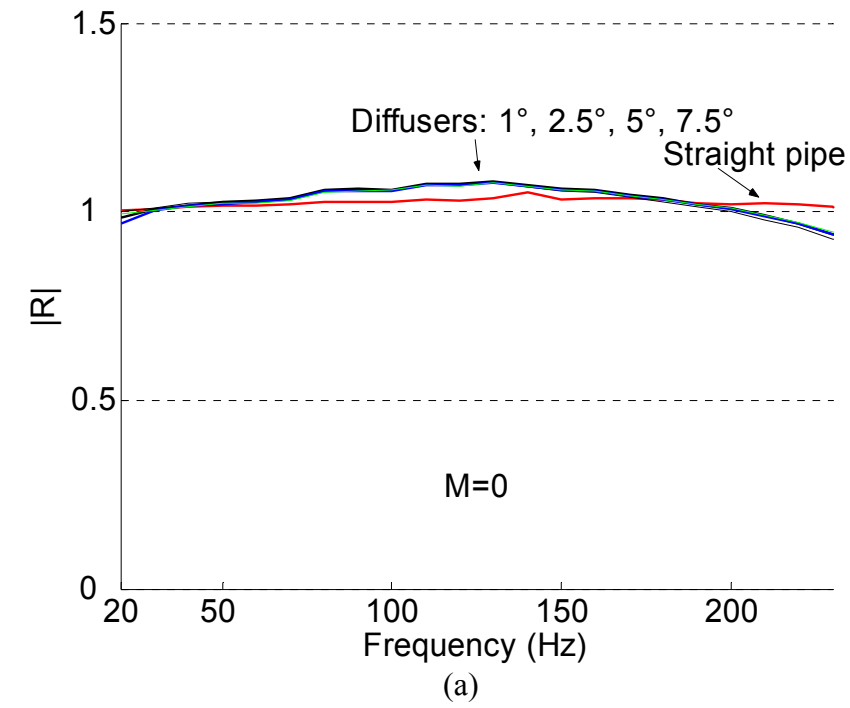


Figure 26 (a), (b): Low frequency reflection coefficient measurements for diffusers ( $M=0, 0.06$ ).



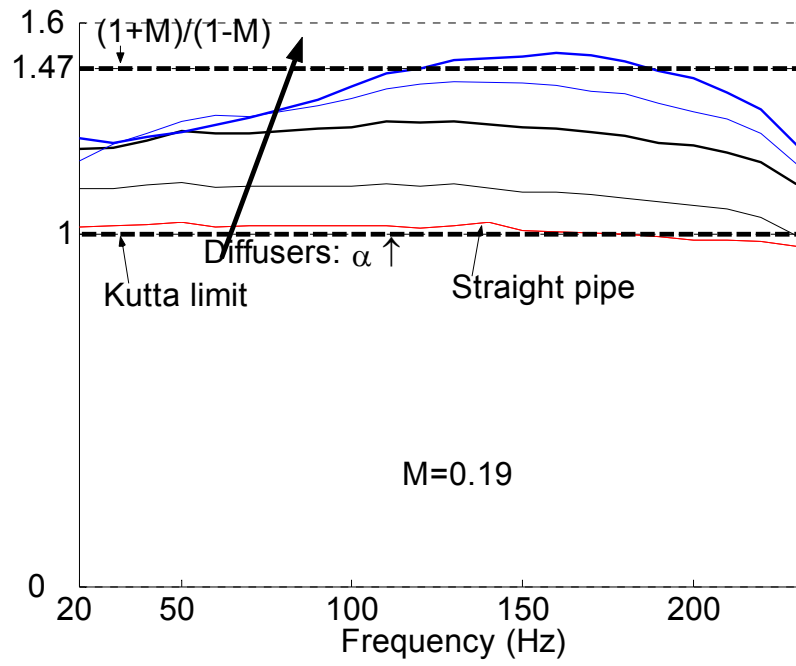
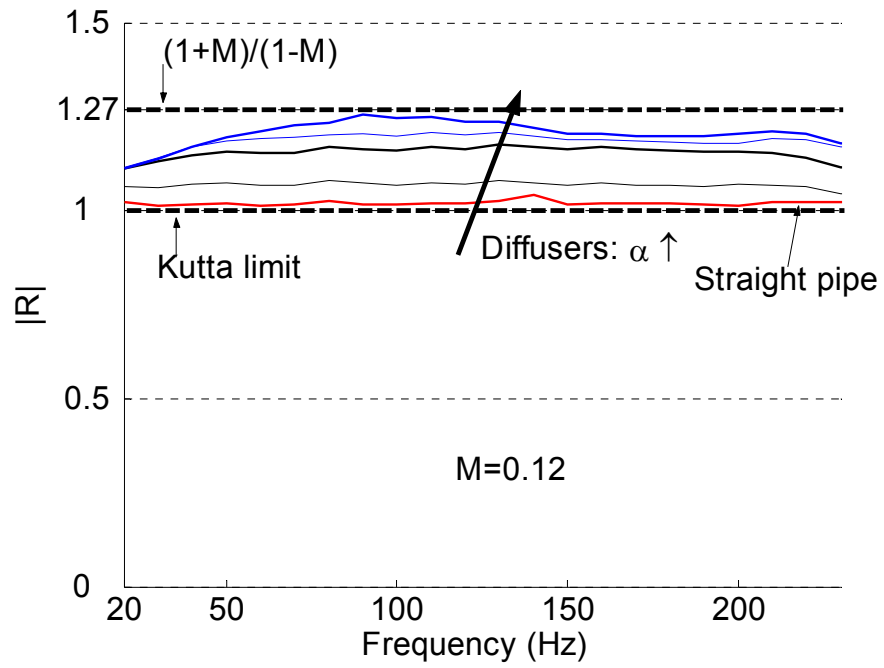


Figure 26 (c), (d): Low frequency reflection coefficient measurements for diffusers ( $M=0.12$ ,  $0.19$ ).

Hirschberg and al. (1988) have studied the vortex sound generated by diffusers. They use the energy reflection coefficient  $R_E$  defined as

$$R_E = |R_B|^2 = |R|^2 \frac{(1 - M^2)}{(1 + M^2)}, \quad (3-5)$$

where  $R_B$  is the enthalpy reflection coefficient and  $R$  is the sound pressure reflection coefficient used throughout this paper. It indicates that for  $R_E$  exceeding unity, sound is amplified by the flow separation mechanism. As seen from Figure 26 the tested diffusers are not producing extra sound. But for angles around  $5-7.5^\circ$  we approach the limit  $((1 + M)/(1 - M))$  of no losses, i.e., all the incident acoustic power is reflected for low frequencies.

### ***Diffuser impedance results***

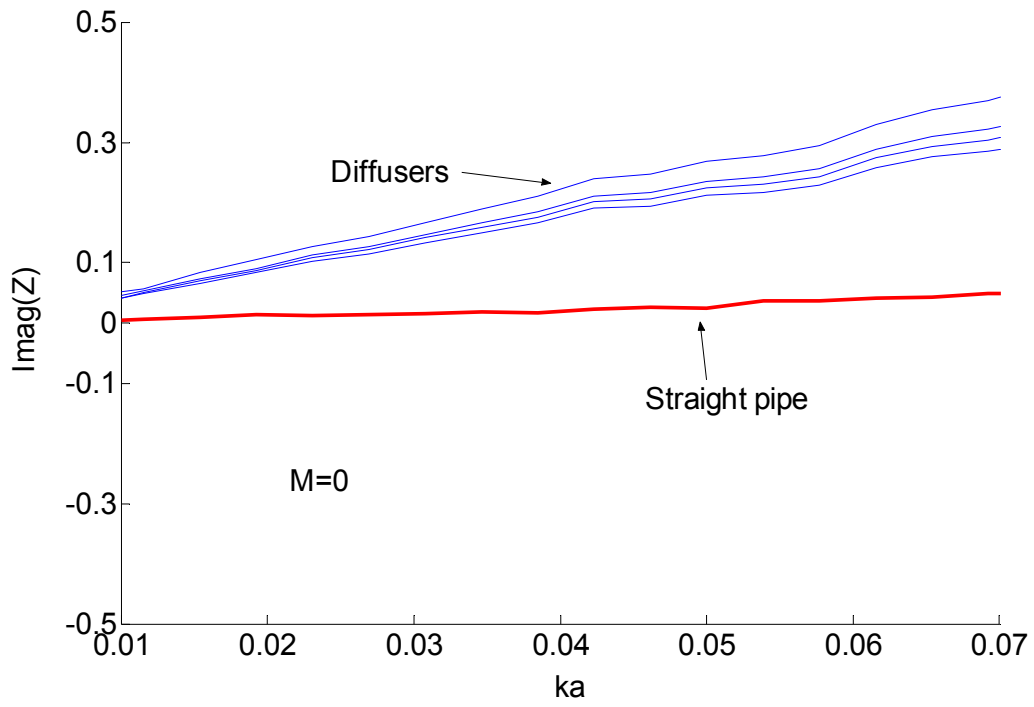
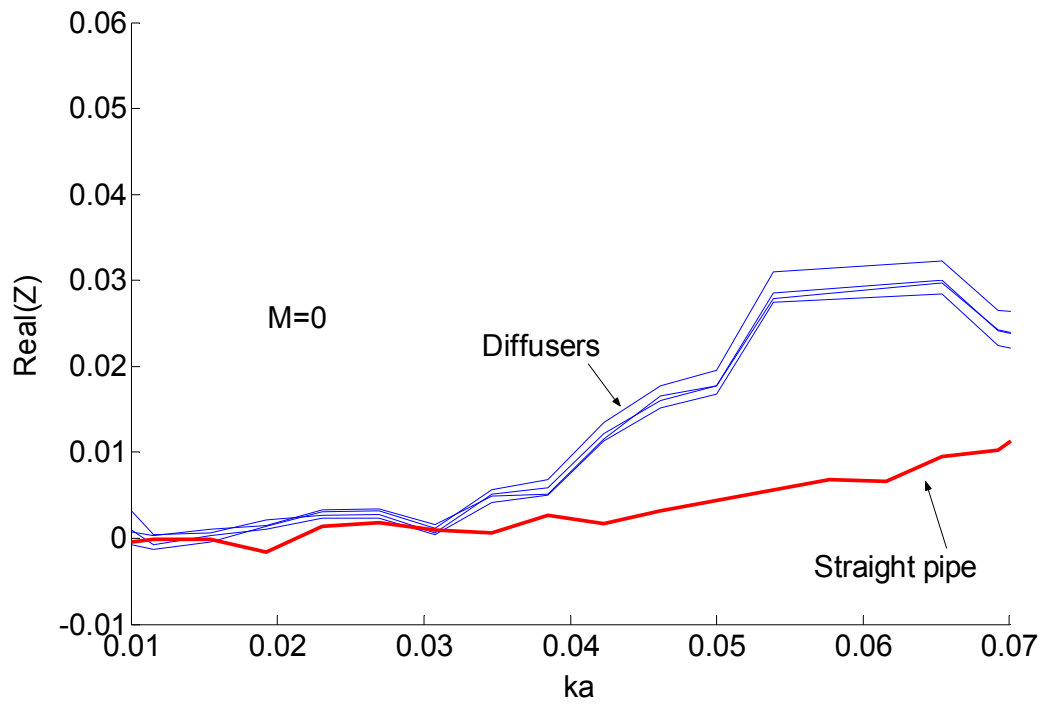
Measurement of the complex pressure reflection coefficient  $R$  enables the derivation of the complex impedance  $Z$  (see (1-1)) for the same low frequency range.

### ***Influence of diffuser half-angle $\alpha$***

The real and imaginary part of the impedance is plotted in Figure 27 as function of the Helmholtz number  $ka$ , the diffuser angle  $\alpha$  and flow Mach number  $M$ . The data was obtained at the microphone reference 1 and moved to the open end by a distance of  $l=150$  mm (cf Figure 1) corresponding to the opening of the straight pipe and to the inlet of the diffusing elements. The length of the elements is constant (105 mm).

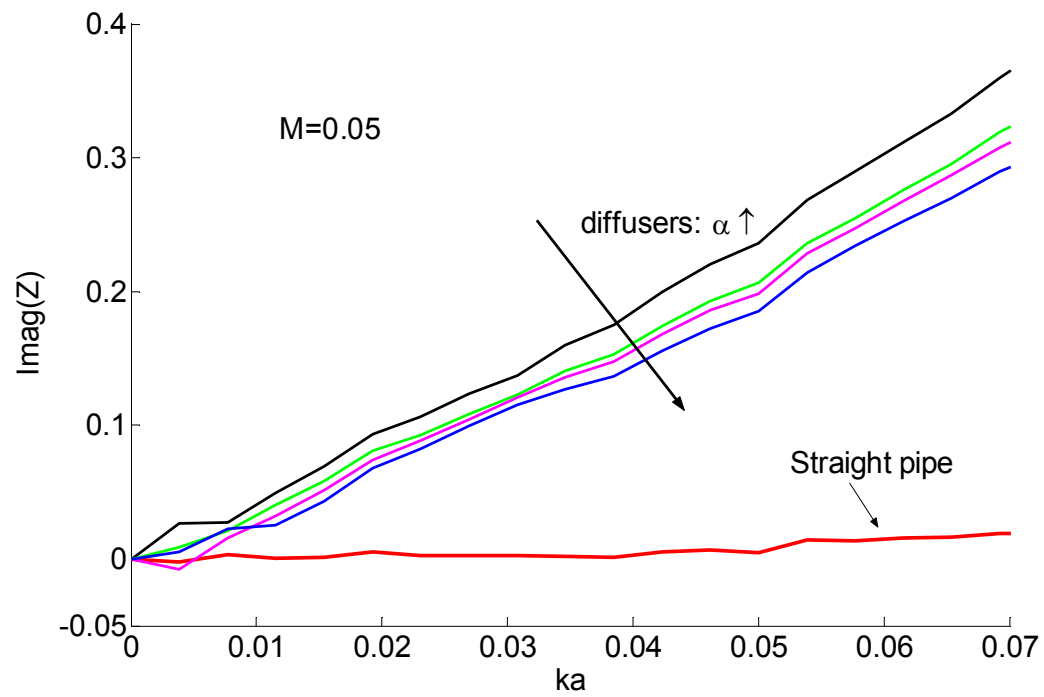
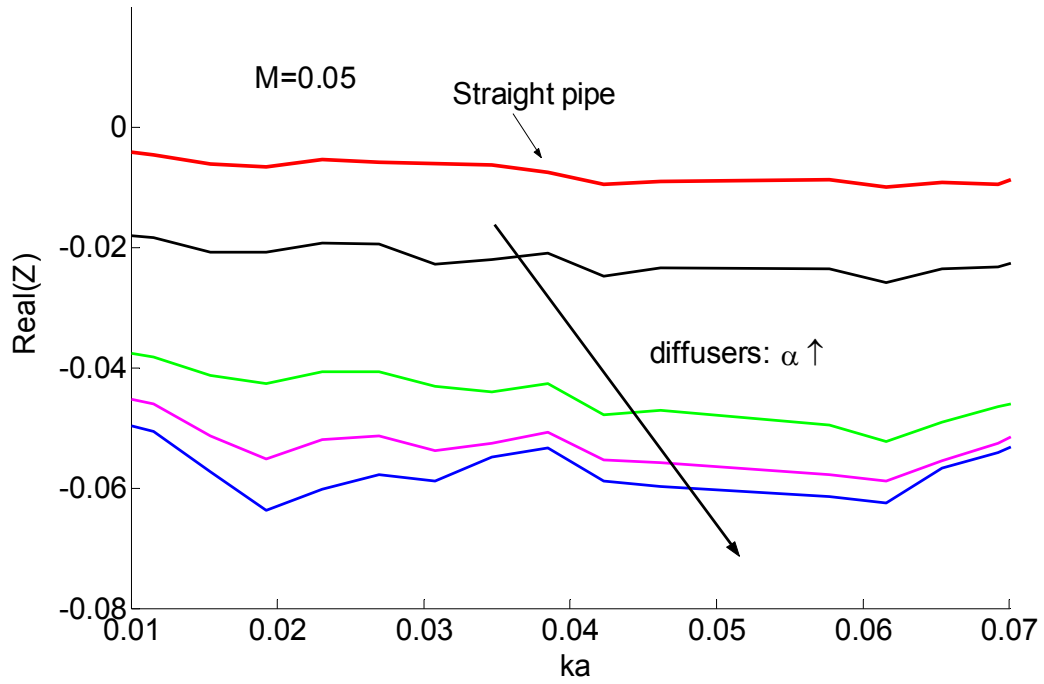
For results with no flow ( $M=0$ ), no deviations are observed between the diffusers. It shows that the diffusers have the same behaviour when no airflow is introduced in the pipe.

In view of the flow results,  $M=0.05$  and  $0.2$ , the trend is for the real part of the impedance (radiation resistance) to decrease as the diffuser angle  $\alpha$  and Mach number  $M$  increase. This observation is of paramount importance when the diffuser is connected to an exhaust line. An optimal design of exhaust system requires to minimise such radiation. Modelling and performance estimation of exhaust line with these measured load impedance data are presented in the section “Modelling of exhaust lines”.



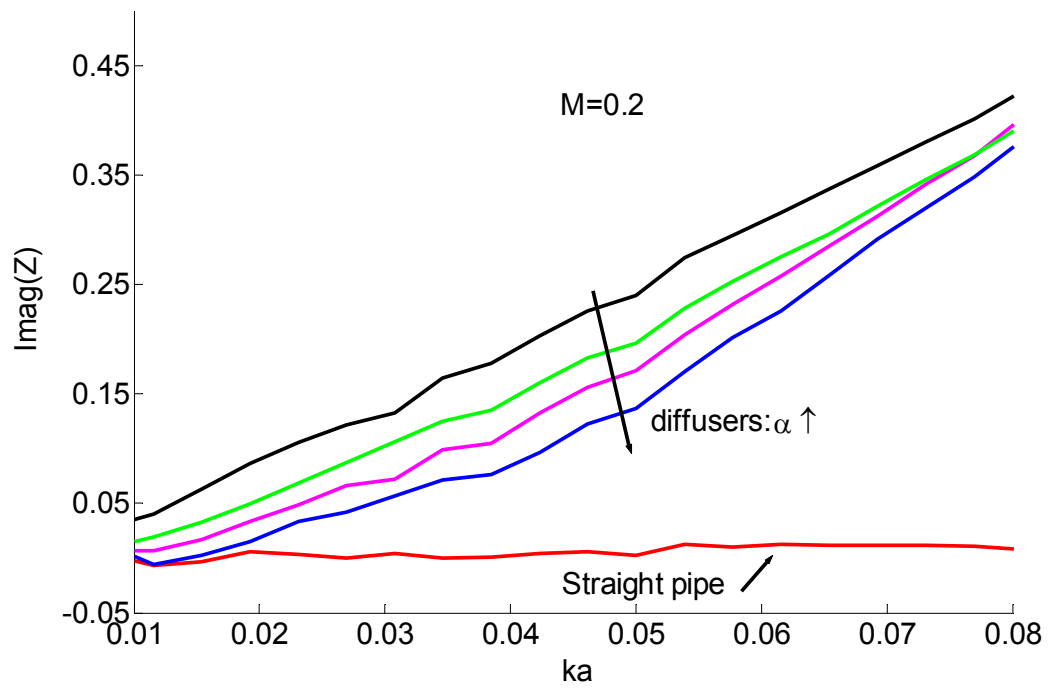
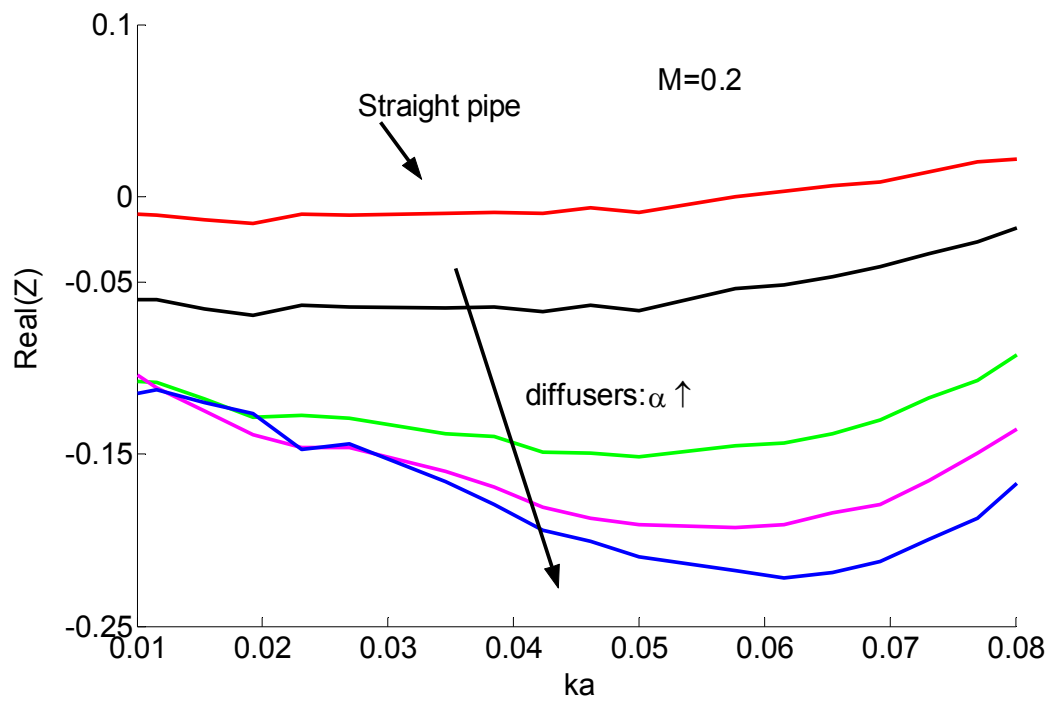
(a)

Figure 27 (a): Normalised inlet impedance measurement at low Helmholtz number for diffuser elements ( $M=0$ ).



(b)

Figure 27 (b): Normalised inlet impedance measurement at low Helmholtz number for diffuser elements ( $M=0.05$ ).



(c)

Figure 27 (c): Normalised inlet impedance measurement at low Helmholtz number for diffuser elements ( $M=0.2$ ).

*Theoretical investigation of the opening acoustics of diffusers*

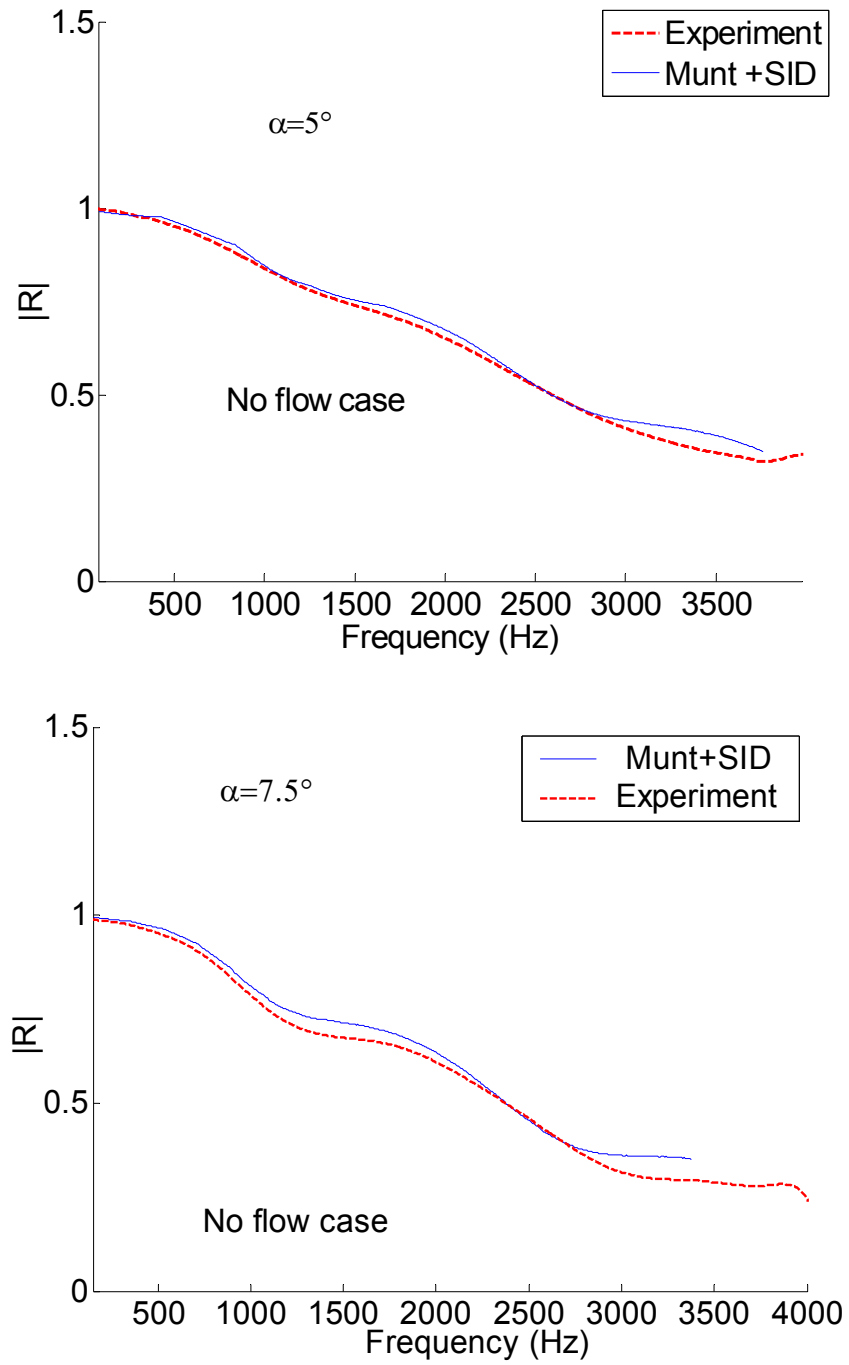


Figure 28: Theoretical and experimental comparison for reflection coefficient for diffusers with no flow.



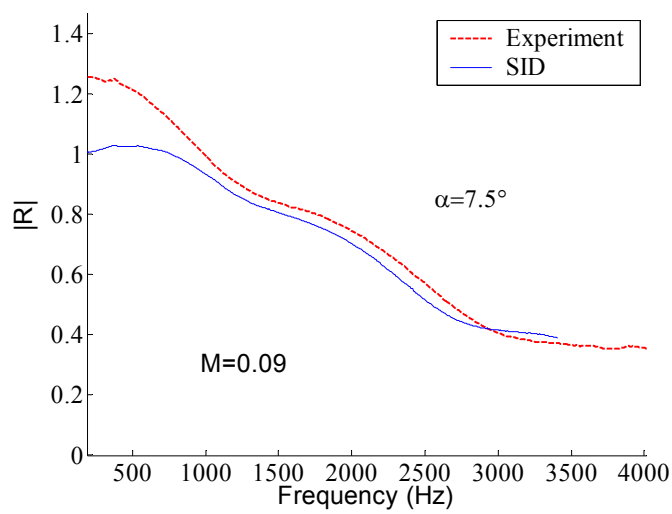
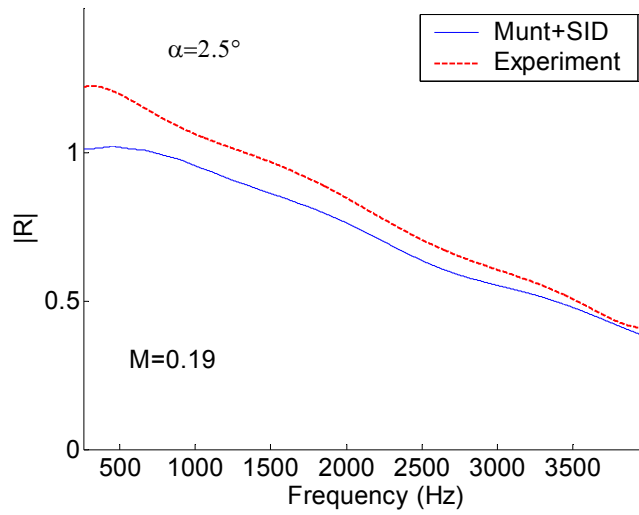
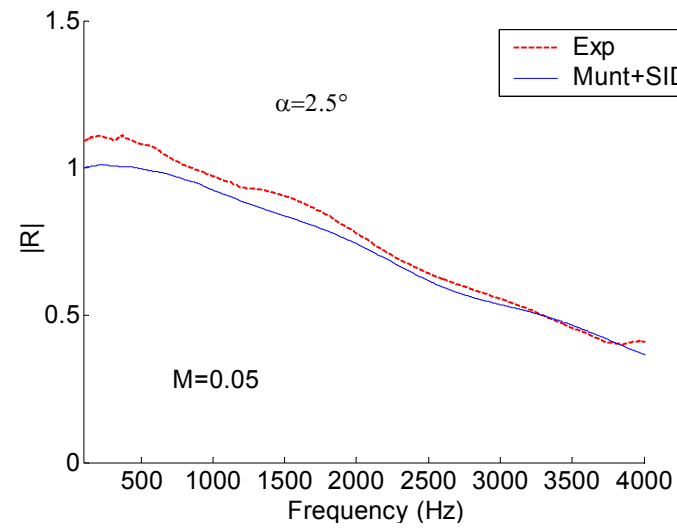


Figure 29: Theoretical and experimental comparison for reflection coefficient for flow diffusers.

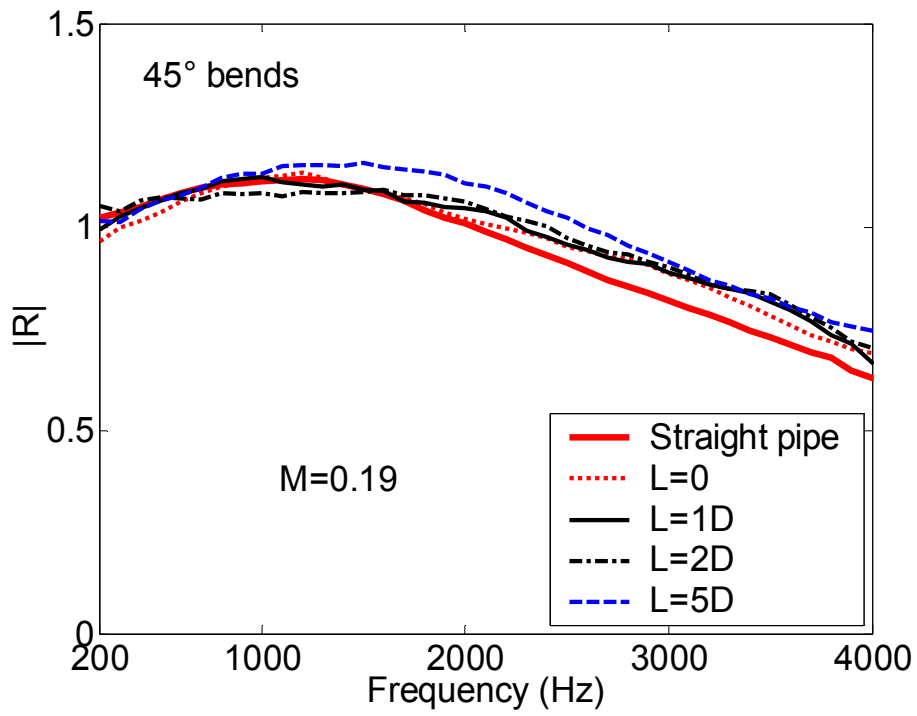
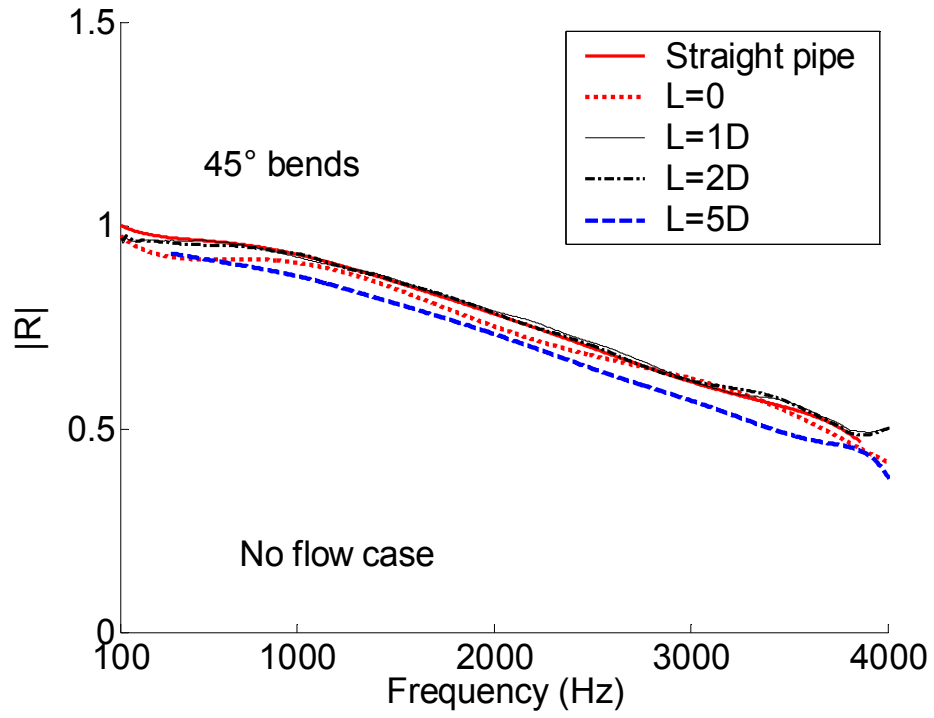
The results presented in Figure 28 from the transfer matrix model used to predict the reflection coefficient for the no flow case agrees well with the experimental data. Modelling of the standing wave pattern (undulation) is achieved theoretically. There is a significant discrepancy between the calculated and experimental values for lower frequency when flow is present in the rig (Figure 29). Dequand and al. (2002) showed for diffusers of this type that the flow separation point is not fixed but moves along the inner walls of the diffuser elements. Munt's model to calculate the pressure reflection coefficient at the outlet cross-section is based on a sharp-edged condition (Kutta condition). Flow separation is assumed to occur solely at the lips in Munt's model. Due to the flow separation within the diffuser element for half-angle greater than  $4^\circ$ , the boundary layer at the opening is substantially thicker violating the simple flow separation model used by Munt.

### ***Bends***

Experimental results for the reflection coefficient of bends and straight-pipe terminations are given in Figure 30 and Figure 31. it emphasises and confirm the findings of Dequand and al. (2002) , i.e., the bends can be replaced by a straight pipe. The curvature of the bend does not affect the internal sound propagation under the present conditions. Dequand and al. (2002) showed that smooth bends do not differ strictly from a straight pipe. Their attempt to predict sound propagation through smooth bends using an incompressible quasi-stationary model failed to give satisfactory data due to the flow separation point moving along the wall. This model is valid for geometries involving sharp edges such as: slit, perforated plates, abrupt expansions. In the case of smooth elements in slowly divergent conical diffusers or smooth bends, other effects come into play that are not well predicted by the quasi-stationary theory. Dequand and al. (2002) demonstrates that modelling the sound propagation through smooth bends using a Fanno model give better agreement with experimental data than using a quasi-stationary model. Such a model characterises the bend as a straight pipe of the same length as the centreline distance between the inlet and outlet of the bend and includes a finite friction factor. The pressure loss used in this Fanno model to estimate the friction magnitude is either obtained experimentally by measuring the pressure drop between the inlet and outlet of the element or can be found in Blevins (1984).



*45° bends*



(a)

Figure 30 (a): Reflection coefficient measurements for 45° bends.

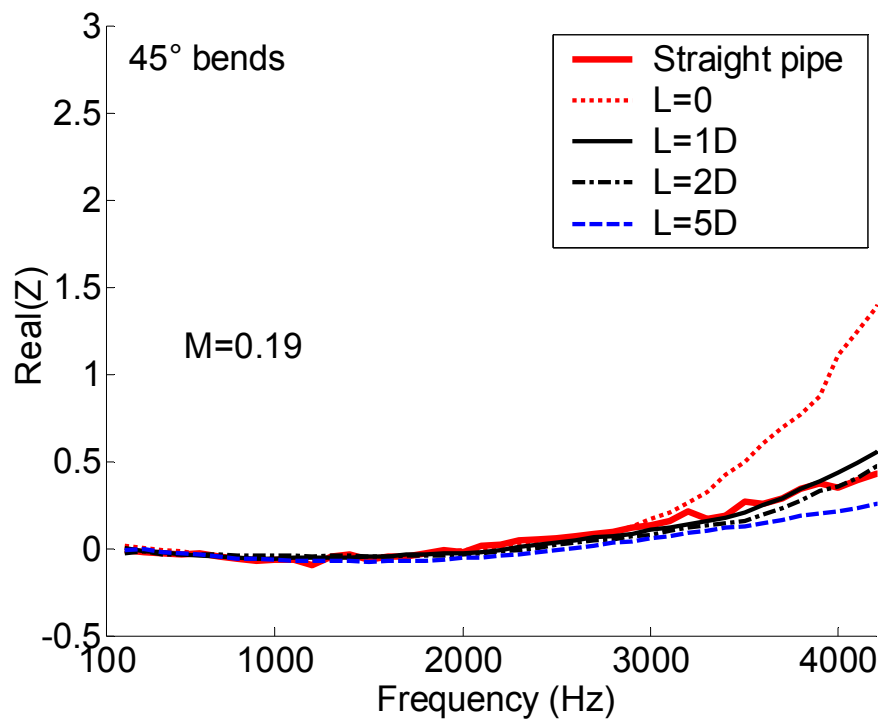
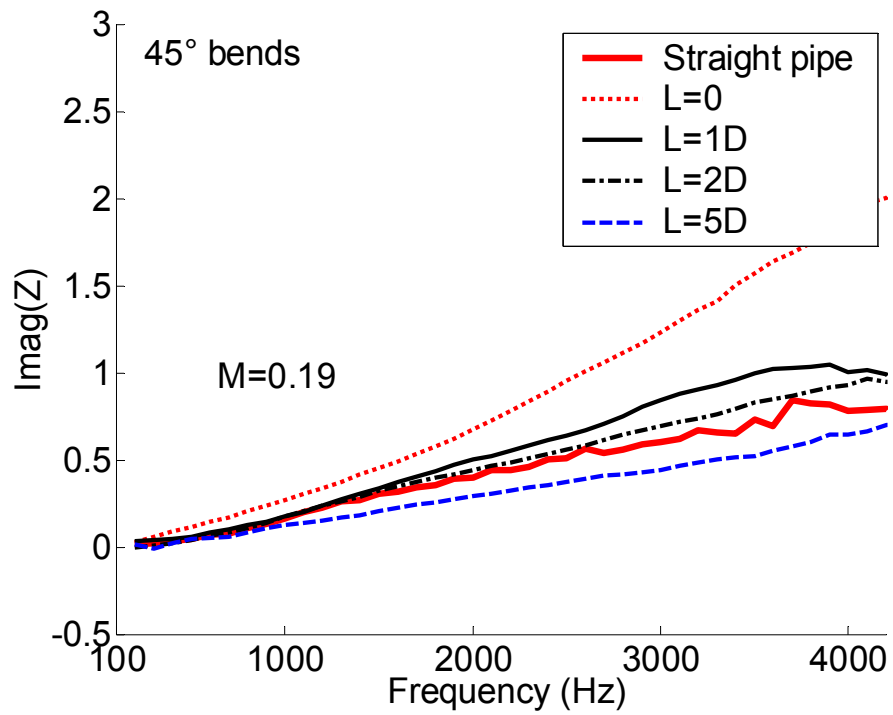
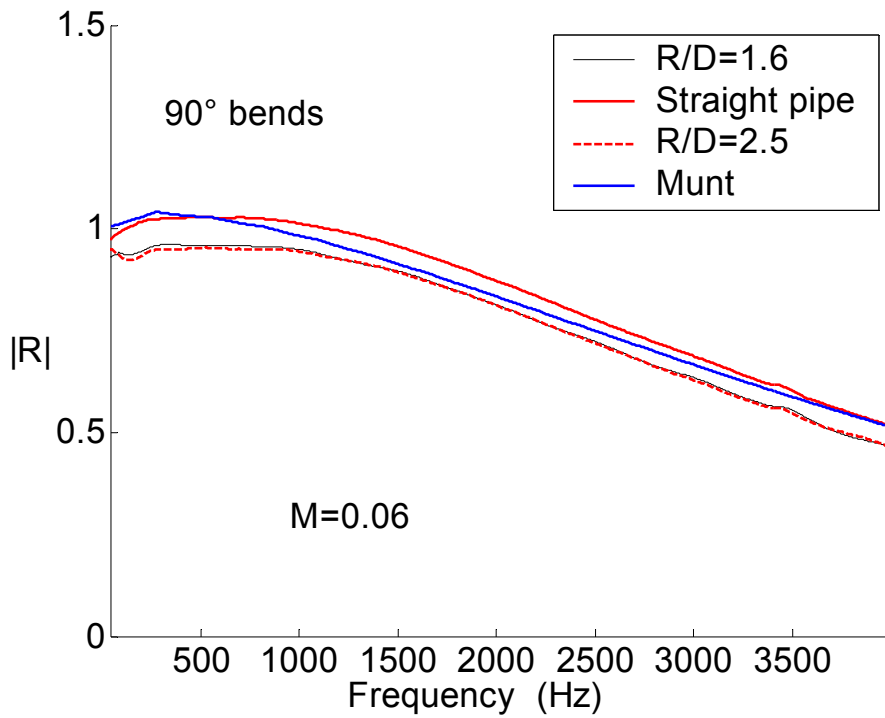
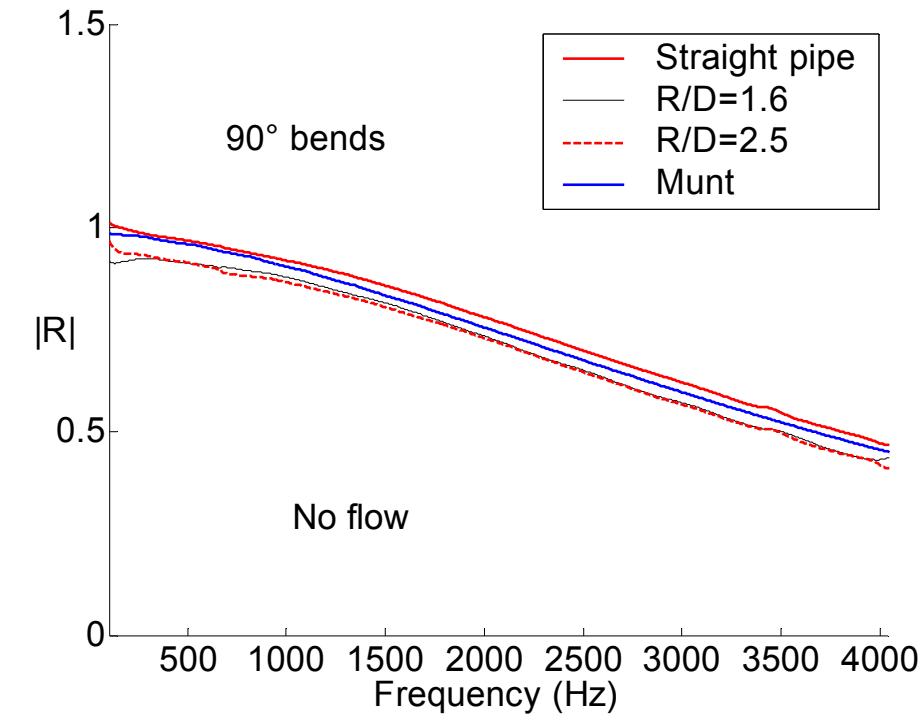


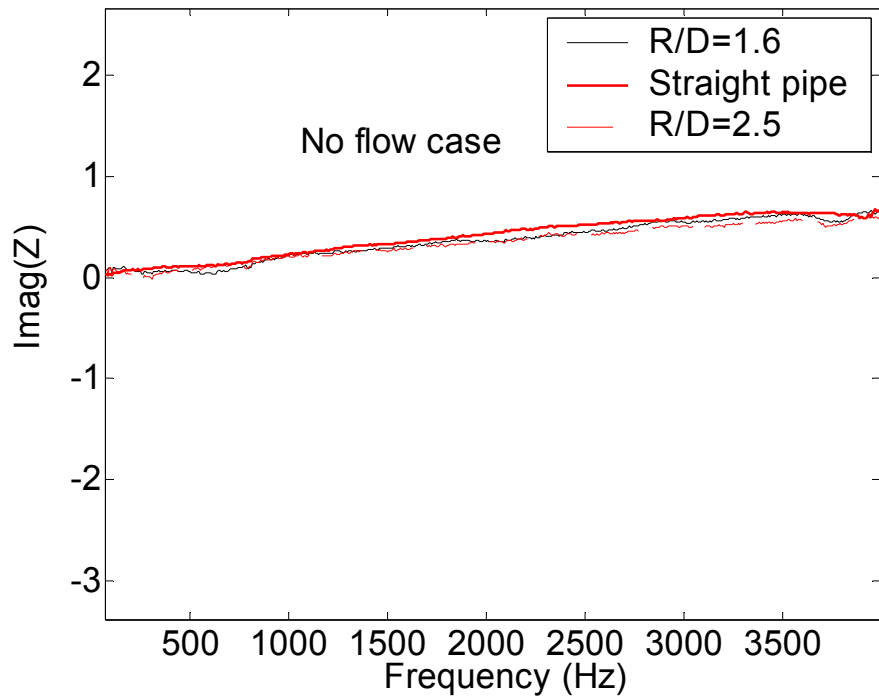
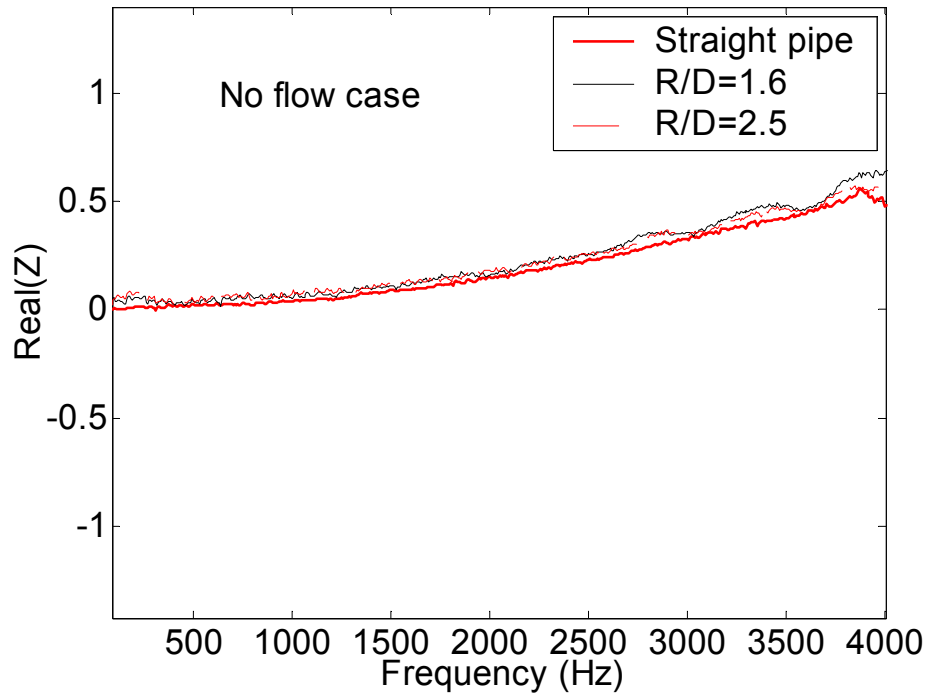
Figure 30: Impedance measurements for 45° bends.

*90° bends*



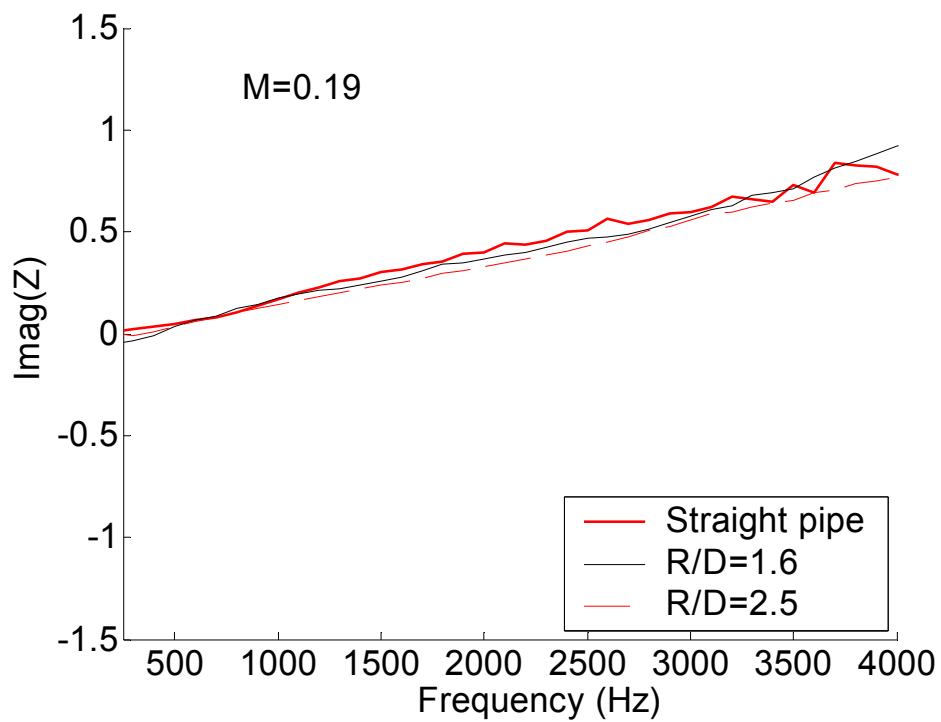
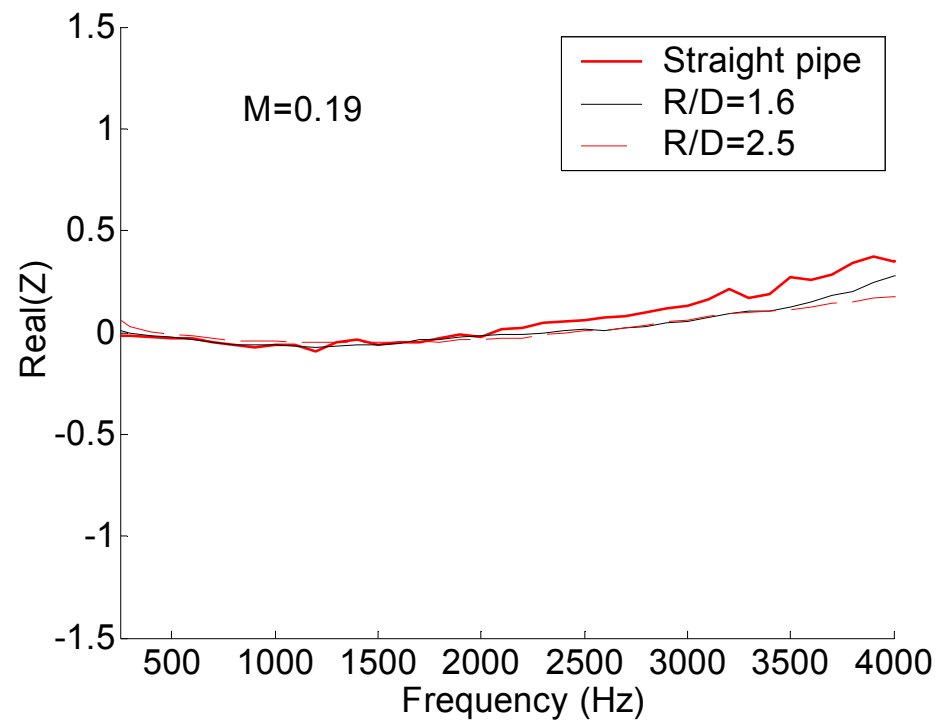
(a)

Figure 31 (a) : Reflection coefficient measurements for 90° bends.



(b)

Figure 31 (b): Impedance measurements for 90° bends ( $M=0$ ).



(c)

Figure 31 (c) : Impedance measurements for 90° bends ( $M=0.19$ ).

### 3.3 Summary

Experimental and theoretical investigations have been performed on various elements terminating a straight pipe. Internal sound propagation in a pipe terminated by elements such as oblique cuts, diffusers and bends have been both experimentally and theoretically studied. The experimental procedure consisted of the standard two-microphone technique. Thus, inlet and outlet data have been obtained for any element by shifting the measured pressure reflection coefficient at the microphone reference to the position of interest. Measurements have been carried out for no flow and for flow up to a Mach number of 0.2. Experimental results show the aeroacoustic behaviour differences between the elements. The theoretical procedure to compute the pressure reflection coefficient or impedance consisted of combining the outlet impedance from a model derived by Munt (1977, 1990) and an element transfer matrix calculated from the SID software. For the oblique cuts a reasonable agreement with experimental data is observed when the obliquity effect is approximated using a number of parallel pipes with varying length. However, this model breaks up at high frequencies due to the lack of non-plane wave effects. A more exhaustive model is required to fully predict the behaviour of the oblique cut elements. Concerning the diffuser elements, the model works well for the no flow case. Discrepancies between the experimental and theoretical results have been observed at low frequencies when flow is present in the rig. Measurements have been repeated at even lower frequencies (0-200 Hz) and confirm such a trend. Results from the straight pipe indicate that the magnitude of the reflection coefficient tends to unity at low frequencies. Diffusers behave differently and show a reflection coefficient magnitude larger than 1 in the low frequency limit. Inspection of the impedance results for diffusers also reveals deviations from the straight pipe behaviour at low frequency. In order to assess the practical applicability of these observations on the diffusers, the results are used in the next chapter to model complete exhaust lines. The purpose of this modelling is to estimate the potential of the diffusers to improve the insertion loss at low frequencies, in particular at tailpipe resonances. Experimental comparison between bends and the straight pipe confirms an observation previously made; the internal sound propagation in bends is similar to that of a straight pipe. Thus, no special transfer matrix calculation is required.

## 4. Modelling of exhaust lines

The experimental investigation on internal noise propagation has highlighted various acoustical phenomena for the tailpipes studied. It is now necessary to implement and estimate these effects in designs of exhaust lines in order to test the usefulness for a typical automotive application of the results. It has been found that the acoustic properties of the oblique cut elements start to deviate from that of a straight pipe at frequencies above 1500 Hz. The dominating pulsations in a diesel engine can be observed at much lower frequencies ( $< 200$  Hz). Deviations from a straight pipe at this low frequency range have been observed for flow diffusers. Thus, diffuser terminations show interesting acoustic properties at low frequencies for automotive applications. The acoustic properties of bends do not differ significantly from the straight pipe over the investigated frequency range ( $< 5000$  Hz).

Two types of exhaust lines (“automotive” and “single pipe”) are modelled using the measured data of the diffuser load impedances,  $Z_L$ .

The automotive exhaust line has been designed in such way that the Insertion Loss IL index has been calculated between two systems having the same source and measured load termination impedance but with different elements. In the case of the single pipe exhaust line, the elements remain the same, only the load termination is changed. The single pipe exhaust line is used to explain the improvements observed for the automotive line.

### 4.1 Description of an exhaust line

A typical schematic of an exhaust line is given in Figure 32. It comprises of a source, elements and termination.

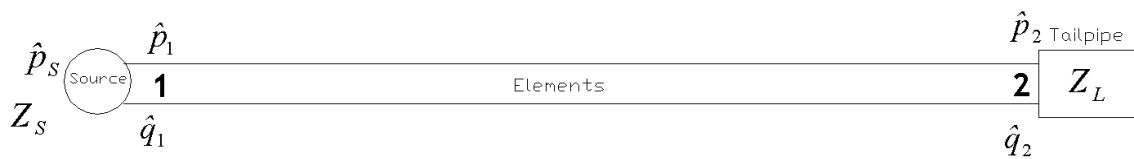


Figure 32: Schematic of a standard exhaust line.

The volume flow speed  $\hat{q}_2$  at the outlet of the exhaust line can be calculated by defining (Bodén (1989)) the source impedance  $Z_s$ , the source pressure  $\hat{p}_s$  (source pressure), the transfer matrices of the elements positioned between the source and the termination and the load impedance. Comparison of the volume flow speed  $\hat{q}_2$  from a reference system enables the determination of the Insertion Loss (IL).

The pressure  $\hat{p}$  and volume flow speed  $\hat{q}$  at the inlet (1) and outlet (2) of the exhaust line depicted in Figure 32 is given by

$$\begin{aligned}\hat{p}_1 &= \hat{p}_s - Z_s \hat{q}_1, \\ \hat{p}_2 &= Z_L \hat{q}_2.\end{aligned}\tag{4-1}$$

The state variables pressure  $\hat{p}$  and volume flow speed  $\hat{q}$  at the inlet (1) and outlet (2) of the entire system is related for any exhaust line through its transfer matrix. The exhaust line transfer matrix  $T_{exh} = \begin{pmatrix} T_{11} & T_{12} \\ T_{21} & T_{22} \end{pmatrix}$  depends on the elements composing the line between the source and the termination. The relation between the pressure  $\hat{p}$  and volume flow speed  $\hat{q}$  at the inlet (1) and outlet (2) is given as

$$\begin{pmatrix} \hat{p}_1 \\ \hat{q}_1 \end{pmatrix} = \begin{pmatrix} T_{11} & T_{12} \\ T_{21} & T_{22} \end{pmatrix} \begin{pmatrix} \hat{p}_2 \\ \hat{q}_2 \end{pmatrix}.\tag{4-2}$$

(4-2) can be rearranged as

$$\begin{aligned}\hat{p}_1 &= T_{11}\hat{p}_2 + T_{12}\hat{q}_2, \\ \hat{q}_1 &= T_{21}\hat{p}_2 + T_{22}\hat{q}_2.\end{aligned}\tag{4-3}$$

The complex pressure reflection coefficient  $R_{ref}$  is measured at the in-duct flush-mounted reference microphone using the two-microphone technique. The value of the reflection coefficient  $R_L$  at the inlet is calculated using (1-3).

The load impedance used in the calculation of the  $IL$  for the exhaust lines is formulated as

$$Z_L = \left( \frac{1 + R_L}{1 - R_L} \right) \frac{\rho_0 c_0}{S},\tag{4-4}$$

where  $S$  is the inlet cross-section area. The results for the normalised load impedances are given in Figure 27.

Due to the low frequency investigation, it is assumed throughout this section that the



sound radiated to the far field is of monopole type, i.e., it is proportional to the volume flow speed  $\hat{q}$  at the outlet of the entire system. The low frequency range studied also implies that the inlet tailpipe impedance is equivalent to the outlet impedance.

Combining (4-1) and (4-3) gives the monopole source strength  $\hat{q}_2$  at the outlet (2) of the exhaust line

$$\hat{q}_2 = \frac{\hat{p}_s}{Z_L T_{11} + T_{12} + Z_s Z_L T_{21} + Z_s T_{22}}. \quad (4-5)$$

## 4.2 The automotive exhaust line

An automotive exhaust line is typically composed of a source, two straight pipes of length  $L_1$  and  $L_2$  respectively and a silencer, as depicted in Figure 33. In some cases, e.g., trucks, it is sometimes necessary to use a long tailpipe  $L_2$ . This is problematic since it will introduce low frequency tailpipe resonances that are in the same frequency range as the engine harmonics.

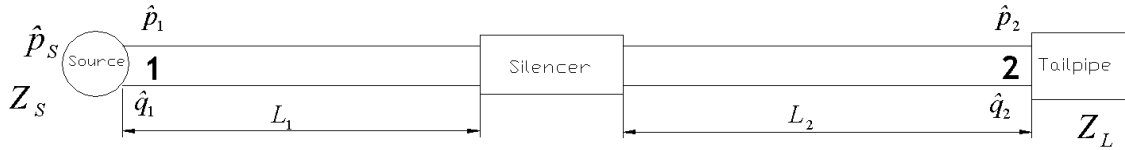


Figure 33: The automotive exhaust line.

For the case studied below a Scania truck exhaust line with  $L_1=1.3\text{m}$  and  $L_2=2.6\text{m}$  is used (Glav (1994)).

The total transfer matrix for the entire system in Figure 33 is calculated from

$$T_{exh} = T_{sp,L_1} \times T_{silencer} \times T_{sp,L_2} = \begin{pmatrix} T_{11exh} & T_{12exh} \\ T_{21exh} & T_{22exh} \end{pmatrix}, \quad (4-6)$$

where the straight pipe transfer matrix  $T_{sp}$  is given in equation (4-11).

The frequency independent source impedance  $Z_s = \rho_0 c_0 \exp(i\pi 7/4)/S$  where  $S$  is the pipe cross-section area is taken from Callow & Peat (1988). No source strength  $P_s$  is required and can be set up to any value as it cancels out when deriving the expression for  $IL$ .

The measured truck silencer transfer matrix is given as

$$T_{silencer} = \begin{pmatrix} T_{11sil} & T_{12sil} \\ T_{21sil} & T_{22sil} \end{pmatrix} \quad (4-7)$$

provided by the Swedish heavy-vehicle manufacturer Scania for no flow condition gives the following transmission loss

$$TL = 10 \log_{10} \left( \frac{1}{4} \left| T_{11sil} + \frac{T_{12sil}}{Z_0} + Z_0 T_{21sil} + T_{22sil} \right|^2 \right). \quad (4-8)$$

The inlet and outlet impedances are equal to  $Z_0 = \rho_0 c_0 / S$  with  $S$  taken as the inlet and outlet silencer cross-section area and equal to  $8.66 \times 10^{-3} \text{ m}^2$ . A plot of the Scania silencer transmission loss is given in Figure 34.

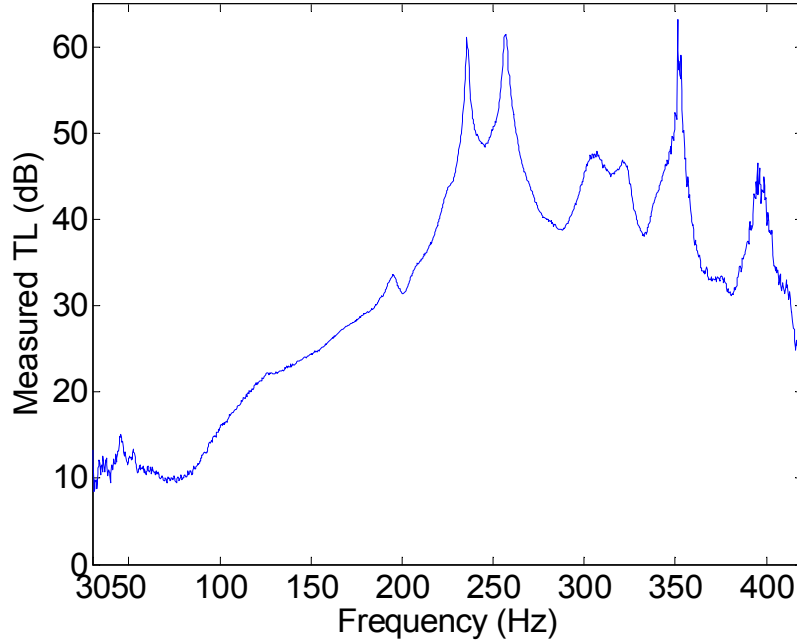


Figure 34: Transmission loss for Scania silencer.

The transfer matrices for the two pipes  $T_{sp,L_1}$  and  $T_{sp,L_2}$  in Figure 33 are computed using (4-11) with  $L_1=1.3\text{m}$  and  $L_2=2.6\text{m}$ .

In order to derive the IL, it is necessary to define a reference system. It is defined as shown in Figure 35 as a source, a pipe of zero length with transfer unit matrix and the measured termination impedance  $Z_L$

$$T_{ref} = \begin{pmatrix} T_{11ref} & T_{12ref} \\ T_{21ref} & T_{22ref} \end{pmatrix} = \begin{bmatrix} 1 & 0 \\ 0 & 1 \end{bmatrix}. \quad (4-9)$$

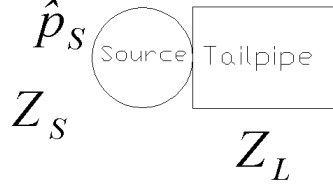


Figure 35: Reference system for the automotive exhaust line.

### Insertion loss

An insertion loss index  $IL$  is calculated for the system in Figure 33 and the reference system in Figure 35 with the same load impedance  $Z_L$ . The  $IL$  is defined as the ratio of the source strength calculated for the automotive exhaust line in Figure 33 ( $\hat{q}_{exh}$ ) to the reference line in Figure 35 ( $\hat{q}_{ref}$ ).

$$IL_{exh} = -20 \log_{10} \left( \frac{\hat{q}_{exh}}{\hat{q}_{ref}} \right) = -20 \log_{10} \left( \frac{Z_L T_{11ref} + T_{12ref} + Z_S Z_L T_{21ref} + Z_S T_{22ref}}{Z_L T_{11exh} + T_{12exh} + Z_S Z_L T_{21exh} + Z_S T_{22exh}} \right), \quad (4-10)$$

where  $T_{11ref}$ ,  $T_{12ref}$ ,  $T_{21ref}$ ,  $T_{22ref}$  elements are given in (4-9),  $T_{11exh}$ ,  $T_{12exh}$ ,  $T_{21exh}$ ,  $T_{22exh}$  elements are obtained from (4-6) and  $Z_L$  is the measured tailpipe load impedance.

The measured load impedance  $Z_L$  is obtained on elements with an inlet diameter of 42 mm. The silencer data provided by Scania corresponds to an inlet and outlet diameter of 105 mm. It was thus necessary to obtain the load impedance for the diffuser using the same dimensionless Helmholtz number  $ka$  based on either the silencer or pipe radius.

### Results

The  $IL$  calculated from (4-10) for systems terminated with the diffuser elements of different semi-angle  $\alpha$  are shown in Figure 36 for the no flow condition. It can be seen from Figure 36 that changing the diffuser element at the termination of the automotive exhaust line do not significantly modify the  $IL$  results in the case of no airflow. The large dip ( $\approx 55$  Hz) comes from the first half-wavelength resonance in the tailpipe  $L_2$ . However, when flow is introduced, it can be seen from Figure 37 that the larger the diffuser half angle  $\alpha$ , the larger the  $IL$  value at the resonance frequency. An increase in

the  $IL$  is interpreted as an improvement as it means that the radiation to the outside of the exhaust line is reduced. It can be noted that the  $IL$  value at the resonance dip is improved with more than 10 dB.

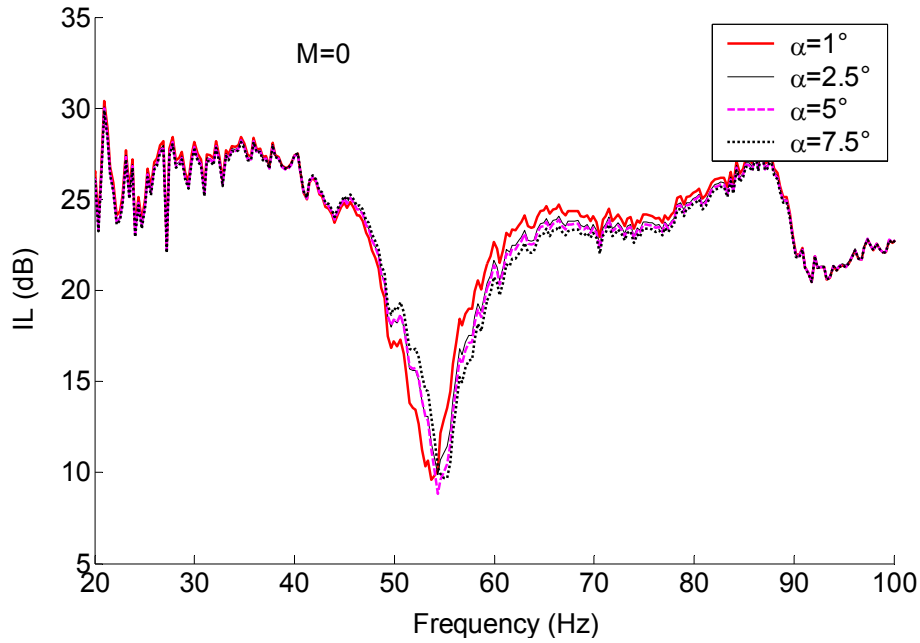


Figure 36: No flow  $IL$  for the automotive exhaust line terminated with diffusers.

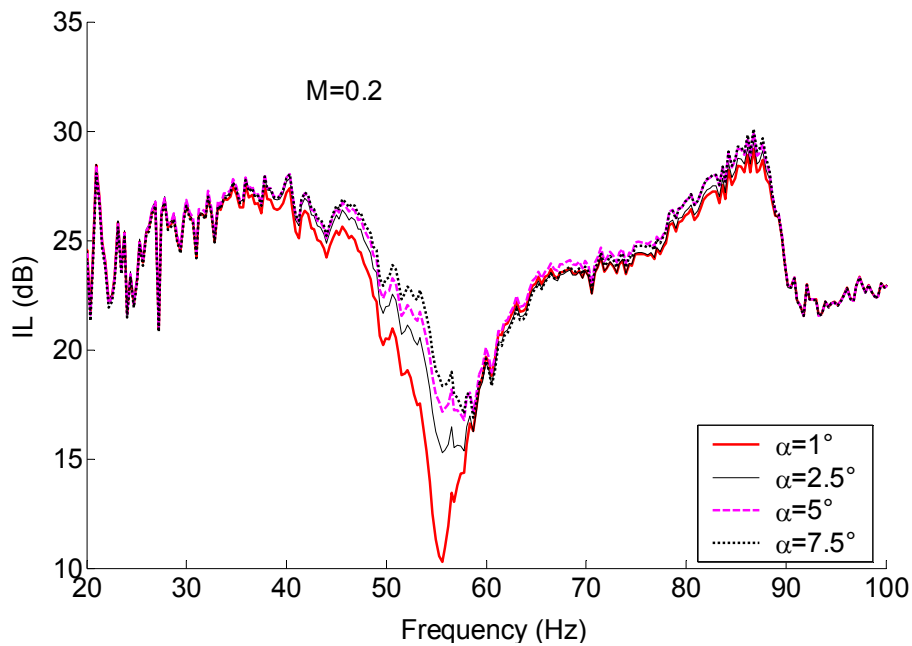


Figure 37:  $IL$  with flow for the automotive exhaust line terminated with diffusers.

Looking at the largest angle ( $\alpha=7.5^\circ$ ) investigated, Figure 38 shows the improvement at different Mach numbers.

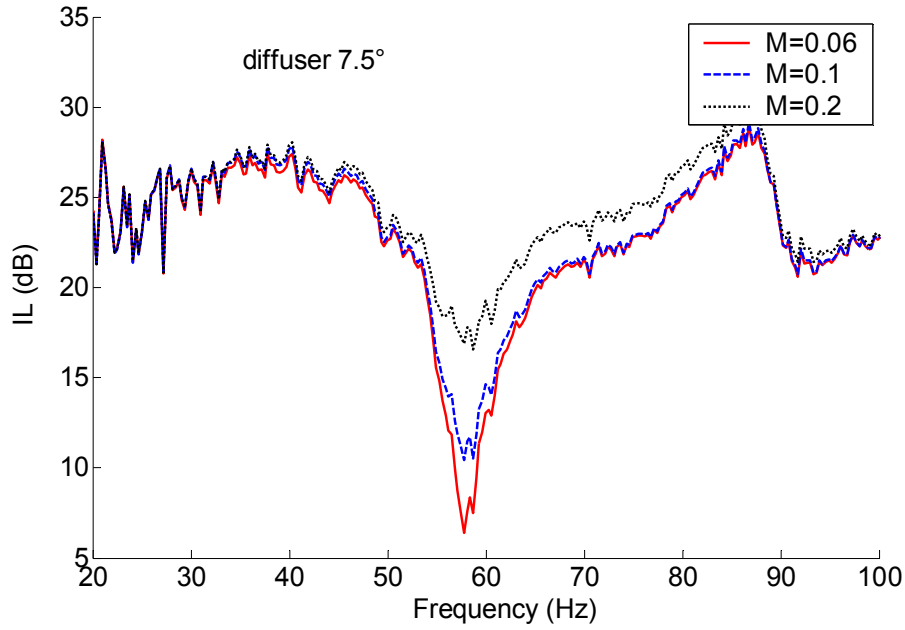


Figure 38: Automotive exhaust line IL for the diffuser  $7.5^\circ$  at various flow Mach number  $M$ .

It appears that the IL is greater when flow Mach number and diffuser angle increase. In order to understand these results on the tailpipe resonance, a simplified system consisting only of a tailpipe is studied next. Since the tailpipe at the upstream end is normally connected to a “large volume” (silencer), it will be assumed that the source impedance  $Z_s$  is zero.

### 4.3 The single pipe exhaust line

This system comprises a pipe of length  $L$  and a source strength  $Z_s=0$  as shown in Figure 39.

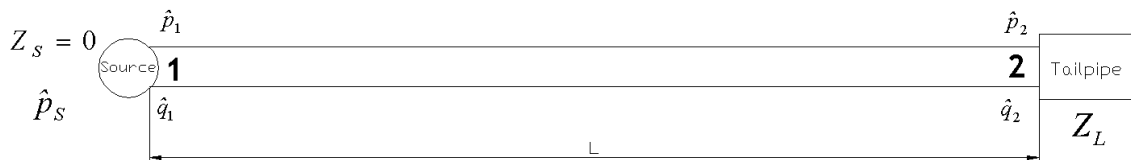


Figure 39: The single pipe exhaust line.

A reference system is taken for the single pipe exhaust line terminated with diffuser of angle  $\alpha=1^\circ$  to ensure overall fixed length. The diffusers have a constant length of 105 mm.

The transfer matrix for a straight pipe element with flow of length  $L$  is

$$T_{sp,L} = \begin{pmatrix} \frac{1}{2} [\exp(ik_+L) + \exp(-ik_-L)] & \frac{\rho_0 c_0}{2S} [\exp(ik_+L) - \exp(-ik_-L)] \\ \frac{S}{2\rho_0 c_0} [\exp(ik_+L) - \exp(-ik_-L)] & \frac{1}{2} [\exp(ik_+L) + \exp(-ik_-L)] \end{pmatrix}, \quad (4-11)$$

where  $k_{+/-} = k/(1 \pm M)$ . A length  $L=2.6\text{m}$  is used.

### Insertion loss

An insertion loss  $IL$  is calculated and is defined as the ratio of the source strength calculated for the exhaust line in Figure 39 ( $\hat{q}_{sp}$ ) terminated with diffusers to the same exhaust line but with the diffuser of angle  $1^\circ$  ( $\hat{q}_{ref}$ ).

$$IL_{sp} = -20 \log_{10} \left( \frac{\hat{q}_{sp}}{\hat{q}_{ref}} \right) = -20 \log_{10} \left( \frac{Z_{Lref} T_{11sp,L} + T_{12sp,L} + Z_S Z_{Lref} T_{21sp,L} + Z_S T_{22sp,L}}{Z_{Ltailp} T_{11sp,L} + T_{12sp,L} + Z_S Z_{Ltailp} T_{21sp,L} + Z_S T_{22sp,L}} \right). \quad (4-12)$$

The elements  $T_{11sp,L}$ ,  $T_{12sp,L}$ ,  $T_{21sp,L}$ ,  $T_{22sp,L}$  are obtained theoretically from (4-11). The measured load impedance for the  $1^\circ$  diffuser ( $Z_{Lref}$ , reference case) and tailpipe  $Z_{Ltailp}$  are taken from the measurement of the pressure reflection coefficient  $R_L$  and (4-4).

### Results

Figure 40 shows the effect of the diffuser angle  $\alpha$  on the  $IL$  for the single pipe exhaust line with flow Mach number  $M=0.2$ .

An improvement at the tailpipe resonance frequencies  $nc_0/2L$ ,  $n=1,2$  is observed. The results are consistent with the observations made on the automotive exhaust line. It is immediately apparent from Figure 40 that a diffuser with an angle larger than  $1^\circ$  improves the  $IL$  at the tailpipe resonance frequencies of the pipe length  $L$ .

Figure 41 displays the influence of the flow Mach number on the  $IL$  for the diffuser angle  $\alpha=7.5^\circ$ . Figure 40 and Figure 41 illustrate and confirm the results obtained from the automotive exhaust line, i.e., the  $IL$  at the tailpipe resonance frequencies increase with the diffuser angle and flow Mach number  $M$ .

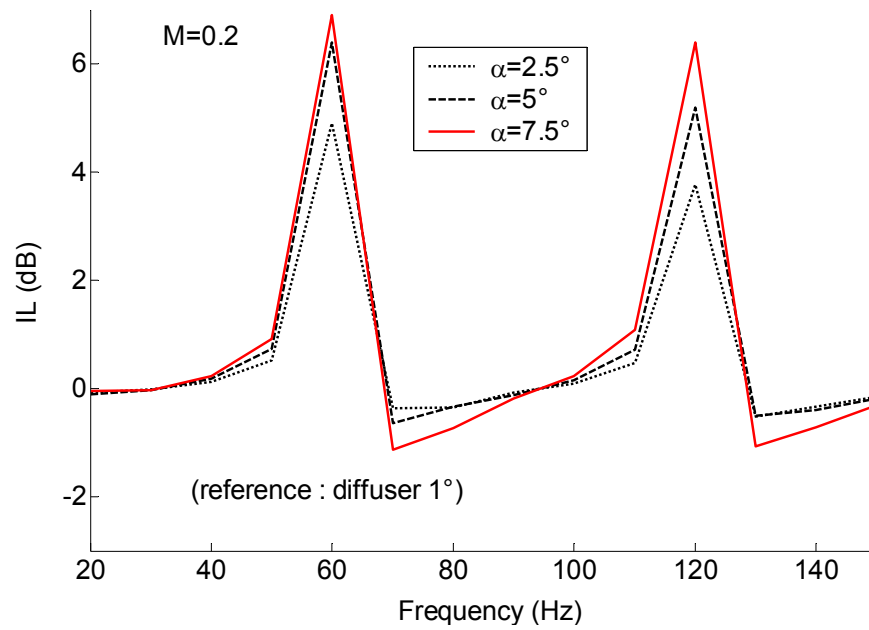


Figure 40: Influence of the diffuser angle for the single pipe exhaust line.

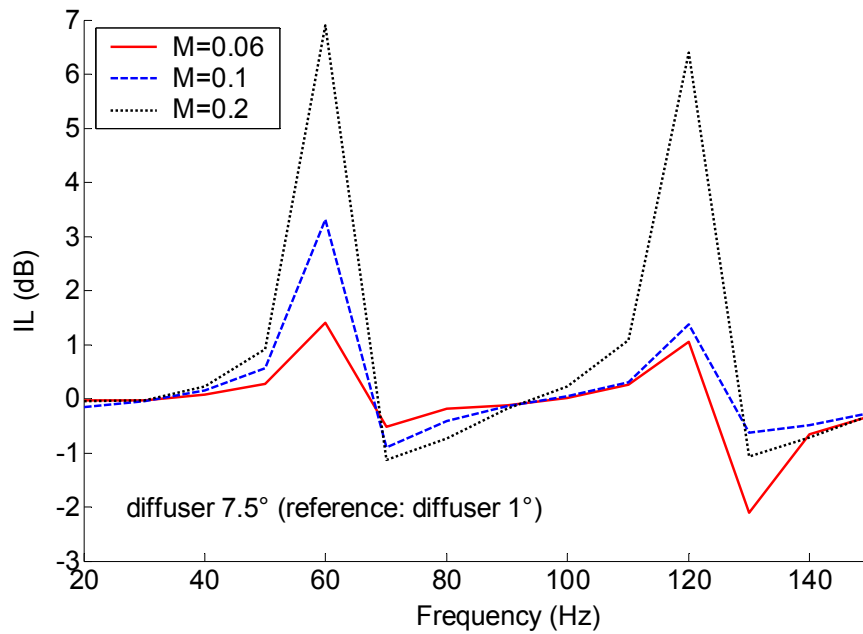


Figure 41: Single pipe exhaust line  $IL$  for the diffuser  $7.5^\circ$  at various Mach number  $M$ .

#### 4.4 Summary

The investigation of the acoustics of diffusers as pipe terminations has showed low frequency deviations from the straight pipe case. The magnitude of the pressure reflection  $R$  at the opening of the diffusers has been experimentally obtained using the two-microphone technique. It has been found that at low frequency ( $< 200$  Hz) and with airflow in the rig, the magnitude of the pressure reflection coefficient  $R$  is greater for the diffusers than for the straight pipe.

The experimental load impedance results for diffusers have been implemented in the calculation of the insertion loss  $IL$  for two types of designs; a Scania truck exhaust and a single pipe system.

In view of the results obtained for both exhaust lines terminated with diffuser elements, it can be concluded that the magnitude of the  $IL$  is increased at the tailpipe resonance frequencies. The effect increases with the diffuser angle and flow Mach number and improvements of up to 10 dB seems possible in practice.

Another important parameter to consider when designing such system is the sound generation due to flow separation. This is treated in the next chapter.



## **5. Flow noise for a straight pipe and tailpipes**

In the previous chapters, noise , produced from loudspeakers located upstream the rig, propagates through the rig and radiates from the termination. An experimental and theoretical investigations have been carried out in the previous chapters on the reflection of this sound with and without airflow. Other sources of sound in this apparatus are the flow noise created by the flow inside the pipe and at the terminations. This noise termed as flow noise or aerodynamic noise is of a broadband type and has been studied by Lighthill and reviewed by Goldstein (1976). The flow noise creation is due to the flow separation that occurs inside the pipe, at the lips of the termination and further downstream when the flow breaks up into turbulence. This chapter analyses the flow noise for a straight pipe with circular open end and for the terminations previously studied (oblique cuts, diffusers, bends). The flow noise measurements are performed using a rotating microphone located in a reverberant room. The chapter starts by estimating the various sound power levels found in a straight pipe in order to identify the dominant flow noise mechanism. This is important as data from the tailpipes are compared with the straight pipe (reference case) for derivation of scaling laws for the flow noise sound power.

### **5.1 Methods and materials**

#### **5.1.1 Measurement of flow-induced noise in a reverberant room**

The comparative method (ISO 3747) was chosen for determination of noise generated at the opening of the rig due to the flow separation. This measurement technique uses a reference sound source in a reverberant room for which the sound power level is known. The reference sound source power levels are provided in 1/3-octave bands. A half-inch microphone mounted on a rotating support measured and averaged sound pressure levels of the signal either generated at the opening or from the reference source into the diffuse field.

### 5.1.2 Flow noise generation for a straight pipe

Flow noise is created in different regions of a straight pipe (Figure 42). The following section aims to compare the sound power levels of the noise produced inside the pipe (1), at the lips (2) and in the jet mixing region located outside the pipe (3).

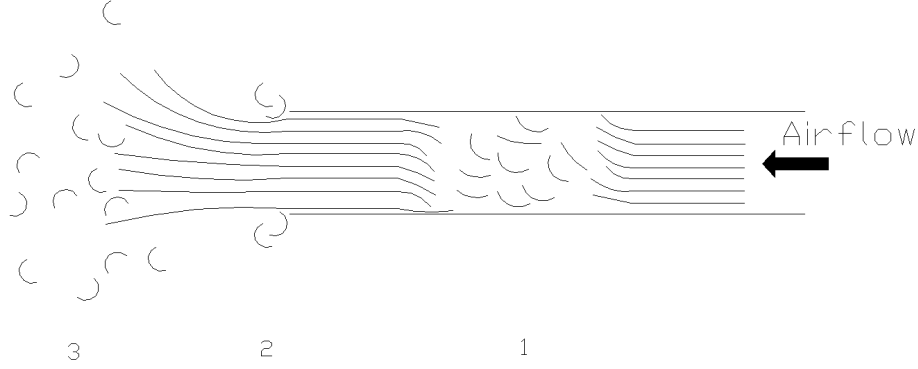


Figure 42: Flow noise generation mechanisms in a straight pipe.

Starting with the internal flow noise in a straight pipe, a semi-empirical model (VDI 3733 (1996)) is presented and used to determine the internal sound power level generated by the flow inside the pipe.

The VDI 3733 guideline gives a semi-empirical model obtained from flow noise induct measurements on long pipes with anechoic terminations. For Mach number ( $M=U/c_0$ ) of less than 0.3, the internal noise generation due to the flow separation inside a straight pipe is dominantly of dipole type (VDI 3733) implying that the flow induced sound power is proportional to  $U^6$ . The flow generated sound power level inside a straight pipe is empirically formulated as

$$L_{w_i} = 10 \log_{10} \left( \frac{W}{W_0} \right) = K + 10 \log_{10} \left( \frac{U}{U_0} \right)^6 + 10 \log_{10} \left( \frac{S}{S_0} \right) + 10 \log_{10} \left( \frac{p}{p_0} \right) - 25 \log_{10} \left( \frac{NT}{N_0 T_0} \right) - 15 \log_{10} \left( \frac{\gamma}{\gamma_0} \right), \quad (5-1)$$

where  $K=8-0.16U$  (correction factor) and the reference values are  $W_0=10^{-12}$  W,  $U_0=1$  m.s<sup>-1</sup> (flow speed),  $S_0= 1$  m<sup>2</sup> (cross-section area),  $p_0= 101325$  Pa (pressure),  $T_0=273$  K (temperature),  $N_0= 287$  J.kg<sup>-1</sup>.K<sup>-1</sup> (specific gas capacity),  $\gamma_0=1.4$  (specific heat ratio).

The internal flow induced sound power level  $L_{w_i,1/3}$  in a straight pipe in 1/3-octave bands is expressed as (VDI 3733).

$$L_{w_i,1/3} = L_{w_i} + \Delta L_{w,oct} - 4.77 \text{ dB}, \quad (5-2)$$

where for  $f/U > 12.5 \text{ m}^{-1}$ , the octave band correction is

$$\Delta L_{W,oct} = 12 - 15.5 \log_{10}(f_{oct}/U), \quad (5-3)$$

where  $f_{oct}$  corresponds to the octave band center frequencies.

It has been assumed in VDI 3733 that the flow induced noise power level given by (5-2) is due to an internal process in the straight pipe. Thus, part of the acoustic energy is reflected at the opening. The external microphone only measures the portion of the sound that is transmitted out of the open end. Therefore, it is necessary to compute transmitted sound power levels for comparison with our data obtained from the external measurement. The ratio of the transmitted sound power  $W_t$  to the incident power  $W_i$  is

$$\frac{W_t}{W_i} = 1 - |R|^2. \quad (5-4)$$

The following empirical formulation (Davies and al. (1980)) is used to predict the pressure reflection coefficient  $R$ .

$$R = 1 + 0.01336ka - 0.59079(ka)^2 + 0.33576(ka)^3 - 0.06432(ka)^4 \quad (5-5)$$

The effect of the flow on the reflection coefficient is here neglected.

In terms of the sound power level, the relation in (5-4) can be rewritten as

$$L_{W_t} = L_{W_i} + 10 \log_{10}(1 - |R|^2) \quad (5-6)$$

Thus, the transmitted sound power level can be rewritten as

$$L_{W_t,1/3} = L_{W_i,1/3} + 10 \log_{10}(1 - |R|^2), \quad (5-7)$$

where  $L_{W_i,1/3}$  is given by (5-2) and corresponds to the empirically predicted internal sound power in 1/3-octave bands.

Figure 43 shows the flow noise measured in the far field together with the internal noise results obtained from (5-7). The flow noise measurement corresponds to the flow noise generated from the inside, from the lips and jet mixing region and picked up by the rotating microphone. The internal flow noise sound power level calculated from (5-7) (VDI 3733) indicates that the flow noise created inside the pipe and transmitted out is not the dominant mechanism for our external measurement. It appears that the measured data correspond to the noise created at the lips and in the jet mixing region under the Mach number range investigated.

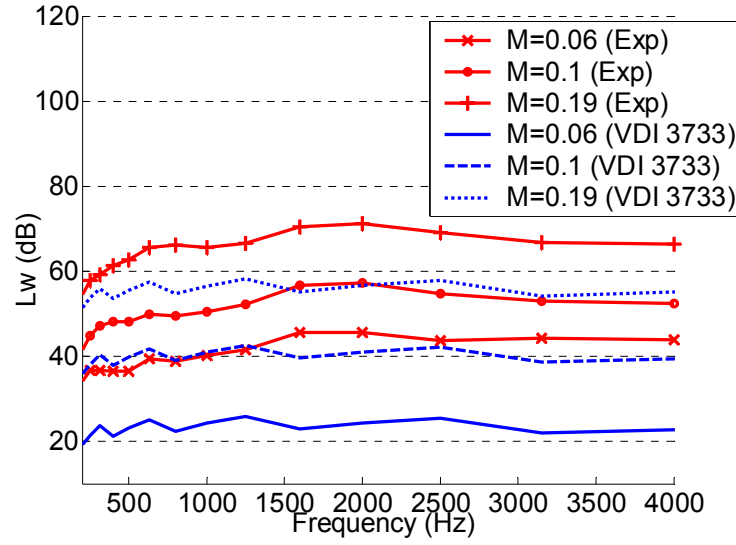


Figure 43: Comparison between the internal noise produced inside the pipe calculated from VDI 3733 with the measured flow noise in the reverberant room.

Kuhn & Morfey (1976) argue that the jet mixing noise produced outside the pipe becomes dominating compared to the noise generated within the pipe and at the lips for flow Mach numbers varying from 0.18 to 0.56. For the tests carried out in this work with Mach numbers up to 0.2, it seems probable that the jet mixing noise (quadrupole) is weaker than the dipole type of noise generated at the lips.

### 5.1.3 Scaling laws

It is of engineering interest to derive semi-empirical laws to predict the sound power level of the flow generated noise. This section is devoted to the general procedure to obtain such predictions. It is based on the method derived by Nelson & Morfey (1981) and Gijrath H. and al. (2001).

Flow induced noise is commonly considered as a dipole-type of source (Nelson & Morfey (1981)), i.e., a fluctuating force acting at the opening is the mechanism of sound production. A general scaling law for the flow generated noise can be written noise as

$$W = \rho_0 U^3 D^2 M^\alpha C_L^2 F(St) \quad (5-8)$$

where  $W$  is the flow induced noise sound power,  $U$  is the flow speed,  $D$  is the pipe diameter,  $\alpha$  is the coefficient determining the aeroacoustic source type,  $F(St)$  is the dimensionless spectra to be calculated for each element,  $St = fU/D$  is the Strouhal

number and  $C_L$  is the pressure loss coefficient.

The essence of this method is the evaluation of the dimensionless spectrum  $F(St)$  in (5-8) as a function of the Strouhal number  $St$ . Ideally, each acoustical element is characterised by a specific dimensionless spectrum  $F(St)$ . In general, the form of this spectrum depends only on the geometry of the tailpipe studied, i.e., oblique cuts, bends and diffusers. Knowing this dimensionless spectrum  $F(St)$ , one can predict the sound power level the element generates by the flow at a different characteristic dimension  $D$ , taken here as the pipe diameter for bends or the outlet diameter for diffusers, and outlet flow speed  $U$ . For diffuser elements, the flow speed is given as  $U = U_{duct} \times (D_{inlet}/D_{outlet})^2$ . The scaling law method requires the external measurement in a reverberant room of the flow induced sound power  $W$  at various measured flow speeds  $U$ . All the dimensionless spectra  $F(St)$  calculated from (5-8) for a specific element and at various Mach number  $M$  are plotted.

A routine is implemented to obtain the optimal value of  $\alpha$  for which minimum standard deviation between the plots is achieved. This procedure is required to obtain only one scaling law for each element.

The value of the coefficient  $\alpha$  in (5-8) depends on the type of frequency bands used (1/3-octave band analysis has been performed in this paper), the type of source (monopole, dipole, quadrupole) and whether the flow noise generated is internally or externally.

It is usually suitable to present the data in logarithmic scale as

$$L_s = 10 \log_{10}(F(St)). \quad (5-9)$$

Others authors prefer the use of the formulation derived by Nelson & Morfey (1981) having the following form

$$L_{s,\Delta f,Nelson\&Morfey}(St) = L_{w,\Delta f} - 10 \log_{10}\left(\frac{\rho_0 c_0^3 S}{16W_{ref}}\right) - 10 \log_{10}(C_L^2) - 10 \log_{10}(M^4). \quad (5-10)$$

The dimensionless spectrum  $L_{s,\Delta f}$  given in equation (5-10) is only applicable in the plane wave range, that is, below the pipe cut-off frequency  $f_c$ , which for a pipe of diameter  $D$  is

$$f_c = \frac{1.84c_o}{\pi D}. \quad (5-11)$$

The experiment was conducted with a pipe of diameter  $D$  of 42 mm (cut-off frequency:

4.8 KHz). Comparisons with other authors scaling laws require the conversion of the Nelson and Morfey's formula (5-10) to the form (5-8) used throughout this analysis. Using (5-8), (5-9) and (5-10) the conversion (for  $\alpha=1$  in (5-8) ) is found to be

$$L_s = L_{s,Nelson\&Morfey} - 13 \text{ dB.} \quad (5-12)$$

Nygård (2000) applied a correction of 3 dB due to the effect of the walls on the in-duct sound pressure level measurement he performed. A quasi-reverberant field is caused by the presence of the pipe walls resulting in an excess level of the sound pressure level by a factor of 0 to 6 dB. VDI 3733 suggests setting this correction factor by 3 dB.

#### ***Determination of the pressure loss coefficient $C_L$***

Table 2 gives the pressure loss coefficient  $C_L$  calculated from the measured pressure drop  $\Delta P$  and flow speed  $U$ .

<b><i>Elements</i></b>	<b><i>Inlet mean Velocity <math>U</math> (m/s)</i></b>			<b><i>Inlet Reynolds number <math>Re</math></i></b>			<b><i>Pressure loss coefficient <math>C_L</math></i></b>
Diffuser 1°	25	44	80	$6 \times 10^4$	$9.9 \times 10^4$	$18 \times 10^4$	0.25
Diffuser 2.5°	27	47	90	$6.1 \times 10^4$	$11 \times 10^4$	$20 \times 10^4$	0.48
Diffuser 5°	27	48	90	$6.1 \times 10^4$	$11 \times 10^4$	$20 \times 10^4$	0.37
Diffuser 7.5°	25	48	91	$5.6 \times 10^4$	$9.9 \times 10^4$	$20 \times 10^4$	0.55
45° Bend L=1D	24	41	80	$5.4 \times 10^4$	$9.2 \times 10^4$	$18 \times 10^4$	0.17
45° Bend L=2D	24	42	80	$6 \times 10^4$	$9.2 \times 10^4$	$18 \times 10^4$	0.16
45° Bend L=5D	24	42	80	$6 \times 10^4$	$9.2 \times 10^4$	$18 \times 10^4$	0.23
90° Bend 1 R/D=1.6	23	41	78	$6 \times 10^4$	$9.2 \times 10^4$	$18 \times 10^4$	0.25
90° Bend 2 R/D=2.5	24	41	78	$6 \times 10^4$	$9.2 \times 10^4$	$18 \times 10^4$	0.24

Table 2: Pressure loss coefficient  $C_L$ .

The pressure loss coefficient  $C_L$  indicates the pressure difference between the inlet and the outlet of an element. For elements (flow constrictions) inside a pipe producing flow noise,  $C_L$  should be used in the scaling law as proposed by Nelson & Morfey (1981). However, for tailpipe terminations, it is not clear that this is useful and therefore  $C_L$  can be omitted in the scaling laws. The flow noise investigation requires the measurement of the airflow pressure drop  $\Delta P$  between the inlet of the elements and the room (Figure 9). It was carried out using an averaging method, where four circumferential holes were drilled in the pipe to measure simultaneously the static pressure difference between the inlet and the outlet of the elements. In turbulent flow the pressure loss coefficient  $C_L = 2\Delta P / \rho_0 U^2$  is essentially independent of the flow speed  $U$  and its magnitude depends solely on the geometry of the elements (Blevins (1984)).

#### ***Scaling laws for bend cases***

The flow generation process for diffusers occurs at the outlet of the elements whereas the sound source of interest to be scaled for bends is located internally at the bends. The sound power level measured is performed externally and corresponds to the flow induced at the bend and at the opening. Thus, two corrections (open end flow noise removal, end reflection) are necessary to compute the proper sound power level generated by flow separation in bends. To remove background noise, i.e., noise produced along the pipe and at the opening, the measured flow induced sound power level of the straight pipe is subtracted from the sound power level measured for each bend. However, part of the flow induced sound generated inside the element is reflected back at the opening as shown in Figure 44. This is corrected using equation (5-7).

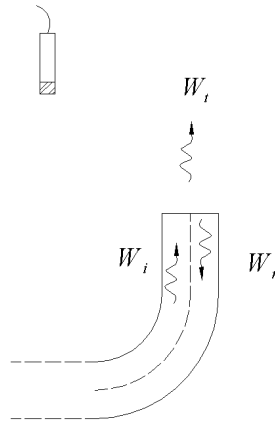


Figure 44: Flow sound power levels in bends.

## 5.2 Results and discussion

### 5.2.1 Scaling law results for a straight pipe

Measurement of flow noise in 1/3-octave band in the reverberant room at various flow Mach numbers  $M$  enables the derivation of scaling law after collapse of sound power level curves as shown in Figure 45.

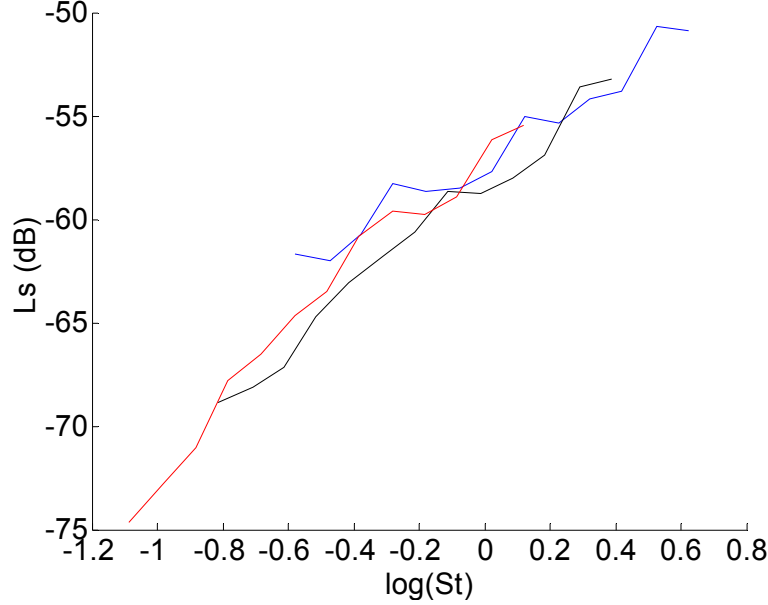


Figure 45: Dimensionless spectrum  $L_s$  for the straight pipe case, formulation used:

$$W = \rho_0 U^3 D^2 M^\alpha F(St), \alpha=3 \text{ for straight pipe (dipole source in free field).}$$

Figure 45 shows the dimensionless spectrum  $L_s$  obtained for the straight pipe. The sound power level of the noise generated by the flow is proportional to  $U^6$  corresponding to flow separation at the lips.

### 5.2.2 Flow-induced noise and scaling law results for tailpipes

This section addresses the noise generated by flow noise for the rig (Figure 9) terminated with elements such as oblique cuts, diffusers and bends. The methodology employed consists of systematically comparing the element flow noise to the straight pipe flow noise. Scaling laws are derived when additional flow noise of more than 3 dB is observed between the element and the straight pipe.



### *Oblique cuts*

The case corresponding to the most pronounced angle ( $60^\circ$ ) is studied as it was observed to be the one creating the highest sound power level. Measured flow noise sound power levels are compared to the results for a straight pipe termination in Figure 46.

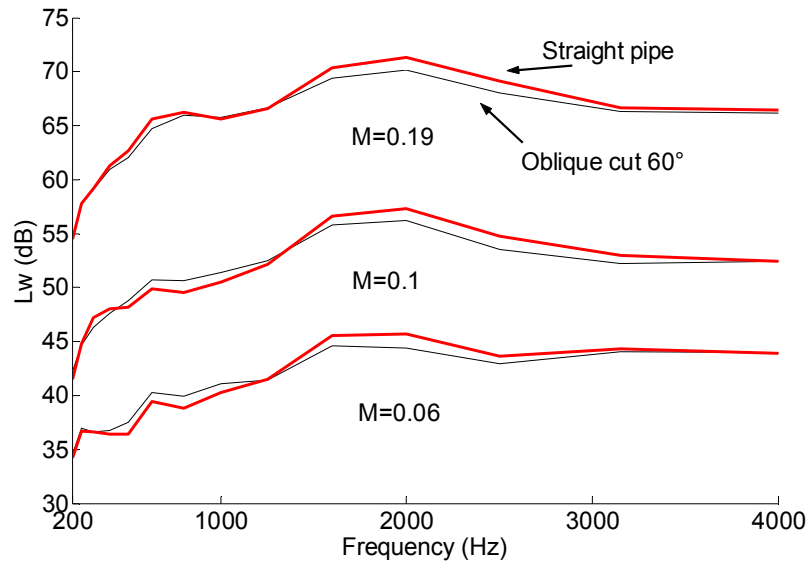
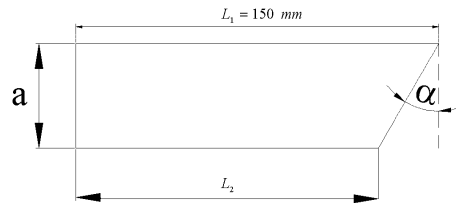


Figure 46: Flow induced sound power levels for oblique cuts.



We note that no significant difference in terms of the sound production by flow is observed between the oblique cuts and the straight pipe termination. In comparison with a straight pipe, no additional noise is generated due to the obliquity. Consequently, the scaling law for this element equals the one derived in the section regarding the straight pipe.

### *Diffusers*

Flow generated noise for diffusers are now presented and compared with the reference case, i.e., the straight pipe termination.

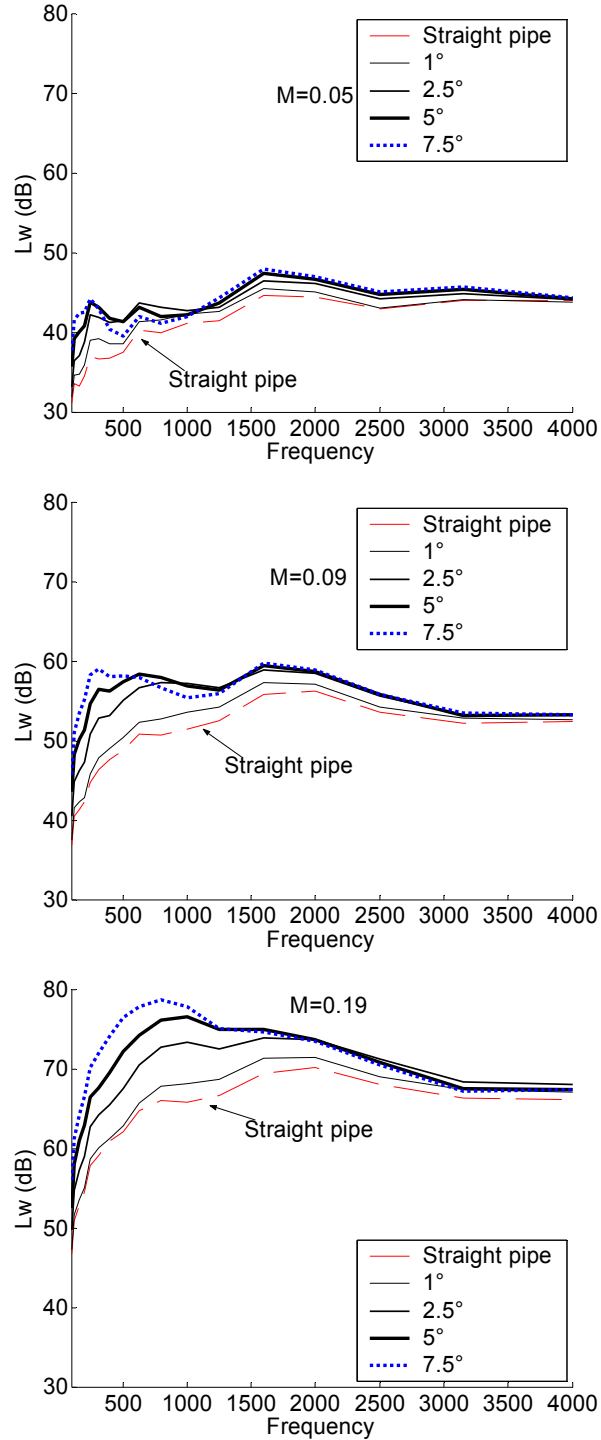


Figure 47: Flow induced sound power levels for diffusers.

The sound generation by flow for diffusers is of dipole type in free field. It means that the sound power generated by the flow is proportional to its velocity  $U^\phi$  since the noise generation occurs mostly at the opening. At low frequencies, a noticeable deviation from the reference case can be observed for all investigated cases. The larger the diffuser angle, the greater the sound power level generated by the flow. It is noted that the diffuser lip circumferential length increases with the diffuser angle since the diffusers have the same length. Consequently, flow separation and flow induced sound power at the lips is most pronounced for diffusers with greater angle and same length although the outlet airflow speed is reduced. The very small difference in the flow induced sound power level  $L_W$  between the diffuser with an angle of  $1^\circ$  and a straight pipe shown in Figure 47 indicates that this diffuser may be regarded as a straight pipe in terms of flow induced noise. Dimensionless spectra  $L_S$  obtained for the diffuser cases according to the formulation  $W = \rho_0 U^3 D^2 M^\alpha C_L^2 F(St)$  are shown in Figure 48.

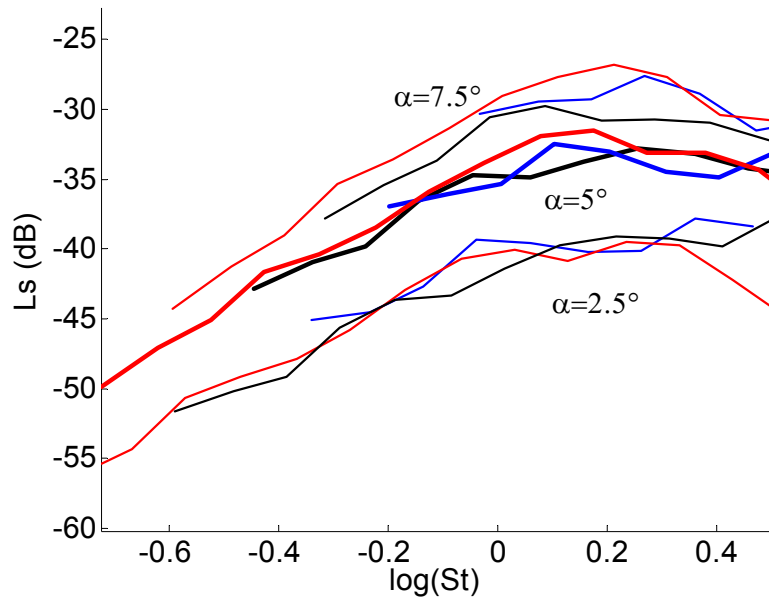


Figure 48: Dimensionless spectra for the diffuser terminations, formulation used:

$$W = \rho_0 U^3 D^2 M^\alpha C_L^2 F(St), \alpha=3 \text{ for diffusers (dipole source in a free field).}$$

The collapse of data shown in Figure 48 for each angle was obtained for a velocity dependence of  $U^\phi$  (outlet velocity, calculated from Pitot-tube measurement inside the rig and outlet cross-section) corresponding to  $\alpha=3$  in  $W = \rho_0 U^3 D^2 M^\alpha C_L^2 F(St)$ .

### 45° bends

Flow noise sound power level results for 45 ° bends are shown in Figure 49.

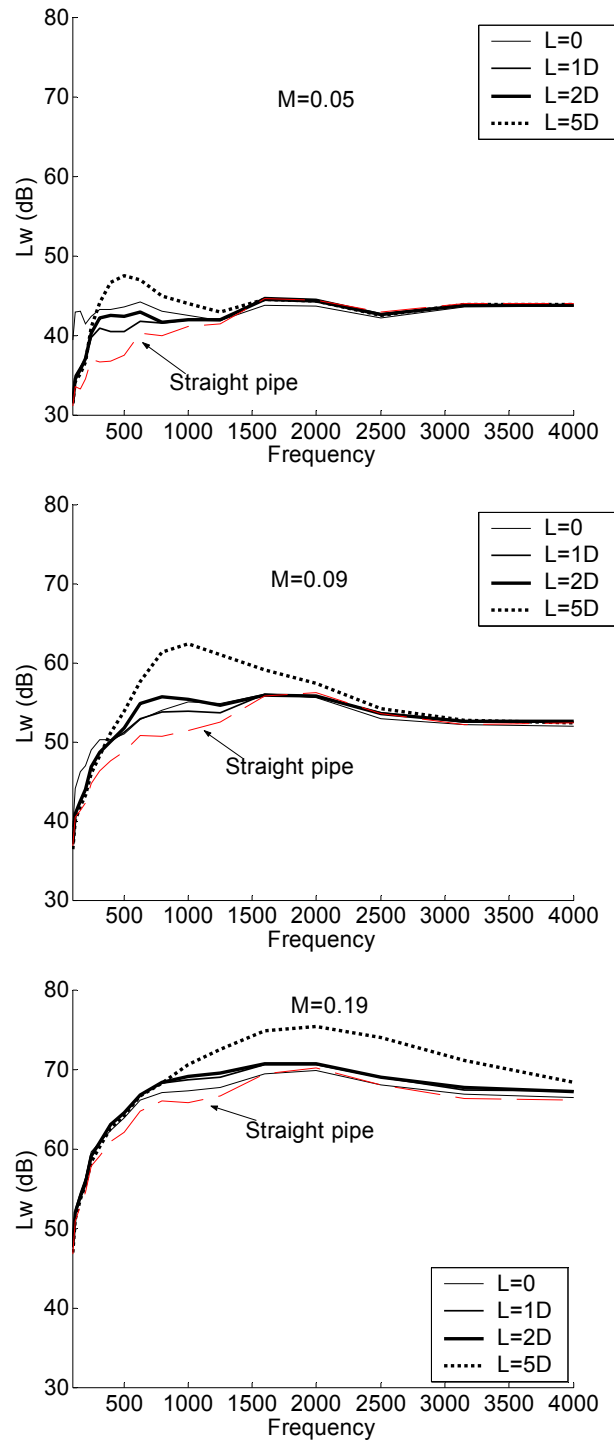


Figure 49: Flow induced sound power levels for 45° bends.

All bend elements behave as a straight pipe in the high frequency region. It is seen from Figure 49 that the greater the flow Mach number, the smaller the deviation compared to the results for a straight pipe. It is due to the flow noise at the opening dominating the internal flow induced noise at the bend. Coupling occurs between the sound sources at the bend and at the opening when the distance separating them is short (Nygård (2000)). The exception to this observation is for the bend with the longest upstream length ( $L=5D$ ). For a length of  $L=5D$ , the internal flow noise generated is greater than the noise generation at the opening. The scaling laws for the  $45^\circ$  bends are shown in Figure 50. It shows more scattering for the shortest upstream lengths ( $L=1D$  and  $L=2D$ ), due to the mixed flow processes at the bend and at the opening. These two processes (internal flow noise, flow noise at the opening) are described by two different velocity exponents. The change in the velocity exponent  $\alpha$  is due to the presence of pipe walls (boundary conditions) for the internal noise mechanism (Nelson & Morfey (1981)). No significant difference between the shortest  $45^\circ$  bend ( $L=0$ ) and the straight pipe in terms of flow noise is observed, thus the results are not presented.

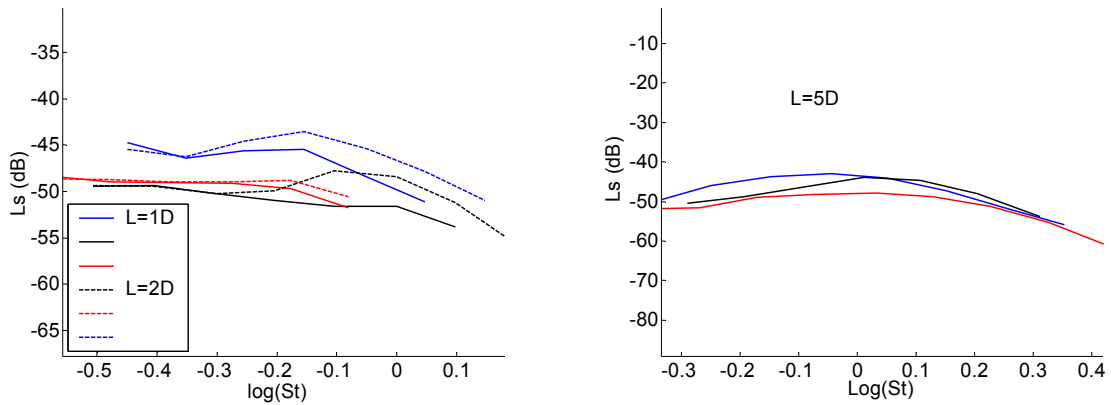


Figure 50: Dimensionless spectra for  $45^\circ$  bend cases, formulation used:

$$W = \rho_0 U^3 D^2 M^\alpha C_L^2 F(St), \alpha=1 \text{ for bends (dipole source in an enclosed field).}$$

The dimensionless spectra shown in Figure 50 have been obtained for a velocity dependence of  $U^4$ .

### 90° bends

Experimental data for flow generated sound for 90° smooth bends are given in Figure 51 together with the derived dimensionless spectra for the two 90° bends investigated (Figure 52).

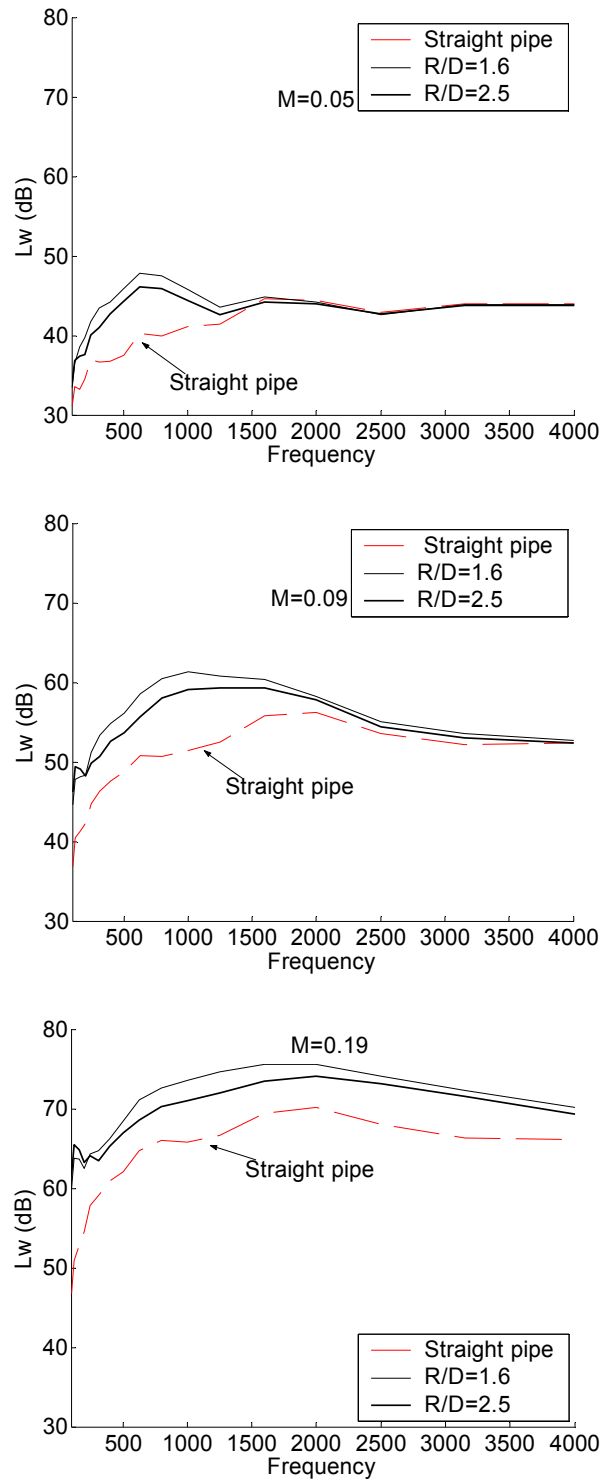


Figure 51: Flow induced sound power levels for 90° bends.

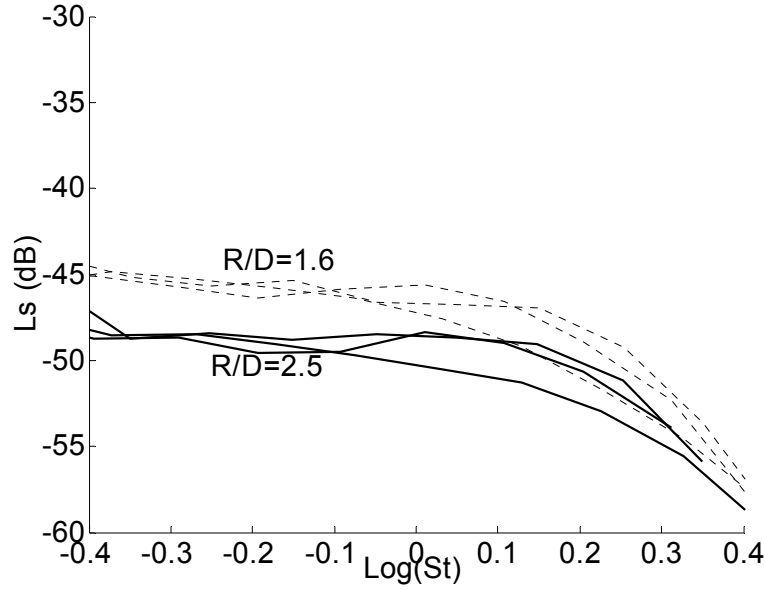


Figure 52: Dimensionless spectra for the 90° bend cases, formulation used:

$$W = \rho_0 U^3 D^2 M^\alpha C_L^2 F(St), \alpha=1 \text{ for bends (dipole source in an enclosed field).}$$

The bend with the largest curvature ( $R/D=1.6$ ) generates the highest sound power level. The dimensionless spectra (Figure 52) for the flow sound power generated in these bends indicate that the sound generation is proportional to the airflow speed  $U^4$ . The velocity exponent  $\alpha=1$  for the bends differs from that of the diffusers, i.e.,  $\alpha=3$ . It is due to the flow sound generation process, which for the diffusers mainly occurs at the opening (free field) whereas it occurs inside the pipe (enclosed field) for the bends.

### 5.2.3 Scaling laws review

Figure 53 shows the scalings laws for diffusers and the straight pipe.

Nygård (2000) has developed scaling laws for other type of bends. However, the formulation based on Nelson & Morfey (1981) used in his derivation of dimensionless spectra is slightly different from the procedure taken throughout this document and needs to be converted. The conversion is given in (5-12). Complete sets of data from Nygård (2000) and our results are shown in Figure 53 together with the formulation used to derive the dimensionless spectra  $L_S$ .

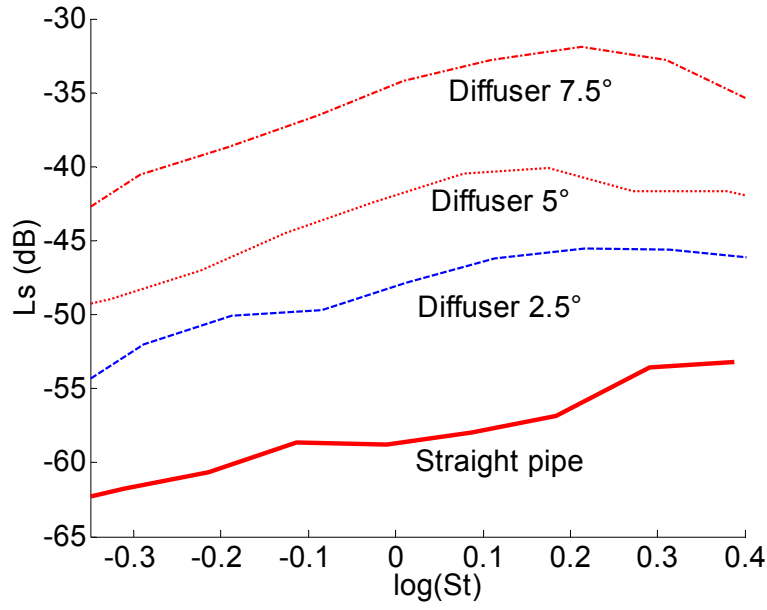


Figure 53: Complete sets of dimensionless spectra obtained from our investigation on diffusers.

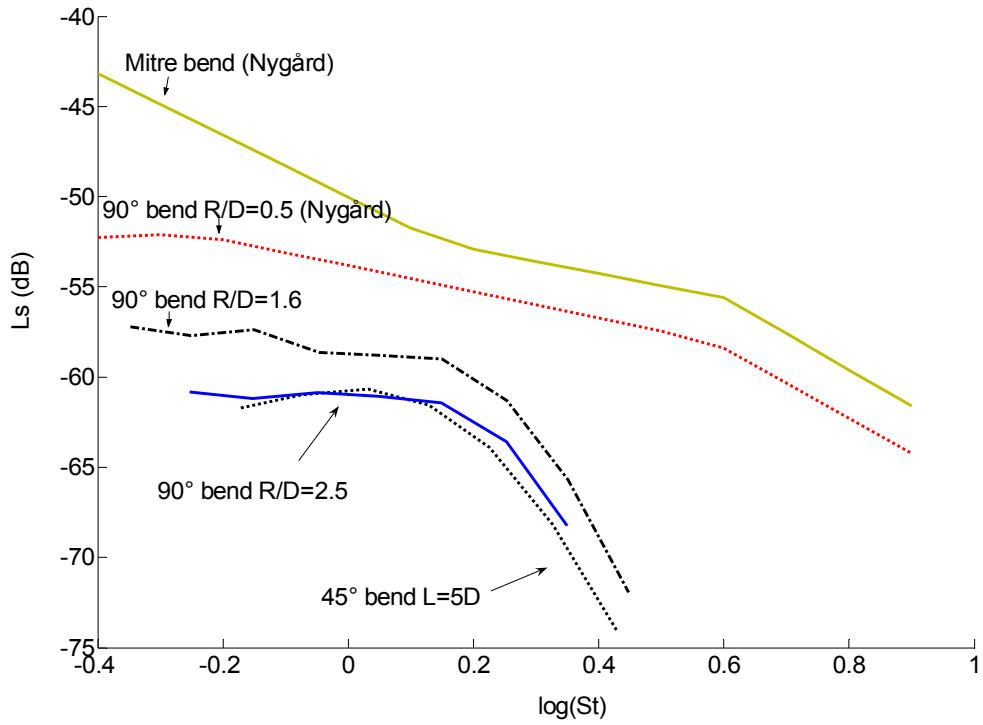


Figure 54: Complete sets of dimensionless spectra obtained from our investigation on diffusers and Nygård (2000) after conversion to the following formulation excluding the pressure loss

$$\text{coefficient } C_L: W = \rho_0 U^3 D^2 M^\alpha F(St).$$



The semi-empirical laws together with coefficients (Table 3) obtained from Figure 53 and Figure 54 and a line fitting procedure are given in (5-13).

$$Ls = C_1 [\log(St)]^5 + C_2 [\log(St)]^4 + C_3 [\log(St)]^3 + C_4 [\log(St)]^2 + C_5 [\log(St)]^1 + C_6 . \quad (5-13)$$

	<b>C<sub>1</sub></b>	<b>C<sub>2</sub></b>	<b>C<sub>3</sub></b>	<b>C<sub>4</sub></b>	<b>C<sub>5</sub></b>	<b>C<sub>6</sub></b>
<b>Straight pipe</b>	-68	-44	28	12	10	-59
<b>Diffuser 2.5°</b>	-82	25	33	-19	10	-48
<b>Diffuser 5°</b>	34	11	-34	-28	15	42
<b>Diffuser 7.5°</b>	19	19	-24	-33	16	-34
<b>45° bend L=5D</b>	100	73	-110	-49	1	-61
<b>90° bend R/D=2.5</b>	-420	-28	-63	-18	0	-61
<b>90° bend R/D=1.6</b>	310	-170	-120	-3	-2	-58
<b>Mitre bend (Nygård)</b>	-150	-6	47	10	-18	-50
<b>90° bend R/D=0.5 (Nygård)</b>	15	-27	10	0	-7.5	-54

Table 3: Coefficients to be used in conjunction with semi-empirical laws derived in (5-13) from scaling laws for each element presented in Figure 53.

### 5.3 Summary

An experimental investigation has been conducted on the noise created by airflow. The experimental technique consists of a rotating microphone located in a reverberant room. Thus, flow induced sound power levels have been measured from a flow rig terminating with different geometries (oblique cuts, diffusers, bends) and at various flow Mach number  $M < 0.5$ . A preliminary investigation on a straight pipe termination has shown that the dominant noise creation process occurs at the lips. Flow noise is also created inside the pipe. However, this internal flow noise is of lesser magnitude compared to the noise produced at the lips or externally for the Mach numbers studied here.

The flow noise sound power levels determined from the geometries have been compared to the straight pipe case and derivations of scaling laws based on these results have been obtained. The results demonstrate the different flow noise behaviours of the elements investigated. It also indicates the relation between the airflow speed and the noise produced due to the flow separation.

It has been found that the diffusers behave as the straight pipe in terms of the flow induced noise process (same velocity exponent), i.e., the flow noise mechanism occur at the outlet. Although, the flow speed is reduced due to the expansion of the diffuser, it has been found that the flow noise at the diffuser outlet is increased compared to that of a straight pipe. It is demonstrated that the diffuser elements behave as a straight pipe in terms of flow induced noise. The sound generation mostly occurs at the opening/lips (dipole sound mechanism). An increase of the angle of the diffuser (fixed length) results in an augmented flow noise production, especially in the low frequency range (see Figure 47). Moreover, for half angle  $\alpha$  greater than  $4^\circ$ , flow separation also occurs within the elements as the flow is detached from the wall. Due to the rather short length of the diffuser, this noise creation inevitably interacts with the noise created at the lips, though it is believed that the latter is of greater magnitude. On the other hand, the oblique cut elements do not generate additional noise and can be treated as a straight pipe. The bends require a special treatment as two flow noise processes can be accounted for. Flow noise is created internally at the bend and externally at the lips. The internal process is of main interest and a correction technique has been applied to retrieve the flow noise at the bend from external measurement. Semi-empirical laws to calculate flow noise sound power levels have been derived for all elements tested.

## 6. Summary and conclusions

An experimental investigation on the propagation and generation of sound through a straight pipe and various tailpipe configurations has been carried out. The aim of this work has been to investigate the sound radiation and the flow noise creation for several opening geometries and to provide guidelines for the design of exhaust systems outlets in the automotive sector.

Starting with the straight pipe taken as a reference case, different aspects were studied. An array of six microphones was employed jointly with an iterative method to experimentally obtain the imaginary part of the complex acoustic wavenumber in the straight pipe. Attenuation of the acoustical energy as the wave travels inside the pipe can thus be determined. It is found that the empirical formulation commonly used for the prediction of acoustical losses when flow is present in the pipe is inadequate. The ad hoc formula suggested by Davies (1988) for the acoustical damping of plane waves in flow ducts can lead to significant smaller damping values than actually measured. An analysis of the end correction was also performed. Opening reflection coefficient and end correction results were confronted with the model of Munt (1977, 1990). It was found that Munt's model predicts well the drop in the end correction at low  $St$ -numbers. Sound radiation measurements enabled the determination of acoustical energy loss through vorticity by comparing induct and reverberation room measurements. An analytical model (Bechert (1980)) treating the opening as monopole and dipole sources, validated the experimental results and confirmed the low frequency mechanism associated with vorticity absorption.

A description and evaluation of flow noise encountered in a pipe system are given together with derivation of an empirical law for straight-pipe flow induced noise. It is found that the major source of flow noise occurred mainly at the lips of the pipe. Internal flow noise generation is of smaller magnitude for Mach numbers less than 0.2.

The geometry at the outlet opening of the straight pipe was varied (oblique cut, diffuser, bend elements) to study its influence on the acoustic radiation. A systematic comparison with the straight-pipe case was the starting point for further analysis to explain any deviations. This is of importance to improve the optimal design of an exhaust line in an

internal combustion engine. Reflection coefficient models for the various tailpipes studied combining Munt's theory and transfer matrix calculations have been tested against measurements performed induct with flush mounted microphones. For the diffusers an interesting deviation from the straight pipe behaviour was found, since the magnitude of the reflection coefficient is larger than 1 in the low frequency limit. This effect gives a significant reduction up to 10 dB of tailpipe resonances. It has been found that the phase difference at various points along the cut needs to be modelled for the oblique cut elements. Bends behave as a straight pipe regarding the internal sound propagation.

In terms of flow noise, scaling laws formulation based on Nelson & Morfey (1981) for calculation of flow induced sound power as function of frequency and characteristic dimension, were obtained in a similar fashion as for the straight pipe. A sixth power velocity dependence was found for the diffuser cases. Bends scale with  $U^4$ . No additional noise is created by the oblique cuts.

Regarding future research, one effect that could be of importance in IC-engine intake and exhaust systems is non-linearities since the pressure amplitude of the fundamental engine harmonics can reach 160-170 dB. Both the diffusers and bends studied are elements for which non-linearities can play a role (Dequand and al. (2002)). Temperature gradients are known to be of little effect.

A more refined analysis on the sound propagation in oblique cuts is needed to model the role of the sharp cut on the acoustics of such elements.

A complete form of the theory of Munt (1977, 1990) gives also the far-field directivity pattern. However, the coded model that was used in this document concerned only the reflection coefficient at the opening from which impedance and end correction were calculated. A refined coding giving the far-field behaviour, compared with the sound transmission measurement obtained here would also give the sound absorption magnitude in the near field. In other words, prediction of acoustical energy losses that occur in the flow could be also performed using Munt's model.

A summary of the main findings for tailpipes are listed in Table 4.

<i>Elements</i>	<b>Reflection coefficient/Impedance</b>	<b>Flow noise</b>
Oblique cuts	Deviates from straight pipe at frequencies $> 1500$ Hz. No effect for low frequencies.	Equivalent to a straight pipe
Diffusers	Kutta condition not valid for $>5^\circ$ Deviations from the straight pipe at low frequencies and with flow	$1^\circ$ : Equivalent to a straight pipe $2.5^\circ, 5^\circ, 7.5^\circ$ : Flow noise sound power level at opening $\propto U^6$
Bends	Equivalent to a straight pipe	$45^\circ$ bend( $L=0$ ): Equivalent to a straight pipe $45^\circ$ bend( $L=5D$ ), $90^\circ$ bends ( $R/D=1.6, 2.5$ ): Flow noise sound power level at the bend $\propto U^4$

Table 4: Comparison between the tailpipes and the straight pipe.



## 7. References

1. Åbom M., 1989, *Studies of sound propagation in ducts and mufflers*, Doctoral Thesis, Department of Aeronautical and Vehicle Engineering, Royal Institute of Technology, Stockholm, Sweden.
2. Åbom M., Bodén H., 1988, *Error analysis of two-microphone measurements in ducts with flow*, Journal of the Acoustical Society of America, **83**, 2429-2438.
3. Allam S., 2004, *Acoustic modelling and testing of advanced exhaust system components for automotive engines*, Doctoral Thesis, Department of Aeronautical and Vehicle Engineering, Royal Institute of Technology, Stockholm, Sweden.
4. Baxa D. E., 1989, *Noise control in combustion engines*, Krieger Pub Co.
5. Bechert D. W., 1980, *Sound absorption caused by vorticity shedding, demonstrated with a jet flow*, Journal of Sound and Vibration, **70**, 389-405.
6. Bierkens J., 2002, *Calculation of the reflection coefficient of a jet pipe with subsonic jet flow*, Master Thesis, Department of Aeronautical and Vehicle Engineering, Royal Institute of Technology, Stockholm, Sweden.
7. Blevins R. D., 1984, *Applied fluid dynamics handbook*, New York : Van Nostrand Reinhold.
8. Bodén H., 1989, *Characterization of fluid machines as sources of fluid borne noise*, Doctoral Thesis, Department of Aeronautical and Vehicle Engineering, Royal Institute of Technology, Stockholm, Sweden.
9. Bodén H., Carlsson U., Glav R., Wallin H. P., Åbom M., 2001, *Ljud och vibration*, Norstedts Tryckeri AB, Stockholm.
10. Boij S., 2003, *Acoustic scattering in ducts and influence of flow coupling*, Doctoral Thesis, Department of Aeronautical and Vehicle Engineering, Royal Institute of Technology, Stockholm, Sweden.

11. Callow G.D., Peat K.S., 1988, *Insertion loss of engine intake and exhaust silencers*, IMechE C19/88, 39-46.
12. Cargill A. M., 1982, *Low frequency acoustic radiation from a jet pipe- a second order theory*, Journal of Sound and Vibration, **83**, 339-354.
13. Davies P.O.A.L., 1988, *Practical flow duct acoustics*, Journal of Sound and Vibration, **124**(1), 91-115.
14. Davies P.O.A.L., Coelho J. L. B., Bhattacharya M., 1980, *Reflection coefficients for an unflanged pipe with flow*, Journal of Sound and Vibration, **72**, 543-546.
15. Dequand S., van Lier L., Hirschberg A., Huijnen J., 2002, *Aeroacoustics response of diffusers and bends: comparison of experiments with quasi-steady incompressible flow models*, Journal of Fluids and Structures, **16**, 957-969.
16. Dokumaci E., 1998, *On transmission of sound in circular and rectangular narrow pipes with superimposed mean flow*, Journal of Sound and Vibration, **210**, 375-389.
17. Ducret F., Åbom M., 2004, *Aeroacoustics behaviour of different exhaust pipe geometries*, Eleventh International Congress on Sound and Vibration, St. Petersburg, Russia.
18. Ducret F., 2005, *Aeroacoustics behaviour of a straight pipe*, Twelfth International Congress on Sound and Vibration, Lisbon, Portugal.
19. Gijrath H., Nygård S., Åbom M., 2001, *Modelling of flow generated sound in ducts*, Eight International Congress on Sound and Vibration, Hong-Kong, China.
20. Glav R., 1994, *On acoustic modelling of silencers*, Doctoral Thesis, Department of Aeronautical and Vehicle Engineering, Royal Institute of Technology, Stockholm, Sweden.
21. Goldstein M., 1976, *Aeroacoustics*, McGraw-Hill, New York.
22. Hirschberg A., Bruggeman J. C., Wijnands A. P. J., Morgenstern M., 1988, *The whistler nozzle and horn as aero-acoustic sound sources in pipe systems*, Proc. Inst. Acoust., 10, 701-708.



23. Howe M. S., 1980, *The dissipation of sound at an edge*, Journal of Sound and Vibration, **70**, 407-411.
24. Howe M. S., 1995, *The damping of sound by turbulent shear layers*, Journal of the Acoustical Society of America, **98**, 1723-1730.
25. Huijnen J.H., 1998, *Aero-acoustics of a bend: quasi-stationary models*, Technische universiteit eindhoven, Report R1476A.
26. Ingard U., Singhal V. K., 1974, *Sound attenuation in turbulent pipe flow*, Journal of the Acoustical Society of America, **55**, 535-538.
27. in't panhuis P., 2003, *Calculations of the sound pressure reflection coefficient and the acoustic end correction of a semi-infinite pipe issuing a subsonic cold or hot jet with co-flow*, Master Thesis, Department of Aeronautical and Vehicle Engineering, Royal Institute of Technology, Stockholm, Sweden.
28. ISO 3741, 1994, *Acoustics: Determination of sound power levels of noise sources using sound pressure, precision methods for reverberation rooms*.
29. ISO 3747, 1998, *Acoustics: Determining the sound power level of noise sources from sound pressure measurement*.
30. Kirchhoff G., 1868, *Über den einfluss der wärmeleitung in einem gase auf die schallbewegung*, Pogg. Ann., **134(6)**, 177-193.
31. Kuhn G.F., Morfey C.L., 1976, *Noise due to fully developed turbulent flow exhausting from straight and bend pipes*, Journal of Sound and Vibration, **44**, 27-35.
32. Levine, H., Schwinger H., 1948, *On the radiation of sound from an unflanged circular pipe*, Physical Review, **73**, 383-406.
33. Morfey C.L., 1971, *Sound transmission and generation in ducts with flow*, Journal of Sound and Vibration, **14(1)**, 37-55.

34. Munt R.M., 1977, *The interaction of sound with a subsonic jet issuing from a semi-infinite cylindrical pipe*, Journal of Fluid Mechanics, **83**, 609-61040.
35. Munt R. M., 1990, *Acoustic transmission properties of a jet pipe with subsonic jet flow: I. the cold jet reflection coefficient*, Journal of Sound and Vibration, **142**, 413-436.
36. Nelson P.A., Morfey C.L., 1981, *Aerodynamic sound production in low speed flow ducts*, Journal of Sound and Vibration, **79**, 263-289.
37. Nygård S, 2000, *Modelling of low frequency sound in duct networks*, Licenciate Thesis, , Department of Aeronautical and Vehicle engineering, Royal Institute of Technology, Stockholm, Sweden, TRITA-FKT 2000:57.
38. Oldham D. J., Ukpoho A. U., 1990, *A pressure-based technique for predicting regenerated noise levels in ventilation systems*, Journal of Sound and Vibration, **140**, 259-272.
39. Peters M.C.A.M., Hirschberg A., Reijnen A.J., Wijnands A.P.J, 1993, *Damping and reflection coefficient measurements for an open pipe at low Mach and Low Helmholtz numbers*, Journal of Fluid Mechanics **256**, 499-534.
40. Pierce A.D., 1989, *Acoustics: an introduction to its physical principles and applications*, Acoustical Society of America, Mc Graw Hill Inc., New York.
41. Rienstra S.W., Hirschberg A., 2004, *An introduction to acoustics*, Report IWDE 01-03 , Eindhoven University of Technology, can be downloaded at <http://www.win.tue.nl/%7Esjoerdr/papers/boek.pdf>
42. Ronneberger D., 1975, *Genaue messung der schalldämpfung und der phasengeschwindigkeit in durchströmten rohren im hinblick auf die weckselwirkung zwischen schall und turbulenz*, Habilitationsschrift mathematische-naturwissenschaftliche fakultät der universität Göttingen.
43. Schlichting H., 1968, *Bounday layer theory*, McCraw Hill Inc., New York.

44. Schlinker R.H., 1979, *The transmission of acoustic plane waves as a jet exhaust*, Journal of Aircraft, **16**(3).
45. Tijdeman H., 1975, *On the propagation of sound in cylindrical tubes*, Journal of Sound and Vibration, **39**, 1-33.
46. van Lier L.J., 1999, *An experimental study of the dynamic response of diffusers with application to gas transport system*, Technische universiteit Eindhoven, Report R-1493-A.
47. van Lier L., Dequand S., Hirschberg A., Gorter J., 2001, *Aeroacoustics of diffusers: An experimental study of typical industrial diffusers at Reynolds numbers of  $O(10^5)$* , Journal of the Acoustical Society of America, **109**, 108-115.
48. VDI3733,1996, Noise at pipes, VDI manual noise reduction guidelines, <http://www.vdi.de/vdi/kontakt/index.php>, Verein Deutscher Ingenieure e.V., VDI Guidelines Department P.O. Box 10 11 39, 40002 Düsseldorf, Germany.

### ***Paper III. Linear and non linear acoustic regimes of perforated plates***

#### **Abstract**

The paper treats the sound transmission through perforated sample. Micro-perforated elements are being tested as a substitute for hazardous porous material used for automotive application. An experimental investigation is performed on the non linearity of samples perforated with different types of apertures (hole, square, rectangular). The parameter of interest is the specific acoustic impedance defined as the ratio of the pressure drop across the thickness of the sample to the particle velocity. Non linear resistive results are used to obtain the perforation area ratio (porosity) of the samples tested. A linear analytical model for the flow impedance is formulated. It is composed of a series of uncoupled internal and external resistance and reactance terms. The model is confronted with the results at low particle velocity (linear regime).



## Table of Contents

1. Introduction .....	1
2. Modelling the acoustics linear regime of perforated plates.....	5
2.1.1    Analytical terms for the acoustic impedance of a single aperture.....	5
2.1.2    Analytical expression for a single aperture (linear regime) .....	9
2.1.3    Analytical expression for panels .....	9
3. Acoustic non linear regime of perforated plates.....	11
4. Experimental apparatus .....	13
4.1    Experimental investigation of the acoustics of perforated panels .....	13
4.1.1    Description of the experimental rig.....	13
4.1.2    Samples.....	15
4.1.3    Presentation of the experimental technique.....	16
5. Results and discussion .....	23
5.1    Comparison between plates .....	28
5.2    General discussion.....	32
5.3    Experimental determination of the porosity .....	32
5.4    Plate modelling.....	33
6. Conclusion.....	41
7. References .....	43



# 1. Introduction

Perforated panels have been used in the automotive industry for decades not primarily as a mean to attenuate sound since the perforations are too large ( $>1$  mm) to provide substantial viscous-thermal dissipation but to guide the airflow to ensure low back pressure, a parameter of paramount importance for the design of silencing systems. A reactive silencer is based on the impedance mismatch due to the expansion chamber. This results in the reflection of incoming waves. An additional acoustic treatment is to line the inside wall of this chamber with porous materials to create a resistive (dissipative) type of silencer element. The separation between the silencer core and the damping cavity is normally provided by a perforated tube. It has been demonstrated that for a perforation area ratio of more than 30%, the panel is acoustically transparent.

The use of micro-perforated (apertures of submillimetre size) material ensures enough losses by itself so that no bulky absorbent material is required. The other advantage over traditional porous/fibre type of materials is the higher attenuation efficiency at low frequency and the reduction of the hazardous risks associated with the handling of brittle material.

Two mechanisms are responsible for the dissipation of the acoustic energy by micro-perforated panels. The visco-thermal boundary layers formed along the inner walls of the aperture and caused by the fluid interacts with the acoustic waves. This interaction cannot be neglected for apertures of small transverse dimension and causes the acoustical energy to be converted into heat. Another mechanism is the acoustic particle jet formation (vorticity) at the opening. The acoustic particle velocity is increased sharply as the wave is squeezed into the minute perforations. A jet is formed as the wave exits the other side of the perforation. For high sound amplitude, this results in the formation of vorticity at the opening. This non-linear phenomenon enhances the dissipation of acoustical energy.

It is known (Ingard (1953), Morfey (1969)) that the acoustics of apertures depends on their geometries. For thin panel and at low frequency, the sound transmission through orifices depends mostly on the perimeter of the opening (Morfey (1969)).

Analytical and experimental investigations have been performed by various authors on the acoustics of panels composed of a single circular hole (Ingard (1953), Ingard &



Ising (1967)) and a single rectangular aperture (Sivian (1935)). Maa (1998) details a unified formulation for the acoustic impedance of panels with multiple micro-circular holes. Maa's analytical model treats the internal and external resistances and reactances. No similar model exists for panels composed of multiple rectangular apertures. Attempts (Gomperts (1964, 1965), Gomperts & Kihlman (1967), Ingerslev & Nielsen (1944)) by building acousticians have been performed on modelling the scattering of sound on cracks in walls or opening around door frames. These models regard the slits as infinitely long and do not treat the viscous dissipation inside and on the edges of the aperture. The cases presented in this paper are on the other hand considered of finite dimensions and the internal and external acoustics behaviours including viscous losses are detailed. Therefore, the building acoustics models are inadequate for the present configurations.

A more closer approach on modelling the acoustics of perforated slitted panels has been carried out by Randeberg (2000, 2002). He describes an analytical model coupled with a finite element model for calculation of the absorption coefficient of double slitted perforated panels.

Based on Maa's method (Maa (1998)) for micro-circular holes and Randeberg's work (Randeberg (2000, 20002)) on slitted plates, an analytical model for the sound transmission through a single panel composed of rectangular apertures is derived in this paper and each of the terms are discussed. The aim of this derivation is to allow easy and flexible calculations of perforated slitted panel properties to attenuate sound.

One of the main assumptions made when modelling the perforated elements is that the apertures do not interact. Therefore, it is convenient to derive the theory for the acoustic impedance of one single aperture and use the perforation area ratio (porosity) to model the entire panel. The normal incident impedance  $Z = \hat{p}/\hat{u}$  over the panel is defined as  $Z = [(1 + R)/(1 - R)]\rho_0 c_0 = \zeta \rho_0 c_0$  where  $R$  is the pressure reflection coefficient  $R = \hat{p}^- / \hat{p}^+$ . The dimensionless normal impedance is defined by  $\zeta = (1 + R)/(1 - R)$ . The specific acoustic flow impedance  $Z_s$  across a sample is expressed as  $Z_s = \Delta\hat{p}/\hat{u} = (\hat{p}_A - \hat{p}_B)/(\hat{u}_A)$ , where  $\hat{u}_A$  is the averaged flow speed over the sample inlet surface  $S$ .

A commercial micro-perforated panel (Acustimet) is also tested in this paper. The

Acustimet panel is composed of small slits obtained after punching aluminium or steel plates. This manufacture process is relatively fast and inexpensive to perform. The micro-perforated Acustimet product has been already implemented with success in cavity to dampen the acoustics modes associated with standing waves. A new area of interest is the use of this material for exhaust systems. The potential for silencers made of this material is still not well known and the effects of high amplitudes and flow on the behaviour should be investigated.

A closer look at the Acustimec product reveals the presence of minute apertures of geometry closer to rectangular than circular orifices. An analytical model based on panels composed of rectangular apertures is therefore required to predict the acoustics of such panels.

Previous works (Ingard (1953), Maa (1998)) have relied mostly upon the measurement on only one side of the sample. The experimental apparatus consists usually of one measuring section (impedance tube) terminated by the sample and a rigid cavity (resonator). Microphones mounted on one section allow determination of the reflection and absorption coefficients. The techniques presented in this paper are related to a rig comprised of two measuring sections. The sample is mounted between these sections with anechoic terminations and measurements are performed on both sides of the sample. Thus, the sample can be characterised more exhaustively.

Non-linear regime implies that the acoustic properties, for example, the flow impedance, are dependent of the acoustic particle velocity (amplitude of the acoustic source). Thus, non-linear parameters are required for prediction of sample properties at high sound intensity. It has been demonstrated (Maa (1998)) that there is not a sharp distinction between the linear and non-linear regimes.



## 2. Modelling the acoustics linear regime of perforated plates

In the following section, an account of the analytical terms describing the impedance at low sound intensity is given for a plate composed of multiple rectangular apertures (subscript  $ra$ ). Smits & Kosten (1951) points out that the rectangular aperture has two dimensional characteristics due to the slow divergence of the airflow whereas the circular hole introduces one dimensional mechanism related to the fast divergence of the airflow. In other word, the apertures have different acoustic behaviour, thus emphasising the importance of separate treatments. The methodology taken by Maa (1998) to obtain the acoustic impedance of plates with micro-circular holes is used to derive a similar expression for an array of rectangular apertures. Interaction effects between neighbouring apertures are also discussed.

### 2.1.1 Analytical terms for the acoustic impedance of a single aperture

Sivian (1935) splits the orifice impedance into two regions: the interior (subscript  $i$ ) corresponding to the inside of the orifice and the external (subscript  $e$ ) related to the opening and near field. Sivian (1935) writes the total impedance for any orifice shown in Figure 2

$$Z_{\text{single aperture}} = Z_i + Z_e = (R_i + jX_i) + (R_e + iX_e) = \Delta\hat{p}/\hat{v}, \quad (2-1)$$

where  $\Delta\hat{p}$  is the acoustic pressure drop through the thickness  $t$  of the orifice and  $\hat{v}$  is the interior acoustic particle velocity. This is related to the external velocity  $\hat{u}_A$  given in equation (4-11). The impedance is composed of a resistance term  $R$  and reactance term  $X$ . The plate is assumed to be thin so the particle velocity  $\hat{v}$  is assumed to be the same on both sides.

The following section sets out the analytical expressions for the various analytical terms for the acoustic impedance of circular and rectangular orifices with geometries depicted in Figure 1.

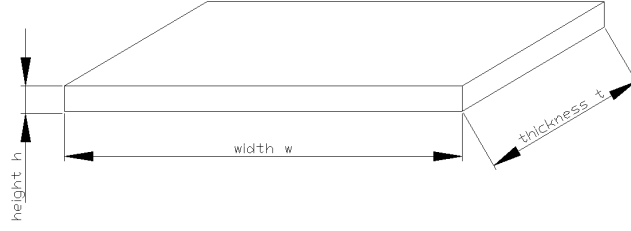


Figure 1: Nomenclature for single rectangular aperture.

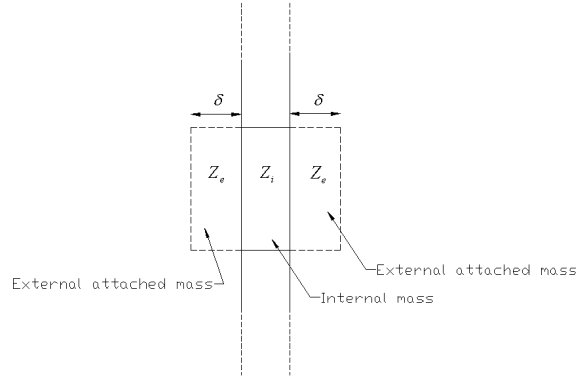


Figure 2: Internal and external impedances for an orifice.

### ***Internal terms***

#### ***Internal viscous losses***

Internal propagation of acoustic waves through narrow apertures causes the acoustical energy to be converted into other forms of energy. The main sound dissipation mechanism encountered in sound propagation through small apertures is of viscous nature. Thermal effect corresponding to the heat conduction between the fluid and the wall is usually neglected.

Allard (1993) derives the complete internal acoustic impedance  $Z_{i,ra}$  of a single rectangular aperture. The internal resistive term  $R_{i,ra}$  for rectangular geometry is taken as the real part of the expression for  $Z_{i,ra}$ .

$$R_{i,ra} = Re \left[ j\omega\rho_0 t \left( 1 - \frac{\tanh\left(\frac{w}{2} \sqrt{\frac{j\omega\rho_0}{\eta}}\right)}{\frac{w}{2} \sqrt{\frac{j\omega\rho_0}{\eta}}} \right)^{-1} \right], \quad (2-2)$$

where  $w$  is the width of the rectangular aperture,  $t$  is the thickness,  $\eta$  (dynamic viscosity)  $= 1.8 \times 10^{-5} \text{ Ns} \cdot \text{m}^{-2}$  and  $\rho_0 = 1.2 \text{ kg} \cdot \text{m}^{-3}$

### ***Internal reactance***

The internal reactance  $X_{i,ra}$  for single rectangular aperture can be extracted by taking the imaginary part of the complete internal impedance formulation  $Z_{i,ra}$  (see equation (2-5)) derived by Allard (1993).

$$X_{i,ra} = Im \left[ j\omega\rho_0 t \left( 1 - \frac{\tanh\left(\frac{w}{2} \sqrt{\frac{j\omega\rho_0}{\eta}}\right)}{\frac{w}{2} \sqrt{\frac{j\omega\rho_0}{\eta}}} \right)^{-1} \right], \quad (2-3)$$

For small transverse dimension, this reduces to

$$X_{i,ra} = j\omega\rho_0 t \quad (2-4)$$

### ***Internal impedance***

The complete internal impedance  $Z_{i,ra}$  for a slit orifice with no thermal effect has been calculated by Allard (1993) and Cremer & Müller (1982). It is calculated from the effective density  $\rho_{\text{eff}}$  of the air inside the slit following Kirchoff's method. It is assumed that the width  $w$  is greater than height  $h$  but less than the acoustic wavelength. The thermal losses are neglected. It is expressed as

$$Z_{i,ra} = j\omega\rho_{\text{eff}}t = j\omega\rho_0 t \left( 1 - \frac{\tanh\left(\frac{w}{2} \sqrt{\frac{j\omega\rho_0}{\eta}}\right)}{\frac{w}{2} \sqrt{\frac{j\omega\rho_0}{\eta}}} \right)^{-1}. \quad (2-5)$$

### ***External terms***

#### ***External friction resistance and radiation resistance***

Under the condition of the non presence of porous materials or screens, the acoustic energy is mostly dissipated through viscous effects and heat conduction on the surfaces of the aperture.

The external resistance  $R_e$  corresponds to these losses caused at the opening due to the friction against the opening surfaces. Ingard (1953) obtains

$$R_{e,ca} = R_s = (1/2)\sqrt{2\rho_0\omega\eta}. \quad (2-6)$$

This formulation is valid for the case of an oscillating flow over a surface. This formula must be modified for the effects of the edges of the opening. Ingard (1953) suggests based on experiments a value of  $4R_s$ . Maa (1998) argues that this value is too high and sets it to  $R_s$  in his model for micro-circular holes. This is probably due to the fact that he uses Crandall's internal resistance term (Crandall (1927)) whereas Ingard (1953) treats the internal losses with an approximate form. Randeberg (2000, 2002) uses a factor of 2 together with the internal resistance predicted by Allard (1993). This model will also be used here, i.e.,

$$R_{e,ra} = \sqrt{2\omega\rho_0\eta} = 2R_s. \quad (2-7)$$

#### ***End correction on one side of the orifice***

Sivian (1935) calculates the air mass reactance on a rectangular aperture based on the following assumptions:

- The particle velocity  $\hat{v}$  normal to the plane of the aperture is constant across the orifice.
- The aperture transverse dimensions (width  $w$ , height  $h$ ) are small compared to the wavelength ( $kw \ll 1$ ,  $kh \ll 1$ ).
- The aperture is located in an infinite baffle.

These assumptions allow him to write a simple and easy to calculate velocity potential based on  $\hat{v}$ . The end correction for one side of a rectangular aperture is then given by

$$\delta_{ra} = \frac{2}{3\pi(w/2)(h/2)} \left[ \frac{(w/2)^3 + (h/2)^3 - ((w/2)^2 + (h/2)^2)^{3/2} +}{3(w/2)(h/2)} \left( \begin{aligned} &(h/2) \ln \left( \frac{(w/2) + ((w/2)^2 + (h/2)^2)^{1/2}}{h/2} \right) \\ &+ (w/2) \ln \left( \frac{(h/2) + ((w/2)^2 + (h/2)^2)^{1/2}}{w/2} \right) \end{aligned} \right) \right]. \quad (2-8)$$

Our analytical model for rectangular apertures includes the end correction on both sides.

### **Mass attached reactance**

The external mass attached reactance  $X_e$  for one side of the aperture derived from the end correction term  $\delta$  is of the form

$$X_e = \rho_0 \omega \delta. \quad (2-9)$$

### **2.1.2 Analytical expression for a single aperture (linear regime)**

It is now time to assemble all the previous terms into a single expression for the acoustic impedance  $Z_{ra}$  of an orifice of rectangular geometry at low sound intensity.

$$Z_{ra} = Z_{i,ra} + Z_{e,ra} = 2R_{e,ra} + Z_{i,ra} + 2jX_{e,ra}$$

$$= \sqrt{2\omega\rho_0\eta} + j\rho_0\omega \left[ \left[ t \left( 1 - \frac{\tanh\left(\frac{w}{2}\sqrt{\frac{j\omega\rho_0}{\eta}}\right)}{\frac{w}{2}\sqrt{\frac{j\omega\rho_0}{\eta}}} \right)^{-1} + \frac{4}{3\pi(w/2)(h/2)} \left[ \frac{(w/2)^3 + (h/2)^3 - ((w/2)^2 + (h/2)^2)^{3/2} +}{3(w/2)(h/2)} \left( \begin{aligned} &(h/2) \ln \left( \frac{(w/2) + ((w/2)^2 + (h/2)^2)^{1/2}}{h/2} \right) \\ &+ (w/2) \ln \left( \frac{(h/2) + ((w/2)^2 + (h/2)^2)^{1/2}}{w/2} \right) \end{aligned} \right) \right] \right] \right]. \quad (2-10)$$

### **2.1.3 Analytical expression for panels**

Having reviewed the expression (2-10) for the acoustic impedance  $Z_{ra}$  for a single rectangular orifice, the next step is to compute the overall acoustic impedance for the panel depicted in Figure 3.



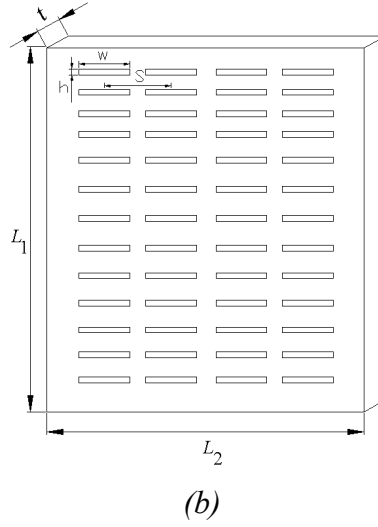


Figure 3: Schematic of perforated samples with  $n$  apertures and cross section  $S=L_1L_2$ .

The total panel acoustic impedance calculated for panels as depicted in Figure 3 and normalised with respect to  $\rho_0 c_0$  is given by

$$\zeta_S = Z_{ra}/\sigma\rho_0 c_0 = Z_S/\rho_0 c_0 = r_S + jx_S = \Delta\hat{p}/(\hat{u}_A\rho_0 c_0), \quad (2-11)$$

where the perforation ratio area (porosity)  $\sigma$  is defined as

$$\sigma = nhw/S, \quad (2-12)$$

where  $n$  is the number of apertures. The particle velocity  $\hat{u}_A$  corresponds to the averaged particle velocity over the entire sample surface of cross section  $S$ .

Equation (2-10) assumes no interaction between the apertures. Melling (1973) indicates that this assumption is valid for a perforation ratio area of less than 4% for panels with circular holes. Ingard (1953) has studied the interaction effect for an array of rectangular apertures and argues that the effect is slightly more pronounced for rectangular apertures than for circular holes. However, we believe that a limit of 4% for the panel of rectangular aperture is also acceptable. As with Maa (1998), the coupling effect is not included in our model for rectangular apertures.

### **3. Acoustic non linear regime of perforated plates**

At low excitation level, the acoustic flow through an aperture is irrotational, laminar and symmetrical, i.e., the behaviour is the same at the inlet and outlet of the orifice. The acoustic dissipation is mostly due to the viscous dissipation as the acoustic flow enters and leaves the orifice. Internal friction against the inside walls of the aperture also causes acoustic energy losses. Above a certain excitation level, turbulence occurs and vorticity is formed at the outlet (see Figure 4). The flow is therefore no longer symmetrical. Maa (1994) theoretically demonstrates that the acoustic non linearity of apertures is an external phenomenon, i.e., the internal impedance is independent of the sound intensity. Melling (1973) presents a clear review about previous work on the non linearity of orifices before proposing a theoretical model for the non linearity of perforated plates. His model is based on the knowledge of the discharge coefficient (the product of the velocity and contraction coefficients). He points out that the discharge coefficient is difficult to estimate and needs to be measured. Sivian (1935) demonstrates that the increase of the acoustic losses when the excitation level is raised is not only due to the turbulence generation as the flow exits the orifice but also comes from the flow separation when the flow enters it. A few decades later, Ingard & Ising (1967) experimentally determined that at low particle velocity (linear regime), the relation between the excitation pressure and the particle velocity is of linear nature whereas under non-linear regime this relationship becomes quadratic. This was a starting point for Ingard & Ising (1967) to further derive novel empirical observations on the non linearity of orifices. According to Ingard & Ising (1967), the suggested non linear terms are frequency independent. They observe that the reactance decreases as the excitation level goes up. Maa (1998) explains this reduction by the presence of the turbulent jet formed in the near field of the orifice. Inspired by Sivian (1935), Ingard & Ising (1967) also apply the Bernoulli's law for orifices in order to get a better understanding of the linear relationship observed between the orifice resistive term and the particle velocity inside the orifice for high particle velocities. They derive the following relation between the non linear resistive term and particle velocity inside a single circular hole

$$R = \rho_0 |\hat{v}| (1 - \sigma^2) / (1 - q_1), \quad (3-1)$$

where  $\sigma$  is the perforation area ratio (porosity) and  $q_1$  is the fraction of the excitation pressure corresponding to the acoustic pressure inside the hole.

Maa (1994) suggests a modified version of this for the case of micro-perforated plates with small porosity  $\sigma$  and expresses the normalised non linear resistance term for a complete perforated panel as

$$r = \hat{v} / (\sigma c_0) = \hat{u}_A / (\sigma^2 c_0), \quad (3-2)$$

where  $\hat{u}_A$  is the acoustic particle velocity on the inlet sample surface.

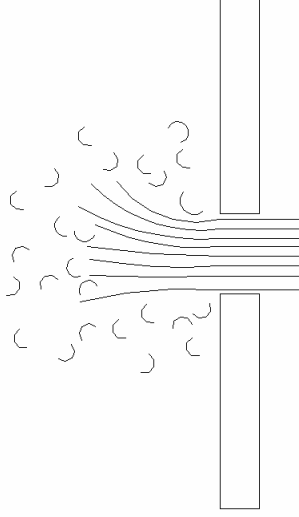


Figure 4: Flow vorticity

## 4. Experimental apparatus

### 4.1 Experimental investigation of the acoustics of perforated panels

In this section, we describe the experimental apparatus and techniques used to measure the sample normalised acoustic impedance  $\xi_s$  and the inlet sample particle velocity  $\hat{u}_A$  and the normalised acoustic impedance  $\xi'_s$  based on the interior particle velocity  $\hat{v}$ .

#### 4.1.1 Description of the experimental rig

The rig shown in Figure 6 and Figure 5 consists of two identical sections. Positions 1 and 2 are part of the upstream<sup>1</sup> section whereas positions 3 and 4 are referred to the downstream<sup>1</sup> section.

The two sections are clamped and tightened together through flanges. To prevent air leakages, rubber joints are installed on each section at the location of the sample.

The walls of the duct are perfectly rigid so that no vibration occurs. The duct is terminated on both sides with porous material to reduce standing waves inside the duct. Mounts for microphones have been manufactured to facilitate the change of position.

The cut-off frequency for this square duct is given by  $f_c = c_0/2L = 2450\text{Hz}$  where  $c_0$  is the speed of sound ( $343 \text{ m} \cdot \text{s}^{-1}$ ) and  $L$  is the duct transverse dimension (70 mm). Plane wave propagation occurs below the cut-off frequency. No higher order modes are investigated.

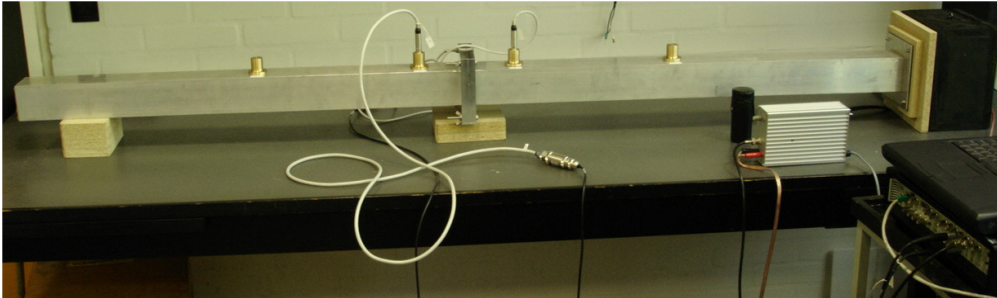


Figure 5: Experimental rig for sample testing.

---

<sup>1</sup> The upstream and downstream sections refer to the rectangular tubes located on both sides of the sample. No airflow has been used in this paper.

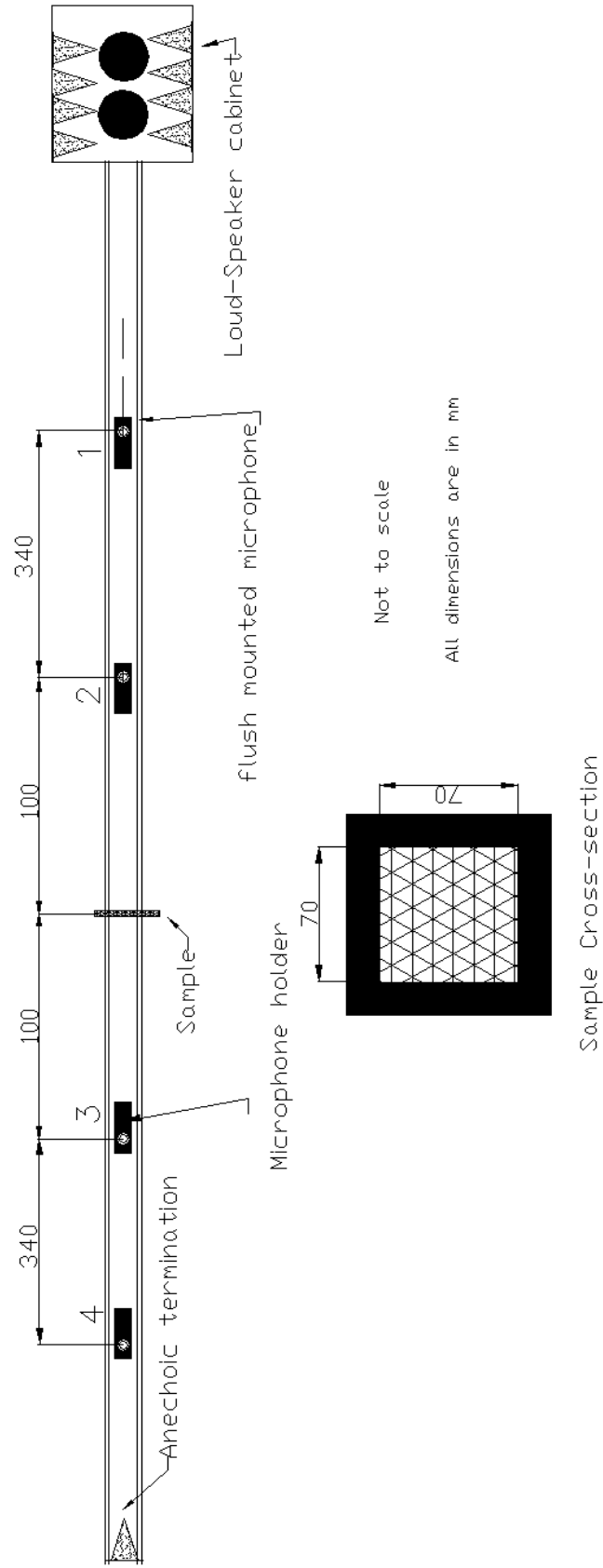


Figure 6: Layout of the experimental rig for sample testing.

### 4.1.2 Samples

Table 1 shows the samples investigated together with their dimensions in mm. The total cross section of the plate is 70 by 70 mm.

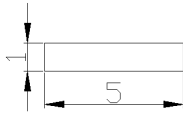


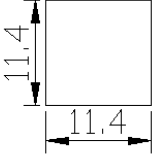
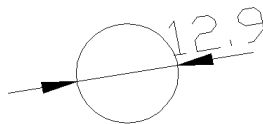

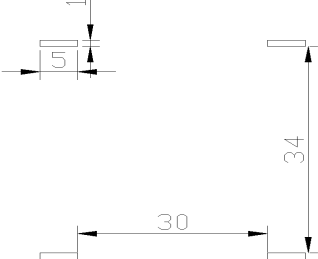
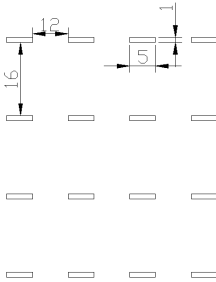

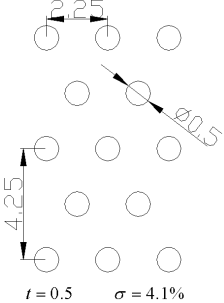
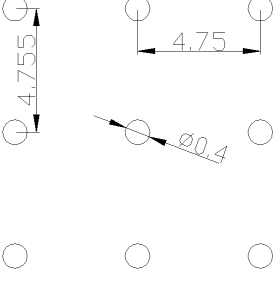
	
	
	
	
	 <p>Acustimet</p>
 <p><math>t = 0.5</math>    <math>\sigma = 4.1\%</math></p>	 <p><math>t = 0.6</math>    <math>\sigma = 0.56\%</math></p>

Table 1: Samples tested.

#### 4.1.3 Presentation of the experimental technique

The main methodology consists of determining the sound fields on either side of the sample. The difference between them is attributed to the properties of the material. No direct measurement is made on the sample. The requirement is to map the propagation of acoustic waves in both sections of the duct (Figure 7).

In order to achieve this, two microphones are used simultaneously. Frequency response (transfer functions) measurements are carried out between the two microphones. The data acquisition system and signal to the loudspeaker was provided by a Brüel & Kjær PULSE system. The PULSE software programming language necessitates to derive the real and imaginary parts of the parameters investigated. The drawback of using of two microphones simultaneously is that a phase and magnitude calibration between the microphones is needed.

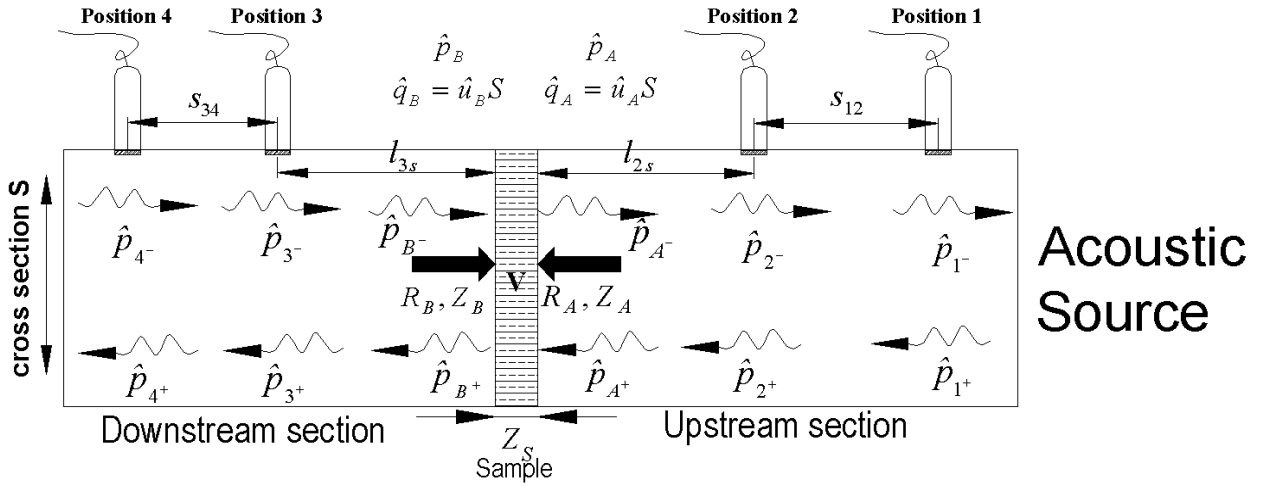


Figure 7: Rig propagating sound waves.

#### *Calibration of the two microphones*

The experimental technique requires a separate phase and magnitude calibration for the two microphones. This calibration procedure in this case consists of placing the two microphones through a coupler mounted on a calibrator producing random noise. By measuring the sound intensity, one can adjust the phase difference within the PULSE software to compensate for any differences. The calibration transfer function  $H_{21\text{ cal}}$

between the two microphones is saved. The index 1 and 2 in the calibration procedure refers to the microphone number (1 and 2) whereas it indicates the duct position number (1 through 4) when they are mounted on the duct. The calibration saved transfer function  $H_{21\text{ cal}}$  is combined with the measured frequency response  $H_{21\text{ meas}}$  to calculate the true frequency response  $H_{21\text{ true}}$  as follows

$$H_{21\text{ true}} = H_{21\text{ meas}} / H_{21\text{ cal}} ,$$

$$\text{Re}(H_{21\text{ true}}) = [\text{Re}(H_{21\text{ meas}})\text{Re}(H_{21\text{ cal}}) + \text{Im}(H_{21\text{ meas}})\text{Im}(H_{21\text{ cal}})] / [\text{Re}(H_{21\text{ cal}}^2) + \text{Im}(H_{21\text{ cal}}^2)], \quad (4-1)$$

$$\text{Im}(H_{21\text{ true}}) = [\text{Re}(H_{21\text{ cal}})\text{Im}(H_{21\text{ meas}}) - \text{Re}(H_{21\text{ meas}})\text{Im}(H_{21\text{ cal}})] / [\text{Re}(H_{21\text{ cal}}^2) + \text{Im}(H_{21\text{ cal}}^2)].$$

From now on, the true frequency response for the automation technique is simply referred to  $H_{21}$ .

### ***Overview of the technique***

The procedure starts by measuring the downstream properties (anechoic termination), i.e., the normal impedance  $\zeta_B$  by placing the microphones at positions 3 and 4 (Figure 7). Ideally, this impedance corresponds to the value of an infinite duct (no reflection at the termination), i.e.,  $\zeta_B = 1$ . In practice this cannot be obtained especially at low frequencies. This normal impedance is thus saved. The microphones are next moved to position 1 and 2 for determination of the normal incident impedance  $\zeta_A$ . Finally, the acoustic impedance  $\zeta_S = \zeta_A - \zeta_B$  is derived after the impedance have been moved to the sample surfaces  $A$  and  $B$ .

### ***Downstream properties***

The calibration procedure is followed by mounting the microphones 1 and 2 onto positions 3 and 4 respectively. The anechoic termination on the downstream is fixed for the entire procedure. Therefore, the downstream section properties are determined only once and used for any sample and excitation level by loading the saved impedance  $\zeta_B$  to determine the sample acoustic impedance  $\zeta_S$  after comparison with  $\zeta_A$ .

The true frequency response  $H_{43}$  (microphone 1 in location 3, reference microphone 2 in



location 4) is calculated from equation (4-1) using the calibration file. The calculation of the pressure reflection coefficient  $R_4$  at position 4 for the downstream condition is further performed. The real and imaginary parts for  $R_4$  are given as

$$R_4 = \frac{-H_{43} + e^{jks_{34}}}{H_{43} - e^{-jks_{34}}},$$

$$Re(R_4) = \frac{-(Re(H_{43}) - \cos(ks_{34}))^2 + (\sin(ks_{34}) - Im(H_{43}))(Im(H_{43}) + \sin(ks_{34}))}{(Re(H_{43}) - \cos(ks_{34}))^2 + (Im(H_{43}) + \sin(ks_{34}))^2}, \quad (4-2)$$

$$Im(R_4) = \frac{2 \sin(ks_{34})(Re(H_{43}) - \cos(ks_{34}))}{(Re(H_{43}) - \cos(ks_{34}))^2 + (Im(H_{43}) + \sin(ks_{34}))^2},$$

where  $s_{34}$  = 340 mm is the distance separating positions 3 and 4.

Assuming no losses, the reflection coefficient  $R_4$  is moved to the sample surface  $B$  (cf Figure 7) through the distance  $s_{34} + l_{3s}$  = 440 mm using the expressions

$$R_B = R_4 e^{-2j(k(s_{34} + l_{3s}))},$$

$$Re(R_B) = Re(R_4) \cos(2k(s_{34} + l_{3s})) + Im(R_4) \sin(2k(s_{34} + l_{3s})), \quad (4-3)$$

$$Im(R_B) = Im(R_4) \cos(2k(s_{34} + l_{3s})) - Re(R_4) \sin(2k(s_{34} + l_{3s})).$$

The normalised normal impedance  $\zeta_B$  on sample surface  $B$  is thus

$$\zeta_B = \frac{1 + R_B}{1 - R_B},$$

$$Re(\zeta_B) = \frac{1 - (Re(R_B))^2 - (Im(R_B))^2}{(1 - Re(R_B))^2 + (Im(R_B))^2}, \quad (4-4)$$

$$Im(\zeta_B) = \frac{2 Im(R_B)}{(1 - Re(R_B))^2 + (Im(R_B))^2}.$$

### Upstream properties

Throughout the course of the experimental investigation, the anechoic termination on the downstream section is unchanged. Therefore, it is assumed that  $\zeta_B$  remains constant and independent of the sample tested. The experimental data corresponding to the normal impedance  $\zeta_B$  on surface B obtained from equation (4-4) with the two microphones mounted at positions 3 (microphone 1) and 4 (microphone 2) are saved within the PULSE software environment and are loaded for further evaluation. The two microphones are then moved to position 1 (microphone 1) and 2 (microphone 2) for determination of the sound field of the upstream section leading to the normal impedance  $\zeta_A$  on the surface A. The wave decomposition is essentially the same as performed for the downstream section to obtain the pressure reflection coefficient  $R_4$  at position 4. However, we now obtain the pressure reflection  $R_2$  at position 2 given as

$$R_2 = \frac{-H_{21} + e^{jks_{12}}}{H_{21} - e^{-jks_{12}}},$$

$$Re(R_2) = \frac{-(Re(H_{21}) - \cos(ks_{12}))^2 + (\sin(ks_{12}) - Im(H_{21}))(Im(H_{21}) + \sin(ks_{12}))}{(Re(H_{21}) - \cos(ks_{12}))^2 + (Im(H_{21}) + \sin(ks_{12}))^2}, \quad (4-5)$$

$$Im(R_2) = \frac{2 \sin(ks_{12})(Re(H_{21}) - \cos(ks_{12}))}{(Re(H_{21}) - \cos(ks_{12}))^2 + (Im(H_{21}) + \sin(ks_{12}))^2},$$

where  $s_{12}$  = 340 mm is the distance separating positions 1 and 2.

The pressure reflection coefficient  $R_2$  is moved to the sample surface A (cf Figure 7) through the distance  $l_{2s}$  = 100 mm using the expressions

$$R_A = R_2 e^{2j(kl_{2s})},$$

$$Re(R_A) = Re(R_2) \cos(2kl_{2s}) - Im(R_2) \sin(2kl_{2s}), \quad (4-6)$$

$$Im(R_A) = Im(R_2) \cos(2kl_{2s}) + Re(R_2) \sin(2kl_{2s}).$$

The normalised normal impedance  $\zeta_A$  on sample surface A is thus

$$\zeta_A = \frac{1 + R_A}{1 - R_A}, \quad (4-7)$$

$$Re(\zeta_A) = \frac{1 - (Re(R_A))^2 - (Im(R_A))^2}{(1 - Re(R_A))^2 + (Im(R_A))^2},$$

$$Im(\zeta_A) = \frac{2 Im(R_A)}{(1 - Re(R_A))^2 + (Im(R_A))^2}.$$

### **Sample flow impedance**

The normal impedance  $\zeta_A$  and saved normal impedance  $\zeta_B$  are further combined to derive the sample normalised acoustic impedance  $\zeta_S$  given as

$$\zeta_S = \frac{\Delta \hat{p}}{\hat{u}_A \rho_0 c_0} = (\zeta_A - \zeta_B) = \left( \frac{1 + R_A}{1 - R_A} - \frac{1 + R_B}{1 - R_B} \right) = r_s + jx_s. \quad (4-8)$$

### **Inlet particle velocity $\hat{u}_A$**

An extra measurement is required on the upstream section. One of the aims of this investigation is to estimate the dependence of the level of excitation on the acoustic impedance of the sample mounted between the two sections. Therefore, one also needs to measure the particle velocity  $|\hat{u}_A|$  on the surface  $A$  (see Figure 7) of the sample using a wave decomposition technique.

The expressions used are

$$\begin{aligned} |\hat{u}_A| &= \sqrt{(Re(\hat{u}_A))^2 + (Im(\hat{u}_A))^2}, \\ Re(\hat{u}_A) &= \frac{[Re(H_{2A^+}) - Re(H_{2A^-})] \sqrt{S_{22}}}{\rho_0 c_0 K_2}, \\ Im(\hat{u}_A) &= \frac{[Im(H_{2A^+}) - Im(H_{2A^-})] \sqrt{S_{22}}}{\rho_0 c_0 K_2}, \\ Re(H_{2A^+}) &= \frac{-Re(H_{21}) \sin(kl_{2s}) + Im(H_{21}) \cos(kl_{2s}) + \sin(k(l_{2s} + s_{12}))}{2 \sin(ks_{12})}, \\ Im(H_{2A^+}) &= \frac{-Re(H_{21}) \cos(kl_{2s}) - Im(H_{21}) \sin(kl_{2s}) + \cos(k(l_{2s} + s_{12}))}{2 \sin(ks_{12})}, \end{aligned} \quad (4-9)$$

$$Re(H_{2A^-}) = \frac{-Im(H_{21})\cos(kl_{2s}) - Re(H_{21})\sin(kl_{2s}) + \sin(k(l_{2s} + s_{12}))}{2\sin(ks_{12})},$$

$$Im(H_{2A^-}) = \frac{Re(H_{21})\cos(kl_{2s}) - Im(H_{21})\sin(kl_{2s}) - \cos(k(l_{2s} + s_{12}))}{2\sin(ks_{12})}.$$

Consequently, it can be seen from equation (4-9) that the experimental derivation of the particle velocity  $|\hat{u}_A|$  at the surface  $A$  requires the measurement of the transfer function  $H_{21}$ , the autospectrum  $S_{22}$  at position 2 (microphone 2) together with the magnitude calibration  $K_2$  [V/Pa] of the microphone 2 located at position 2. For a thin sample, the particle velocity is the same on either side, i.e.,  $\hat{u}_A = \hat{u}_B$ .

#### ***Acoustic impedance based on the interior particle velocity $\hat{v}$***

The normalised acoustic impedance based on the interior particle velocity  $\hat{v}$  is defined as

$$\xi'_S = \frac{\Delta\hat{p}}{\hat{v}\rho_0c_0} = \frac{\Delta\hat{p}}{(\hat{u}_A/\sigma)\rho_0c_0} = \xi_S\sigma = r'_S + j'x_S \quad (4-10)$$

#### ***Interior particle velocity $\hat{v}$***

The particle velocity  $\hat{v}$  inside the orifice is obtained from

$$\hat{v} = \hat{u}_A/\sigma, \quad (4-11)$$

where  $\hat{u}_A$  corresponds to the averaged particle velocity over the inlet sample cross sectional area given in equation (4-9) and  $\sigma$  is the porosity.



## 5. Results and discussion

Empirical observations and comparisons are first made on the different plates investigated. The transitional particle velocity  $\hat{v}_t$  is defined as the threshold for the internal acoustic velocity for which non linearity is observed. Non-linearity resistive results are further exploited to determine experimentally the porosity of the samples. The second part treats the modelling of the plates with the model previously described. Unless specified, all the plates have a thickness of 1 mm.

### *Experimental results*

#### *Plate with a single aperture*

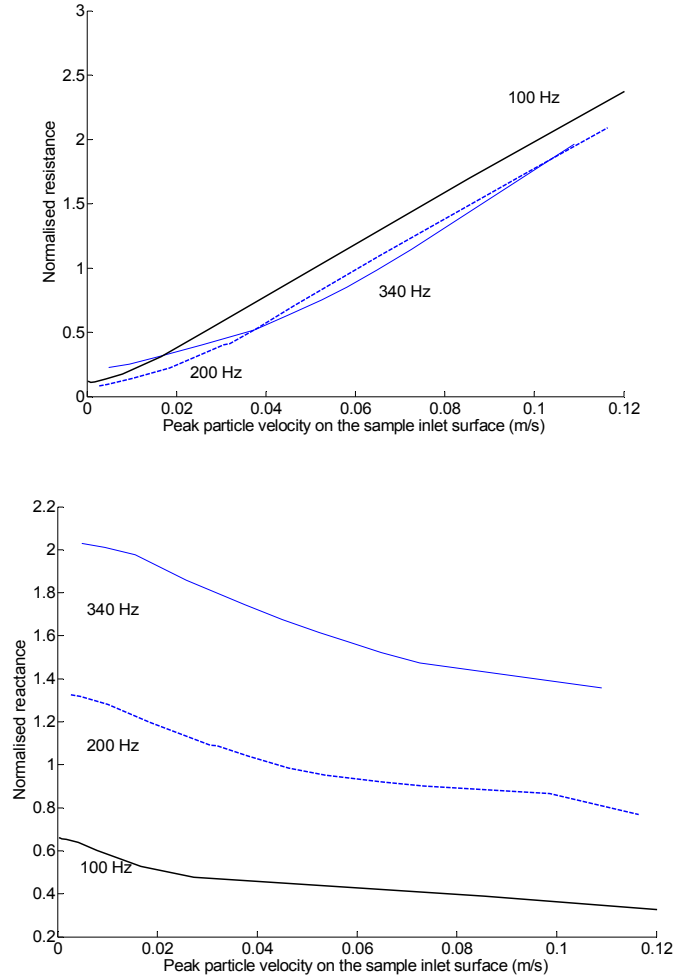


Figure 8: Normalised impedance  $\zeta_s$  for the rectangular aperture ( $w=50$  mm,  $h=1$  mm,  $\sigma=0.0102$ ).

*Plate with multiple apertures*

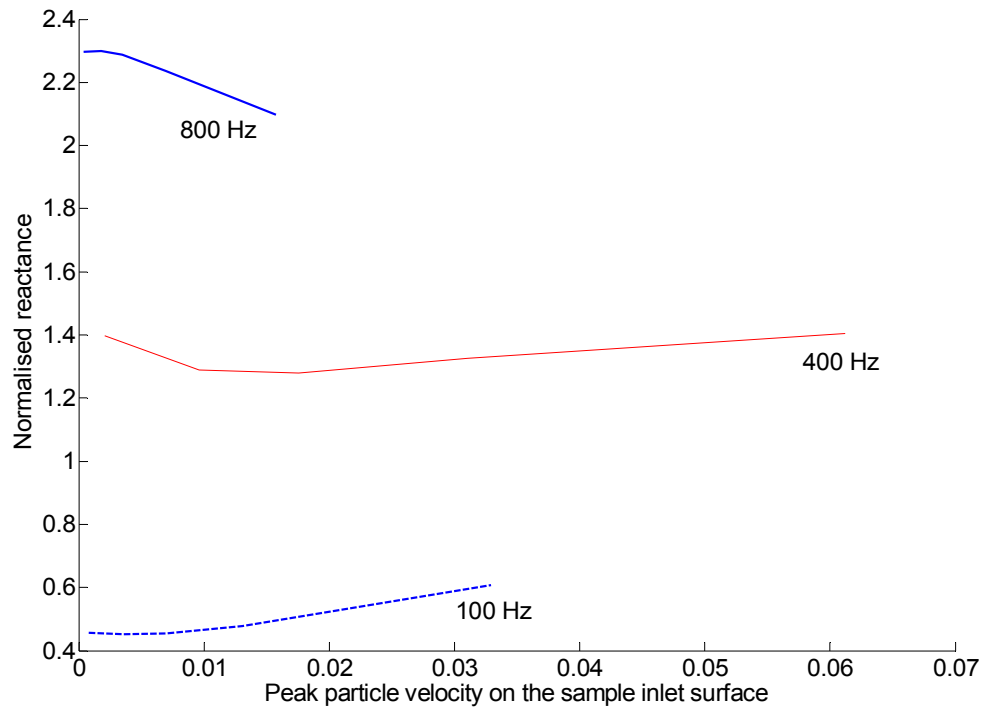
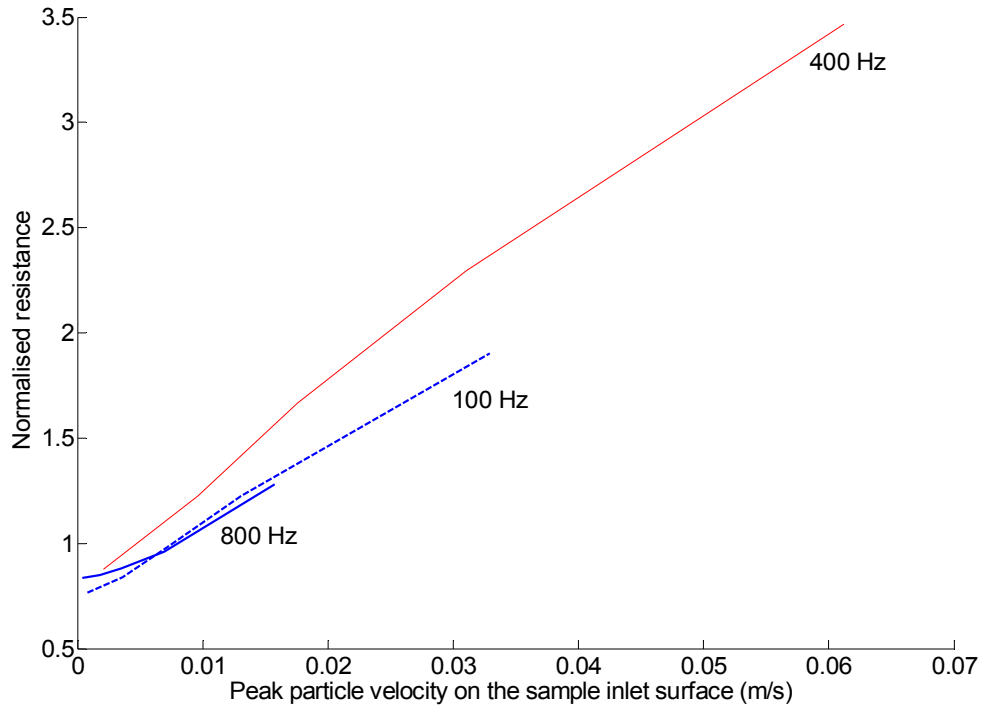


Figure 9: Normalised impedance  $\zeta_s$  for a plate with multiple circular holes ( $d=0.4$  mm,  $t=0.6$  mm  $\sigma=0.0056$ ).

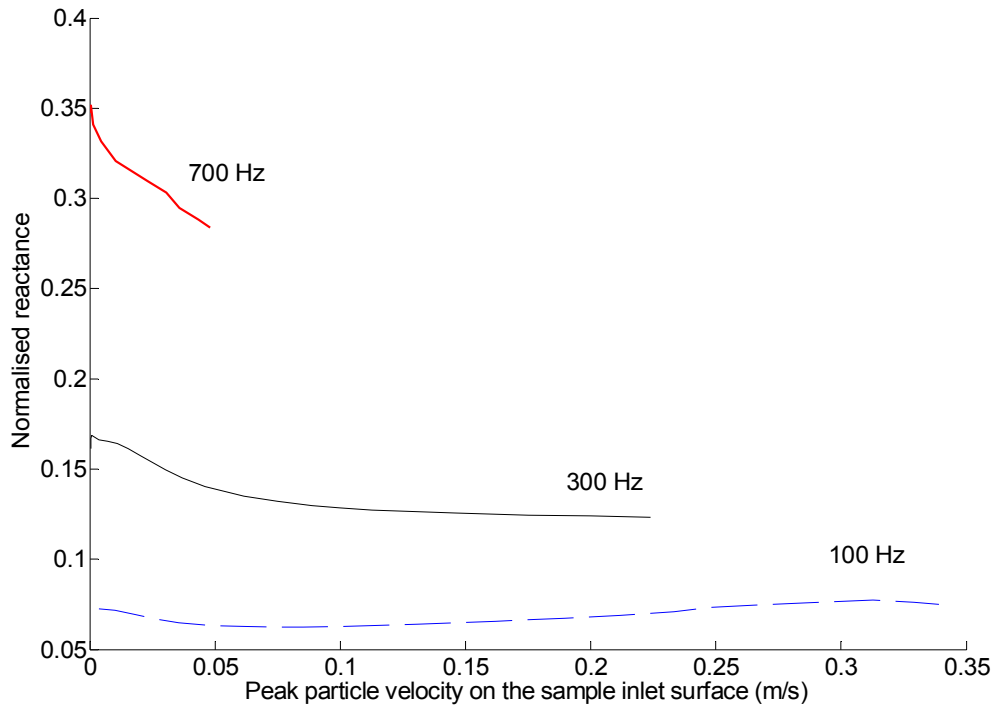
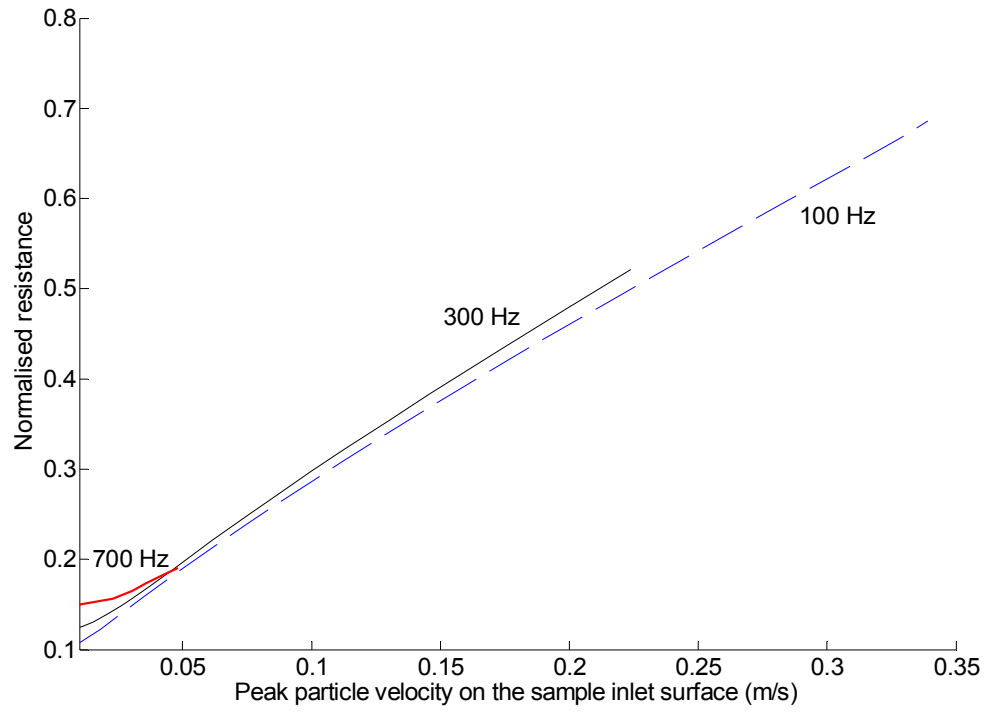


Figure 10: Normalised impedance  $\zeta_s$  for a plate with multiple circular holes ( $d=0.5$  mm,  $t=0.5$  mm  $\sigma=0.041$ ).



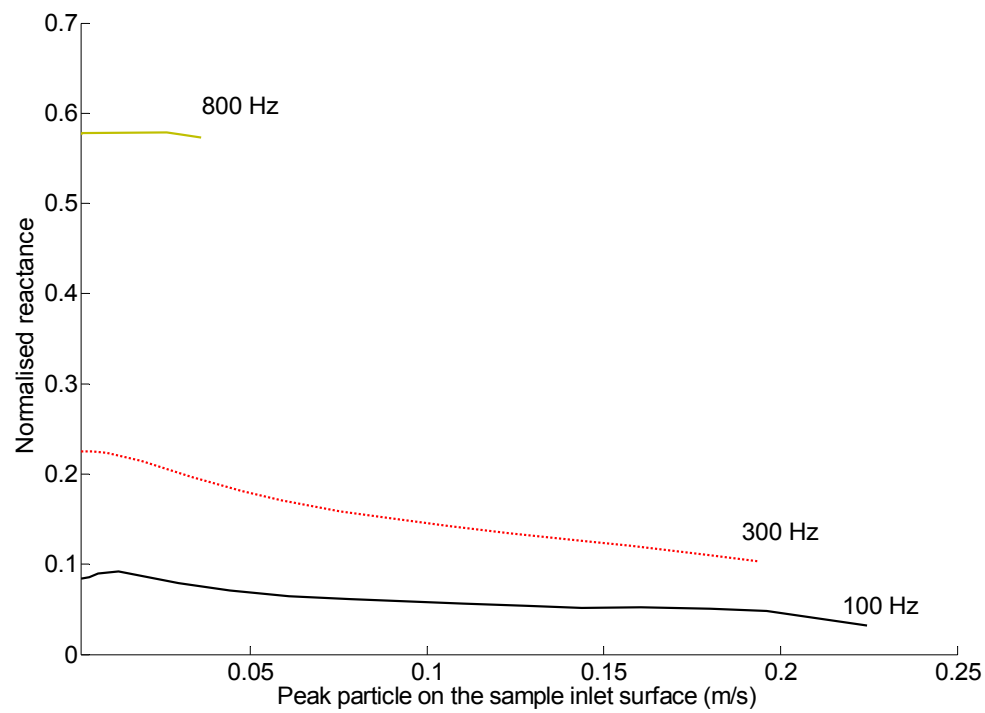
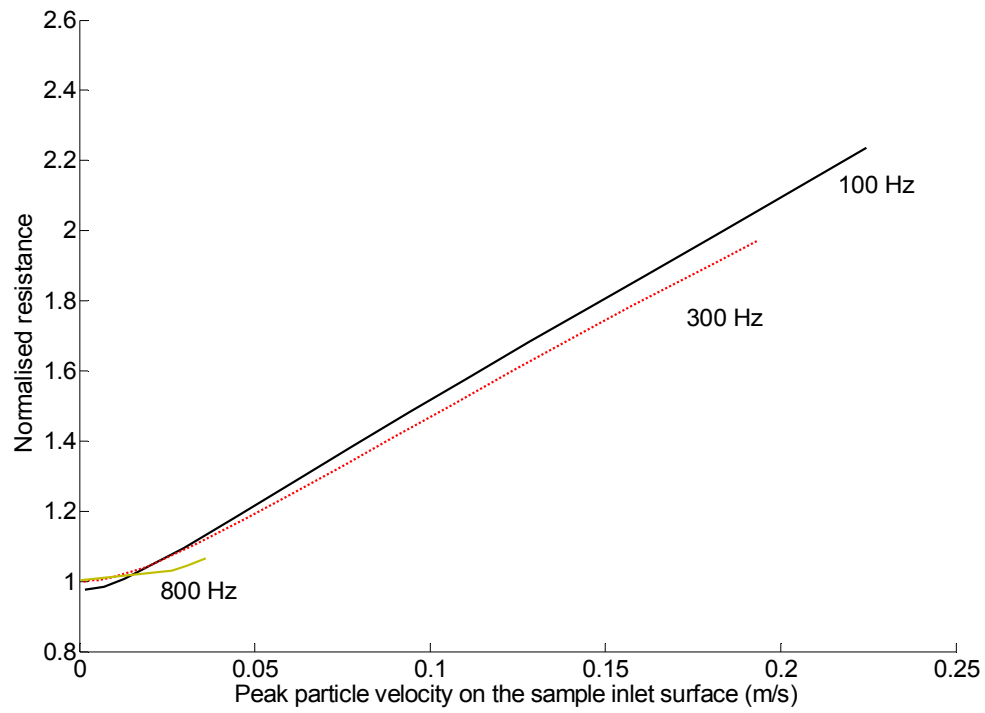


Figure 11: Normalised impedance  $\zeta_s$  for the Acustimet micro-perforate sample.

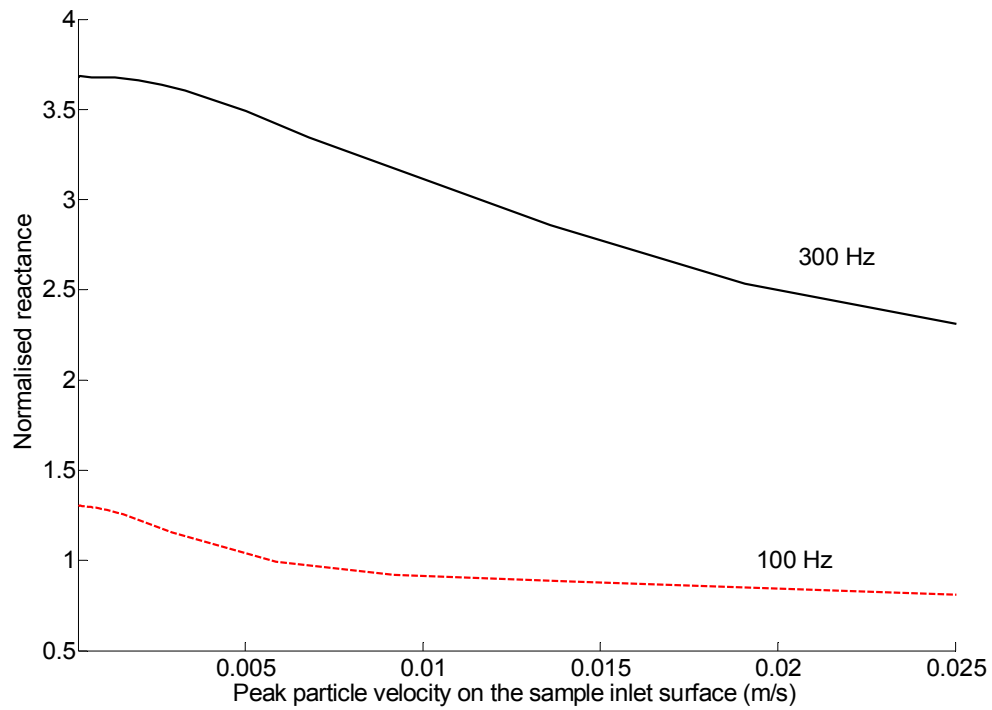
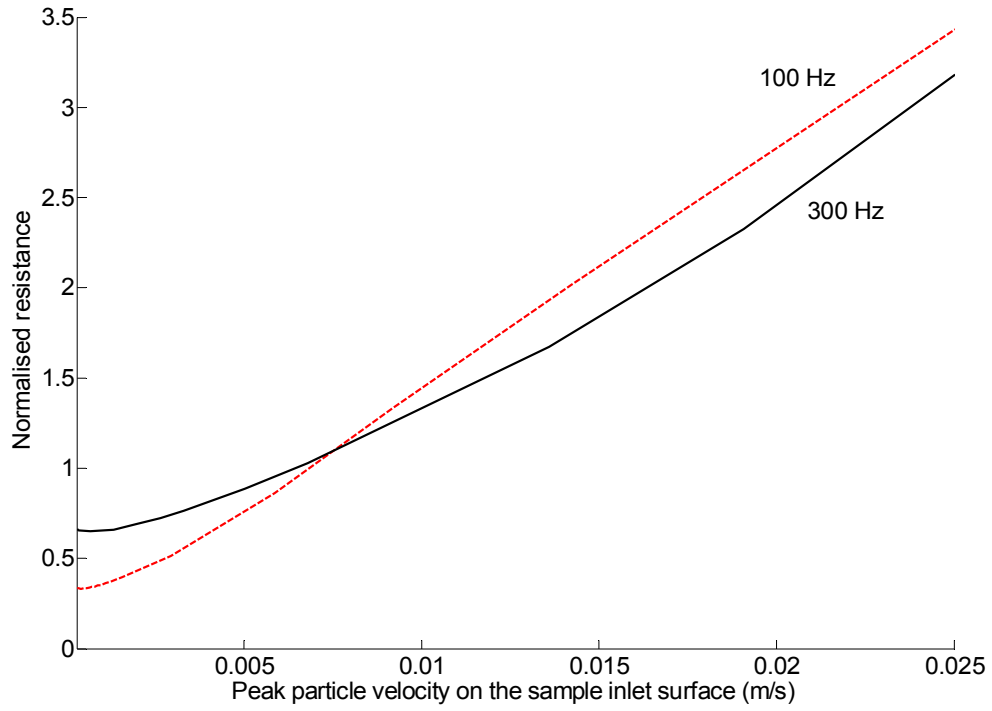


Figure 12: Normalised impedance  $\zeta_s$  for a plate with four rectangular apertures ( $w=5$  mm,  $h=1$  mm,  $\sigma=0.004$ ).

## 5.1 Comparison between plates

The normalised impedance  $\zeta'_s$  based on the internal acoustic particle velocity  $\hat{v}$  is chosen in this section to facilitate the comparison of results for the various plates investigated.

### *Single aperture*

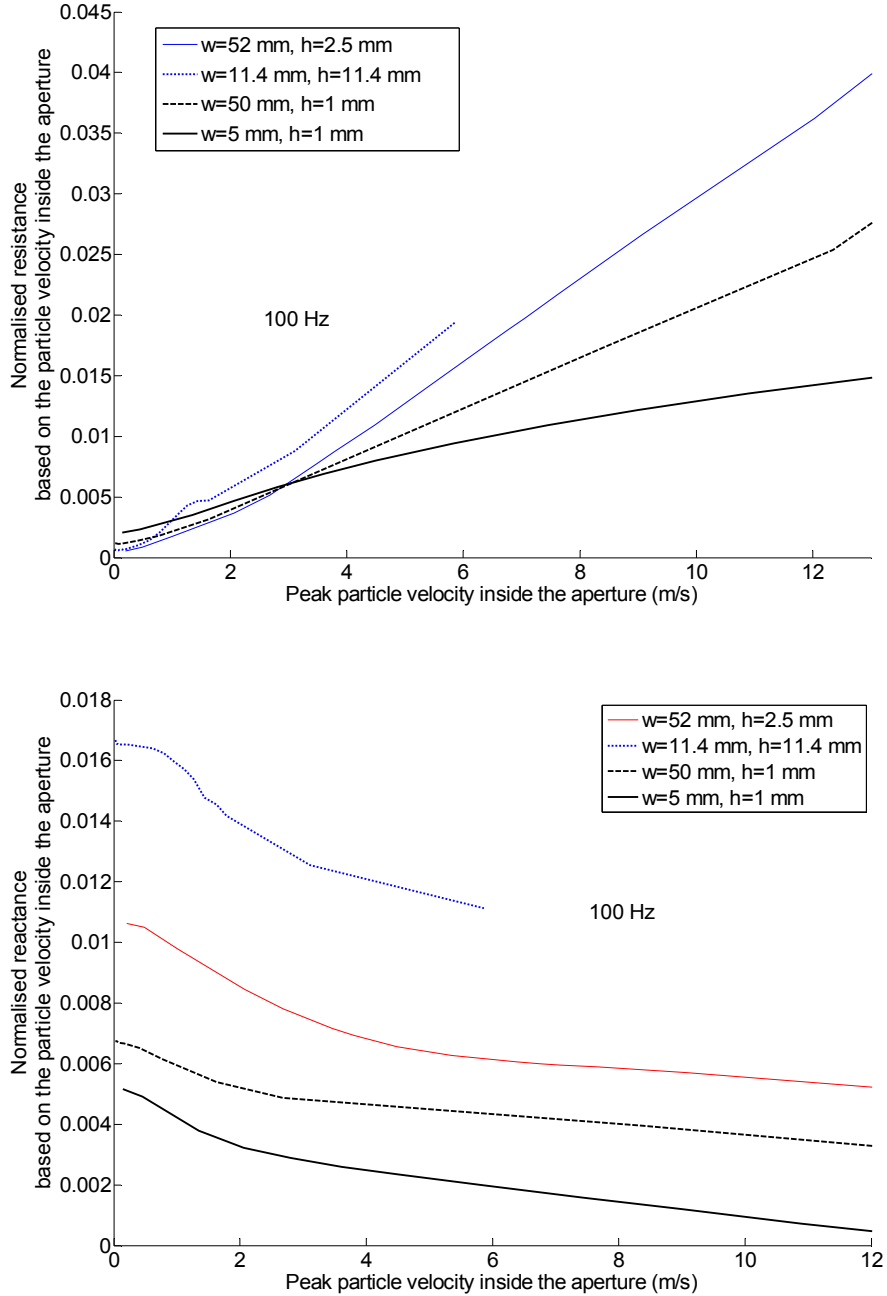


Figure 13: Normalised impedance  $\zeta'_s$  based on the interior particle velocity  $\hat{v}$  for plates with single square and rectangular apertures.

Figure 14 shows the acoustic impedance based on the internal particle velocity  $\hat{v}$  for different excitation levels for plates with the same porosity and different single aperture geometries.

It is immediately apparent from Figure 14 that the overall acoustic behaviours for both regimes are not related to the type of geometry. The square, rectangular, hole apertures all show a linear increase of the resistive  $r_S$  and a drop of the reactance  $x_S$  above a certain transitional acoustic particle velocity  $\hat{v}_t$ .

It can be seen from Figure 14 that the linear and non linear normalised resistances  $r_S$  appear to be independent of the frequency. The normalised resistance is related mostly to the porosity of the sample.

The normalised reactance  $x_S$  is the same for the square and circular orifices with same porosity. An elongation of the aperture results in a reduction of the end correction. The transitional particle velocity  $\hat{v}_t$  increases with the frequency. Figure 13 indicates that an elongated aperture causes the particle velocity  $\hat{v}_t$  to be reduced. This can be explained on the basis that vorticity is more likely to be formed as the aperture narrows.

Figure 13 emphasises the point previously discussed concerning the transitional particle velocity  $\hat{v}_t$ . The narrower the dimensions, the smaller the particle velocity  $\hat{v}_t$ . The square and rectangular apertures ( $w=52$  mm,  $h=2.5$  mm) have the same porosity implying the same averaged particle velocity  $\hat{u}_A$  over the entire sample cross section. Comparison between these two geometries shows that an elongated aperture results in a lower reactance. This is due to the end correction term, the external reactance being nearly identical due to the same thickness  $t=1$  mm.

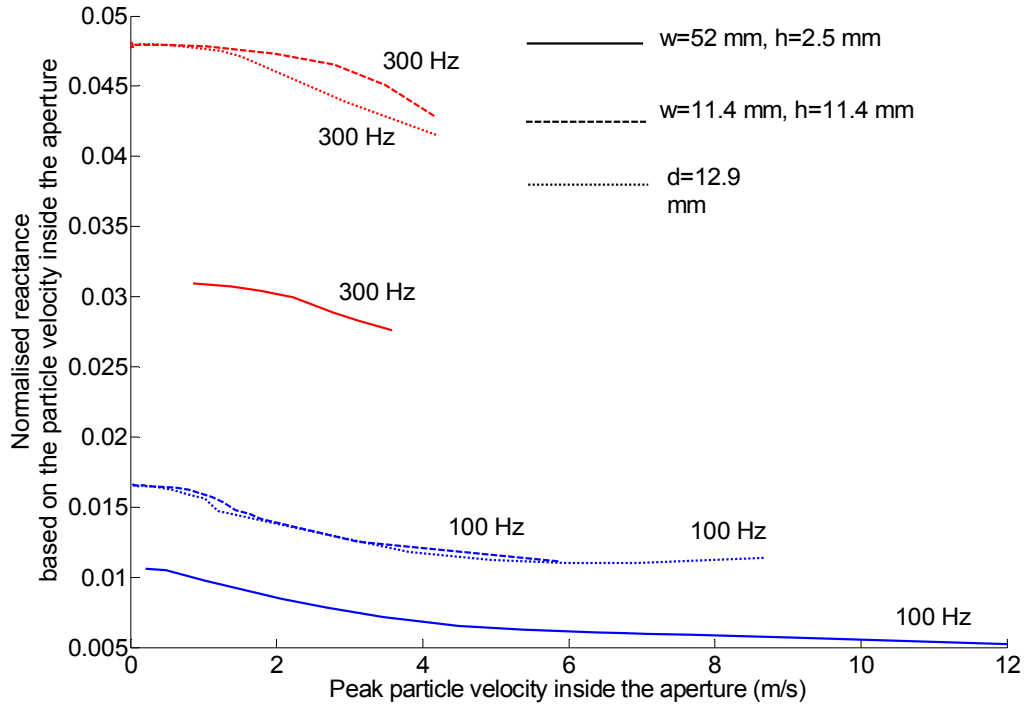
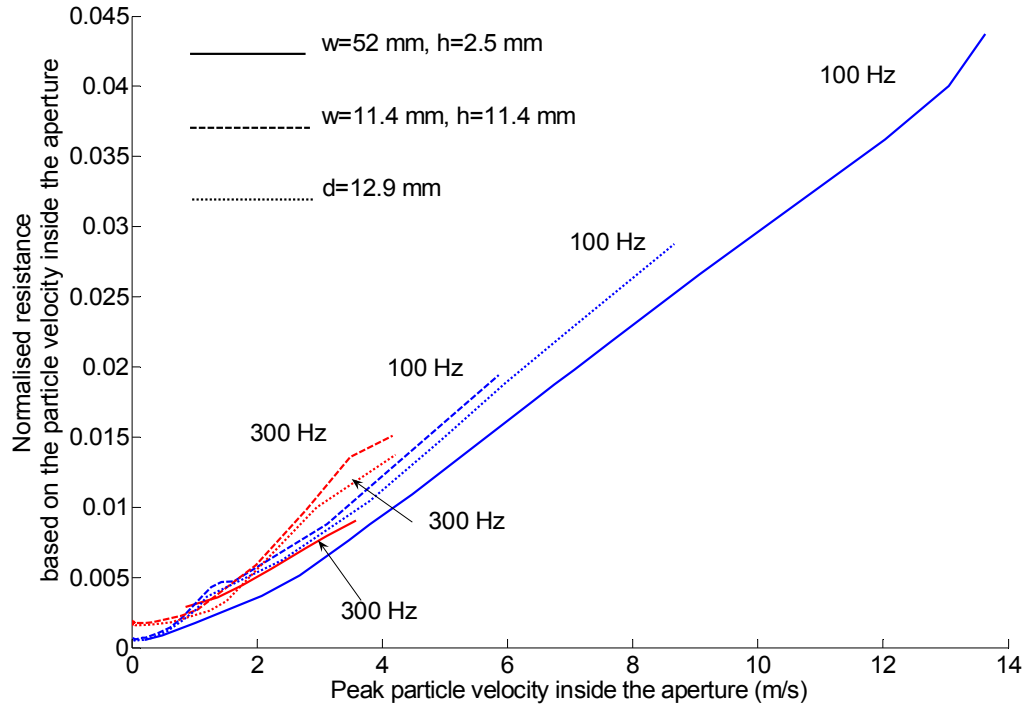


Figure 14: Normalised impedance  $\zeta'_s$  based on the interior particle velocity  $\hat{v}$  for plates with single square, rectangular and hole orifices ( $\sigma=0.0265$ ).

### Multiple apertures

Figure 15 shows the impedance for a plate composed of the same slit dimension ( $w=5$  mm,  $h=1$  mm) and different porosity values  $\sigma$ .

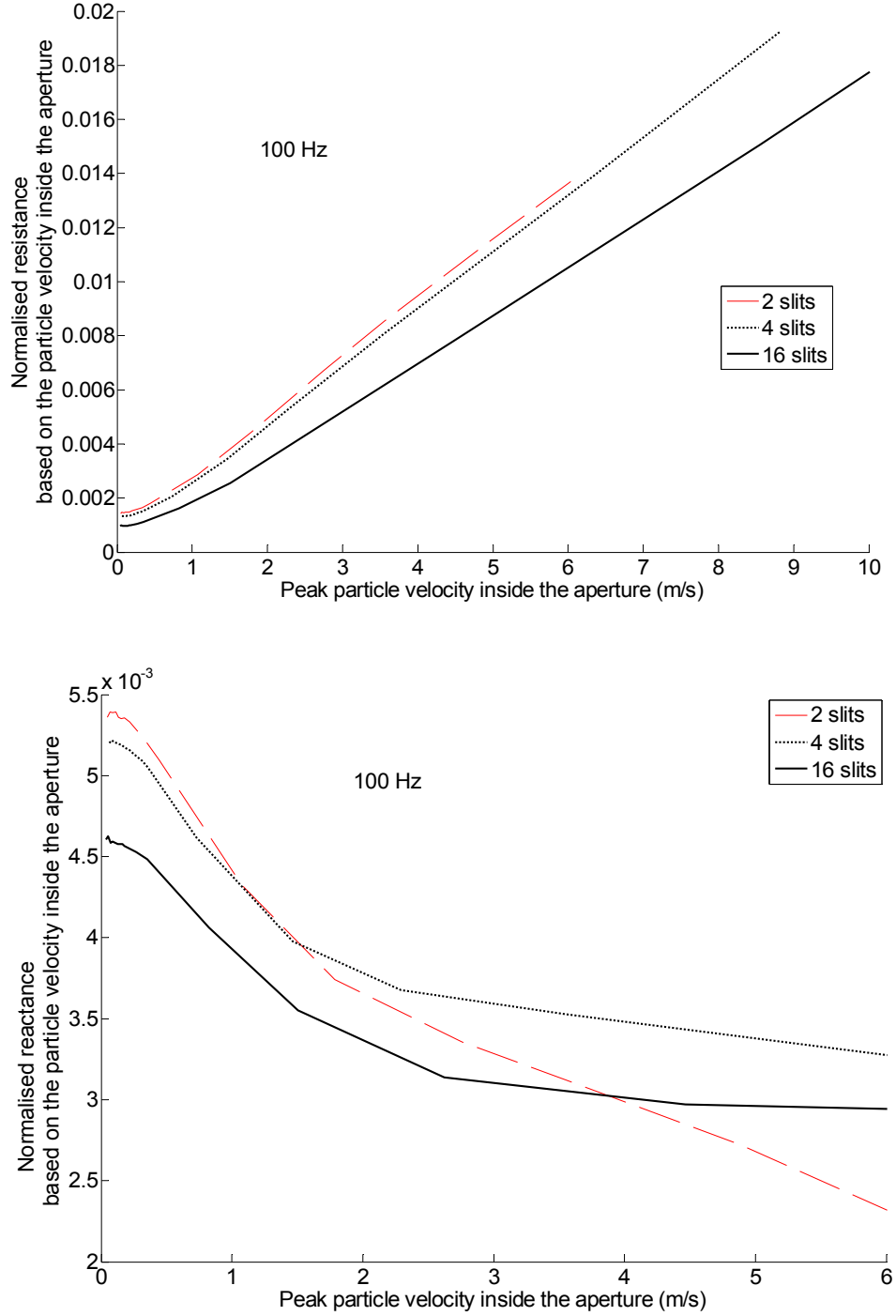


Figure 15: Single aperture normalised impedance  $\zeta'_s$  for plates with multiple rectangular aperture ( $w=5$  mm,  $h=1$  mm).

Figure 15 demonstrates the effect of the coupling between adjacent rectangular apertures as Ingard (1953) and Melling (1973) have discussed for circular orifices. An increase of porosity results in a reduction of both the resistance and reactance linear results. It also appears than the limit of 4% for the porosity previously assumed has been overestimated. Coupling effects take place for lower porosity values in the case of aperture of rectangular geometry.

## 5.2 General discussion

In view of the experimental results obtained, some empirical observations can be made. The linear limit seems more or less independent of the frequency for the resistive term. For the reactance the linear limit on the other hand is frequency dependent and increases with the frequency. Commenting the non-linear regime now, the resistive term is linearly proportional to the peak particle velocity increases and independent of the frequency. The non-linear reactance is reduced as the particle velocity  $\hat{u}_A$  rises. From Figure 14 it is clear that the transition between the linear and non-linear regime is dependent of the geometry of the orifice. Non-linearity effects are triggered for lower interior particle velocity  $\hat{v}_i$  for the rectangular aperture than for the square aperture. This is due to the narrower dimension causing the acoustic flow to break down into vorticity. This observation emphasises the argument of Maa (1994) that non-linearity is an external phenomenon. Maa (1994) states that the internal impedance is independent of the sound intensity.

## 5.3 Experimental determination of the porosity

Following Ingard (1953) and Maa (1998) treatments of the non linear resistive impedance, a procedure is now discussed to measure the perforation ratio area of the samples. At high (non-linear regime) sample inlet particle velocity  $\hat{u}_A$ , the normalised resistance of the sample is observed (Figure 8-Figure 12) to be linearly related to the particle velocity  $\hat{u}_A$ . Using a line fitting technique, the slope of the normalised resistance as function of the particle velocity  $\hat{u}_A$  is obtained for the non-linear regime. According to Maa (1998), the slope is equal to  $1/(\sigma^2 c_0)$ . Therefore, the perforation ratio area  $\sigma$  is obtained from the measured non-linear normalised flow resistive term  $r_S$ .

Results for the samples investigated are given in Table 2 and show good agreement with the true porosity calculated from the dimensions of the orifice and the entire plate.

Samples	Measured porosity	Calculated porosity
Single rectangular aperture ( $w=5$ mm, $h=1$ mm)	0.0013 (200 Hz)	0.001
Two rectangular apertures ( $w=5$ mm, $h=1$ mm) separated by a distance of 20 mm	0.0023 (100 Hz)	0.002
Single rectangular aperture ( $w=50$ mm, $h=1$ mm)	0.0121 (100 Hz)	0.0102
Four rectangular apertures ( $w=5$ mm, $h=1$ mm)	0.0047 (100 Hz)	0.004
Sixteen rectangular apertures ( $w=5$ mm, $h=1$ mm)	0.02 (100 Hz)	0.016
Single square aperture ( $w=11.4$ mm, $h=11.4$ mm)	0.0249 (100 Hz)	0.0265
Single rectangular aperture ( $w=52$ mm, $h=2.5$ mm)	0.0246 (100 Hz)	0.0265
Single circular hole ( $d=12.9$ mm)	0.0238 (100 Hz)	0.0267
Multiholed plate 1 ( $d=0.4$ mm)	0.0093 (100 Hz) 0.0084 (400 Hz)	0.0056
Multiholed plate 2 ( $d=0.5$ mm)	0.041 (100 Hz)	0.041
Sontech Acustimet micro-perforated sample	0.0224 (100 Hz)	

Table 2: Porosity measurement technique results.

#### 5.4 Plate modelling

The plain straight line corresponds to the calculated value for the linear regime based on equation (2-10).



*single aperture*

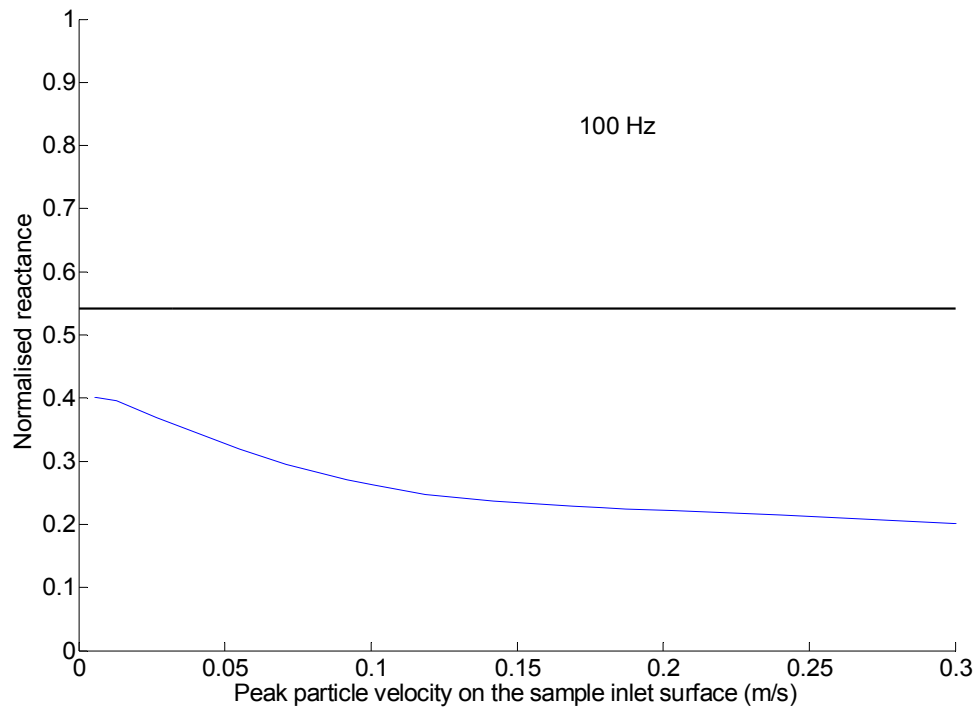
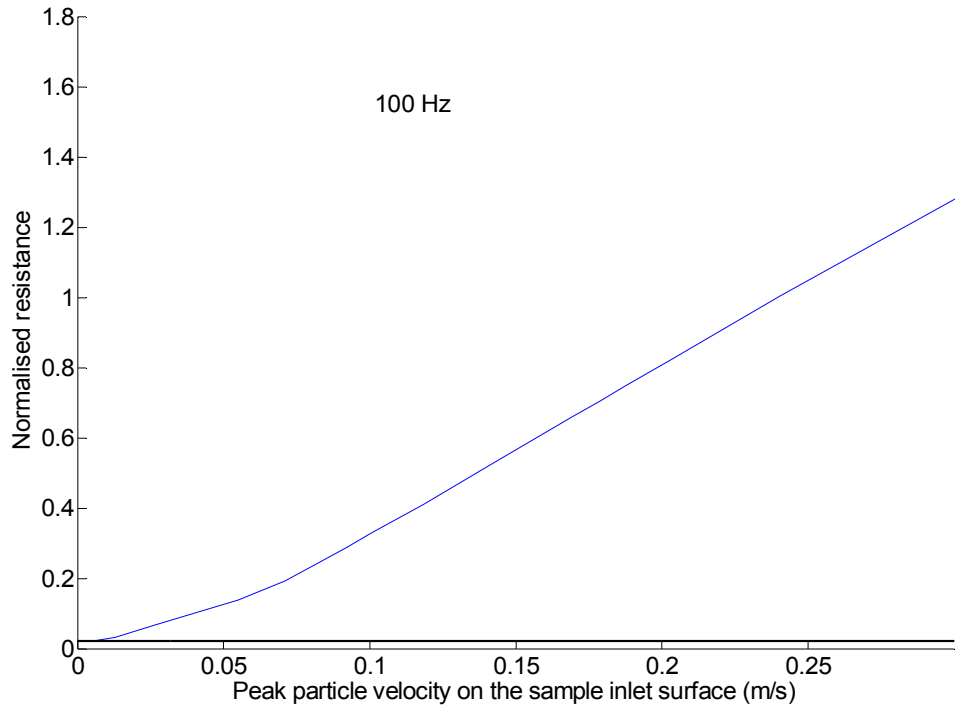


Figure 16: Normalised impedance  $\zeta_s$  for a plate with one rectangular aperture ( $w=52$  mm,  $h=2.5$  mm,  $\sigma=0.0265$ ).

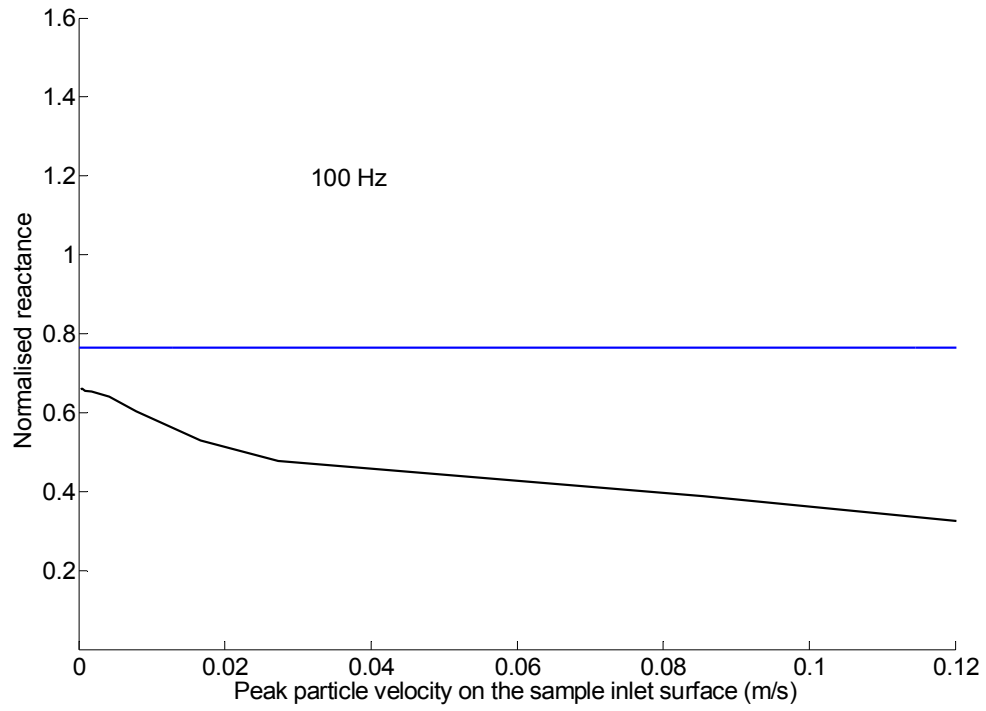
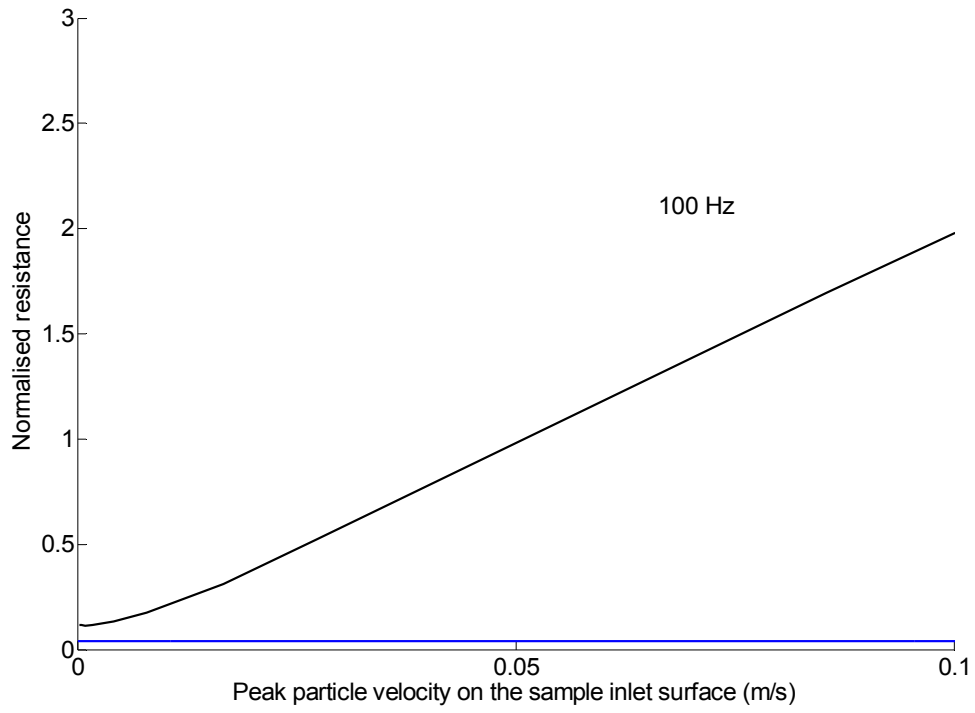


Figure 17: Normalised impedance  $\zeta_s$  for a plate with one rectangular aperture ( $w=50$  mm,  $h=1$  mm,  $\sigma=0.0102$ ).

*multiple apertures*

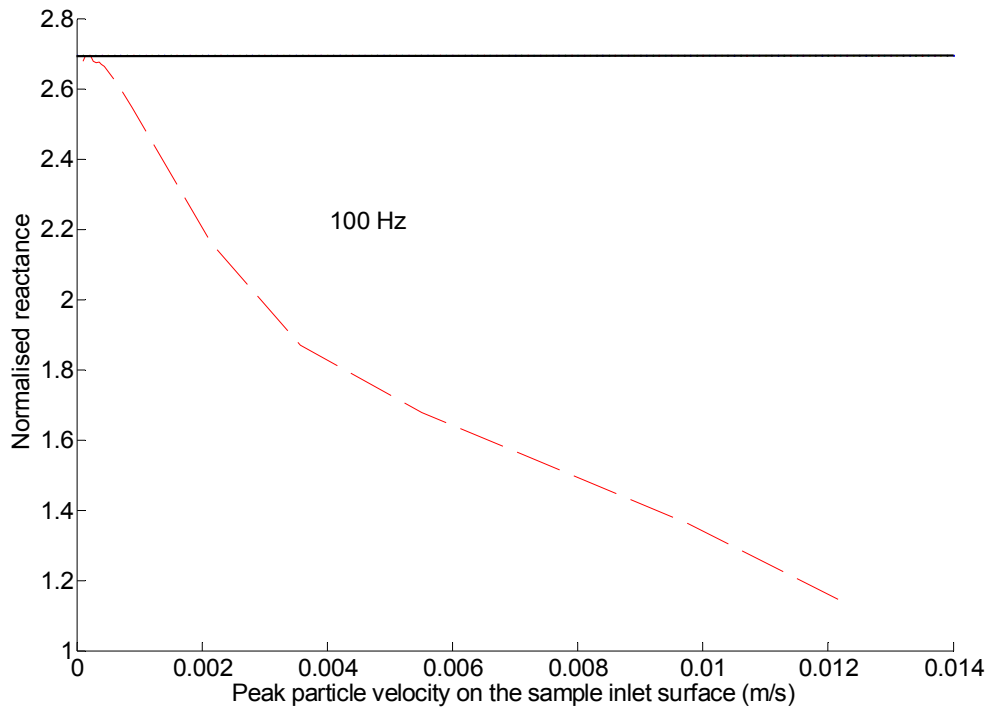
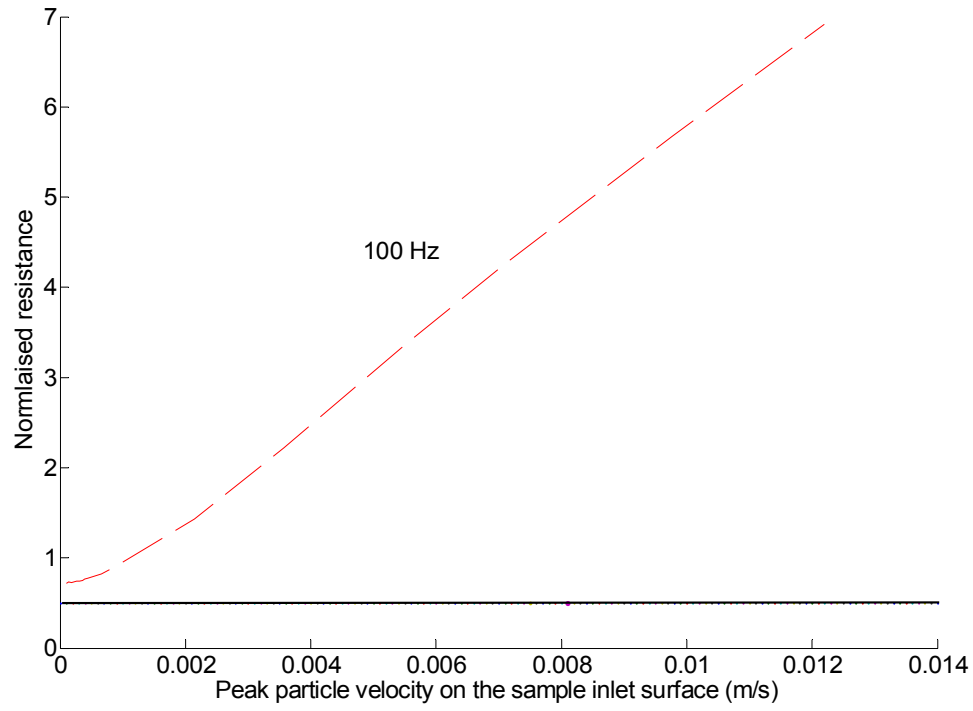


Figure 18: Normalised impedance  $\zeta_s$  for a plate with two rectangular apertures ( $w=5$  mm,  $h=1$  mm,  $\sigma=0.002$ ).

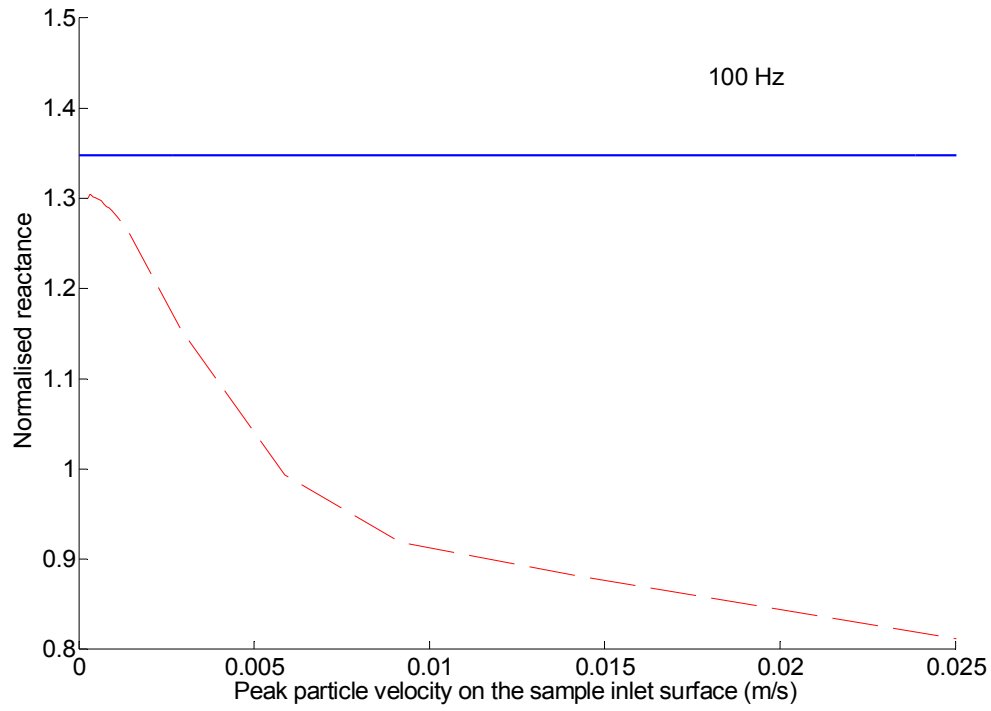
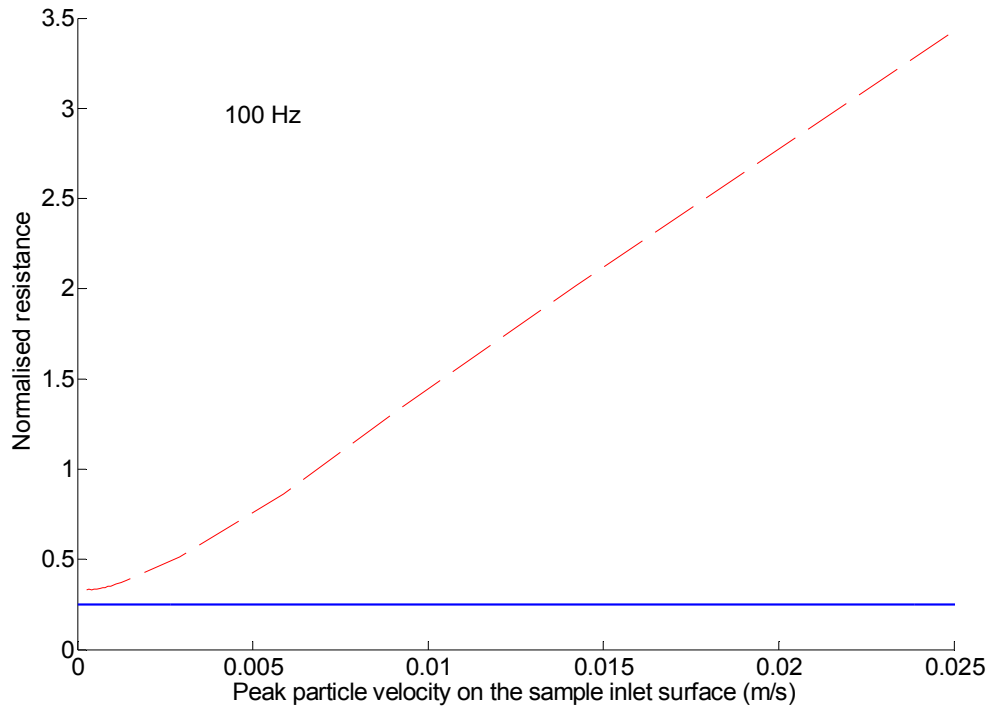


Figure 19: Normalised impedance  $\zeta_s$  for a plate with four rectangular apertures ( $w=5$  mm,  $h=1$  mm,  $\sigma=0.004$ ).

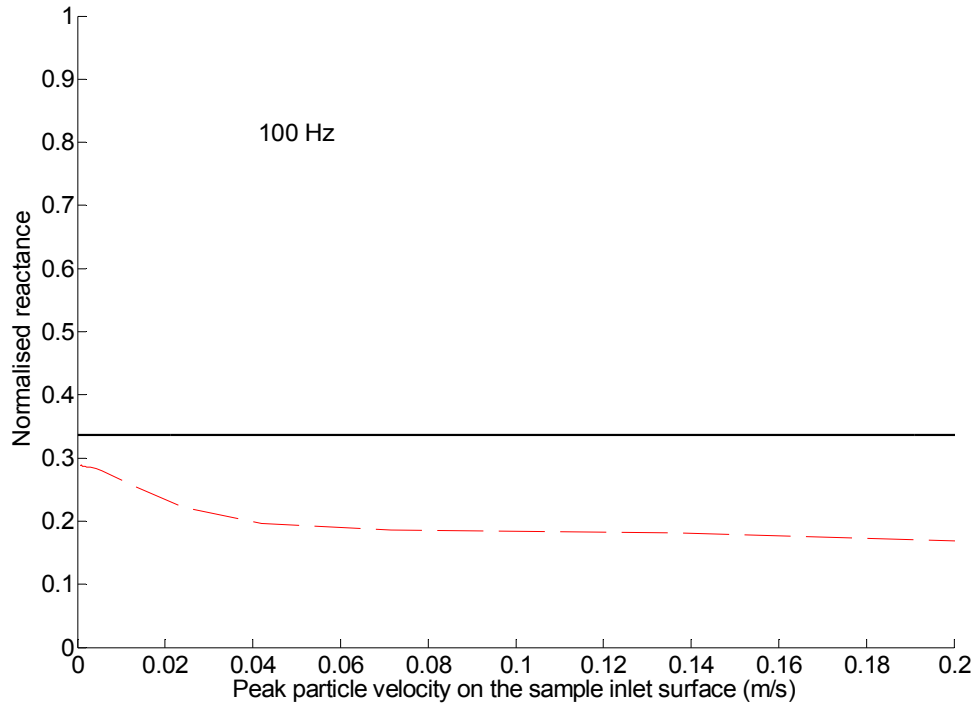
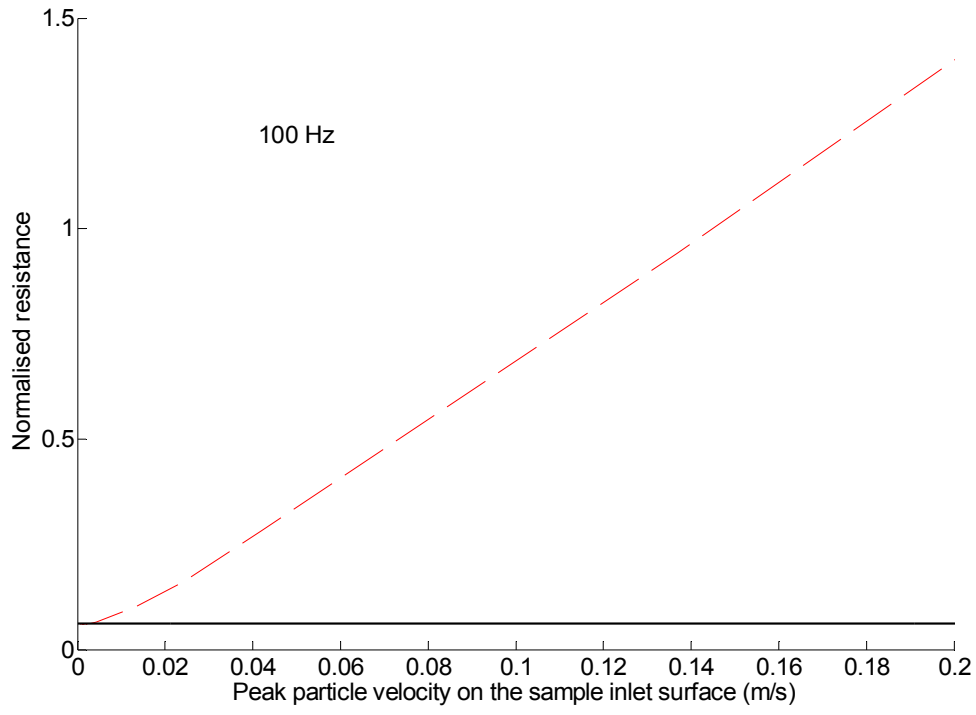


Figure 20: Normalised impedance  $\zeta_s$  for a plate with sixteen rectangular apertures ( $w=5$  mm,  $h=1$  mm,  $\sigma=0.016$ ).

Results from Figure 16 to Figure 20 show that the normalised resistive term  $r_s$  is well predicted for the samples investigated. Nevertheless, the tendency is to underpredict the losses. This can be explained on the fact that the external friction resistance  $R_s$  is greater or at least of the same magnitude than the internal resistance  $R_{i,ra}$  over the width  $w$  investigated ( $\geq 5$  mm). The external friction resistance  $R_s = (1/2)\sqrt{2\rho_0\omega\eta}$  has been empirically obtained from the Ingard investigation on circular orifices (Ingard (1953)). The magnitude of the external friction resistance  $R_s$  has been multiplied by a factor of 2. This appears to be not sufficient and need to be treated in more detail.

In the case of the plates with multiple slits and at high porosity, the underprediction is compensated by the coupling effect. It has been said and experimentally shown that as the separation between the apertures gets smaller, the resistance and reactance reduce. The theoretical values for the normalised reactance  $x_s$  tend to be overpredicted for samples with larger porosity. This can be explained by the coupling effects between neighbouring apertures for the plates with multiple apertures. These effects are not taken into account in the models.



## 6. Conclusions

The experimental determination of the acoustic impedance for plates with single, multiple circular and rectangular apertures have revealed the major differences regarding the linear and non linear regimes of these plates.

It has been observed than an elongated aperture show a reduction in the normalised reactance due to the smaller end correction. The non-linear transitional particle velocity  $\hat{v}_t$  is also reduced for elongated rectangular geometries. A model for plates with multiple rectangular apertures has been carried out to predict the acoustic impedance for the samples. An overprediction has been observed for the reactance of samples with higher porosity. Previous experimental works have relied upon the means of a rigid cavity backing up the sample together with measurement of absorption coefficient by using the impedance tube method. A similar experimental approach could be taken in the future for complementary validation of our model for slits. The measured non-linear resistive results have been used to derive experimentally the porosity of the samples. The technique gives satisfactory results.





## 7. References

- 1 Åbom M., 1999, *Determination of porous material data via two-port measurements*, Inter-Noise 99, Florida, USA, 589-594.
- 2 Allard J.F., 1993, *Propagation of sound in porous media, modelling sound absorbing materials*, Elsevier, London.
- 3 Chung J.Y., Blaser D.A., 1980, *Transfer function method of measuring in-duct acoustic properties I. Theory*, Journal of the Acoustical Society of America, **68**, 907-913.
- 4 Crandall I. B., 1927, *Theory of vibrating systems and sound*, Appendix A: Resistance coefficients for cylindrical conduits, Macmillan and co, limited.
- 5 Cremer L., Müller H. A., 1982, *Principles and applications of room acoustics*, vol. II, Applied Science Publisher, London.
- 6 Ducret F., Jacobsen F., Åbom M., 2005, *Development of micro-perforated acoustic elements for vehicle applications*, Twelfth International Congress on Sound and Vibration, Lisbon, Portugal.
- 7 Elnady T., 2004, *Modelling and characterization of perforates in lined ducts and mufflers*, Doctoral Thesis, KTH Aeronautical and Vehicle Engineering.
- 8 Fenech B., 2004, *Damping the acoustic modes in a closed cavity using a micro-perforated plate*, MSc Thesis, Acoustic Technology, Ørsted, DTU, Denmark.
- 9 Gomperts M.C., 1964, *The “sound insulation” of circular and slit-shaped apertures*, Acustica, **14**(1), 1-16.
- 10 Gomperts M.C., 1965, *The influence of viscosity on sound transmission through small circular apertures in walls of finite thickness*, Acustica, **15**(4).
- 11 Gomperts M.C., Kihlman T., 1967, *The sound transmission loss of circular and slit-shaped apertures in walls*, Acustica, **18**, 144-150.

- 12 Ingard U., 1953, *On the Theory and Design of Acoustic Resonators*, Journal of the Acoustical Society of America, **25**(6), 1037-1061.
- 13 Ingard U., Ising H., 1967, *Acoustic nonlinearity of an orifice*, Journal of the Acoustical society of America, **42**(1), 6-17.
- 14 Ingerslev F., Nielsen A. K., 1944, *On the transmission of sound through small apertures and narrow slits*, Publication Nr.1 from The Acoustical Laboratory of the Academy of Technical Sciences, Copenhagen.
- 15 Jacobsen F., 2005, *Propagation of sound waves in ducts*, Note 31260, Acoustic Technology, Ørsted-DTU, Denmark.
- 16 Kristiansen U.R., Vigran T.E., 1994, *On the design of resonant absorbers using a slotted plate*, Applied Acoustics, **43**, 39-48.
- 17 Lamb H., 1910, *The dynamical theory of sound*, London.
- 18 Maa D-Y., 1983, *Direct and accurate impedance measurement of microperforated panel*, Inter Noise, Edinburg, UK.
- 19 Maa D-Y., 1987, *Microperforated-panel wideband absorbers*, Noise Control Engineering Journal, **29**(3).
20. Maa D-Y., 1994, *Microperforated panel at high sound intensity*, Inter Noise, Yokohama Japan, August 29-31.
- 21 Maa D-Y., 1998, *Potential of microperforated panel absorber*, Journal of the Acoustical Society of America, **105**(5), 2861-2866.
- 22 Mechel F.P., 1994, *Helmholtz resonators with slotted neck plates*, Acustica, **80**, 321-331.
- 23 Melling T.H., 1973, *The acoustic impedance of perforates at medium and high sound pressure levels*, Journal of Sound and Vibration, **29**(1), 1-65.
- 24 Morfey C.L, 1969, *Acoustic properties of openings at low frequencies*, Journal of Sound and Vibration, **9**(3), 357-366.

- 25 Morse, P.M., Ingard K.U., 1968, *Theoretical acoustics*, McGrawHill, St.Louis.
- 26 Lord Rayleigh, 1878, *The theory of sound*, Macmillan and Co.
- 27 Randeberg R. T., 2002, *Adjustable slitted panel absorber*, Acta Acustica/Acustica, **88**, 507-512.
- 28 Randeberg R.T., 2000, *A Helmholtz resonator with a lateral elongated orifice*, Acta Acustica/Acustica, **86**, 77-82.
- 29 Sauter A., Soroka W.W., 1970, *Sound transmission through rectangular slots of finite depth between reverberant rooms*, Journal of the Acoustical Society of America, **47**(1), 5-11.
- 30 Sivian L.J., 1935, *Acoustic impedance of small orifices*, Journal of the Acoustical Society of America, **7**, 94-101.
- 31 Smits J.M.A, Kosten C.W., 1951, *Sound absorption by slit resonators*, Acustica, **1**, 114-122.